Western Graduate&PostdoctoralStudies

Western University
Scholarship@Western

Electronic Thesis and Dissertation Repository

12-1-2016 12:00 AM

Development of Design Loads for Transmission Line Structures Subjected to Downbursts Using Aero-elastic Testing and Numerical Modeling

Amal Elawady
The University of Western Ontario

Supervisor
Ashraf El Damatty
The University of Western Ontario

Graduate Program in Civil and Environmental Engineering
A thesis submitted in partial fulfillment of the requirements for the degree in Doctor of Philosophy
© Amal Elawady 2016

Follow this and additional works at: https://ir.lib.uwo.ca/etd

Part of the Civil Engineering Commons, and the Structural Engineering Commons

Recommended Citation

Elawady, Amal, "Development of Design Loads for Transmission Line Structures Subjected to Downbursts Using Aero-elastic Testing and Numerical Modeling" (2016). *Electronic Thesis and Dissertation Repository*. 4242.
https://ir.lib.uwo.ca/etd/4242

This Dissertation/Thesis is brought to you for free and open access by Scholarship@Western. It has been accepted for inclusion in Electronic Thesis and Dissertation Repository by an authorized administrator of Scholarship@Western. For more information, please contact wlswadmin@uwo.ca.

ABSTRACT

The failure of transmission line structures due to severe High Intensity Wind (HIW) events is one of the major problems facing the electrical utility companies in various places around the globe including Canada. An extensive research program focusing on this problem started about fifteen years ago at The University of Western Ontario (UWO). In this Thesis, two major milestones are achieved leading to the advancement of the knowledge in this field. The first milestone is conducting, for the first time, a test on an aero-elastic model of a multi-span transmission system under reduced–scale simulated downbursts. The first objective of the experimental program is to assess the dynamic response of the conductors and the towers resulting from the transient nature of both the mean and the fluctuating components of downbursts. The second objective is to use the experimental results to validate a numerical model previously developed in-house at UWO for the analysis of transmission line structures under downbursts.

The second milestone achieved in this Thesis is the development, for the first time, of a set of load cases that simulates the critical effects of downbursts on transmission line structures taking into account the variation in the location and size of the wind events. A load case that is particular for downbursts results in a velocity profile on the line that is non uniform and unequal along the conductor spans adjacent to the opposite sides of a tower. This leads to unequal tensions in the two spans adjacent to the tower and the difference in tensions leads to a force transmitted to the tower along the longitudinal direction of the line. This force is believed to be the cause of the failure of many towers. A procedure that is simple enough for application and for estimation such a force is developed in this study. Finally,

through conducting an extensive parametric study for a number of transmission line systems, a comprehensive and simple procedure for estimating critical downburst loads on both the tower and the conductors is developed and presented in a simplified manner for possible implementation in the codes of practice.

Keywords

High Intensity Wind, Downburst, Transmission Line, Transmission Tower, Dynamic Response, Conductor, Cable, Longitudinal Force, Downburst Critical Load Cases.

CO-AUTHORSHIP

This thesis has been prepared in accordance with the regulations for an Integrated Article format thesis stipulated by the School of Graduate and Postdoctoral Studies at Western University. Statements of the co-authorship of individual chapters are as follows

Chapter 2: Aero-elastic Testing of Multi-Spanned Transmission Line Subjected to Downbursts

All the numerical and experimental work was conducted by A. Elawady under close supervision of Dr. A. A. El Damatty, Dr. G. Bitsuamlak and Dr. H. Aboshosha and the guidance of Dr. H. Hangan for the experimental work conducted in the WindEEE facility. Drafts of Chapter 2 were written by A. Elawady and modifications were done under supervision of Dr. A. A. El Damatty and Dr. G. Bitsuamlak. A paper co-authored by A. Elawady, A. A. El Damatty, H. Aboshosha G. Bitsuamlak, H. Hangan, and A Elatar will be submitted to the *Journal of Wind Engineering & Industrial Aerodynamics.*

Chapter 3: Aero-Elastic Response of Transmission Line System Subjected to Downburst Wind: Validation of Numerical Model Using Experimental Data

All the numerical and experimental work was conducted by A. Elawady under close supervision of Dr. A. A. El Damatty and Dr. H. Aboshosha. Drafts of Chapter 3 were written by A. Elawady and modifications were done under supervision of Dr. A. A. El Damatty and Dr. H. Aboshosha. A paper co-authored by A. Elawady, A. A. El Damatty, and H. Aboshosha will be submitted to the *Journal of Wind and Structures.*

Chapter 4: Longitudinal Force on Transmission Towers due to Non-Symmetric Downburst Conductor Loads

All the numerical work was conducted by A. Elawady under close supervision of Dr. A. A. El Damatty. Drafts of Chapter 4 were written by A. Elawady and modifications were done under supervision of Dr. A. A. El Damatty. A paper co-authored by A. Elawady and A. A. El Damatty has been published in the *Journal of Engineering Structures.*

Chapter 5: Critical Load Cases for Lattice Transmission Line Structures Subjected to Downbursts: Economic Implications for Design of Transmission Lines

All the numerical work was conducted by A. Elawady under close supervision of Dr. A. A. El Damatty. Drafts of Chapter 5 were written by A. Elawady and modifications were done under supervision of Dr. A. A. El Damatty. A paper co-authored by A. A. El Damatty and A. Elawady will be submitted to the *Journal of Engineering Structures.*

To my beloved mother ***Thanaa Elshafie***

To my sister ***Amira*** and my brothers ***Ahmed and Islam***

To my soulmate and my trusted friend **Mary**

For patience, support, encouragement, and sharing these years of hard work

To my nephews ***Ahmed, Seif, Ibrahim, Mohamed*** and my niece ***Mariam***

For filling my life with joy and happiness

To the soul of my beloved father **Mohamed Kamel Elawady** and the soul of my beloved brother **Ibrahim**

To my supervisor, ***Dr. Ashraf A. El Damatty***
For his continuous support and guidance as well as sharing his experience during these years

ACKNOWLEDGMENTS

These few words are a simple yet sincere attribute to express my gratitude to all those who helped me through the past years, to reach the end of a journey that would have never been possible without their help.

My utmost gratitude goes to my professor, Dr. Ashraf El Damatty, who taught me far beyond academics. To him I owe the knowledge and skills I rely on to pursue my career in academia. I am extremely grateful for all these hours he spent to motivate me and to sincerely give me as much as he could of his valuable experience.

I would like to thank the to thank Hydro One company, Ontario Centre of Excellence (OCE), O. H. Ammann Fellowship awarded by ASCE for their kind funding.

The support of my friends in Western is deeply appreciated. Many thanks must go to (M. Hamada, A. Ansary, A. Musa, A. Ibrahim, A. Hamada, H. Aboshosha, A. El Shaer, I. Ibrahim, A. Shehata, C. Santos, P. Sultana, N. El Gharably). I am extremely thankful for the support I received from Dr. Girma Bistuamlak and Dr. Ayman El Ansary who immensely helped on various aspects of my academic life at Western. I am indebted to the opportunity that surrounded me with such a group of helpful colleagues. The years I spent in my PhD couldn't possibly be any better without you.

Lastly, I would like to thank my sincere friend Mary for her valuable time, support, patience, and advices during all the stage of my PhD. Words fall short to describe my gratitude, admiration and adore to my amazing family; my ever loving, caring and supporting mom, my cheerful siblings. Thanks for your patience and support through this important period of my life. To my lighthearted niece and nephews, I hope one day you feel inspired and proud of what I have achieved. To my beloved family, you are everything I ever wanted.

TABLE OF CONTENTS

ABSTRACT ii

CO-AUTHORSHIP iv

ACKNOWLEDGMENTS vii

TABLE OF CONTENTS viii

LIST OF TABLES xiv

LIST OF FIGURES xvi

LIST OF SYMBOLS xxi

CHAPTER 1 1

INTRODUCTION 1

1.1 Background 1

1.2 Downburst Wind Field 6

1.2.1 Downburst Field Measurements 6

1.2.2 Experimental Studies for Downburst Wind Field 7

1.2.3 Numerical Studies for Downburst Field Characterization 7

1.3 Studies on TLs Response to Downbursts 10

1.4 Research Conducted at UWO On the Effect of Downbursts on TLs 11

1.5 Research Gaps 15

1.6 Scope of the Current Study 16

1.7 Organization of The Thesis 17

1.7.1. Aero-elastic Testing of Multi-Spanned Transmission Line Subjected to Downbursts 17

1.7.2. Aero-Elastic Response of Transmission Line System Subjected to Downburst Wind: Validation of Numerical Model Using Experimental Data 17

1.7.3. Critical Load Cases for Lattice Transmission Line Structures Subjected to Downbursts: Economic Implications for Design of Transmission Lines 18

1.7.4. Longitudinal Force on Transmission Towers due to Non-Symmetric Downburst Conductor Loads 19
1.7.5. Summary and Conclusions 19
1.8 References 19

CHAPTER 2 25

AERO-ELASTIC TESTING OF MULTI-SPANNED TRANSMISSION LINE SUBJECTED TO DOWNBURSTS 25

2.1. Introduction 25

2.2. Downburst Simulation at WindEEE 33

2.2.1. Mean and fluctuating wind decomposition 35
2.2.2. Turbulence intensity 37
2.2.3. Velocity profile validation 39
2.3. Aero-elastic Modeling of Transmission Line System 41

2.3.1. Prototype description 41
2.3.2. Aero-elastic model scaling parameters 45
2.3.2.1. Tower model 47
2.3.2.2. Conductor model selection 49
2.3.2.3. Support boundary conditions 50
2.3.2.4. Instrumentation 51
2.3.2.5. Aero-elastic model free vibration test 54
2.3.3. WindEEE downburst test plan 56
2.3.3.1. Layout 1: Maximum longitudinal loads (Angle of attack Θ = 90º) 58
2.3.3.2. Layout 2: Maximum transverse loads (Angle of attack Θ = 0 º) 58
2.3.3.3. Layout 3: Maximum oblique loads (Angle of attack Θ = 52 º) 59
2.4. Results and Discussions 61

2.4.1. Identification of Critical Configurations 61
2.4.2. Decomposition of the responses 62
2.4.3. Quantifying the dynamic effect for different downburst velocities and configurations 68
2.4.4. Dynamic Amplification Factor (DAF) 71

2.5. Conclusion 76

2.6. Acknowledgment 78

2.7. References 79

CHAPTER 3 82

AERO-ELASTIC RESPONSE OF TRANSMISSION LINE SYSTEM SUBJECTED TO DOWNBURST WIND: VALIDATION OF NUMERICAL MODEL USING EXPERIMENTAL DATA 82

3.1. Introduction 82

3.2. Brief about the numerical tools 87

3.2.1. Tower simulation using finite element model (FEM) 88

3.2.2. Conductors semi-analytical technique 90

3.3. Wind Tunnel Testing at WindEEE 91

3.3.1. Downburst wind field 91

3.3.2. Aero-elastic transmission line model 96

3.3.2.1. Full-scale transmission line system 96

3.3.2.2. Aero-elastic modelling of the line system 99

3.3.2.3. Instrumentations and data acquisition system 99

3.3.3. Experimental Test plan 100

3.3.3.1. Layout 1: Maximum longitudinal loads (Angle of attack of 90º) 102

3.3.3.2. Layout 2: Maximum transverse loads (Angle of attack of 0 º) 103

3.3.3.3. Layout 3: Maximum oblique loads (Yaw angles of attack): 104

3.4. Variation of peak and mean responses of the aero-elastic model with the downburst location 105

3.4.1. Layout 1: Maximum Longitudinal Loading (Θ=90˚, Fig. 3-17) 106

3.4.2. Layout 2: Maximum Transverse Loading (Θ=0˚, Fig. 3-18) 107

3.4.3. Layout 3: Maximum Oblique Loading (Θ=0˚, Fig. 3-19 and 3-20) 108

3.5. Results obtained from the numerical models 113
3.5.1. Validation of the external forces evaluation: 114
3.5.2. Validation of the conductor solution 114
3.5.3. Validation of straining action distributions 115
3.6. Conclusions 117
3.7. Acknowledgment 119
3.8. References 119
CHAPTER 4 124
LONGITUDINAL FORCE ON TRANSMISSION TOWERS DUE TO NON-SYMMETRIC DOWNBURST CONDUCTOR LOADS 124
4.1. Introduction 124
4.2. Downburst Wind Field 128
4.3. Variation of Longitudinal Force with the Conductor parameters 137
4.4. Longitudinal force charts 144
4.5. Transverse force 149
4.6. Validation 150
4.7. Example 151
4.8. Conclusion 153
4.9. Acknowledgement 155
4.10. Appendix A 156
4.11. References 172
CHAPTER 5 175

CRITICAL LOAD CASES FOR LATTICE TRANSMISSION LINE STRUCTURES SUBJECTED TO DOWNBURSTS: ECONOMIC IMPLICATIONS FOR DESIGN OF TRANSMISSION LINES 175

5.1. Introduction 175

5.2. Methodology 180

5.2.1. Downburst Wind Field 180
5.2.2. Modelling Technique and Method of analysis 183
5.2.3. Structural Characteristics of Analyzed Transmission Line Systems 186
5.3. Results and Discussion 189

5.3.1. Tower response 189
5.3.1.1. Guyed towers 190
5.3.1.2. Self-supported towers 192
5.3.1.3. Conductor forces 193
5.3.2. Proposed Downburst Load Cases 195
5.3.2.1. Load case#1: $R/D_J=1.3$, $\Theta=90^o$, $D_J=500$ m 198
5.3.2.2. Load case#2: $R/D_J=1.3$, $\Theta=0^o$, $L/D_J=0.5$ 199
5.3.2.3. Load case#3: $R/D_J=1.6$, $\Theta=30^o$, $L/D_J=0.5$ 201
5.3.3. Load Cases Validation 202
5.3.4. Economic Implications 205
5.4. Conclusion 211

5.5. Acknowledgements 214

5.6. References 214

CHAPTER 6 217

SUMMARY AND CONCLUSIONS 217

6.1. Summary 217

6.2. Conclusions 218

6.3. Recommendation for future work 220

LIST OF TABLES

Table 2-1. Scaling ratio for various physical parameters of the model..... 46

Table 2-2. Frequencies and mode shapes of the full-scale tower and the required frequencies of the aero-elastic model. 54

Table 2-3. Dynamic properties of the tested conductors..... 55

Table 2-4. Test layouts. 57

Table 2-5. DAF analysis..... 72

Table 3-1. Test layouts 101

Table 3-2. Selected test cases for validating the numerical models..... 113

Table 4-1. Conductors used to assess the effect of the conductor's parameters on R_X.. 141

Table 4-2. Group range for the evaluation of R_X. 145

Table 4-3. Validation for the R_X and R_Y values obtained from the proposed approach 151

Table 5-1. Properties of selected towers 187

Table 5-2. Downburst configurations causing maximum R_X 194

Table 5-3. Results of the economic study 208

Table 5-4. Failed members under downburst load case of a jet speed equal to 50 m/s. 210

Table 5-5. Summary of the economic implications of the downburst. 211

LIST OF FIGURES

Fig. 1-1 Guyed transmission tower components..... 3

Fig. 1-2 Lattice self-supported transmission line..... 4

Fig. 1-3. Numerical modeling methods of downburst winds..... 9

Fig. 2-1. Guyed tower failure in Ontario, (Hydro One Report, 2006)..... 27

Fig. 2-2. Downburst characteristic parameters. 27

Fig. 2-3. Schematic of testing chamber and downburst simulation at WindEEE..... 34

Fig. 2-4. Cobra probe devices. 35

Fig. 2-5. Decomposition of the downburst radial velocity at R/D=0.9 and Z/D=0.06. 39

Fig. 2-6. Contour lines of Wind field characteristics..... 39

Fig. 2-7. Peak radial wind profile along the tower height under. 41

Fig. 2-8. Schematic 3D view of the study line. 43

Fig. 2-9. Schematic of the test layout and the names of the tested towers. 43

Fig. 2-10. 3D view of the prototype transmission tower. 44

Fig. 2-11. Steel angle dimensions of the tower. 44

Fig. 2-12. Half-length of the assembled line. 45

Fig. 2-13. Pictures of D, E, F, and G frames. 45

Fig. 2-14. Test picture of A, B, and C towers..... 46

Fig. 2-15. (a) Spine dimensions (in mm), (b) Schematic of the full-scale guyed tower... 48

Fig. 2-16. Model boundary conditions details. 51

Fig. 2-17. Instrumentations of the tower. 52

Fig. 2-18. Accelerometers and strain gauges. 53

Fig. 2-19. Cobra Probe measurements during testing..... 53

Fig. 2-20. Summary of downburst-structure orientations for the considered layouts. 57

Fig. 2-21. Test layout 1. 58

Fig. 2-22. Test layout 2. 59

Fig. 2-23. Test layout 3. 60

Fig. 2-24. Base shear comparison for the three tested layouts. 62

Fig. 2-25. Response decomposition flow chart. 66

Fig. 2-26. Illustration of "no resonance" response case, in Layout 1, R/D = 0.9 and V_{RD}=35 m/s. 67

Fig. 2-27. Illustration of "resonance" response case in Layout 2, R/D = 0.9 and V_{RD}=35 m/s. 67

Fig. 2-28. Tower responses of Layout 1 at R/D = 0.9 (Cont.). 69

Fig. 2-29. Tower responses of Layout 2 at R/D = 0.8. 69

Fig. 2-30. Tower responses of Layout 3 at R/D = 0.8 and X/L = 1.25. 70

Fig. 2-31. Dynamic amplification factor DAF for the studied layouts. 73

Fig. 2-32. Load path. 76

Fig. 3-1. Guyed tower failure (Hydro One report, 2006) 85

Fig. 3-2. Downburst characteristic parameters 85

Fig. 3-3.Testing chamber 92

Fig. 3-4. Downburst formation snapshot at WindEEE 93

Fig. 3-5. Wind Field measurement using cobra probe devices 95

Fig. 3-6. Repeatability of the downburst wind field 95

Fig. 3-7. Evolution of downburst radial profiles at time = 4.84 seconds 95

Fig. 3-8. Instantaneous of radial wind profiles 96

Fig. 3-9. Schematic of the test layout 97

Fig. 3-10. 3-D view of the prototype tower 98

Fig. 3-11. Half-length of the assembled line 98

Fig. 3-12. Summary of downburst-structure orientations for the considered layouts 101

Fig. 3-13. Test layout 1 102

Fig. 3-14. Test layout 2 103

Fig. 3-15. Test layout 3 104

Fig. 3-16 Sample response of the middle tower subjected to downburst loads 106

Fig. 3-17. Layout 1 maximum peak responses of the tower B 107

Fig. 3-18. Layout 2 maximum peak responses of the tower B 108

Fig. 3-19. Layout 3 maximum peak responses of tower B 110

Fig. 3-20. Layout 3 maximum mean responses of tower B 111

Fig. 3-21. Base shear validation 114

Fig. 3-22. Base moment validation 114

Fig. 3-23. Free body diagram of the cross arm system under the oblique case 115

Fig. 3-24. conductor's model validation 115

Fig. 3-25. Guys tension validations 116

Fig. 3-26. center support force validation 116

Fig 3-27. Mid-height moment validation 116

Fig. 4-1. Downburst characteristic parameters. 130

Fig. 4-2. Radial velocity profile along the height. 131

Fig. 4-3. Vertical velocity profile along the height 131

Fig. 4-4. Time history of the radial velocity at a point in space 131

Fig. 4-5. Velocity distribution along multiple spans in the case of an oblique downburst. 135

Fig. 4-6. Variations of A_D with different downburst diamaters..... 136

Fig. 4-7. Location of downburst corresponding to conductor's maximum longitudinal force. 136

Fig. 4-8. Transvsre velocity distribution for the critical oblique load case (R/D=1.6 and Θ=30° and L/D_J=0.5). 137

Fig. 4-9. Distribution of transverse forces on the conductor due to the critical oblique downburst case. 140

Fig. 4-10. Variations of R_X with h. 143

Fig. 4-11. Variations of R_X with α. 143

Fig. 4-12. Variations of R_X with S_L. 143

Fig. 4-13. Variations of R_X with w. 143

Fig. 4-14. Flow chart of the interpolation process to obtain the conductor's longitudinal force under the critical oblique downburst load case..... 149

Fig. 4-15. Direction of the conductor forces R_X and R_Y..... 150

Fig. 5-1. Downburst characteristic parameters. 179

Fig. 5-2. Radial velocity profile along the height. 182

Fig. 5-3. Axial velocity profile along the height. 183

Fig. 5-4. Time history of the radial velocity at a point in space 183

Fig. 5-5 Transmission Line System (G_1) 188

Fig. 5-6 Transmission Line System (G_2) 188

Fig. 5-7. Transmission Line System (G_3) 189

Fig. 5-8. Transmission Line System (S_1)..... 189

Fig. 5-9. Transmission Line System (S_2)..... 189

Fig. 5-10. Transmission Line System (S_3)..... 189

Fig. 5-11. Conductor reactions under downburst wind field..... 194

Fig. 5-12. Radial velocity distribution along line spans at R/D_J=1.3 and Θ=0°..... 197

Fig. 5-13. Radial velocity distribution along tower height- Θ=90°..... 198

Fig. 5-14. Radial velocity distribution along tower height Θ=0°..... 199

Fig. 5-15. Radial velocity distribution over six conductor spans Θ=0° 200

Fig. 5-16. Downburst span reduction factor 200

Fig. 5-17. Radial velocity distribution along tower height at R/D_J=1.5 and L/D_J=0.5, and Θ=30°..... 202

Fig. 5-18. Radial velocity distribution over six conductor spans at R/D_J=1.5 and L/D_J=0.5, and Θ=30° 202

Fig. 5-19. Load cases validation..... 205

LIST OF SYMBOLS

Symbol	Description
λ_a	Acceleration scaling ratio.
A_1	Area under the squared transverse velocity curves for the conductor spans located on the right side
A_2	Area under the squared transverse velocity curves for the conductor spans located on the left side.
A_D	Difference between the squared values of A1 and A2 normalized by the length of three spans of the line: $A_D= (A_{12}-A_{22})/3L$.
a_m	Model acceleration.
a_p	Prototype acceleration.
B	Background component.
λ_{BM}	Bending and torsional moment scaling ratio.
C_D	Drag coefficient.
D	WINDEEE downburst diameter.
DAF	Dynamic amplification factor.
D_J	Downburst jet diameter.
D_{Jm}	Downburst size in the model-scale.
D_{JP}	Downburst size in the full-scale.
d_p	Single wire projected diameter perpendicular on the transvers direction of the downburst velocity.
EA	Conductor's axial stiffness factor.
λ_{EA}	Elastic stiffness scaling ratio.
λ_{EI}	Elastic stiffness scaling ratio.
F	Fluctuating component.
λ_f	Force per unit length scaling ratio.
λ_F	Force scaling ratio.
f_1	Conductor's fundamental frequency.

FC	Forces from critical loading cases.
$F_{Capacity}$	The member force capacity.
f_{cut}	Cut off frequency.
F_{DB}	Peak internal forces due to downburst loading.
F_m	Model force.
f_{mean}	Mean component of frequencies.
FP	Forces from parametric study.
F_p	Prototype force.
$f_{shedding}$	Shedding frequency.
h	Insulator length.
H	Physical height of jet.
λ_I	Mass moment of inertia per unit length scaling ratio.
λ_I	Mass moment of inertia scaling ratio.
I_{ur}	Turbulence intensity in radial direction.
L	Line span.
λ_L	Length scaling ratio.
L_m	Model length.
L_p	Prototype length.
m	Conductor’s mass.
λ_m	Mass per unit length scaling ratio.
λ_M	Mass scaling ratio.
M_{Ca}	Moment in cross arms.
M_{i1}	Moment at mid-height for the first leg.
M_{i2}	Moment at mid-height for the second leg.
M_{Xb}	Base moment in X direction.
M_{Yb}	Base moment in Y-direction.
Q_X	Base shear in X direction.
Q_y	Base shear in Y direction.
R	Distance between the downburst center to the structure of interest center.
R_X	Conductor's force in the longitudinal direction.

R_X (1-2)	Cable longitudinal force corresponds to the selected design group minimum weight, minimum insulator length, and the line's actual α.
R_X (3-4)	Cable longitudinal force corresponds to the selected design group maximum weight, minimum insulator length, and the line's actual α.
R_X (5-6)	Cable longitudinal force corresponds to the selected design group minimum weight, maximum insulator length, and the line's actual α.
R_X (7-8)	Cable longitudinal force corresponds to the selected design group maximum weight, maximum insulator length, and the line's actual α.
R_X (h max)	Cable longitudinal force corresponds to the selected design group maximum insulator length, the line actual α, and the line's actual w.
R_X (h min)	Cable longitudinal force corresponds to the selected design group minimum insulator length, the line's actual α, and the line's actual w.
R_X	Downburst critical longitudinal unbalanced force based on the proposed design charts corresponds to the actual insulator length.
R_{X1}	Cable longitudinal force under downburst critical case #3 corresponding to specific design group (w_{min}, h_{min}, α_{min}).
R_{X2}	Cable longitudinal force under downburst critical case #3 corresponding to specific design group (w_{min}, h_{min}, α_{max}).
R_{X3}	Cable longitudinal force under downburst critical case #3 corresponding to specific design group (w_{max}, h_{min}, α_{min}).
R_{X4}	Cable longitudinal force under downburst critical case #3 corresponding to specific design group (w_{max}, h_{min}, α_{max}).
R_{X5}	Cable longitudinal force under downburst critical case #3 corresponding to specific design group (w_{min}, h_{max}, α_{min}).
R_{X6}	Cable longitudinal force under downburst critical case #3 corresponding to specific design group (w_{min}, h_{max}, α_{max}).
R_{X7}	Cable longitudinal force under downburst critical case #3 corresponding to specific design group (w_{max}, h_{max}, α_{min}).
R_{X8}	Cable longitudinal force under downburst critical case #3 corresponding to specific design group (w_{max}, h_{max}, α_{max}).
R_Y	Conductor force in the transverse direction.
R_Z	Reaction at tower of interest in Z direction.
S	Percentage of the cable sag divided by line span.
S_t	Strouhal number.
T	Conductor’s tension.

λ_T	Time scaling ratio.
T_{Guy}	Tension in guys.
T_m	Model time period.
t_{max}	Time correspond
T_p	Prototype time period.
λ_v	Velocity scaling ratio.
V_{eqC}	Equivalent uniform velocity distribution for conductors.
V_{eqT}	Equivalent uniform velocity distribution for tower.
V_{eqTL}	Equivalent uniform velocity distribution for transmission line.
V_J	Downburst jet velocity.
V_{Jm}	Downburst jet velocity in the model-scale.
V_{JP}	Downburst jet velocity in the full-scale.
V_m	Model velocity.
V_p	Prototype velocity.
V_{RD}	The radial (horizontal) component of the downburst velocity.
V_{RDmax}	Peak radial velocity.
V_{TR}	A component of the radial velocity of the downburst that acts perpendicular to the conductor's direction.
V_{VR}	The vertical component of the downburst velocity.
w	Single wire weight per unit length.
X	Distance from jet center in X direction.
X-axis	The axis that passes along the line direction (longitudinal direction).
Y	Distance from jet center in Y direction.
Y-axis	The axis perpendicular to the line direction (transverse direction).
Z	Height from ground level.
α	The wind pressure ($0.5*\rho*VJ2 * dp$).
ΔT_L	The increase in the tension force of the conductors on the left hand side of the tower of interest due to the downburst loads.
Δt_m	Time step used in the CFD model.
Δt_p	Time step used in the full-scale analysis.

ΔTR	The increase in the tension force of the conductors on the right hand side of the tower of interest due to the downburst loads.
ζ	Aerodynamic damping.
Θ	Angle between the vertical plane of the transverse direction and the vertical plan connecting the downburst and the structure of interest centers.
λ_{ξ}	Damping scaling ratio.
ρ	Air density.
λ_{ρ}	Density scaling ratio.
σ_{urmax},	Root mean square of fluctuating component.

CHAPTER 1

INTRODUCTION

1.1 Background

Electricity is carried by Transmission Lines (TLs) from the source of generation to the distributing system. A transmission line system consists of support towers, conductors, insulators and ground wires. The conductors are responsible for transmitting the electricity and they are attached to the towers using the insulators. The ground wires protect the line from the lightning strike. Two main structural systems for the towers can be used; a) guyed towers and b) self-supported towers. **Fig. 1-1** shows an example of a guyed lattice transmission tower and the line components. The figure shows that the support system for this specific guyed tower consists of four guys and a hinge at the base. **Fig. 1-2** shows another example of self-supported lattice transmission line, where the tower is supported only at the base of its legs. Other tower systems include H-frame, steel, concrete and wood poles. The current study focuses on the steel lattice towers systems only.

A downburst is defined as an intensive downdraft air that induces very strong wind in all directions when striking the ground. Specifically, Fujita (1985) defined a downburst as a mass of cold and moist air that drops suddenly from the thunderstorm cloud base, impinges on the ground surface, and then horizontally diverges from the centre of impact. The ubiquity and full integration of electronics into modern life means that power outages due to TLs failure are unacceptable because of the associated social and economic losses. In many countries, past reports highlighted that the main cause of modern transmission line failures is the extreme High Intensity Wind (HIW) localized events in the form of downbursts and tornadoes. For instance, Hawes and Dempsey (1993) stated that 90% of

the transmission line failures in Australia were induced by downbursts. In southwestern Slovakia, Kanak et al. (2007) studied a downburst event that occurred in 2003 where at least 19 electricity transmission towers collapsed. In China, Zhang (2006) reported the failures of 18 towers belonging to 500 kV lines and 57 towers belonging to 110 kV lines due to strong wind events such as downbursts, tornadoes and typhoons. Most recently, in September 2016, 23 transmission towers failed during a series of downburst events in South Australia (Australian Wind Alliance, 2016). Also, several failures of transmission line system under downburst events have been reported in Canada such as the failure of 19 transmission towers located near Winnipeg, Manitoba reported by McCarthy and Melsness (1996), and the failure of two guyed towers belonging to Hydro One, Ontario (Failure report, 2006).

Despite the recurrence of the transmission line failures during downburst events, no detailed guidelines are available yet in the current standards to assist practitioners to adequately consider the effect of those extreme events in designing new towers or in the rehabilitation of existing ones. ASCE 74 (2010) states that downburst wind speed can be taken in accordance with the intensity defined for an F2 tornado. ASCE 74 (2010) suggest considering two or three spans to be affected by the downburst winds. No further details are provided in this guideline regarding downburst loading. For certain areas in Australia, AS/NZS:7000 (2010) suggests some modifications in the wind pressure equations in order to account for the downburst loads. These modifications include a topography factor, span reduction factor, and terrain-height factor. Again, the guidelines are not detailed enough and do not address many aspects of the downbursts including the effect of their localized nature.

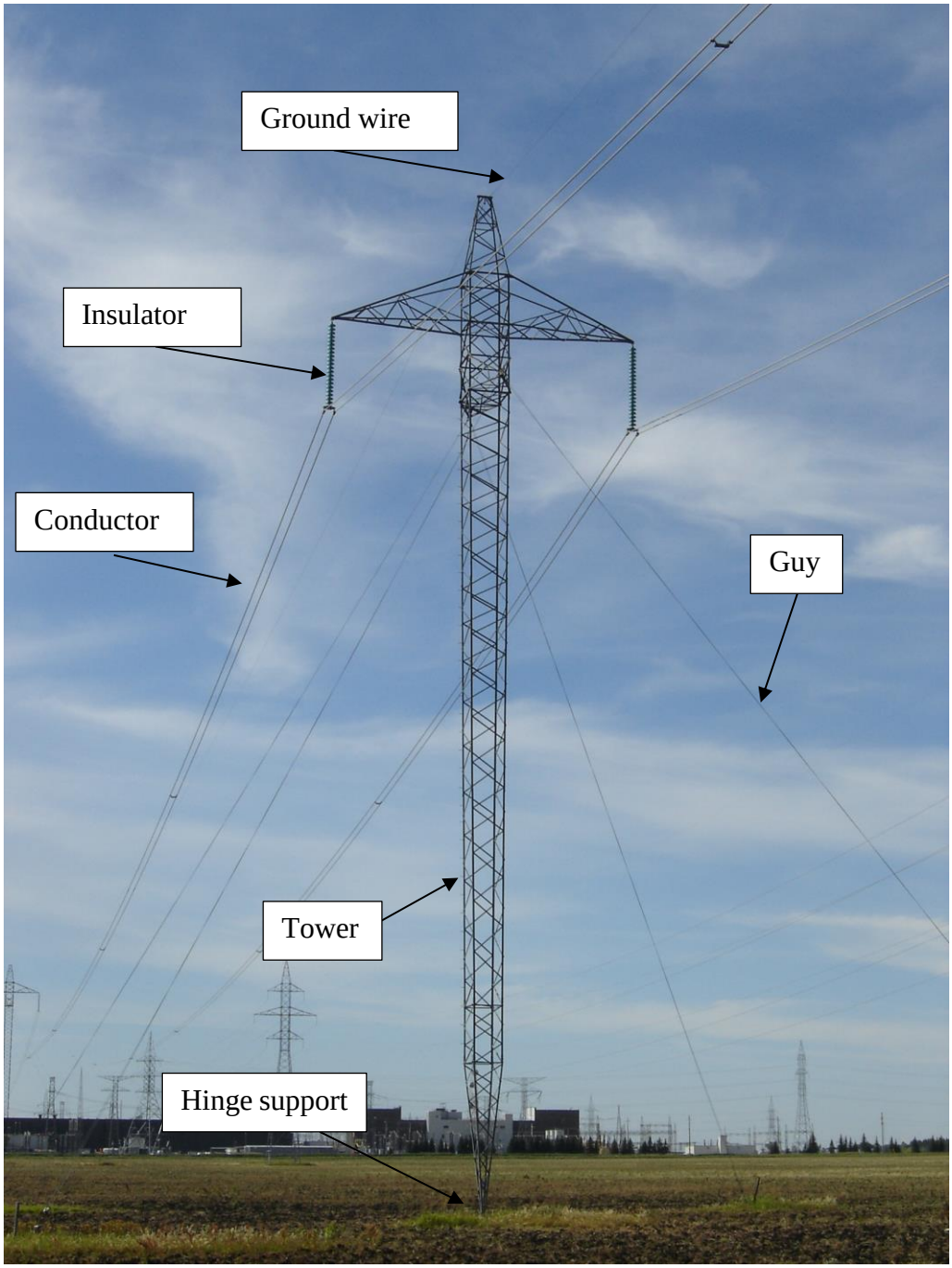

Fig. 1-1 Guyed transmission tower components (Source: Wikipedia: https://en.wikipedia.org/wiki/Transmission_tower).

Fig. 1-2 Lattice self-supported transmission line (Source: Wikipedia: https://en.wikipedia.org/wiki/Transmission_tower).

According to Hjelmfelt (1988), the diameter of a downburst, D_J, can vary between 500 m and 2 Km. The typical conductor's span of a transmission line system varies between 200 m and 500 m and sometimes it exceeds that. This means that the size of the downburst can be in the same order of magnitude as the conductor span. As a result, the loads experienced by the tower and the attached conductors would vary depending on the size and the location of the downburst relative to this specific tower. Depending on the location of the downburst, the loads on the conductors might not be uniform and might vary from conductor span to another. This feature characterizes the localized wind events such as downbursts and tornadoes and does not exist for large scale events such as hurricanes and typhoons. As a result, it is expected that a number of critical load profiles leading to peak internal forces in various members of a transmission tower might exist depending on the downburst location. Determining those critical loading profiles for a general steel lattice transmission tower is the ultimate goal of this study. In this chapter, a literature review pertaining to the problem of transmission line structures under downbursts is presented. The review focuses first on the downburst wind field where field measurement and numerical studies available in literature are presented. This is followed by coverage for the studies conducted on the structural response of transmission lines under downbursts. An extensive research program was conducted on this subject by the research group of the author's supervisor at The University of Western Ontario (UWO). The current Thesis builds on this research and expand it. As such, the progress of research conducted by the research group at UWO is presented in a separate section. The gaps existing in the literature are then presented in view of the outlined literature summary. This is followed by presenting the objectives and the scope of the Thesis.

1.2 Downburst Wind Field

1.2.1 Downburst Field Measurements

Because of their localized nature in both space and time, field measurements of downbursts are quite limited. Those include the measurements conducted by the Northern Illinois Meteorological Research (NIMROD) and the Joint Airport Weather Studies (JAWS), which were reported by Fujita (1990) and the FAA/Lincoln Laboratory Operational Weather Studies (FLOWS) measurement reported by Wolfson et al. (1985). Wilson et al. (1984) used the Doppler weather radar data from the JAWS project and reported the horizontal and vertical profiles of the microburst. Holmes and Oliver (2000), Savory et al. (2001), and Orwig and Schroeder (2007) indicated that the downburst wind speed recorded during the measured events ranged between 50 m/s to 70 m/s. Lombardo et al. (2014) analyzed the archived data obtained by Automated Surface Observing System ASOS to identify a number of downburst thunderstorms and compared them to synoptic wind events. The results showed that a shorter averaging times (15–60 s) can be used for downbursts compared to 10 min for synoptic winds. In addition, the study revealed that gust factors corresponding to those thunderstorm events differ from synoptic winds. Based on the field measurements at different ports in Europe such as in Genova, Savona, La Spezia, Livorno, and Bastia, De Gaetano et al. (2014) analyzed the set of data recorded using a semi-automated procedure to separate different downburst events. The authors stated that separating the synoptic and non-synoptic events is a hard task due to the presence of third-class events that has intermediate properties between the main two classifications of winds. Solari et al. (2015) reported the thunderstorms recorded through the ‘‘Wind and Ports” project. Using an in-situ wind monitoring network, they analyzed the main properties of a

number of thunderstorm records detected in the Ports of Genoa, La Spezia and Livorno during the period of 2011 to 2012. Solari et al (2015) reported the mean values and the coefficient of variation of three wind velocity ratios that are believed to have a significant effect on structures.

1.2.2 Experimental Studies for Downburst Wind Field

Different approaches were used to simulate the downburst wind field physically inside wind tunnel laboratories. Donaldson and Snedeker (1971) considered simulating a small-scale downburst using a jet flow issuing from a circular convergent nozzle and impinging on a wall. Using a similar set-up, Didden and Ho (1985) utilized a jet of a diameter of 0.0381 m and a wall positioned at a distance of 0.1524 m from the jet. This represented a height "H" to diameter "D_J" ratio, H/D_J, equal to 4.0. Similar experimental simulations were conducted and reported by Osegura and Bowles (1988), Lundgren et al. (1992), Alahyari and Longmire (1994), Yao and Lundgren (1996), Choi (2000), Wood et al. (2001) and Chay and Letchford (2002) where a jet was impinged normally onto a flat plate in the laminar boundary layer. The simulation of the wind field in Chay and Letchford (2002) study considered a 0.5 m jet diameter against a flat wall located at 0.85 m distance. This represented an H/D_J ratio of 1.7. The study did not represent the transient nature of the downburst. Simulating the downburst wind-like profile is another experimental approach that is specially used in structural applications to model the effect of the downburst winds on structures (Lin et al., 2012).

1.2.3 Numerical Studies for Downburst Field Characterization

Different studies attempted modelling the downburst wind field numerically using Computational Fluid Dynamics (CFD) simulations. The numerical studies found in the

literature simulated downbursts using one of the following techniques: a) Ring Vortex Model, b) Impinging Jet (Impulsive Jet) Model, and c) Cooling Source (Buoyancy-Driven) Model, which are illustrated in **Fig. 1-3**. The Ring Vortex Model (Zhu and Etkin, 1985; Ivan, 1986; Vicroy, 1992; Savory et al., 2001) simulates the vortex ring that is formed during the descent of the downdraft air column. Savory et al. (2001) reported that the Ring Vortex Model is not accurate in simulating the downburst field near the ground after the air column touches the ground. The Impinging Jet Model (suggested by Fujita, 1985 and used in Kim and Hangan, 2007, Sengupta and Sarkar, 2008, Aboshosha et al., 2015, Hadzˇiabdic´, 2005, Chay et al., 2006, Gant, 2009) is based on the analogy between an impulsive jet impinging upon a flat surface and a downburst. Mason et al. (2009) implemented the cooling source method based on a dry, non-hydrostatic, sub-cloud and axisymmetric model. One year later, Mason et al. (2010) extended this work to a three-dimensional model. In both studies, the Scale Adaptive Simulation (SAS) method developed by Menter and Egorov (2005) was used, which is an improvement for the unsteady Reynolds-Averaged Navier–Stokes (URANS) method employed to predict unsteady turbulent flow. However, Gant (2009) reported that the SAS method appears to be over-predicting the turbulent viscosity of jet-type flows. Vermeire et al. (2011) simulated the downburst using the cooling source approach with Large Eddy Simulation (LES) and the results showed a good agreement with those reported by Mason et al. (2009) and a disagreement with the impinging jet models.

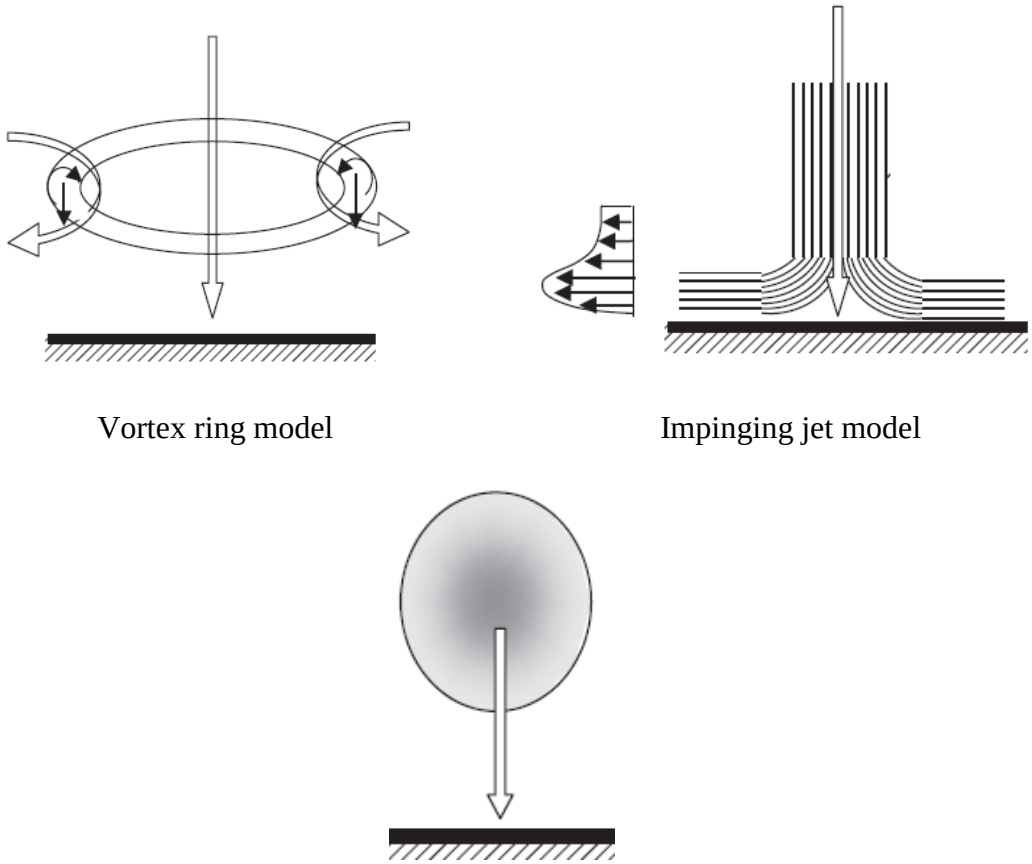

Fig. 1-3. Numerical modeling methods of downburst winds.

For both the experimental and the numerical studies, the dimensions of the wind field domain were reported to influence the characteristics of the resulting radial velocities of the downburst. Previous studies linked the dimensions of the wind field domain in terms of the height, H, and the downburst diameter, D_J to the ratio H/D_J reported from field measurements of real downburst events. Hjelmfelt (1988) reported that the physical ratio H/D_J varies between 1.2 and 6. The numerical simulations conducted by Kim and Hangan (2007), Vermeire et al. (2011), and Aboshosha et al. (2015) employed an H/D_J of 4.0, 4.0 and 2.0, respectively, to simulate the downburst wind field using the impinging jet method. Experimentally, Didden and Ho (1985) and Chay and Letchford (2002) used an H/D_J ratio

of 4.0 and 1.7, respectively. The comparison conducted by Kim and Hangan (2007) for the peak vertical profile of the radial velocity resulting from different simulations using different H/D_J ratios indicated that the peak profile of the radial velocity is independent from the ratio H/D_J.

1.3 Studies on TLs Response to Downbursts

Few number of studies focused on the response of transmission line systems subjected to downburst winds. Savory et al. (2001) studied the failure of transmission towers under both tornado and downburst wind loading. In their study, the conductor loads were neglected and, as a result, failures were only associated with the tornado loading while no failure was observed with the downburst loading. This is because downbursts are larger in size and are expected to load a larger portion of the conductors compared to tornadoes. Mara and Hong (2013) studied the inelastic response of a transmission tower subjected to both a downburst and a synoptic wind field. The study showed a dependency of the tower capacity on the wind direction for both wind fields. Wang et al. (2009) studied the dynamic effect of a downburst on tall transmission towers. The study showed that the size of the downburst has a negligible effect on the dynamic response of the tower. However, the size of the downburst event affected the displacement response of the tower. Yang and Zhang (2016) analyzed two transmission towers under both normal and downburst winds. In their study, the resultant of the conductor's forces was calculated and applied on the tower at the insulator-conductor's connection. All of the above studies did not account for the spatial variation of the downburst wind field.

Other studies assessed the dynamic response of the components of transmission line systems subjected to wind loads in general. Loredo-Souza and Davenport (2001) assessed

the dynamic response of TL conductors subjected to synoptic wind using horizontally distorted conductors to indirectly accommodate the large length of the span into the wind tunnel lab. The study showed that the response of the conductors was mainly background response. In a number of cases, the study showed that the resonance contribution may increase depending on the aerodynamic damping of the conductors. This agreed with the findings reported by Battista et al. (2003) and Gani and Legeron (2010) who emphasized on the importance of considering the dynamic effects of the conductors. Lin et al. (2012) tested a single span aero-elastic model of a guyed lattice tower under both the synoptic and the downburst winds at a conventional boundary layer wind tunnel lab. In their study, a number of 57 downburst-like profiles were simulated. The study showed that the resonance component of the conductor reactions can be as high as the background. It is clear that no clear definite conclusion about the contribution of the resonant component in the response of transmission line structures to wind loads in general and downbursts in particular can be found in the literature.

1.4 Research Conducted at UWO On the Effect of Downbursts on TLs

The research at UWO was initially funded by Manitoba Hydro, Manitoba, Canada, and then by Hydro One, Ontario, in order to investigate the reasons behind the chain of TLs failures that occurred in those two Canadian provinces. Shehata et al. (2005) developed a finite element model that simulates the tower members and the guys using two-nodded linear three-dimensional frame element with three translational and three rotational degrees of freedom per node. Each tower member was simulated using one element while each guy was modeled using five elements. Rigid connections were assumed between the tower members as these are physically connected using multi-bolted connections that can transfer

moments. In their study, Shehata et al. (2005) considered a number of six spans per line where the conductors were simulated using 2-D non-linear consistent beam element developed by Koziey and Mirza (1994) and modified later by Gerges and El Damatty (2002) to include the effect of geometric nonlinearity. The model accounted for the conductor's pretension force, the conductor's sag, and the insulator stiffness. In their model, Shehata et al. (2005) developed a procedure to scale up the model-scale impinging jet wind field data provided by Hangan et al. (2003) and validated later by Kim and Hangan (2007). Using the structural analysis model developed by Shehata et al. (2005), Shehata and El Damatty (2007) conducted a parametric study to investigate the critical downburst configurations by varying the downburst jet diameter (D_J) and the location of the downburst center relative to the tower (R). The study considered only the mean component of the downburst wind field. Shehata et al. (2005) reported that the effective period of the mean component of the downburst wind speed ranges between 20 and 22 s while the vibration frequencies for the transmission tower and the conductors were about 0.58 s and 8.25 s, respectively. This means that no strong dynamic effect for the tower would be expected. The downburst parameters, in terms of the size of the event and its location relative to the tower, leading to maximum forces in the tower members, were identified. The study revealed that the critical downburst parameters vary based on the type and location of the members. Unsurprisingly, the chord members, diagonal members and cross arm members had different critical downburst configurations. Shehata and El Damatty (2008) extended their numerical scheme by including a failure model for the tower members, which was used to study the progressive collapse of the tower failure. An optimization routine was implemented by Shehata et al. (2008) to predict the critical

downburst parameters and the corresponding forces on a transmission line through an automated procedure. A similar parametric study conducted by Darwish and El Damatty (2011) focused on assessing the response of a self-supported tower. Shehata and El Damatty (2007) predicted different failure modes for transmission towers subjected to downburst winds. One of the critical failure modes, that was also reported by and Darwish and El Damatty (2011), was found to be due to the significant variation in the longitudinal tensile forces developing in the conductors adjacent to the tower of interest from both sides. Shehata et al. (2005) revealed that a longitudinal force transmitting to the tower cross arms leads to an out-of-plane bending moment in this region. The studies conducted by Shehata and El Damatty (2007, 2008) and Darwish and El Damatty (2011) agreed that changing the location of the downburst has a strong effect on the value of the internal forces developing in tower members.

Later, Ladubec et al. (2012) improved upon the linear analysis conducted by Shehata and El Damatty (2008) by including the P–Δ effect in the tower's using nonlinear space frame elements to simulate the tower members. The study showed an increase of 20% in the peak axial forces in the chord members of the main legs, as compared to the results from a linear analysis.

The inclusion of the turbulent component in the structural analysis might magnify the response due to the combined effects of the fluctuating (background) component and the resonant component. Darwish et al. (2010) extracted the turbulence from the field measurements of a downburst conducted by Holmes et al. (2008). They used this turbulence measurement to study the dynamic response of the conductors. The study found that there is almost no variation in the dynamic characteristics of the conductors under the

different loading configurations. Also, the study reported that the resonant component is negligible due to the large aerodynamic damping of the conductors. This might be attributed with the assumption made in this study regarding the spatial variation of the turbulence field. Darwish et al. (2010) utilized the turbulence measured at a single point in space and assumed that this measurement is the same along six spans of the conductors; i.e., assumed full correlation. In addition, Darwish et al. (2010) employed Davenport (1962) expression to calculate the aerodynamic damping of the conductors. This expression was developed for the case of synoptic winds which does not account for the effect of the spatial localization of the downbursts. Hamada (2014) assessed the dynamic response of an aero-elastic model of a transmission line subjected to normal winds. The study reported a high resonant response of the conductors at low wind speeds as a result of the low aerodynamic damping of the conductors at those speeds.

The high flexibility and the expected nonlinear behavior of the conductors result in significant computational time when finite element modeling is used to predict the response of conductors under downburst loading. This is because a large number of analyses in order to consider potential size and location of the downburst in estimating the peak structural response. Aboshosha and El Damatty (2014-a) developed a semi-analytical technique to analyze multi-spanned conductors under HIW. This technique represents the first semi-closed form solution for a multi-spanned conductor system under non-uniform loading taking into account the insulator flexibility. The technique was reported to be approximately 185 times faster than finite element analysis.

Aboshosha et al. (2015) simulated the downburst wind field using both the impinging jet model and the Large Eddy technique. In their approach, they considered various terrain

exposures using the fractal surface method. Using the turbulent wind field developed by Aboshosha et al. (2015), Aboshosha and El Damatty (2015) studied the dynamic and the quasi-static responses of a single span and multi spanned transmission line conductors under both the synoptic and the downburst loads. For multi-spanned lines, the study showed that the contribution of the resonant component is in order of 6% of the peak reactions assuming different wind intensities. However, for single span conductor, the contribution of the resonant component to the peak responses was higher (in order of 16%) at low speeds. Aboshosha and El Damatty (2014-b) simulations evaluated the span reduction factor of the downburst radial velocities along the longitudinal direction. The study reported that the span reduction factor of the downburst wind field varies between 1 and 0.85. This results agreed with the findings reported by Holmes et al. (2008).

1.5 Research Gaps

Although different components of the numerical model developed by the UWO team were validated individually, no experimental validation was done for the entire model under simulated downbursts. Also, no experimental study under simulated downbursts was conducted to quantify the dynamic effect resulting from the turbulence component of the downburst for both the tower and the conductors. The recent establishment of the WindEEE dome provides a unique opportunity for simulating large-scale downbursts. WindEEE is a one-of-a-kind three-dimensional wind testing chamber with a hexagonal shape of 25 m in diameter. The facility allows simulating different terrain exposures using automated roughness elements mounted on the ground floor of the testing chamber. The bell mouth-opening diameter (D) is 3.2 m while the height of the testing chamber (H) is 3.8 m. This allows reproducing a downburst wind field with an H/D ratio of 1.2. It allows

also testing of relatively large scale aero-elastic model under simulated downbursts. Such a test can be used to conduct the needed studies mentioned above involving quantifying the dynamic effect and validating the numerical models. The research conducted at the UWO on the effect of downbursts on transmission line structures should lead at the end to the development of velocity profiles and load cases that can simulate the critical effect of downbursts on lattice transmission line structures. Those load cases need to be simple enough, not requiring complicated non-linear analyses, so they can be easily applied by practitioners.

1.6 Scope of the Current Study

The thesis aims to address the gaps mentioned in the above section. As such, the objectives of the thesis are:

1. Assess experimentally the dynamic response of lattice transmission lines and their attached conductors to the downburst induced loads.
2. Assess the effect of downburst spatial variation on the response of transmission lines.
3. Validate experimentally previously developed numerical models used predict the response of transmission line structures to downbursts.
4. Identify the critical downburst load cases that can be used to design generic tangent transmission lines to resist downburst winds.
5. Develop a simple approach that can be used to predict the conductor forces transmitted from the conductors to the towers as a resulting of a downburst oblique load case.

1.7 Organization of The Thesis

This thesis has been prepared in an "Integrated-Article" format. In Chapter 1, a review of the studies and approaches related to downburst wind field and the transmission line response under downbursts is provided. This is followed by achieving the main objectives of the study. These objectives are addressed in detail in the following four chapters.

1.7.1. Aero-elastic Testing of Multi-Spanned Transmission Line Subjected to Downbursts

In this chapter, an aero-elastic multi-spanned TL is designed and tested at the WindEEE dome in order to assess the dynamic response of a multi-spanned transmission line due to the downburst-induced loads. The chapter starts by characterizing the downburst wind field measured at WindEEE using cobra probes devices. The study then provides a detailed information of the design of the aero-elastic tower and the attached conductors. A number of test configurations are selected based on the findings of previous numerical studies. Those configurations cause the peak internal forces in the tower members due to the downburst loads. The study proposes a decomposition approach to extract the resonance and the background components from the measured fluctuating responses of the tower and the conductors. The study shows the Dynamic Amplification Factor (DAF) for different structural responses of the tower and the conductors subjected to downburst wind loads.

1.7.2. Aero-Elastic Response of Transmission Line System Subjected to Downburst Wind: Validation of Numerical Model Using Experimental Data

In this chapter, the results of the test described in chapter 1 is used to validate the built in-house numerical models developed by Shehata et al. (2005) and Aboshosha and El Damatty (2014-a). These numerical models are used later in this research to conduct the numerical

studies described in chapter 4 and 5. The chapter starts by characterizing the downburst wind field measured at WindEEE. The study then gives a summary about the aero-elastic model and the test layouts used. The results of the test are then used to assess the effect of the spatial variations of the downburst with respect to the tower of interest. A number of selected test cases are utilized to validate the above mentioned numerical models. The validation process considers the external force calculations, shielding and drag effect, forces distribution, and internal force calculations.

1.7.3. Critical Load Cases for Lattice Transmission Line Structures Subjected to Downbursts: Economic Implications for Design of Transmission Lines

This chapter is triggered by the fact that codes of practice and guidelines provide very limited information regarding the critical load profiles associated with the downbursts and acting on the towers and conductors of a transmission line system. The complexity of finding this critical load profiles results from the localized nature of such events which depends not only on the magnitude of the event but also on its size and its location relative to the center of the tower. In this chapter, an extensive parametric study is conducted on a number of real lattice transmission line systems, to evaluate their critical response to downburst loads. The study considers the variation in the downburst location, the angle of attack, and the size to understand the effect of changing these parameters on the response of the transmission line system. At the end of study, a number of critical load cases are identified for possible implantation in the design codes. The study then assesses the economic implication of applying the proposed load cases using the increase of the weight of the structure as a measure for the increase of cost.

1.7.4. Longitudinal Force on Transmission Towers due to Non-Symmetric Downburst Conductor Loads

The objective of this chapter is to develop a simple procedure that can be used by practitioners to estimate the maximum longitudinal force developing in TL conductors subjected to downburst. This longitudinal force develops when the downburst winds are acting on the line with an oblique angle. The oblique configuration of the downburst loads leads to an uneven and unequal distribution of the wind forces along the conductor spans located at opposite sides of the tower of interest. This results in a difference between the tension forces developing in the right and the left hand sides spans adjacent to the tower of interest. This difference in tension forces will lead to a net longitudinal force acting on the cross arm of the tower. The regular estimation of this force requires conducting a nonlinear iterative analyses of the conductors under the variable loading conditions of the downburst, while taking into account a number of key parameters including the flexibility of the insulators and the conductor's pretension force. This force is believed to be the reason for the failure of a number of towers during downbursts.

1.7.5. Summary and Conclusions

This chapter presents summary and conclusions of the entire thesis together with recommendations for further research work.

1.8 References

Aboshosha, H., and El Damatty, A., (2014-a), "Effective technique for the reactions of transmission line conductors under high intensity winds", Wind and Structures. 18(3), 235-252.

Aboshosha H., El Damatty, A., (2015). "Dynamic effect for transmission line conductors under downburst and synoptic winds", Wind Struct Int J 2015;21(2):241–72.

Aboshosha, H., Bitsuamlak, G., El Damatty A., (2015), "Turbulence characterization of downbursts using LES", Journal of Wind Engineering and Industrial Aerodynamics. 136, 44–61.

Aboshosha, H., El Damatty, A., (2014-b), "Span Reduction Factor of Transmission Line Conductors under Downburst Winds", Journal of Wind and Engineering 11(1), 13-22.

American Society of Civil Engineers (ASCE), (2010) "Guidelines for electrical transmission line structural loading", ASCE manuals and reports on engineering practice, No. 74, New York, NY, USA.

Alahyari, A., Longmire, E., (1994), "Particle image velocimetry in a variable density flow: application to a dynamically evolving downburst", Experiments in Fluids 17, 434–440.

Australian Standard/New Zealand Standard (AS/NZS) 7000, (2010) "Overhead line design detailed procedures", Standards Australia Limited/Standards New Zealand, North Sydney, Australia.

Australian Wind Alliance, (2016): http://www.windalliance.org.au/

Battista, R., Rodrigues, R., Pfeil M., (2003), "Dynamic behavior and stability of transmission line towers under wind forces", J Wind Eng Ind Aerodyn, 91:1051–67.

Chay, M., Albermani, F. and Wilson, R., (2006), "Numerical and analytical simulation of downburst wind loads", Engineering Structures 28(2), 240-254.

Chay, M., Letchford, C., (2002), "Pressure distributions on a cube in a simulated thunderstorm downburst - part a: stationary downburst observations", Journal of Wind Engineering and Industrial Aerodynamics 90, 711–732.

Choi, ECC., (2000), "Wind characteristics of tropical thunderstorms", Journal of Wind Engineering and Industrial Aerodynamics 84, 215–26.

Darwish, M., El Damatty A., and Hangan, H., (2010), "Dynamic characteristics of transmission line conductors and behaviour under turbulent downburst loading", Wind and Structures 13(4), 327-346.

Darwish, M., and El Damatty, A., (2011), "Behavior of self-supported transmission line towers under stationary downburst loading", Wind and Structures 14(5), 481-4.

Davenport, A.G., (1962), "Buffeting of a suspension bridge by storm winds", J. Struct. Div. - ASCE, 88(3), 233-264.

De Gaetano, P., Repetto, MP., Repetto, T., Solari, G., (2014), "Separation and classification of extreme wind events from anemometric records", J Wind Eng Ind Aerodyn;126:132–43.

Didden, N., and Ho, C., (1985), "Unsteady separation in a boundary layer produced by an impinging jet", Journal of Fluid Mechanics 160, 235–256.

Donaldson, C., and Snedeker, R., (1971), "A study of free jet impingement, Part 1. Mean properties of free and impinging jets", Journal of Fluid Mechanics 45, 281–319.

Failure Investigation Report, HYDRO ONE NETWORKS INC. "Failure of towers 610 and 611, circuit X503E – 500 kV guyed towers near the Township of Waubaushene", Ontario, August 2, 2006", Line Engineering, 2006.

Fujita, T., (1985), ''The downburst: microburst and macroburst", SMRP research paper 210. University of Chicago, USA.

Fujita, T., (1990), "Downbursts: meteorological features and wind field characteristics", Journal of Wind Engineering and Industrial Aerodynamics 36, 75–86.

Gani, F., and Legeron, F., (2010), "Dynamic response of transmission lines guyed towers under wind loading", Can. J. Civ. Eng., 37(3), 450-465.

Gant, S., (2009), "Reliability issues of LES-related approaches in an industrial context", Flow, Turbulence and Combustion 84, 325-335.

Gerges, R., and El-Damatty, A., (2002), "Large displacement analysis of curved beams", Proceedings of the Canadian Society of Civil Engineering Conference, Montreal, Canada, ST 100.

Hadzˇiabdic´, M., (2005), "LES, RANS and Combined Simulation of Impinging Flows and Heat Transfer", Ph.D. thesis, University of Sarajevo, 185.

Hamada, A., (2014), "Numerical and experimental studies of transmission lines subjected to tornadoes", Ph.D. thesis, The University of Western Ontario.

Hangan, H., Roberts, D., Xu, Z., and Kim, J., (2003), "Downburst simulation. Experimental and numerical challenges", Proceedings of the 11th International Conference on Wind Engineering, Lubbock, TX, USA.

Hawes, H., Dempsey, D., (1993), "Review of recent Australian transmission line failures due to high intensity winds". Proceedings of the Task Force of High Intensity Winds on Transmission Lines, Buenos Aires.

Hjelmfelt, M., (1988), “Structure and life cycle of microburst outflows observed in Colorado”, Journal of Applied Meteorology 27, 900–927.

Holmes, J., and Oliver, S., (2000), "An emperical model of a downburst", Engineering Structures 22, 1167-1172.

Holmes, J., (2008), “Recent developments in the specification of wind loads on transmission lines”, Journal of Wind and Engineering 5(1), 8-18.

Ivan, M., (1986), “A ring-vortex downburst model for flight simulations” Journal of Aircraft 23, 232-236.

Kanak, J., Benko, M., Simon, A. and Sokol, A. (2007), "Case study of the 9 May 2003 windstorm in southwestern Slovakia", Atmos. Res., 83, 162-175.

Kim, J. and Hangan, H., (2007), “Numerical simulations of impinging jets with application to downbursts”, Journal of Wind Engineering and Industrial Aerodynamics 95(4), 279-298.

Koziey, B., and Mirza, F., (1994), “Consistent curved beam element”, Computers and Structures 51(6), 643–654.

Ladubec, C., El Damatty, A., and El Ansary, A., (2012), “Effect of geometric nonlinear behaviour of a guyed transmission tower under downburst loading”, Proceedings of the International Conference on Vibration, Structural Engineering and Measurement, Shanghai, China, Trans. Tech. Publications, 1240-1249.

Lin, W., Savory, E., McIntyre, R., Vandelaar, C., and King, J., (2012), “The response of an overhead electrical power transmission line to two types of wind forcing”, Journal of Wind Engineering and Industrial Aerodynamics 100(1), 58-69.

Lombardo F., Smith D., Schroeder J., Mehta K., (2014), “Thunderstorm characteristics of importance to wind engineering”, Journal of Wind Engineering and Industrial Aerodynamics 125, 121–32.

Loredo-Souza, A., and Davenport, A., (2001), “A novel approach for wind tunnel modelling of transmission lines”, Journal of Wind Engineering and Industrial Aerodynamics 89, 1017–1029.

Lundgren, T., Yao, J., and Mansour, N., (1992), “Microburst modelling and scaling”, Journal of Fluids Mechanics 239, 461–488.

Mara, T., and Hong H., (2013), "Effect of wind direction on the response and capacity surface of a transmission tower", Engineering Structures 57, 493–501.

Mason, M., Fletcher, D., and Wood, G., (2010), "Numerical simulation of idealized three-dimensional downburst wind fields", Engineering Structures 32(11), 3558-3570.

Mason, M., Wood, G., Fletcher, D., (2009), "Numerical simulation of downburst winds", Journal of Wind Engineering and Industrial Aerodynamics 97(11-12), 523-539.

McCarthy, P., Melsness, M., (1996) "Severe weather elements associated with September 5, 1996 hydro tower failures near Grosse Isle". Manitoba, Canada. Environment Canada, Winnipeg, Canada.

Menter, F., Egorov, Y., (2005), "A scale adaptive simulation model using two- equation models". Proceedings of 43rd AIAA Aerospace Sciences Meeting and Exhibit, American Institute of Aeronautics and Astronautics.

Orwig K., Schroeder, J., (2007), "Near-surface wind characteristics of extreme thunderstorm outflows", Journal of Wind Engineering and Industrial Aerodynamics 95, 565–84.

Oseguera R., and Bowles R., (1988) "A simple, analytics 3-dimensional downburst model based on boundary layer stagnation flow" NASATM- 100632. Hampton (VA): NASA Langley Research Center.

Savory, E., Parke, G., Zeinoddini, M., Toy, N., and Disney, P., (2001), "Modelling of tornado and microburst-induced wind loading and failure of a lattice transmission tower", Engineering Structures 23(4), 365-375.

Sengupta, A., Sarkar, P., (2008) "Experimental measurement and numerical simulation of an impinging jet with application to thunderstorm microburst winds", Journal of Wind Engineering and Industrial Aerodynamics 96, 345–365.

Shehata, A., Nassef, A., and El Damatty, A., (2008), "A coupled finite element-optimization technique to determine critical microburst parameters for transmission towers", Finite Elements in Analysis and Design 45(1), 1-12.

Shehata, A., and El Damatty, A., (2007), "Behaviour of guyed transmission line structures under downburst wind loading", Wind and Structures 10(3), 249-268.

Shehata, A. and El Damatty, A., (2008), "Failure analysis of a transmission tower during a microburst", Wind and Structures 11(3), 193-208.

Shehata, A., El Damatty, A., and Savory, E., (2005), "Finite element modeling of transmission line under downburst wind loading", Finite Elements in Analysis and Design 42(1), 71-89.

Solari, G., De Gaetano, P., Repetto, M., (2015) "Thunderstorm response spectrum: fundamentals and case study", Journal of Wind Engineering and Industrial Aerodynamics 143, 62-77.

Vermeire, B., Orf, L., Savory, E., (2011), "Improved modelling of downburst outflows for wind engineering applications using a cooling source approach", Journal of Wind Engineering and Industrial Aerodynamics 99, 801–814.

Vicroy, D., (1992), "Assessment of microburst models for downdraft estimation", Journal of Aircraft 29, 1043-1048.

Wang, X., Lou, W., Li, H., and Chen, Y., (2009), "Wind-induced dynamic response of high-rise transmission tower under downburst wind load", Journal of Zhejiang University 43(8), 1520-1525.

Wilson, J., Roberts R., Kessinger, C., McCarthy, J., (1984), "Microburst wind structures and evaluation of Doppler radar for airport wind shear detection", Journal of Climate Applied Meteorology 23, 898–915.

Wolfson, M., DiStefano, J., Fujita, T., (1985), "Low-altitude wind shear characteristics in the Memphis, TN area", Proceedings of the 14th conference on severe local storms, American Meteorological Society, Indianapolis, IN, USA., 322–7.

Wood, G., Kwok, K., Motteram, N., and Fletcher, D., (2001), "Physical and numerical modelling of thunderstorm downbursts", Journal of Wind Engineering and Industrial Aerodynamics 89, 535-552.

Fengli, Yang., and Hongjie, Zhang., (2016), "Two case studies on structural analysis of transmission towers under downburst", Vol. 22, No. 6, 685-701.

Yao, J., Lundgren, T.S., (1996), "Experimental investigation of microbursts", Experiments in Fluids 21, 17–25.

Zhang, Y., (2006), "Status quo of wind hazard prevention for transmission lines and countermea sures", East China Electric Power, 34(3), 28-31

Zhu, S., and Etkin, B., (1985), "Model of the wind field in a downburst", Journal of Aircraft 22, 595-601.

CHAPTER 2

AERO-ELASTIC TESTING OF MULTI-SPANNED TRANSMISSION LINE SUBJECTED TO DOWNBURSTS

2.1. Introduction

Downbursts together with tornadoes are commonly referred to as high intensity wind (HIW) events. In particular, downbursts, which contain masses of convective downdraft air, are usually associated with thunderstorms. Fujita (1985) defined a downburst as a severe descending mass of cold air that impinges on the ground and then transfers horizontally. Different design guidelines such as those of CIGRE (2009) and AS/NZS 7000 (2010) have highlighted the fact that HIW events are of the main cause of transmission line failures in various countries. In Canada, many transmission line failures occurred in the past two decades during HIW events. For example, a chain of transmission towers belonging to the Manitoba Hydro Company failed near Winnipeg during a series of downburst events (McCarthy and Melsness, 1996). Other incidents include the collapse of two 500 kV single circuit guyed towers that failed during a severe thunderstorm in August 2006, and belonged to Hydro One, Ontario, Canada (Hydro One failure report, 2006). The inspection of the line's debris indicated that the anchors and the guy assemblies, were all in a good condition with no failures in the conductors or the insulators. This localized failure, where only two towers failed in different lines passing through the same area, was an indication of an HIW event. This was confirmed by a meteorological analysis, which revealed that a high intensity microburst with wind speeds of approximately 50 m/s caused that particular failure. A picture from the site of one of the failed towers is provided in **Fig. 2-1.** Similar transmission line failures have been

widely reported in other parts of the world due to HIW events. For example, in China, Zhang (2006) reported the failure of 18 (500 kV) and 57 (110 kV) transmission line structures in 2005 under HIWs. Most recently, in September 2016, 23 transmission towers failed during a series of downburst events in South Australia (Australian Wind Alliance, 2016).

Standards and guidelines for designing transmission lines provide detailed information about the loading effect of synoptic winds. However, current codes and standards lack the critical loading information and the necessary guidelines regarding the impact of downburst winds. This lack of information initiated the undertaking of several numerical and experimental studies at The University of Western Ontario, Canada, to investigate the behaviour of transmission line structures when subjected to downburst events. The results of these studies, such as those conducted by Shehata and El Damatty (2005), and Darwish and El Damatty (2011), indicated that the main challenge in analyzing the response of a transmission line under downburst loads is the localized nature of the event. Shehata and El Damatty (2007) showed that the spatial configurations of a downburst (illustrated in **Fig. 2-2**) expressed in terms of the distance between the respective centers of the downburst and the tower "R", the downburst diameter "D", and the angle of attack "Ɵ" have a significant effect on the wind profiles acting on both the tower and its attached conductors. In addition, Shehata and El Damatty (2007) emphasized the dependency of the forces developing in the conductors on the ratio between the line span (L) and the downburst diameter (L/D ratio). The existence of many parameters that define the downburst loading acting on a transmission line system necessitates the consideration of many analysis cases in order to evaluate the peak internal forces of the tower members

resulting from the downburst loads. In addition, the transient characteristics of the downburst's mean velocity further complicates the problem as the mean wind speed changes with time.

Fig. 2-1. Guyed tower failure in Ontario, (Hydro One Report, 2006).

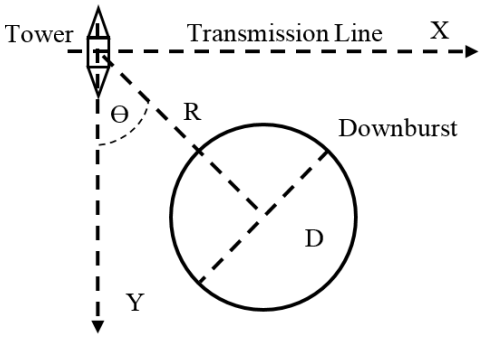

Fig. 2-2. Downburst characteristic parameters.

The localized nature of downbursts both in time and space is the main difficulty that encounters field measurements of those events. Fujita (1985) reported the results of downburst measurements through Northern Illinois Meteorological Research (NIMROD) and the Joint Airport Weather Studies (JAWS) where a characterization of the event size and intensity was attempted. A similar study was conducted by Hjelmfelt (1988) where a summary of the statistics of downbursts measured in Colorado was provided. Later, different field measurement studies such as by Choi and Hidayat (2002), Holmes et al. (2008), and Solari et al. (2015) discussed various decomposition approaches to extract the mean component of the thunderstorm winds. Solari et al. (2015) estimated the possible values of the turbulence intensity of downbursts using the data recorded for more than 90 downburst events as part of the "Wind and Ports" project.

Numerical modeling is an alternative mean to simulate the downburst non-stationarity nature. Different numerical simulation methods have been reported in the literature such as the Impinging Jet and the Cooling Source techniques. Kim and Hangan (2007) utilized the Impinging Jet approach to produce a time and space dependent downburst wind field based on the Reynolds Averaged Navier–Stokes (RANS) method. Using a Large Eddy Simulation (LES), Aboshohsa et al. (2015) characterized the downburst field under four different exposures based on an Impinging Jet model. Vermeire et al. (2011) conducted a comparison study between the Cooling Source and the Impinging Jet approaches using LES. The study showed that the cooling source and the impinging jet profiles produced serious discrepancies at high elevations.

Other attempts included experimental investigations of the downburst wind field such as the studies conducted by Donaldson and Snedeker (1971), Didden and Ho (1985) and Chay and Letchford (2002) in which downbursts were simulated using an axisymmetric jet impinging on a flat wall. Didden and Ho (1985)'s experiment utilized a jet of a diameter of 3.81 cm and a wall positioned at a distance of 15.24 cm from the jet. Simulating the flow of a reduced-scale downburst of 0.5 m jet diameter against a flat wall located at 0.85 m distance, Chay and Letchford (2002) reported that the maximum wind speed was found at a distance equal to the jet diameter. The study emphasized that the quasi-static simulation was limited in its ability to represent the transient features of the downburst. Other studies considered simulating downburst-like profiles in conventional boundary layer laboratory. For instance, Lin et al. (2012) simulated the downburst radial velocity profile by adjusting the ratios between the radial velocities along the height of the testing chamber to desired values. The establishment of the WindEEE dome; a unique

wind testing chamber capable of simulating hurricanes, tornados and downbursts at large scales, provides an opportunity to understand the characteristics of downbursts and to test aero-elastic models of structures under such events.

Special precautions should be taken with respect to the dimensions of a domain of a wind field in downburst wind simulations in both numerical and experimental studies. The diameter of a real downburst ranges between 600 m and 1700 m while the cloud height ranges from ~ 2000 m to 3500 m (Hjelmfelt, 1988). Therefore, the physical height to diameter (H/D) ratio ranges between 1.2 and 6. Numerical and experimental studies in the literature utilized different H/D ratios to simulate the downburst wind field. For instance, Didden and Ho (1985) and Chay and Letchford (2002) used an H/D ratio of 4.0 and 1.7, respectively, to experimentally simulate a downburst wind. Kim and Hangan (2007) and Aboshosha et al. (2015) numerically simulated a downburst using an H/D value of 4.0 and 2.0, respectively, using the impinging jet method. On the other hand, Vermeire et al. (2011) utilized the cooling source method assuming an H/D of 4.0. The agreement found between those studies regarding the vertical profiles of the downburst radial velocity produced using different H/D ratios indicated that the radial velocity profile is independent from the H/D ratio. However, the ratio H/D should be sufficient to permit the formation of the main vortex rings as recommended by Kim and Hangan (2007).

Many studies examined the dynamic response of the components of transmission line systems to synoptic winds. For example, the experimental studies conducted by Loredo-Souza and Davenport (2001) showed that the response of the tested conductors was all background at the design velocity level for the case of synoptic winds. However, limited

number of studies considered the dynamic response of the entire transmission line system under downdraft winds. The comparison between the frequency of the mean component of a downburst and the natural frequencies of the structure is an important factor in the examination of the dynamic response of the structure. Lin et al. (2012) experimentally assessed the dynamic response of a 1:100 single span conductors under synoptic and downburst-like winds. Lin et al. (2012) estimated the average resonance contribution to the cross arm out-of-plane moment to be as high as 45% of the fluctuating component. This was based on calculating the resonance and fluctuating areas of the power spectral density curve for the cross arm moment. However, their study did not provide a comprehensive explanation for the decomposition method for downburst-induced responses. Numerically, Darwish et al. (2010) modified the conductor model developed by Shehata et al. (2005) to study the dynamic response of the transmission line conductors under downburst winds. Darwish et al. (2010) extracted the turbulence component from the full-scale data reported by Holmes et al. (2008) and then added the turbulence to the mean component of the downburst developed numerically by Kim and Hangan (2007) in order to assess the dynamic response of transmission line conductors. In their model, Darwish et al. (2010) evaluated the aerodynamic damping of the conductors using Davenport (1967) where an average value of the wind speed is assumed which means that the study neglected the localized nature of the downburst in both time and space. Darwish et al. (2010) concluded that the dynamic response of the conductors is mainly background. Similar conclusion was obtained by Aboshosha and El Damatty (2015) who reported that for multi-spanned conductors subjected to downburst wind loads, a dynamic excitation in order of 6% is expected. Most of the previously conducted

numerical studies considered only the quasi-static response of the tower and of the conductors to downburst loads. This approach was justified using the following two arguments: (1) the towers typically have natural frequencies greater than 1.0 Hz, which is considerably higher than the mean wind frequencies, which range between 0.01 and 0.05 Hz (Holmes et al., 2008), (2) while the conductors have lower natural frequencies varying between 0.05 and 0.3 Hz that can be excited by the downburst wind, they posses a very high aero-dynamic damping that tends to attenuate the dynamic effect (Darwish et al. 2010, Gattulli et al. 2007, and Aboshosha and El Damatty 2015). The uncertainty regarding the dynamic response of an entire transmission line system, including the towers and conductors, requires conducting aero-elastic studies to assess the dynamic effect. The main challenge of conducting experimental studies on multi-spanned transmission lines, which extend for several kilometres, is the selection of the appropriate length scale within the constraint imposed by the size of the testing facilities. In addition, the aero-elastic model of the multi-spanned transmission line system should consider the main dynamic properties in terms of the aerodynamics, the mass, and the stiffness. In order to overcome this difficulty, Loredo-Souza and Davenport (2001) considered horizontally distorted conductors in order to accommodate the extended length of a single span in a wind tunnel laboratory.

Ideally, an aero-elastic scaling of a structure must include both a geometric scaling of the exterior dimensions and a corresponding scaling for all the forces influencing its structural behaviour. This step includes scaling the elastic, inertia, and the viscous as well as the gravity and damping forces. However, previous practical experience with aero-elastic modeling revealed a difficulty in satisfying all of these requirements (Loredo-

Souza and Davenport, 2001). The difficulty of simulating the transmission line structure subjected to a downburst wind field is even more complicated than the case of synoptic wind testing. This is due to the high degree of dependency of the structure's response on the spatial configurations and the temporal localization of the downburst (Shehata et al., 2005).

The present chapter describes and reports the results of an experimental program conducted, for the first time worldwide, at the WindEEE facility on an aero-elastic multi-spanned transmission line model subjected to simulated downbursts. The goal of the study is to evaluate the dynamic response of various components of the transmission line when subjected to downburst-induced loads.

The specific objectives of the current study can be summarized as follows: (i) characterize the downburst wind field measured at WindEEE; and (ii) assess the dynamic effects of this downburst wind field on the transmission line under study.

The chapter is divided into two main parts. The first part reports the results of processing the downburst wind field measured at WindEEE. A decomposition approach proposed to separate the mean from the fluctuating components of the downburst's radial velocities is first presented. Based on that, the turbulence intensities of the wind field are estimated. The location of the maximum radial speeds is then identified and the vertical profile of the maximum radial velocity is compared versus previous numerical studies. The second part focuses on assessing the dynamic response of an aero-elastic model simulating a multi-span transmission line system under the downburst wind field generated at WindEEE. It starts by providing a description of the considered transmission line system, the details of the aero-elastic model including the instrumentations and the test

plan and configurations. A decomposition approach is presented to separate the mean, background and resonant components of the response and is used to assess the dynamic effect, which is expressed in the form of a dynamic magnification factor. Finally, conclusions drawn from the study are presented.

2.2. Downburst Simulation at WindEEE

WindEEE is a one-of-a-kind three-dimensional wind testing chamber with a hexagonal shape of 25 m diameter (wall to wall) as shown in **Fig. 2-3**. Five of the chamber walls contain an array of eight reversible fans in addition to other 40 fans on the main wall coupled with a louvre system that can produce different kinds of wind systems such as tornados, downbursts, gust fronts, and low-level currents as well as multi-scale wind simulations. The ground floor of the testing chamber is equipped with automated roughness elements, which are designed to generate various exposure conditions. The chamber height (H) is 3.8 m and the bell mouth-opening diameter (D), which is mounted on the ceiling of the chamber, is 3.2 m (see **Fig. 2-3**). As such, the height to diameter ratio, H/D, is ~ 1.2, which is close to the ratios used previously in numerical and experimental simulations of downbursts. The downburst flow at WindEEE is produced using a flow enforce methodology similar to that used in impinging jet simulations where the air is pressurized into the bell mouth by mechanical louvers. The simulation of the downburst winds at WindEEE starts by running the six fans in the upper plenum while the bell mouth opening is kept closed to develop the desired pressure, which is controlled by the percentage of the fans' power. After reaching the required pressure ratio, the bell mouth is opened to create the downburst flow. The perimeter fans of the testing chamber are used to recirculate the flow. The bell mouth opening is kept fully open during the

wind field simulation. The mechanical system of the downburst simulation at WindEEE is capable of creating a translating downburst. This translation is not considered in this study and, therefore, the bell mouth opening is kept stationary above the turntable.

Twelve cobra probe devices, distributed evenly on two columns, are used to measure the downburst radial velocity using a sampling frequency of 156 Hz as illustrated in **Fig. 2-4**. The velocity field of the downburst is measured in an area extending radially from *R/D* = 0.7 to 3.0 and vertically from Z/D = 0.03 to 0.3. The tips of the cobra probe devices are oriented toward the center of the bell mouth. The size of the roughness elements is selected to produce an open terrain profile using trial and error criteria. In the next section, the method used to separate the mean and fluctuating wind velocities of the measured downburst winds is explained.

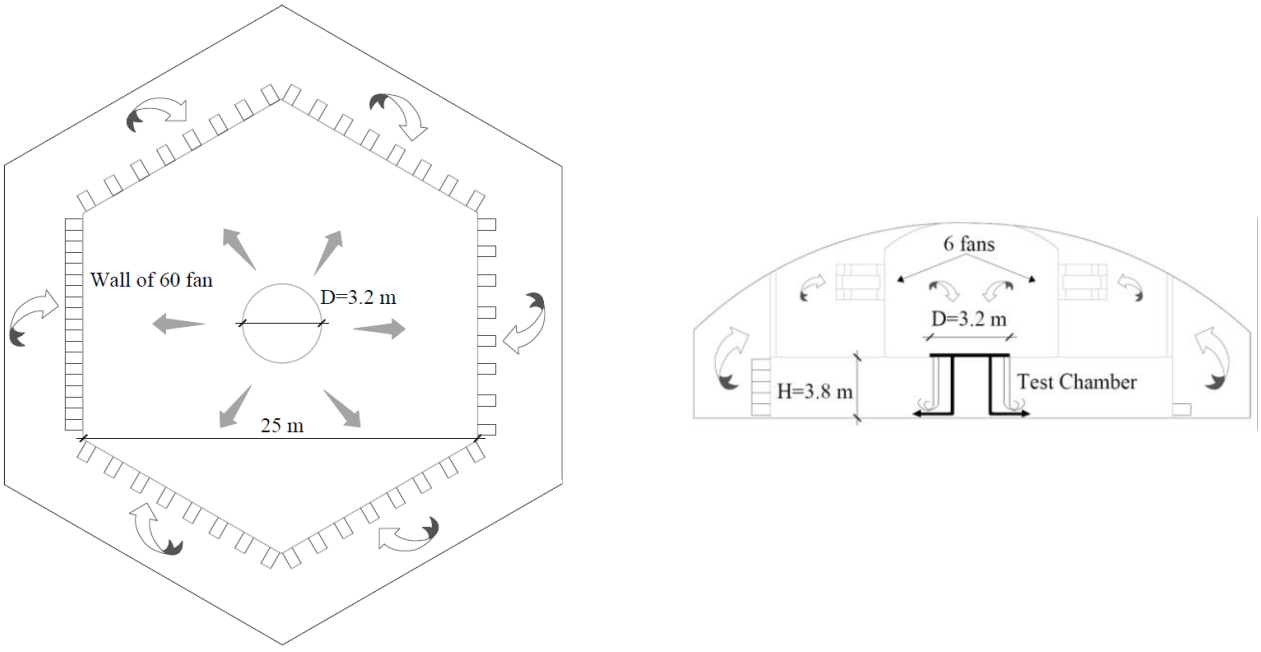

(a) Floor plan (b) Elevation view

Fig. 2-3. Schematic of testing chamber and downburst simulation at WindEEE.

Fig. 2-4. Cobra probe devices.

2.2.1. Mean and fluctuating wind decomposition

One of the major differences between a synoptic and a downburst event is the non-stationary nature of the latter. Choi and Hidayat (2002) and Holmes et al. (2008) proposed decomposing the downburst wind field into two components: running-mean and turbulence. This procedure requires using a moving average window, i.e., temporal averaging, along the time history of the event in order to calculate the mean component. In the current study, temporal averaging is conducted using the decomposition technique described by Kim and Hangan (2007) and Aboshosha et al. (2015) which is based on the value of the shedding frequency. Kim and Hangan (2007) defined the shedding frequency associated with the shedding of the ring vortices as $f_{shedding}=S_t\ V_{RD}/D$ where St is the Strouhal number which is taken as 0.35 as recommended by Didden and Ho (1985), D is the jet diameter, and V_{RD} is the radial velocity of the downburst. Kim and Hangan (2007) and Aboshosha et al. (2015) suggested that the cutting frequency, f_{cut}, of the mean component to be higher than that of the shedding frequency. As such, in the current study, the f_{cut} is considered to be equal to 1.5 $f_{shedding}$ as shown in **Equation (2-1)**.

$$f_{cut} = 1.5 f_{shedding} = 1.5 \frac{S_t V_{RD}}{D} \quad (2\text{-}1)$$

The factor of 1.5 is selected such that the cut-off frequency of the mean component of the velocities does not exceed the lowest structural frequency. This means that the expected resonance frequencies will be higher than the frequency of the mean wind velocity. Further discussion on this equation is provided in the response decomposition description, which is provided in the results section.

Four downburst maximum radial speeds, V_{RD}, of 5, 6.3, 7, and 9 m/s are considered in the current study. The decomposition procedure is applied on the entire downburst wind field measured at WindEEE for the four considered downburst velocities. For example, substituting D = 3.2 m, the downburst diameter used in the test, and V_{RD} = 7 m/s into **Equation (2-1)**, a value of 1.15 Hz is obtained for f_{cut}. Other decomposition approaches are found in the literature such as those provided by Holmes et al. (2008) and Solari et al. (2015). Holmes et al. (2008) suggested a fixed averaging period of 40 seconds for the radial velocities of the real event that occurred near Lubbock, Texas (2002). The Lubbock downburst diameter was estimated to be 600 m with a radial velocity of approximately 35 m/s. By substituting the size and intensity of the Lubbock event into **Equation (2-1)**, f_{cut} is approximately equal to 0.03 Hz; i.e., a 33-second averaging period, which is close to the value suggested by Holmes et al. (2008). This value agrees with the averaging period of 30 sec suggested by Solari et al. (2015) based on statistical analyses for 93 thunderstorm field measurements.

Fig. 2-5 shows a sample of the time history of the peak, the mean and the turbulent components of the radial velocity measured at a point located at R/D = 0.9 and Z/D = 0.06. The figure shows that the peak velocity is localized in a narrow zone, referred to as

zone “P”. In addition, the figure shows that the fluctuating velocities have a strong contribution at the peak zone.

For a certain downburst jet velocity, the entire wind field is measured, processed, decomposed, and the time histories of the mean radial velocities are obtained. At each of the measured locations; i.e., R/D = 0.7 to 3.0 and Z/D = 0.03 to 0.3, the maximum mean radial velocity is recorded. The processing of the mean radial velocities shows that the peak V_{RD} occurs at an approximate distance ratio R/D of 0.9 and a height ratio Z/D of 0.03. The envelope of the mean radial velocities recorded for the entire wind field is then normalized to the absolute maximum mean radial velocity measured in the entire space; i.e., at R/D = 0.9 and Z/D = 0.03. **Fig. 2-6**-a shows a contour lines of the maximum radial velocities normalized to the maximum value measured along a radial distance ratio R/D that varies between 0.7 and 3.0 and a height ratio that varies between 0.03 and 0.3. It is worth mentioning that these maximum radial velocities are recorded at different time instants. In the next section, the procedure used to estimate the turbulence intensity of the radial wind component is described.

2.2.2. Turbulence intensity

The turbulence intensities of the transient velocity (similar to the sample shown in **Fig. 2-5**) is expected to vary at different time intervals. From structural engineering point of view, the interest is in the evaluation of the peak responses, which is expected to occur in zone P shown in **Fig. 2-5**. As such, the analysis conducted for the evaluation of the turbulence intensities is confined to this zone, which is assumed to be bounded between $t_1 = t_{\max} \pm \frac{1}{2 f_{cut}}$ and $t_2 = t_{\max} \pm \frac{1}{2 f_{cut}}$ as recommended by Aboshosha et al.

(2015). The following processing steps are considered for each of the measured radial velocities to calculate the turbulence intensities, $I_{ur:}$

1) The peak radial velocity V_{RDmax} is recorded.
2) The fluctuating component of the radial velocity is obtained using the cutting frequency f_{cut} filter.
3) The peak zone bounds t_1 to t_2 are determined and marked.
4) σ_{urmax}, the r.m.s of the fluctuating radial velocity, is calculated along the time interval of t_2-t_1.
5) The turbulence intensity, I_{ur}, is calculated using **Equation (2-2)**.
6) Contour lines representing the turbulence intensities are plotted in **Fig. 2-6**-b.

$$I_{ur} = \frac{\sigma_{ur\max}}{V_{RD\ \max}} \tag{2-2}$$

where $V_{RD\ max}$ is the maximum radial velocity at the time instant t_{max}, and σ_{urmax} is the r.m.s of the fluctuating radial velocity calculated at the peak zone shown in **Fig. 2-5**. **Fig. 2-6**-b shows that I_{ur} tends to decrease with an increase in the height. The figure also shows that close to the location of the peak radial velocity; i.e., when R/D ranges between 0.8 and 0.9, I_{ur} ranges between 0.11 and 0.14. This finding agrees well with the findings reported by Solari et al. (2015) and Holmes et al. (2008) for real downburst events. The analysis shows that the turbulence intensity of the downburst is much less than that of one typically found for synoptic winds, which ranges between 0.17 and 0.3 (Solari et al. 2015). In the next section, a comparison between the vertical profile of the measured downburst radial velocity and the corresponding profiles previously developed numerically is shown.

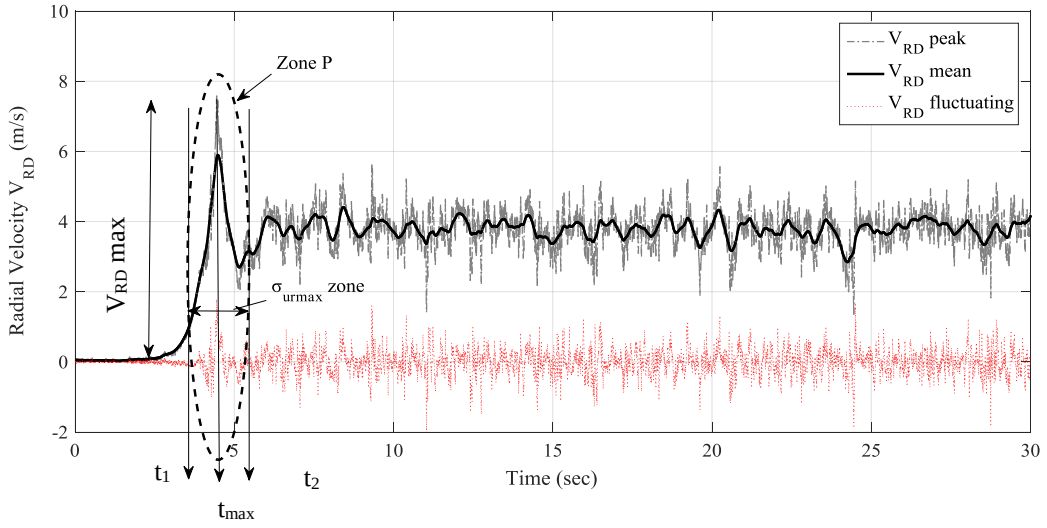

Fig. 2-5. Decomposition of the downburst radial velocity at R/D=0.9 and Z/D=0.06.

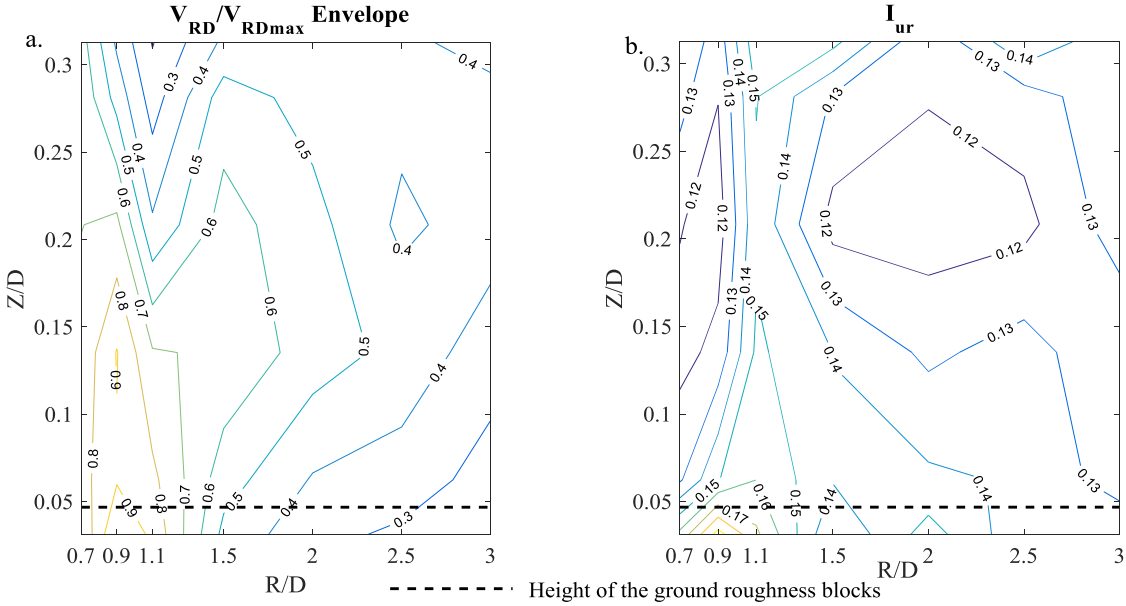

(a) Normalized V_{RD} (b) Turbulence intensity I_{ur}

Fig. 2-6. Contour lines of Wind field characteristics.

2.2.3. Velocity profile validation

This section provides a comparison between the mean wind profiles measured in the location of the maximum radial velocity at the WindEEE testing chamber to the

maximum profiles reported by the numerical simulations conducted by Kim and Hangan (2007), and Aboshosha et al. (2015). As mentioned earlier, the experimental measurements indicate that the maximum radial velocity occurs at radial distance between to 0.8~1.0D. **Fig. 2-7**-a shows the envelope vertical profile of the mean radial velocity normalized to the maximum radial velocity (V_{RD}/V_{RDmax}) along the height at three locations corresponding to R/D = 0.8, 0.9, and 1.0, respectively. The figure shows that the absolute maximum radial velocity occurs at a distance ratio R/D = 0.9 and a height ratio Z/D = 0.03. The location of the maximum radial velocity differs from the values reported at the previous numerical studies; R/D=1.2~1.3 according to Kim and Hangan (2007), and Aboshosha et al. (2015). This is primarily attributed to the difference between the H/D ratios used in the numerical studies (H/D = 2 in Aboshosha et al. (2015) and H/D = 4 in Kim and Hangan, (2007)) and the current experimental study (H/D ~ 1.2). If the vertical profile at maximum velocity is similar, this difference is expected to have a minimal effect on the structural response of the tested system. The measured maximum radial velocity profile is compared in **Fig. 2-7**-b to the profiles produced previously by Aboshosha et al. (2015) using Large Eddy Simulation (LES) and Kim and Hangan (2007) using Reynolds Averaged Navier–Stokes Simulations (RANS). The comparison reveals an excellent match with the LES profile developed by Aboshosha et al. (2015) and a good match with the RANS profile developed by Kim and Hangan (2007). This conclusion confirms that the vertical profile of the maximum radial wind velocity of the downburst is independent from the assumed value of H/D as long as this ratio allows the formation of the main vortices.

In summary, the characterization of the downburst wind field conducted in the current study shows that the downburst turbulence intensity is in order of 0.14. In addition, the vertical profile of the maximum mean radial velocity is in an excellent agreement with the numerical modeling based on the impinging jet approach and the LES simulations.

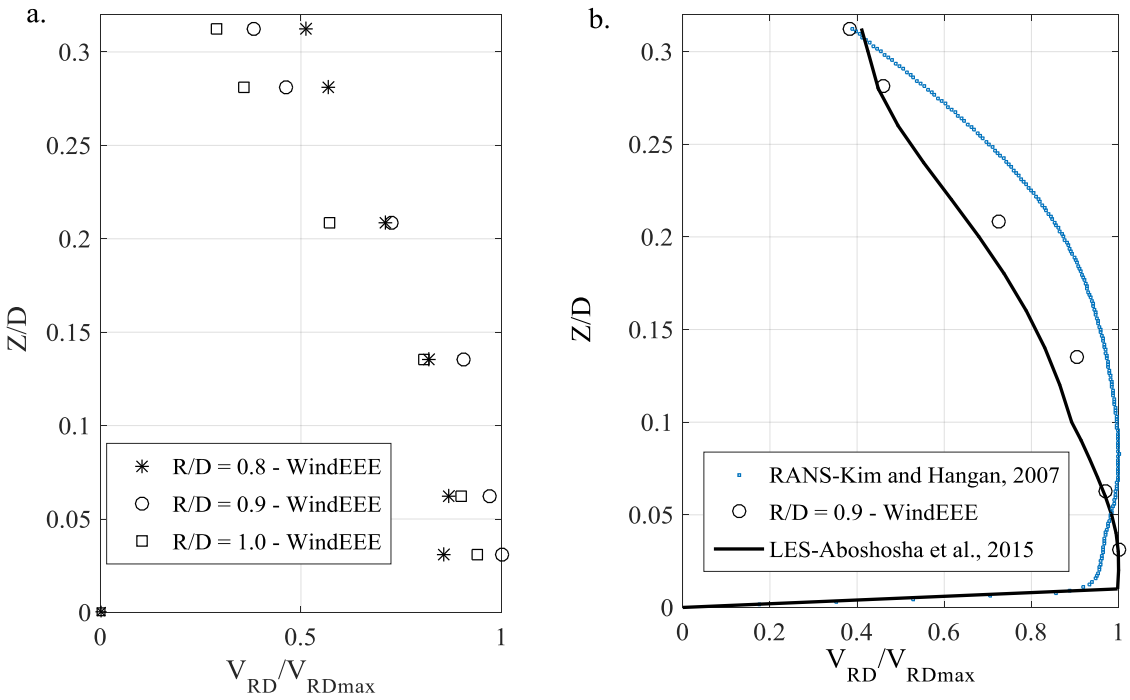

(a) Mean radial profiles (b) Validation

Fig. 2-7. Maximum mean radial wind profile along the height.

2.3. Aero-elastic Modeling of Transmission Line System

2.3.1. Prototype description

The studied transmission line is one of the systems used by Hydro One Company, Ontario, Canada and is shown in **Fig. 2-8** The tower is a light weight structure that is easy to construct in remote areas but its vulnerable to failure when subjected to downbursts (failure instance for similar line is shown in **Fig. 2-1**). The simulated portion of the line

includes seven towers, identified as A to G, as shown in the layout provided in **Fig. 2-9**. A 3D perspective of the transmission line system is shown in **Fig. 2-10**. The system consists of guyed lattice towers; each tower is supported by four guys attached at a height of 40.72 m above the foundation level. Two horizontal cross arms protrude from the inclined tower shafts 40.72 m above the foundation level (main girder level) extending 6.5 m in the transverse direction and ending at the location of the insulator (see **Fig. 2-10**). Three conductor bundles are attached to the tower through the insulators; two at the tip of each cross arm and one at the center point of the main girder. Each conductor bundle has 4-wires and each wire has a diameter of 0.022 m and a weight per unit length of 8.67 N/m. The conductor bundle has a square shape with a separation distance of 0.48 m. The bundles are supported by insulators with a length of 4.27 m. The tower members are steel L-shaped angles with different cross sections as mapped out in **Fig. 2-11**. Galvanized steel guy wires of a diameter of 0.019 m are used to prevent displacements at the anchorage level. The straight length of the guys is 50 m. A pretension force of 11 kN is applied to all the guys. The tower is mounted at the ground level on a pivotal (i.e. hinged) support that allows the rotations at the tower center. The total weight of the tower is approximately 60 kN and has a height of 46.5 m. Two conductor span cases of 125 m and 250 m with a sagging of 3.25 m and 6.5 m, respectively, are considered in the current study.

A test picture showing half of the assembled line is provided in **Fig. 2-12**. Three fully-cladded aero-elastic towers and four other rigid frames (to represent a total of seven towers) are considered. A picture of the rigid frames, D, E, F, and G is provided in **Fig. 2-13**. **Fig. 2-14** shows a picture of towers A, B, and C

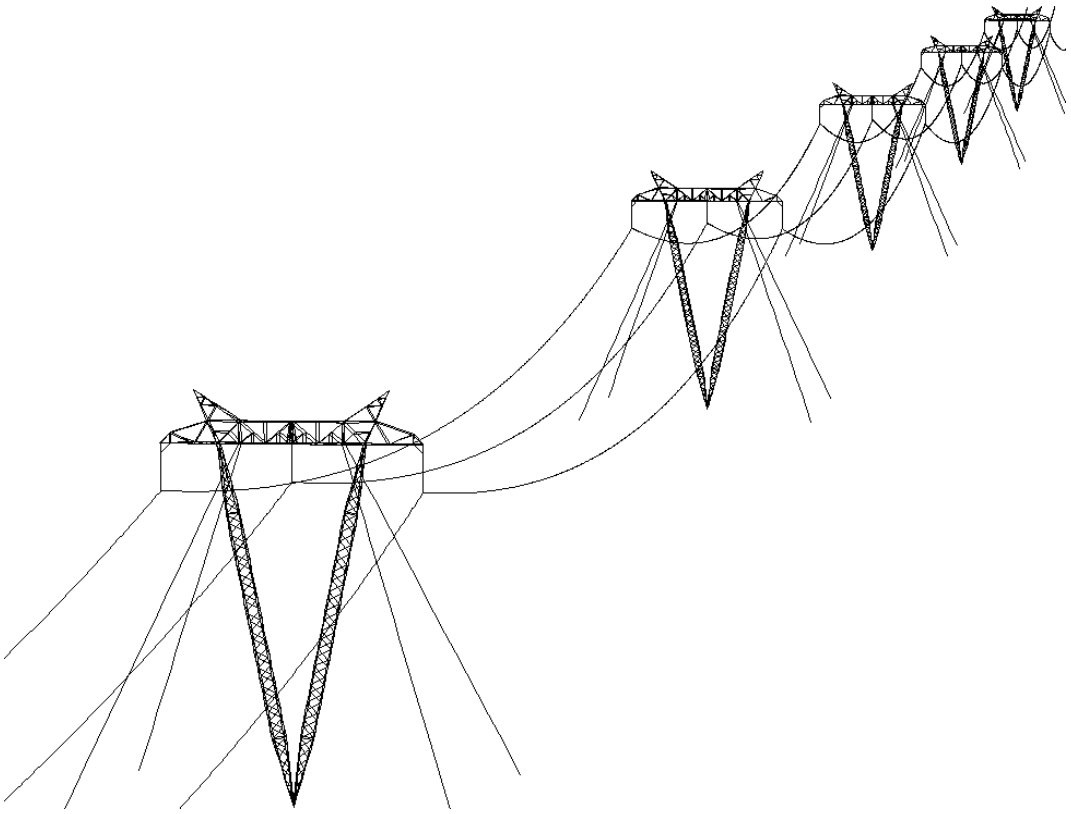

Fig. 2-8. Schematic 3D view of the study line.

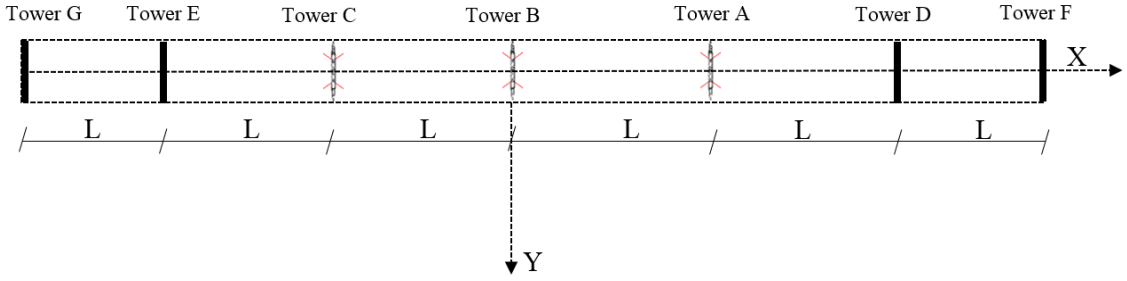

Fig. 2-9. Schematic of the test layout and the names of the tested towers.

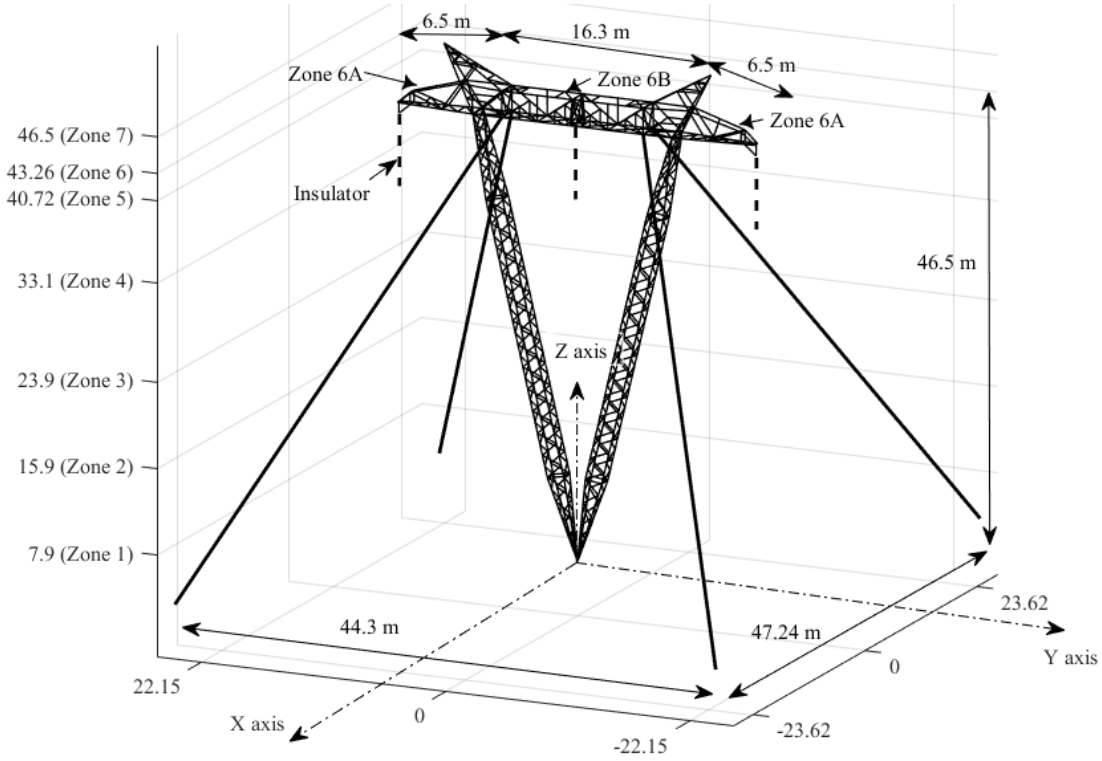

Fig. 2-10. 3D view of the prototype transmission tower.

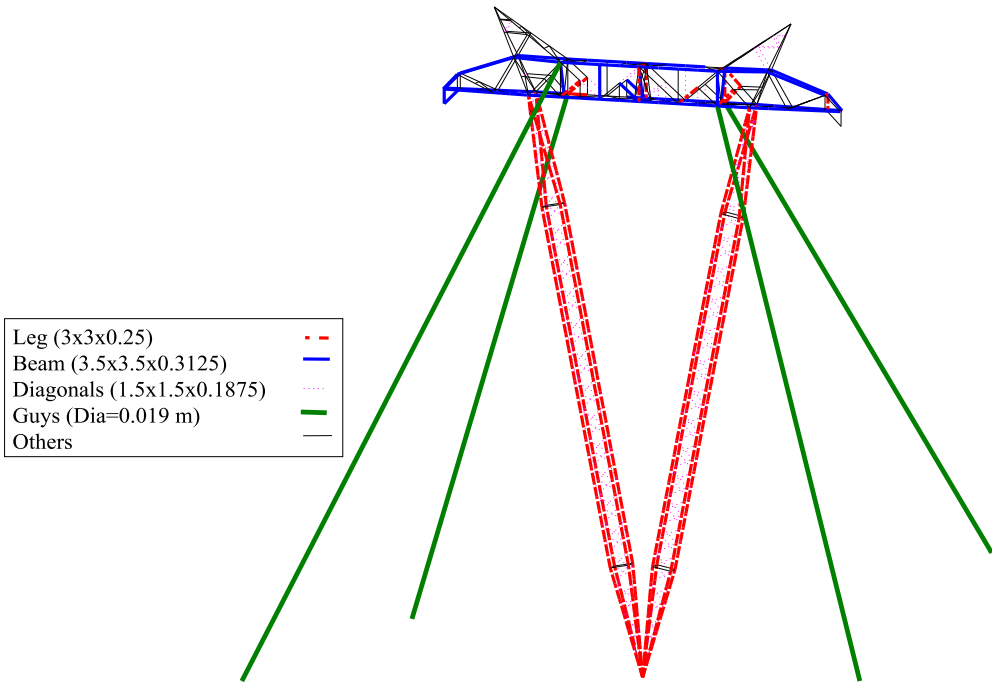

Fig. 2-11. Steel angle dimensions of the tower.

2.3.2. Aero-elastic model scaling parameters

Because of the large size of the WindEEE testing chamber compared to typical wind tunnels, a relatively large length scale of 1:50 is possible to use in this study as shown in **Table 2-1**. Froude number scaling, which characterizes the ratio between the inertial forces of the fluid and the gravitational and elastic forces of the structure, is preserved. This is achieved by linking the velocity scale to the square root of the length scale (i.e. 1:7.07). The scaling ratios for the physical parameters of interest are functions in the length and velocity scales and are summarized in **Table 2-1**. The stiffness and masses of the tower, conductors and insulators are scaled down. Details of the design are provided in the following sections.

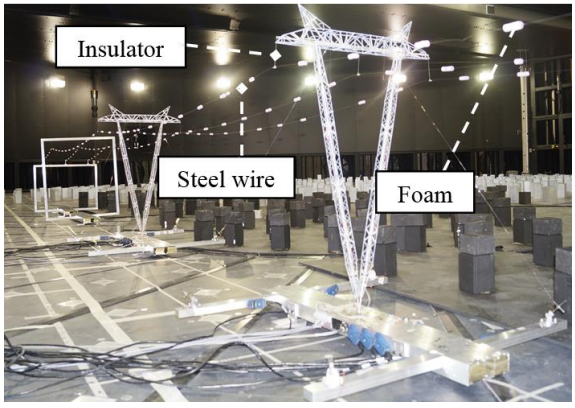

Fig. 2-12. Half-length of the assembled line.

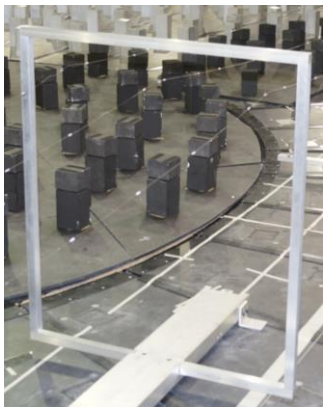

Fig. 2-13. Pictures of D, E, F, and G frames.

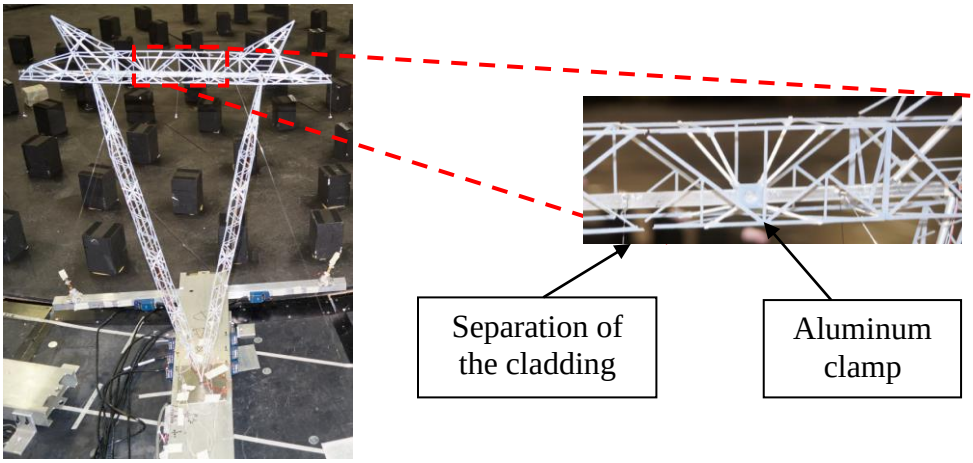

Fig. 2-14. Test picture of A, B, and C towers.

Table 2-1. Scaling ratio for various physical parameters of the model

Parameter	Scaling ratio
Length	$\lambda_L = L_m/L_p = 1{:}50$
Velocity	$\lambda_v = \lambda_L^{0.5} = V_m/V_p = 1{:}7.07$
Time	$\lambda_T = T_m/T_p = \lambda_L/\lambda_V = 1{:}7.07$
Density	$\lambda\rho = \rho_m/\rho_p = 1{:}1$
Mass per Unit Length	$\lambda_m = \lambda_\rho \lambda_L^2 = 1{:}2500$
Mass	$\lambda_M = \lambda_\rho \lambda_L^3 = 1{:}125{,}000$
Mass Moment of Inertia per Unit Length	$\lambda_i = \lambda_m \lambda_L^2 = 1{:}6{,}250{,}000$
Mass Moment of Inertia	$\lambda_I = \lambda_M \lambda_L^2 = 1{:}312{,}500{,}000$
Acceleration	$\lambda_a = a_m/a_p = \lambda_v/\lambda_T = 1{:}1$
Damping	$\lambda_\zeta = \zeta_m/\zeta_p = 1{:}1$
Elastic Stiffness	$\lambda_{EI} = \lambda_{GC} = \lambda_V^2 \lambda_L^4 = 312{,}500{,}000$ $\lambda_{EA} = \lambda_V^2 \lambda_L^2 = 1{:}125{,}000$
Force per Unit Length	$\lambda_f = \lambda_V^2 \lambda_L = \lambda_L^3 / \lambda_T^2 = 1{:}2500$
Force	$\lambda_F = F_m / F_p = \lambda_V^2 \lambda_L^2 = 1{:}125{,}000$
Bending and Torsional Moment	$\lambda_{BM} = \lambda_V^2 \lambda_L^3 = 1{:}625{,}000$

*Subscripts m, and p represent the model and the prototype scale, respectively.

As mentioned earlier, two different spans are considered in the test; 125 m and 250 m which correspond to 2.5 m and 5 m for the model scale, respectively. This means that the

span to the downburst diameter ratio, L/D, is equal to 0.78 and 1.56 for the two conductor cases, respectively. The L/D ratio affects the peak loads acting on the tower and the conductors according to Shehata and El Damatty (2007 and 2008). In these studies, it was reported that the maximum transvers loads acting on the line occurs at an L/D ratio equal or larger than 1.0 while the peak oblique loads on the line occurs with lower L/D ratios. Therefore, in the current study, the short and long spans of the line, 2.5 m and 5 m, are selected to examine both the peak transverse and the peak oblique downburst loadings acting on the line.

2.3.2.1. Tower model

The tower is modeled by continuous structural elements that are referred to here as a "spine". An aluminum spine is selected as an alternative to the prototype steel material to satisfy the mass scaling requirement. Since the tower is V-shaped with two legs, a V-shaped spine is used. In order to design the spine along the tower height, the prototype tower is divided into seven zones (see **Fig. 2-10**) where the stiffness for each one is calculated and preserved in the model. The aerodynamics are maintained by modeling the structure's geometry using non-structural plastic elements, which are referred to as "cladding".

2.3.2.1.1. Spine design

The spine has two functions with respect to the global response of the aero-elastic model. Firstly, to model the flexural and torsional stiffness of a single tower. Secondly, to provide a portion of the required mass and aerodynamics to simulate the real tower. A circular cross section is selected for the tower zones (except for zone 6) to avoid the

discrepancies in the flow separation and consequently avoid the discrepancies in the tower responses under the oblique angles of attack (Kong et al., 2009). The spine dimensions are given in **Fig. 2-15**-a. The shape of the spine coincides with the as built-elevation view of the full-scale tower shown in **Fig. 2-15**-b. A high strength aluminum circular section of tube 3.969 mm in diameter with a wall thickness of 0.356 mm is used to simulate the lateral bending and torsional stiffness of the tower zones except zone six.

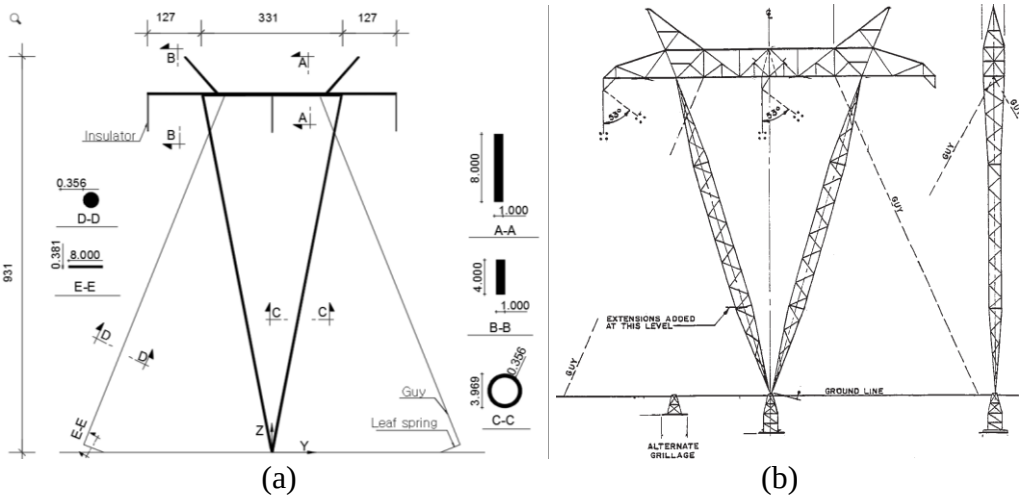

Fig. 2-15. (a) Spine dimensions (in mm), (b) Schematic of the full-scale guyed tower.

Two rectangular aluminum bars are selected to simulate the lateral and the torsional stiffness of the tower's main girder. The middle part (zone 6B) has a thickness of 1 mm and a depth of 8 mm. The two edged cantilevers (zone 6A) have a thickness of 1 mm and a depth of 4 mm. The supporting guys are modeled using a 0.356 mm steel wire. The diameter is chosen to simulate the actual diameter and mass of the prototype. However, the axial stiffness of the selected wire turns to be much greater than the targeted axial stiffness of the prototype guys that is calculated based on the scaling factor shown in **Table 2-1** ($\lambda_{EA} = \lambda_V^2 \lambda_L^2 = 1:125{,}000$). Knowing that the guys make a significant

contribution to the global stiffness of the structure and consequently its natural frequencies, a stiffness correction is done by adding a leaf spring system. The leaf spring is a steel sheet 0.381 mm thickness and 8 mm width with a total length of 25 mm. The leaf spring and the guy's stiffness are assembled to act in series, which creates the needed reduction in the equivalent axial stiffness of the guys. The leaf springs are designed such that the global characteristics of the aero-elastic model are close to the scaled characteristics of the prototype tower.

2.3.2.1.2. Cladding design

The cladding modules are constructed such that each cladding zone is disconnected from the consecutive module and fixed at a single point to the structural spine using an aluminum clamp as shown in **Fig. 2-14**. This is done to prevent the cladding from contributing to the structural stiffness. The figure also shows that a small gap between the cladding modules is included to separate the segments.

2.3.2.2. Conductor model selection

The design of the aero-elastic conductor assumes the case of unshielded wires as recommended by ASCE-74 (2010) where the four wires are simulated using a single conductor model. The cable sag ratio is 2.6% of the line span, which is maintained throughout the test. An equivalent diameter of 0.4064 mm of aircraft cables is used to provide the required mass for the scaled bundle. Thus, the pretension force in the conductors is preserved as well by adjusting the conductor's sag to the desired value; i.e., 0.13 m and 0.065 m for the span values of 5 m and 2.5 m, respectively. However, to satisfy the aerodynamic requirements of the prototype bundle, additional cylindrical foam

bullets (30 mm in length and 10 mm in width at a spacing of 220 mm) are attached to the cable at discrete locations along the cable's length as shown in **Fig. 2-12**. This leads to the testing of an equivalent diameter of 0.0017 m.

The insulator's flexibility is considered at the middle spans using an aluminum rod of 0.0854 m in length and of 0.0005 kg in weight to provide the reduced scale mass and stiffness. The insulators are attached to the girder through a bolted connection that connects the holes in the girder spine and the top of the insulator as shown in **Fig. 2-12**. The conductors then pass through the bottom hole of the insulator.

2.3.2.3. Support boundary conditions

The studied tower, shown in **Fig. 2-10**, has five points of support; four guy supports and one central point. The modeled aero-elastic tower is designed to have a central hinged support using a two-degrees of freedom gimballed system, and a 2D Universal Base Support, as photographed in **Fig. 2-16**-a. All translation as well as the torsional motions are restrained while only the rotations are allowed. The pretensioned guys are supported by the leaf springs (see **Fig. 2-16**-b). The leaf spring system restrains both the rotations and the translations in the horizontal plane while it allows the translation only in the plane perpendicular to the guy's direction in order to give flexibility to the guys to deform under compression or tension. The intermediate support of the conductors is modeled using an insulator rod as previously described. At the end of the line, the conductors are connected to leaf springs having a thickness of 0.381 mm, a width of 8 mm and a length of 50 mm. The leaf springs are then fixed to rigid support frames (towers F or G) as shown in **Fig. 2-16**-c.

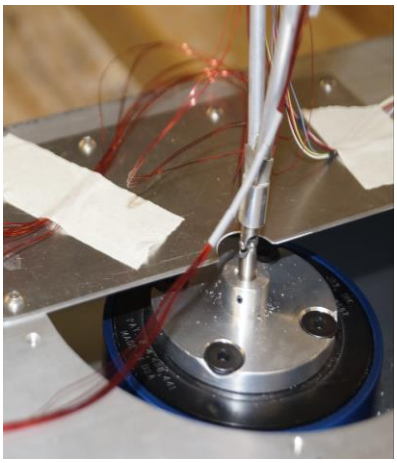

(a) 2-DOF Universal Base

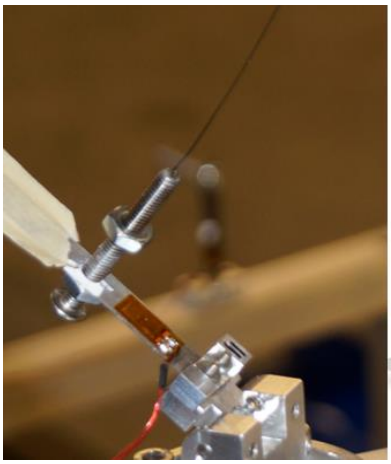

(b) Supporting guy anchorage

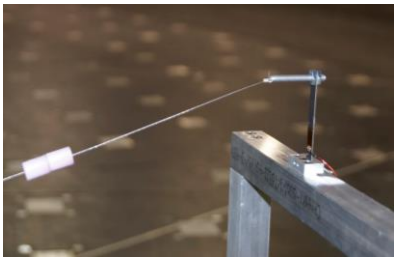

(c) Conductor end support

Fig. 2-16. Model boundary conditions details.

2.3.2.4. Instrumentation

Fig. 2-17 shows the location and devices utilized to acquire different measurements during the test. Strain gauges are mounted at the mid height of the tower and at the cross arm level. This arrangement enables the measuring of the out-of-plane (X direction-line direction) and the in-plane (Y direction-perpendicular to the line direction) bending moments at the mid height of the tower (M_{1X} and M_{1Y}, respectively) and of the out-of-plane bending moment (in X direction) at the cross arm cantilever (M_C) as shown in **Fig. 2-18**. Strain gauges are also mounted on the leaf springs to allow adjustments to reach the desired pretension forces of the tower guys and the conductor's end supports before applying the wind loads on the line and subsequently measuring their tensions during the test as shown in **Fig. 2-16**-b. The strain gauges are calibrated before the test by taking their readings for incrementally increasing known moments using free-standing cantilevered segments. A multi-axis load cell (JR3) is mounted underneath the instrumented tower, as shown in **Fig. 2-16**-a, to measure the center point forces in three directions. Therefore, the measurements of the guys' strain gauges and the center force

balance are used to calculate the base shears (Q_{bX} in X direction and Q_{bY} in Y direction) and the base moments of the tower (M_{bX} in X direction and M_{bY} in Y direction). The base shears and the base moments recorded in the current study are calculated as following:

- Base shear=Σ Guys force in the direction of interest + center support force in the direction of interest.
- Base moment= Σ Guys force in the direction of interest x the lever arm measured from the guy's support to the center support in the direction of interest.

Four 3-axis accelerometers are mounted at specific locations on the tower of interest (see **Fig. 2-17** and **Fig. 2-18**). The accelerometers are used to evaluate the natural frequencies of the tower and of the conductors. A sampling frequency of 100 Hz is used for the test measurements. During the test, four cobra probe devices (see **Fig. 2-19**) are used to measure the downburst wind speed at an elevation of 0.47m, which is almost the mid-height of the tower. The measurements are recorded in the form of time history during the duration of the simulated downburst, which is 30 seconds corresponding to a duration of3.5 minutes for the full-scale.

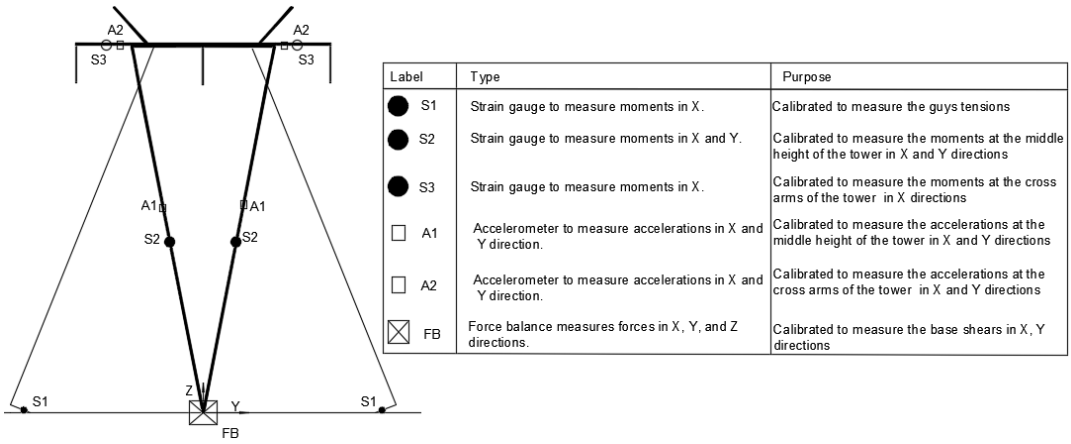

Label	Type	Purpose
S1	Strain gauge to measure moments in X.	Calibrated to measure the guys tensions
S2	Strain gauge to measure moments in X and Y.	Calibrated to measure the moments at the middle height of the tower in X and Y directions
S3	Strain gauge to measure moments in X.	Calibrated to measure the moments at the cross arms of the tower in X directions
A1	Accelerometer to measure accelerations in X and Y direction.	Calibrated to measure the accelerations at the middle height of the tower in X and Y directions
A2	Accelerometer to measure accelerations in X and Y direction.	Calibrated to measure the accelerations at the cross arms of the tower in X and Y directions
FB	Force balance measures forces in X, Y, and Z directions.	Calibrated to measure the base shears in X, Y directions

Fig. 2-17. Instrumentations of the tower.

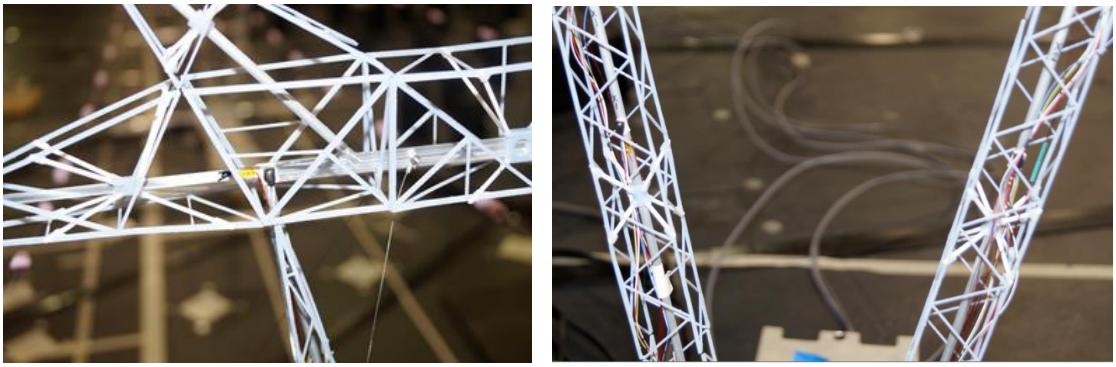

Fig. 2-18. Accelerometers and strain gauges.

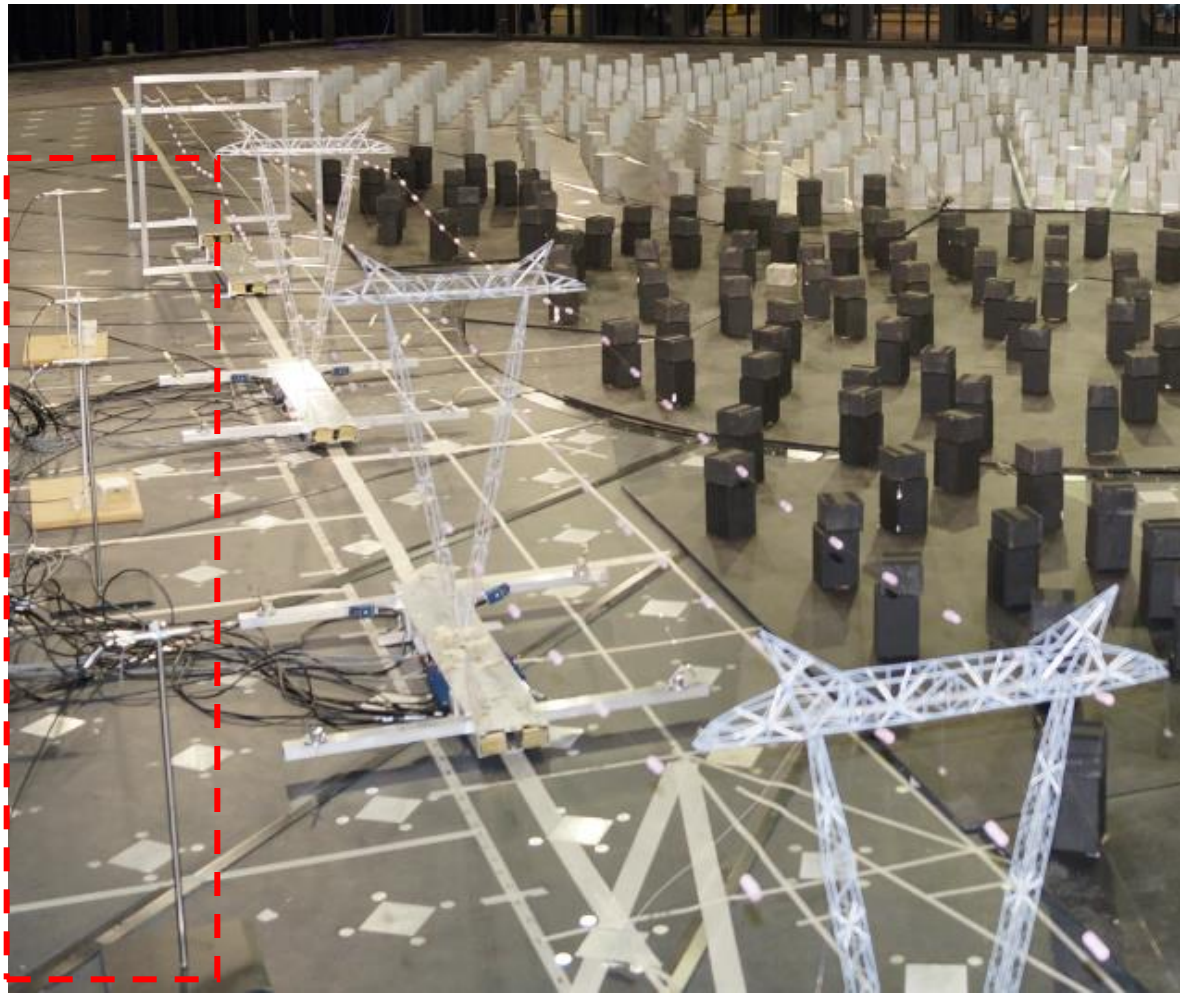

Fig. 2-19. Cobra Probe measurements during testing.

2.3.2.5. Aero-elastic model free vibration test

The dynamic properties of the prototype in terms of the essential mode shapes should be carefully captured and considered in the design of the aero-elastic model.

Single tower

Table 2-2 shows the natural frequencies and the fundamental mode shapes of the prototype tower evaluated using the commercial finite element code SAP2000 (Computer and Structures, Inc., CSI). The table also shows the corresponding frequencies targeted for the model, which are obtained by multiplying the prototype frequencies by the factor λ_v defined in **Table 2-1**. Free vibration tests are conducted to estimate experimentally the natural frequencies and mode shapes of the built model. The comparison between the target and the measured frequencies of the model, which is shown in **Table 2-2**, indicates a strong agreement with a maximum difference of 8% in the third mode.

Table 2-2. Frequencies and mode shapes of the full-scale tower and the required frequencies of the aero-elastic model.

Mode no.\ Description	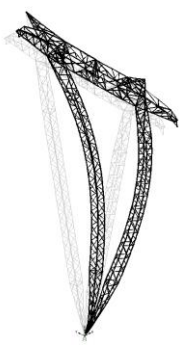	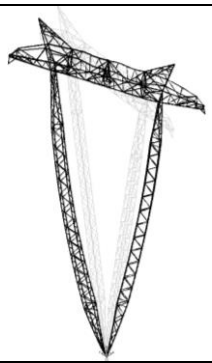	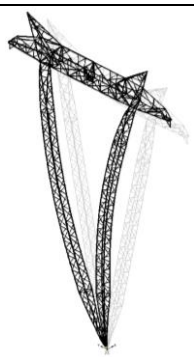
	Mode 1, Out-of-plane bending	Mode 2, Torsional bending	Mode 3, In-plane bending
Proto. Frequency (Hz)	1.44	1.88	2.44
Target Frequency (Hz)	10.18	13.3	17.25
Model Frequency (Hz)	10.3	14.3	18.7
Difference	1.3 %	7.8 %	8.0 %

The measured damping ratio from the aero-elastic model is found to be in order of 3% which is lower than the values recommended by the ASCE-74 (~ 4%). This measured damping ratio agrees with the values reported by Momomura et al. (1997) for full-scale transmission tower damping of 1.7 to 3.3% critical damping ratios.

Assembled line

The conductor's fundamental frequency is estimated using **Equations (2-3)** and **(2-4)**, which were derived by Irvine (1974) for a single spanned conductor.

$$f_1 = \frac{1}{2L}\sqrt{\frac{T}{m/L}} \tag{2-3}$$

$$T = \frac{wL^2}{8\,S} \tag{2-4}$$

where L is the conductor's length (m), m is the conductor's mass (kg), and T is the conductor's tension (N) as calculated in **Equation (2-4)**, S is the line sag, and w is the cable weight per unit length. In addition, a finite element model of six spans conductors of the line described in the current study is developed simulating the exact boundary conditions of the line to evaluate their fundamental frequencies.

A free vibration test is conducted for the assembled line including both the towers and the conductors, considering the 2.5 m and 5 m spans, in order to estimate the fundamental frequency of the conductors.

Table 2-3 shows both the calculated and the measured conductors' frequencies for the prototype, for the two considered span values. The table shows an excellent agreement between the target and tested conductor frequencies.

Table 2-3. Dynamic properties of the tested conductors.

Span (m)	Sag (m)	Weight (N/m)	Calculated Frequency (Irvine, 1974) (Hz)	Frequency (Hz) using SAP (2000)	Tested conductor frequency (Hz)	% Difference
250	6.5	39.05	0.217	0.27	0.23	-17.4
125	3.25	39.05	0.307	0.33	0.31	-6.45

2.3.3. WindEEE downburst test plan

The test configurations and layouts are selected in light of the findings of Kim and Hangan (2007), Shehata and El Damatty (2007) and Darwish and El Damatty (2011) along with the downburst field characterization conducted in the current study. Shehata and El Damatty (2007) reported that most of the guyed tower members experienced peak internal forces at a downburst angle of attack equal to $\Theta = 90^{o}$ where the wind field is parallel to the line direction and consequently no conductor forces exist in such a configuration. This is because the system of the guyed tower acts as an over hanging beam where the conductor forces, acting on the cantilever part, tend to reduce the internal forces developing between the beam supports. As such, in the current study, a single tower is tested under this configuration; i.e., $\Theta = 90^{o}$, while no conductors are attached to the tower. In contrast, Darwish and El Damatty (2011) reported that, for a self-supported tower that acts as a cantilever, a critical load case occurs when the downburst acts with an angle of attack of $\Theta = 0^{o}$. This is because the case of $\Theta = 0^{o}$ causes maximum transverse

forces on both the conductors and the tower leading to peak internal force in this cantilever system. Shehata and El Damatty (2007) reported a third critical case where the cross arms of the towers experienced large longitudinal forces due to a downburst oblique configuration, which causes unsymmetrical wind loads acting on the conductor spans adjacent to the considered tower.

With respect to the distance between the tower and the center of the downburst, the wind field's characterization at WindEEE conducted in the current study indicated that the maximum radial speed occurs at R/D = 0.8 ~ 1.0. Based on the above findings, three layouts are considered (see **Fig. 2-20**) to assess the dynamic response of the studied transmission line under critical downburst load cases. **Table 2-4** summarizes the considered layouts and the parameters used in the tests. The table shows the location of the middle tower of the line (tower B in **Fig. 2-9**) with respect to the center of the downburst in terms of X and Y distances and the R/D ratio where X and Y are the distances measured from the downburst center to the tower center in the line direction and the direction perpendicular to the line, respectively. The table also shows the span value used in each of the tested layouts and the number of spans considered. The tests consider four different downburst velocities defined by the peak radial velocity, as shown in **Table 2-4**. As shown in the table the peak velocities vary between 5 m/s and 9 m/s which corresponds to a full-scale velocities varying between 35 m/s to 64 m/s. The description of the three test layouts is provided in the next sub-sections.

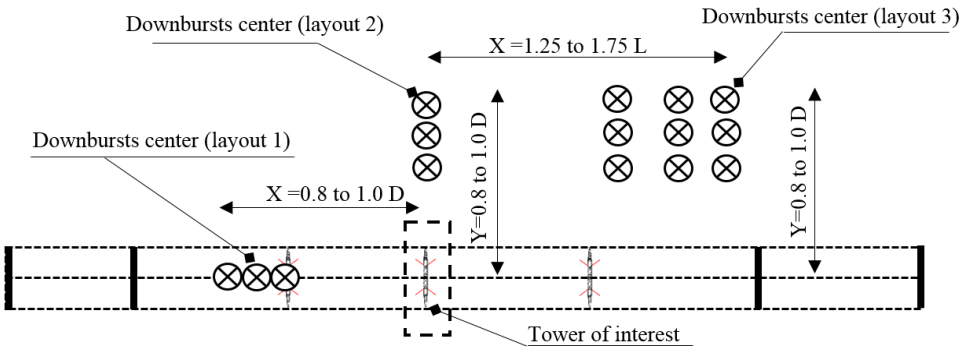

Fig. 2-20. Summary of downburst-structure orientations for the considered layouts.

Table 2-4. Test layouts.

Layout	Θ (degree)	Middle tower location			Line span (m)	No. of spans	Peak V_{RD} (m/s)
		X (m)	Y (m)	R/D			
1	90	2.56, **2.88**, 3.2	0	0.8, **0.9**, 1.0	-	-	35, 45, 50, 64
2	0	0	**2.56**, 2.88, 3.2	**0.8**, 0.9, 1.0	5	4	35, 45, 50, 64
3	52	**3.125,** 3.75, 4.375	**2.56,** 2.88, 3.2	**1.26** to ~1.7	2.5	6	35, 45, 50, 64

2.3.3.1. Layout 1: Maximum longitudinal loads (Angle of attack Θ = 90º)

This layout focuses on evaluating the response of a single tower when the downburst field acts in the longitudinal direction, X, of the line. **Fig. 2-21**-a shows the locations of the tested tower relative to the downburst center. The center of the downburst is located at a distance X = 2.56 m, 2.88 m, and 3.2 m, respectively, from the center of the tested tower. This corresponds to distance ratios R/D = 0.8, 0.9, and 1.0, respectively. **Fig. 2-21**-b shows a picture for test layout 1 inside WindEEE.

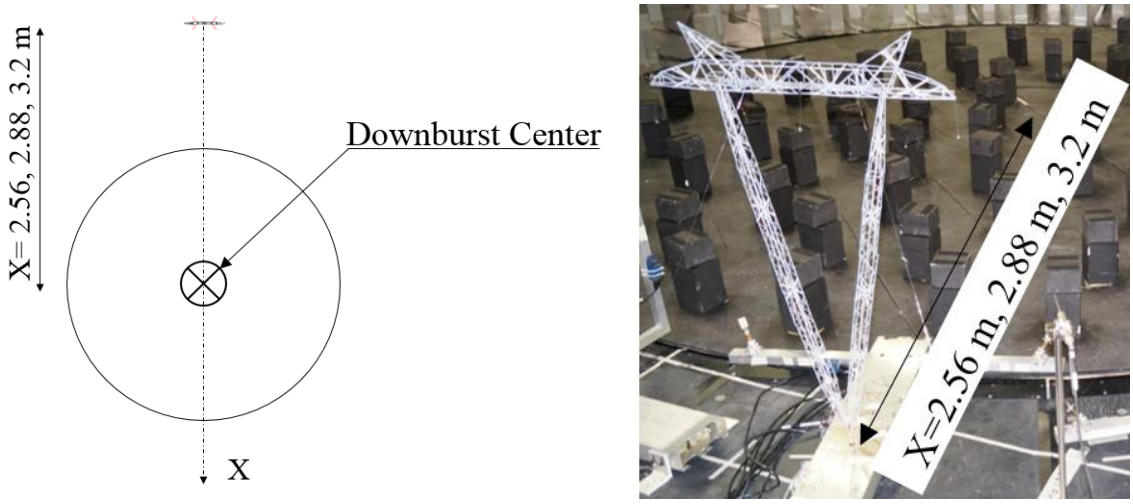

(a) Schematic plan view of layout 1

(b) Layout 1 testing at WindEEE

Fig. 2-21. Test layout 1.

2.3.3.2. Layout 2: Maximum transverse loads (Angle of attack Θ = 0 º)

This layout focuses on evaluating the tower's response when the downburst wind field acts in a transverse direction, Y, relative to the tower and the conductors. Four line spans each of 5 m are considered for this layout. **Fig. 2-22**-a shows the locations of the middle tower with respect to the downburst center at WindEEE. The tower is placed at transverse distances Y= 2.56 m, 2.88 m, and 3.2 m corresponding to distance ratios R/D= 0.8, 0.9, and 1.0, respectively. **Fig. 2-22**-b is a picture of this layout at WindEEE.

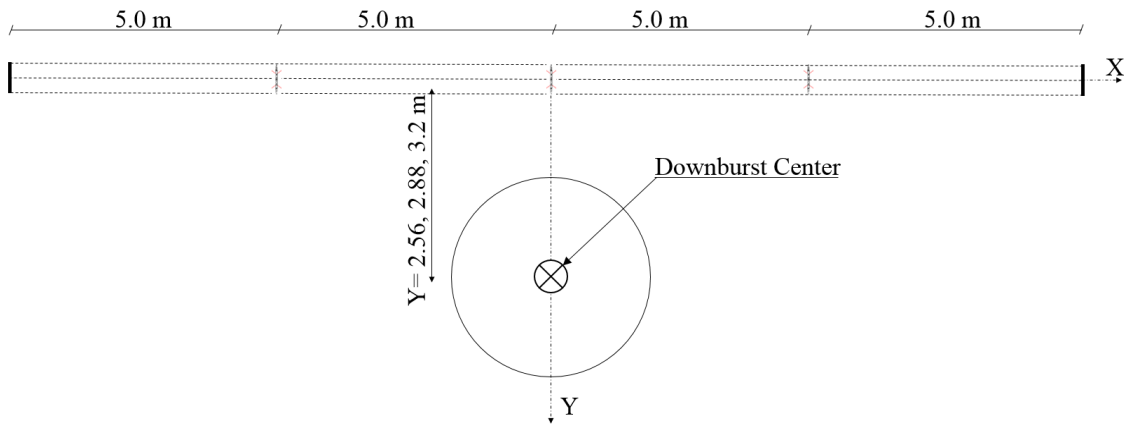

(a) Schematic plan view of layout 2

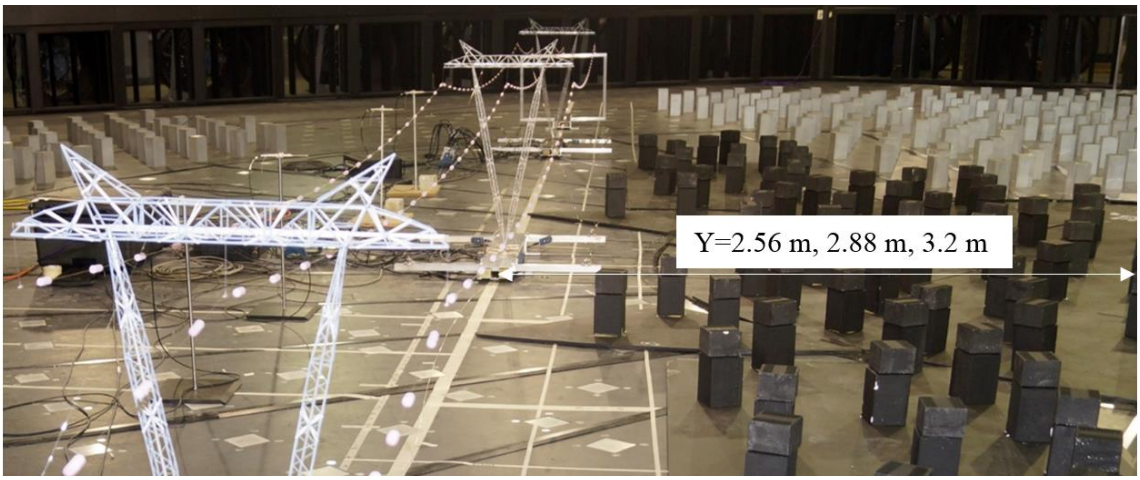

(b) Layout 2 testing at WindEEE

Fig. 2-22. Test layout 2.

2.3.3.3. Layout 3: Maximum oblique loads (Angle of attack Θ = 52 º)

This layout focuses on evaluating the tower's response when a downburst is attacking the line at an oblique angle. The tower is placed at distances (3.125 m, 3.75 m, 4.375 m) and (2.56 m, 2.88 m, 3.2 m) in X and Y directions, respectively, as shown in **Fig. 2-23**-a and **Table 2-4**. This means that the downburst center of the line is located at distances representing the permutation of a distance to span ratio (X/L) of 1.25, 1.5, and 1.75

measured from the tower of interest in X direction and Y/D ratios of 0.8, 0.9, and 1.0 measured from the tower of interest in Y direction.

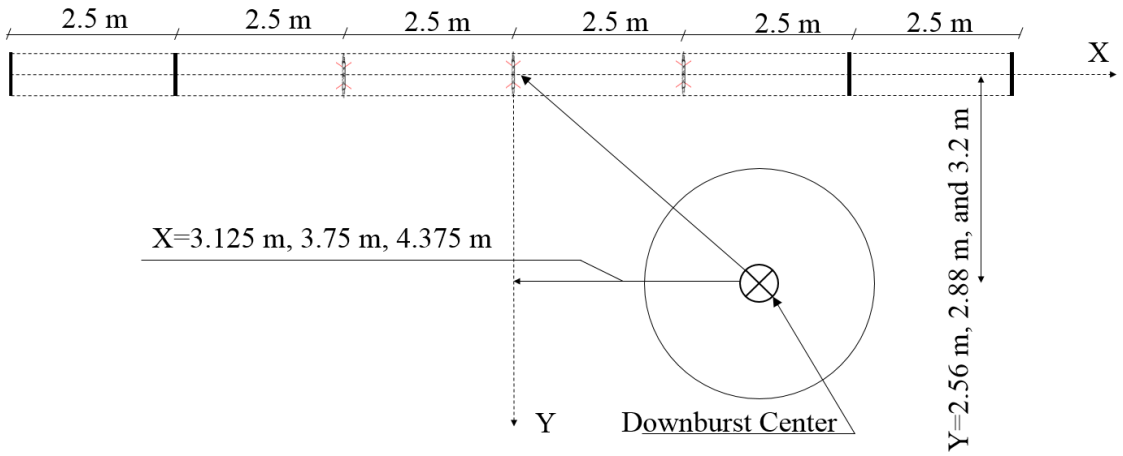

(a) Schematic plan view of layout 3

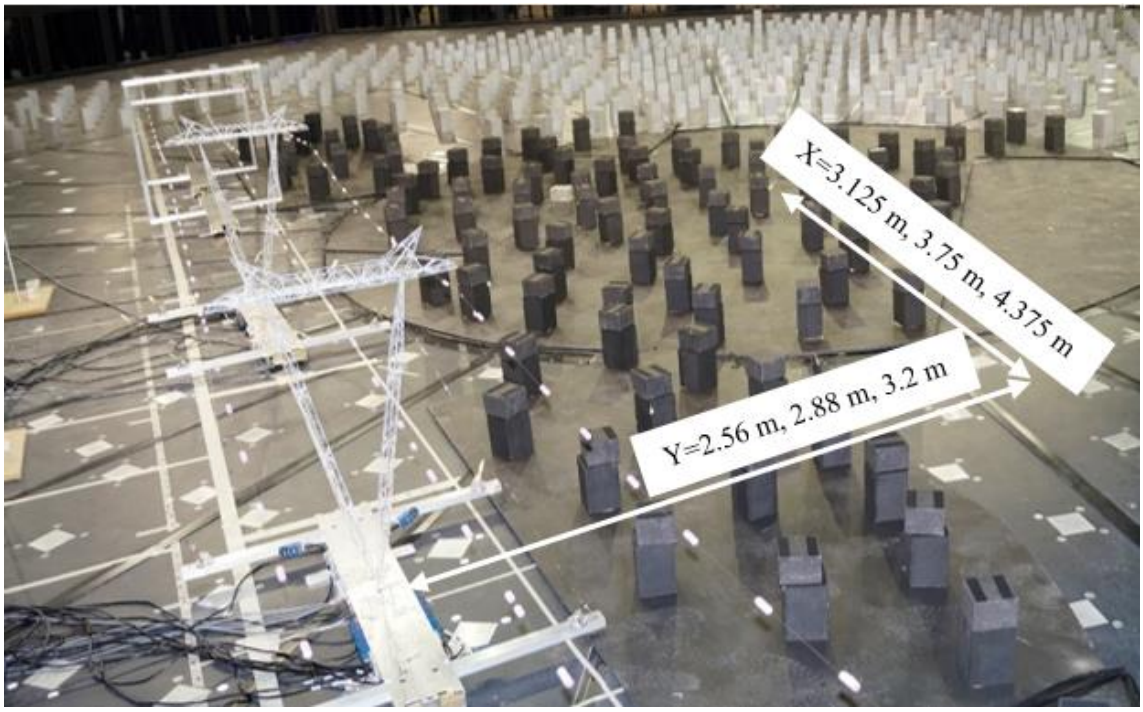

(b) layout 3 testing at WindEEE

Fig. 2-23. Test layout 3.

In the next section, the results obtained from the testing of the described transmission line configurations under downburst loads are discussed with a focus on evaluating the dynamic responses of the tower and the conductors.

2.4. Results and Discussions

A downburst is a non-stationary and dynamic wind system that might result in a non-stationary dynamic structural response. In order to quantify the dynamic response, a decomposition approach of the line response has been adopted and is presented in the following section. The measured responses are first decomposed into mean and fluctuating components. Then, the fluctuating component is decomposed into its background and resonant components. Further, the dynamic effect, expressed by an amplification factor for the tower and for the conductors, is evaluated. Since the tests are conducted for many downburst locations, it is decided to focus only on the critical locations (configurations) resulting in maximum base shear values acting on the tower. As such, those cases are first identified in the next section.

2.4.1. Identification of Critical Configurations

The base shear responses corresponding to all the downburst locations are determined for the case of wind speed V_{RD} = 50 m/s case. **Fig. 2-24** shows the maximum base shear values recorded for those cases. This Figure shows that for Layout 1, the absolute maximum base shear in the X direction (Q_X) occurs when the center of the tower of interest is located at a distance X = 2.88 m (R/D = 0.9) from the downburst center. For Layout 2, the absolute maximum base shear in Y direction (Q_Y) occurs when the center of the tower of interest is located at a distance Y = 2.56 m (R/D = 0.8) from the

downburst center. For Layout 3, the absolute maximum base shears in both the X and Y directions occur when the tower center is located at X = 3.125 m and Y = 2.56 m (R/D = 1.26). Based on these observations, the test data will be processed and decomposed into mean, background, and resonance responses for those cases causing peak responses in the tower for each of the test layouts, i.e., in the case of X = 2.88 m in Layout 1, case of Y = 2.56 m in Layout 2, and case of X = 3.125 m and Y = 2.56 m in Layout 3.

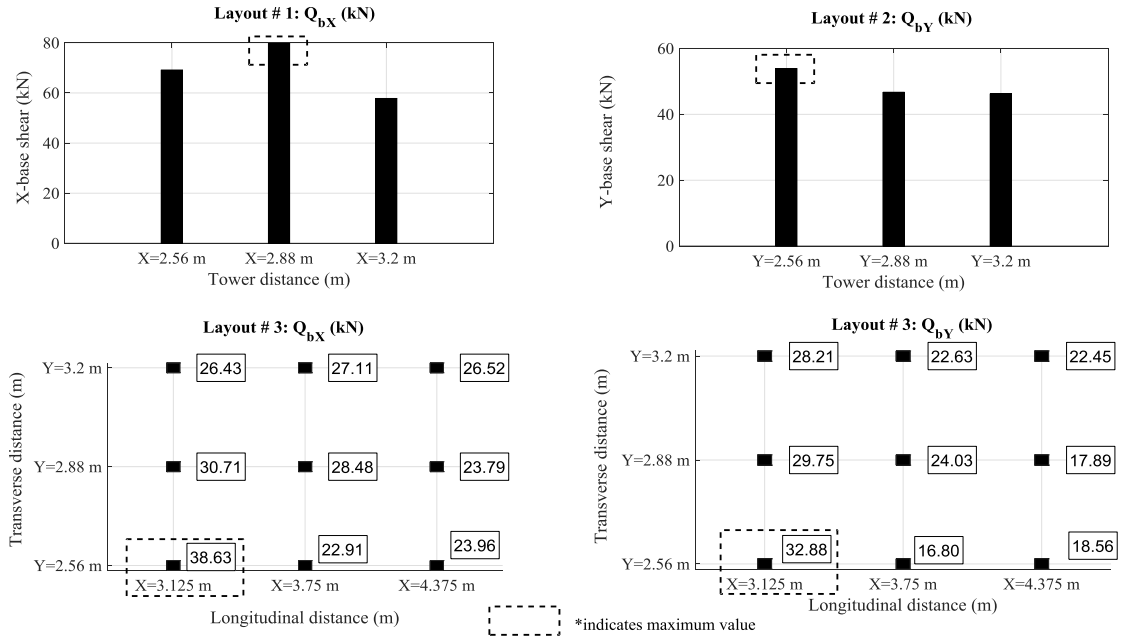

Fig. 2-24. Base shear comparison for the three tested layouts.

2.4.2. Decomposition of the responses

Identifying the resonant component of the structural response due to downburst loads is challenging because of the non-stationarity nature of the wind event. In synoptic wind studies, the resonance is distinguished from the background response by applying the -5/3 law (Kolmogorov Spectrum Theory, 1941) to the power spectral density (PSD) of the fluctuating response. However, the PSD of the fluctuating response induced by downburst winds differs substantially when compared with that resulting from a synoptic

wind (Aboshosha et al. 2015; Solari et al. 2015). In the current study, the approach described in the flowchart shown in **Fig. 2-25** has been developed to extract the resonance component for each of the measured responses.

In this approach, the mean and fluctuating components are separated by extracting the frequencies, which are less than 1.5 times the shedding frequency, i.e. $f_{mean}<1.5\ f_{shedding}$ (step 1 in **Fig. 2-25**). The remaining part of the response is composed of background and resonance responses. In order to distinguish between the background and resonant components, the power spectral density of the fluctuating response and the corresponding frequencies are calculated and plotted using a Fast Fourier Transform application (step 2 in **Fig. 2-25**). The cumulative power spectral density, (cumulative PSD), at each identified frequency is calculated and normalized to the variance of the fluctuating response PSD (step 3 in **Fig. 2-25**). This leads to a cumulative PSD equal to 1.0 at the highest frequency. The average slope of the common logarithmic values of the cumulative PSD is then calculated (step 4 in **Fig. 2-25**). The ratio between the slope of the common logarithm values of the cumulative PSD of the fluctuating response and the average slope is evaluated (step 5 in **Fig. 2-25**). The resonance frequencies are identified when this ratio exceeds a chosen threshold value ($R_{threshold}$) (step 6 in **Fig. 2-25**). This threshold ratio is selected based on a trial and error basis. The criterion in selecting this threshold value is to find the ratio ($R_{threshold}$) above which the resonance contribution remains the same. This implies that when the ratio between the slope of the common logarithm values of the cumulative PSD and the average slope is greater than $R_{threshold}$, the developed approach marks this frequency as a resonance frequency. After identifying the resonance frequencies, a Bandstop filter is utilized to separate the resonance frequencies

from the fluctuating responses and as a result, the background response is identified (step 7 of **Fig. 2-25**). The quasi-static response of the tower is calculated as the linear summation of the mean and the background responses. For the three identified critical downburst configurations, this procedure has been conducted for all the measurements recorded during the tests. Some measurements have shown a high contribution of the resonant component while others did not. Two extreme cases with "no resonance" and "high resonance" responses are presented below. **Fig. 2-26** shows the results of processing the mid-height moment of the tower response at R/D = 0.9 in Layout 1 at V_{RD}=35 m/s. The plot shown in **Fig. 2-26**-a indicates that the cumulative PSD of this measurement is gradually increasing with no sudden change in the slope. This indicates that no resonant response is detected in this measurement for this particular configuration. **Fig. 2-26**-b shows the decomposition of the time history response of the measurement, which also shows that the resonant component of the response is approximately equal to zero. Since no dynamic effect is expected in this case, the quasi-static response is almost equal to the peak response of the structure. On the contrary, **Fig. 2-27** provides the results of processing the base shear measurement of the tower in Layout 2 at R/D = 0.9 and V_{RD}=35 m/s. The cumulative PSD plotted in **Fig. 2-27**-a shows several fluctuations at the frequencies of the distinctive peaks of the PSD. This means that the resonant component significantly contributes to the structural response. **Fig. 2-27**-b shows the time history of the base shear response decomposed into mean, resonant, and background. The figure shows that the resonant component is approximately equal to the background component. As a result, the figure shows that the quasi-static response is less than the peak response.

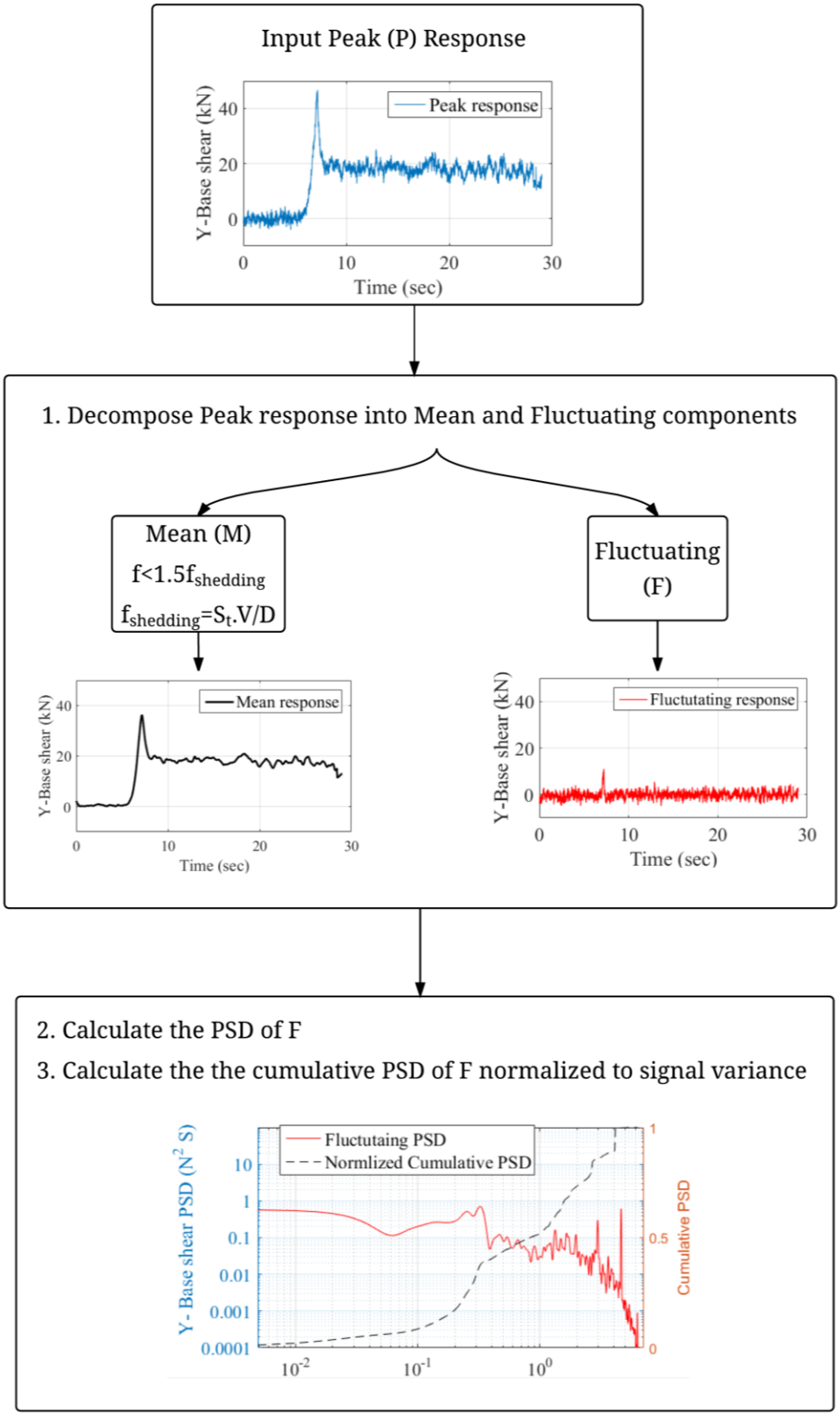
Input Peak (P) Response
Peak response
Y-Base shear (kN)
Time (sec)
1. Decompose Peak response into Mean and Fluctuating components
Mean (M)
f<1.5f_shedding
f_shedding=S_t.V/D
Fluctuating (F)
Mean response
Fluctutating response
2. Calculate the PSD of F
3. Calculate the the cumulative PSD of F normalized to signal variance
Fluctutaing PSD
Normlized Cumulative PSD
Y - Base shear PSD (N^2 S)
Cumulative PSD

4. Calcualte the average slope of the log cumulative PSD

5. Calculate the ratio between the slope of the log cumulative PSD at each of the two successive frequencies and the average slope in the log scale.

6. Ratios greater than a chosen threshold represnets the resonance (R).

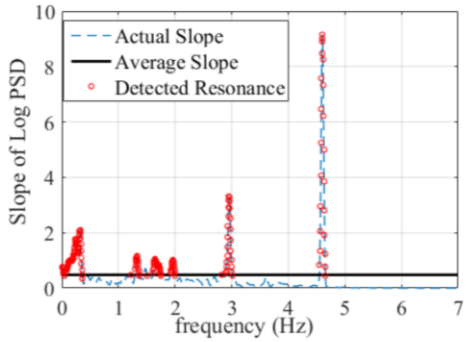

7. Background component (B) is calculated using bandstop filter: B=F-R

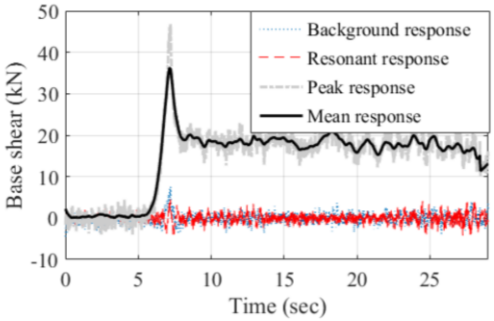

Fig. 2-25. Response decomposition flow chart.

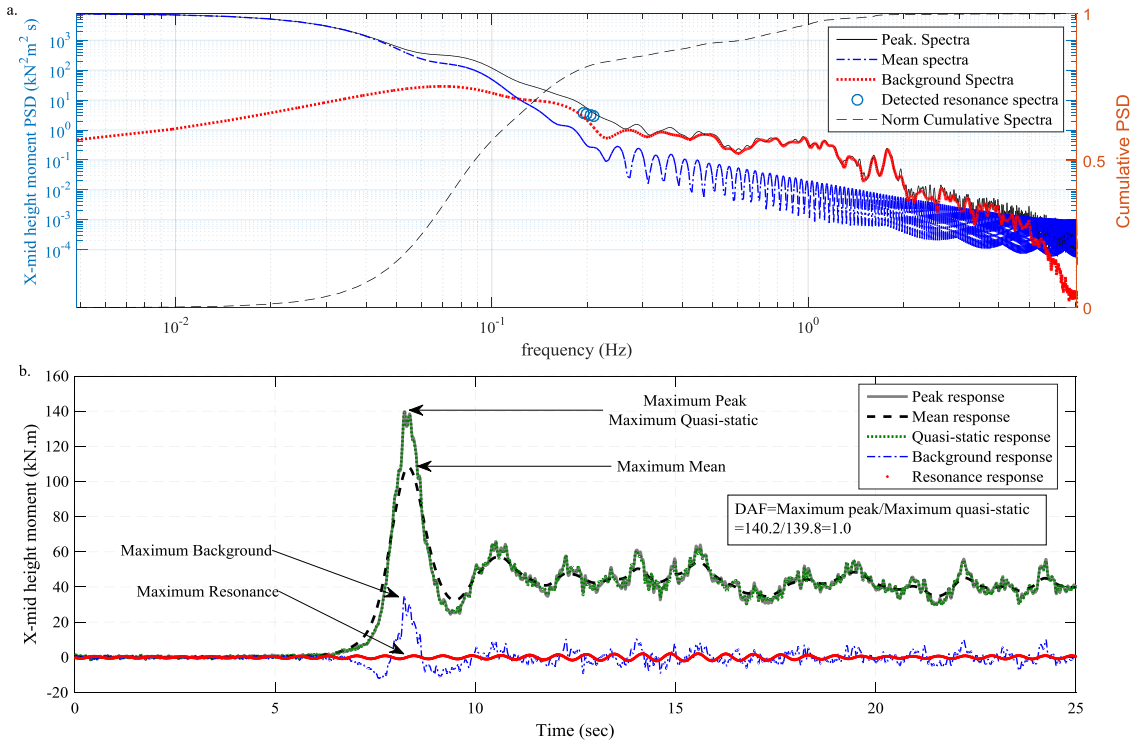

Fig. 2-26. Illustration of "no resonance" response case, in Layout 1, R/D = 0.9 and V_{RD}=35 m/s.

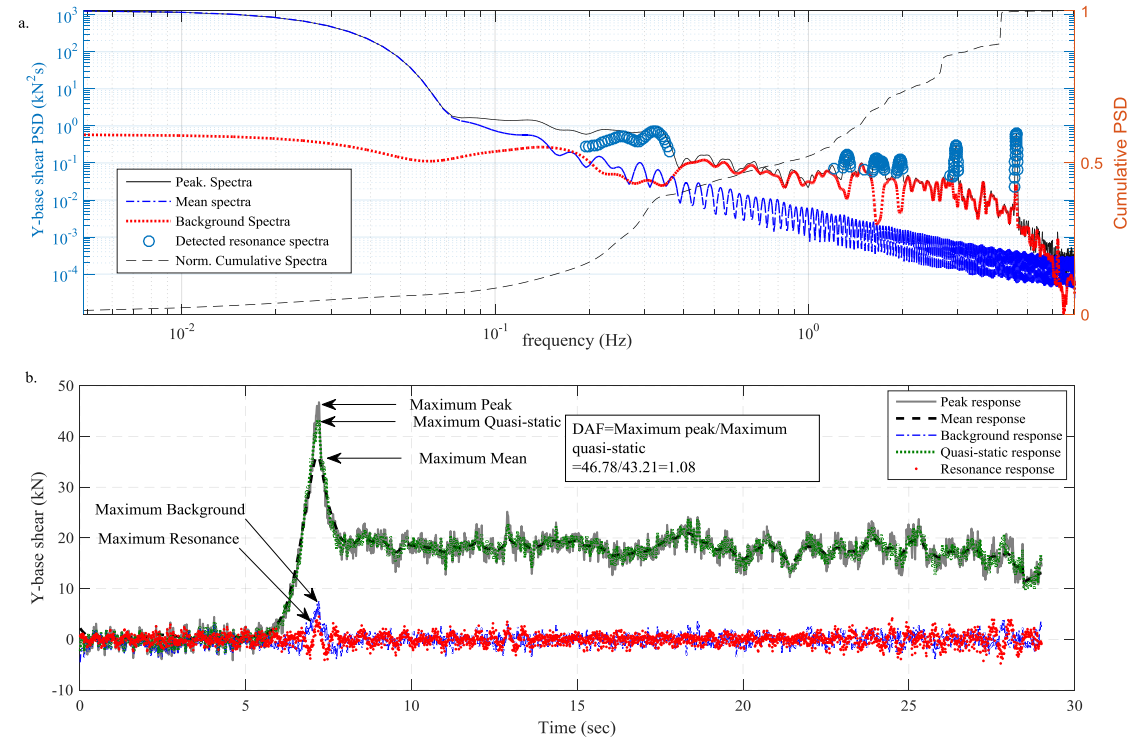

Fig. 2-27. Illustration of "resonance" response case in Layout 2, R/D = 0.9 and V_{RD}=35 m/s.

2.4.3. Quantifying the dynamic effect for different downburst velocities and configurations

The procedure described in the pervious section is applied for other quantities measured in the selected critical configurations of the three test layouts at different downburst velocities. The objective of this section is to show the variation of different components of the response with the downburst velocities. **Fig. 2-28** to **30** show the values of the maximum peak, quasi-static, and mean responses of various measurements under different downburst velocities. In general, the figures show that the responses vary nonlinearly with the changes in the wind speed. In addition, the results reveal that there is no general trend regarding the ratio between the peak and both the quasi-static and the mean responses for the different structural responses measured in various tests. In the next section, a Dynamic Amplification Factor (DAF), expressed as the ratio between the peak and the quasi-static responses, is calculated and used to assess the importance of the dynamic effect for different quantities.

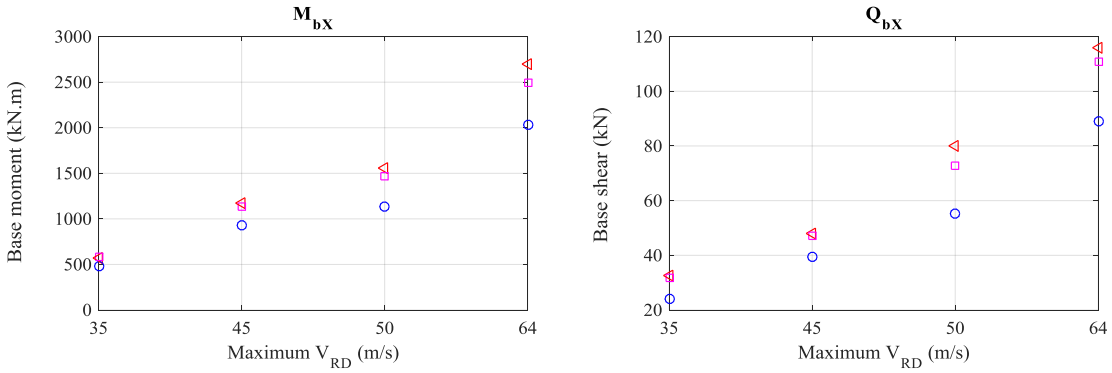

Fig. 2-28. Tower responses of Layout 1 at R/D = 0.9.

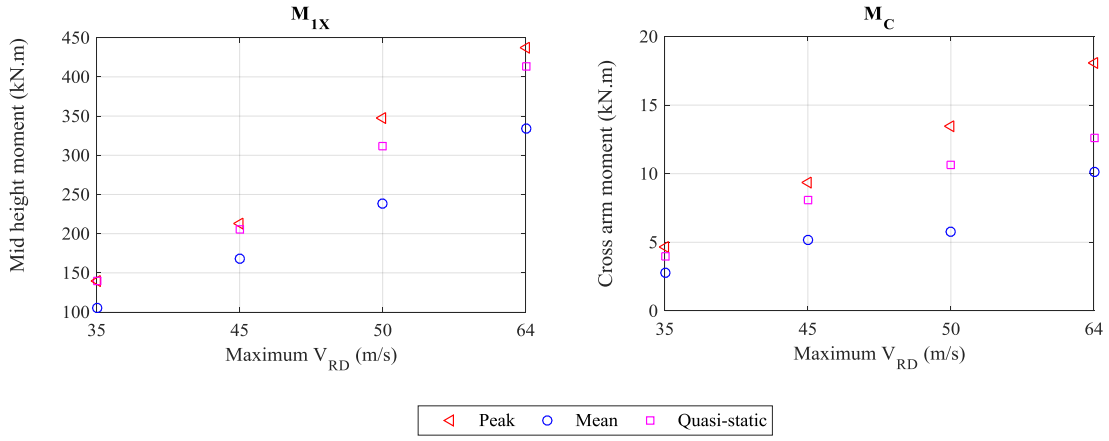

Fig. 2-28. Tower responses of Layout 1 at R/D = 0.9 (Cont.).

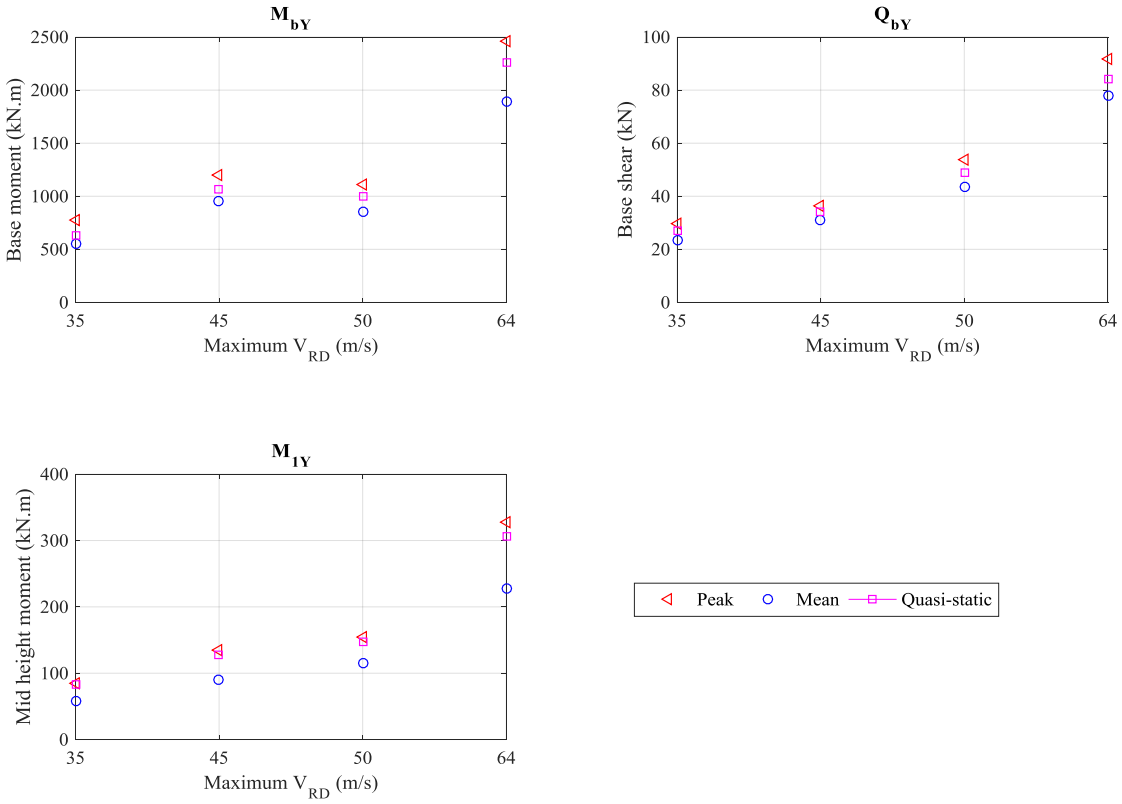

Fig. 2-29. Tower responses of Layout 2 at R/D = 0.8.

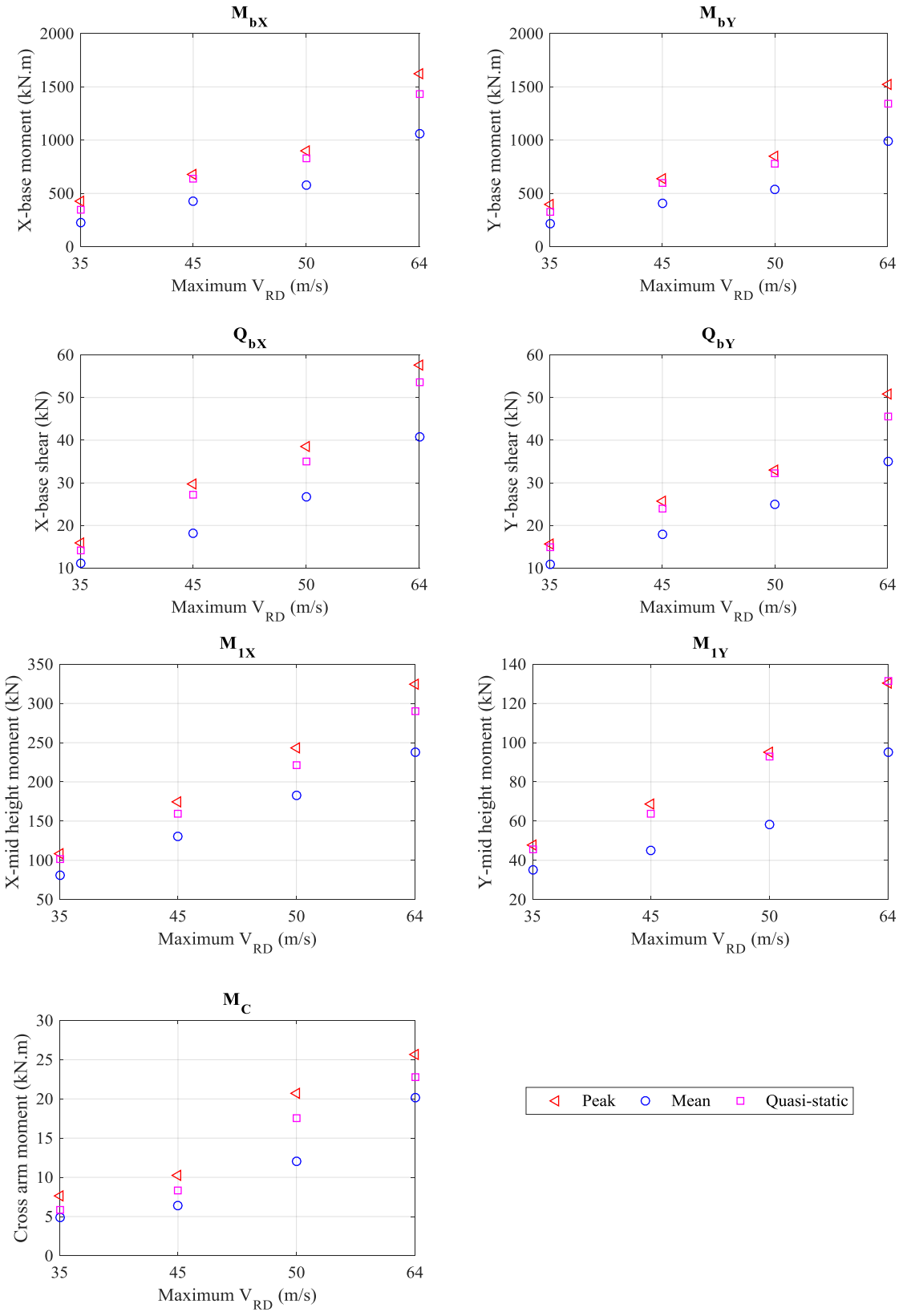

Fig. 2-30. Tower responses of Layout 3 at R/D = 0.8 and X/L = 1.25.

2.4.4. Dynamic Amplification Factor (DAF)

A Dynamic Amplification Factor, DAF, is calculated using **Equation (2-5)**.

$$DAF = \frac{Maximum\ Peak\ response}{Maximum\ Quasi-static\ response} \quad (2\text{-}5)$$

The values of the DAF should be greater than or equal to 1.0. The higher the ratio, the more is the contribution of the resonant response toward the total response. A DAF value of 1.0 indicates that the peak and the quasi-static responses are equal and this implies that there is no dynamic effect.

The variations of the DAF with the downburst velocity obtained from the processing of different measurements of the three considered tests are provided in **Fig. 2-31** and summarized in **Table 2-5**. **Fig. 2-31** shows the DAF for the considered measurements, which are the base moment, the base shear, the mid height moment, and the cross arm moment for four different radial downburst velocities. In **Table 2-5**, the DAF factor is shown for the tower measurements only at the velocity bounds; i.e., at V_{RD}= 35 m/s and 64 m/s.

Table 2-5. DAF analysis.

Layouts	Measurements	DAF		Trend	Remarks
		V_{RD}= 35 m/s	V_{RD}= 64 m/s		
Layout 1	Cross arm moment	1.15	1.15	Constant	High local flexibility
	Base moment	1	1.09	Increasing	
	Mid-height moment	1	1.08	Increasing	
	Base shear	1.03	1.05	Increasing	
Layout 2	Cross arm moment	N/A			
	Base moment	1.23	1.08	Decaying	Aerodynamic damping effect
	Mid-height moment	1.03	1.08	Increasing	
	Base shear	1.09	1.09	Constant	
Layout 3-X	Cross arm moment	1.3	1.13	Decaying	Aerodynamic damping effect
	Base moment	1.23	1.07	Decaying	Aerodynamic damping effect
	Mid-height moment	1.07	1.1	Increasing	
	Base shear	1.13	1.07	Decaying	Aerodynamic damping effect
Layout 3-Y	Cross arm moment	N/A			
	Base moment	1.23	1.08	Decaying	Aerodynamic damping effect
	Mid-height moment	1.04	1.04	Constant	
	Base shear	1.06	1.06	Constant	

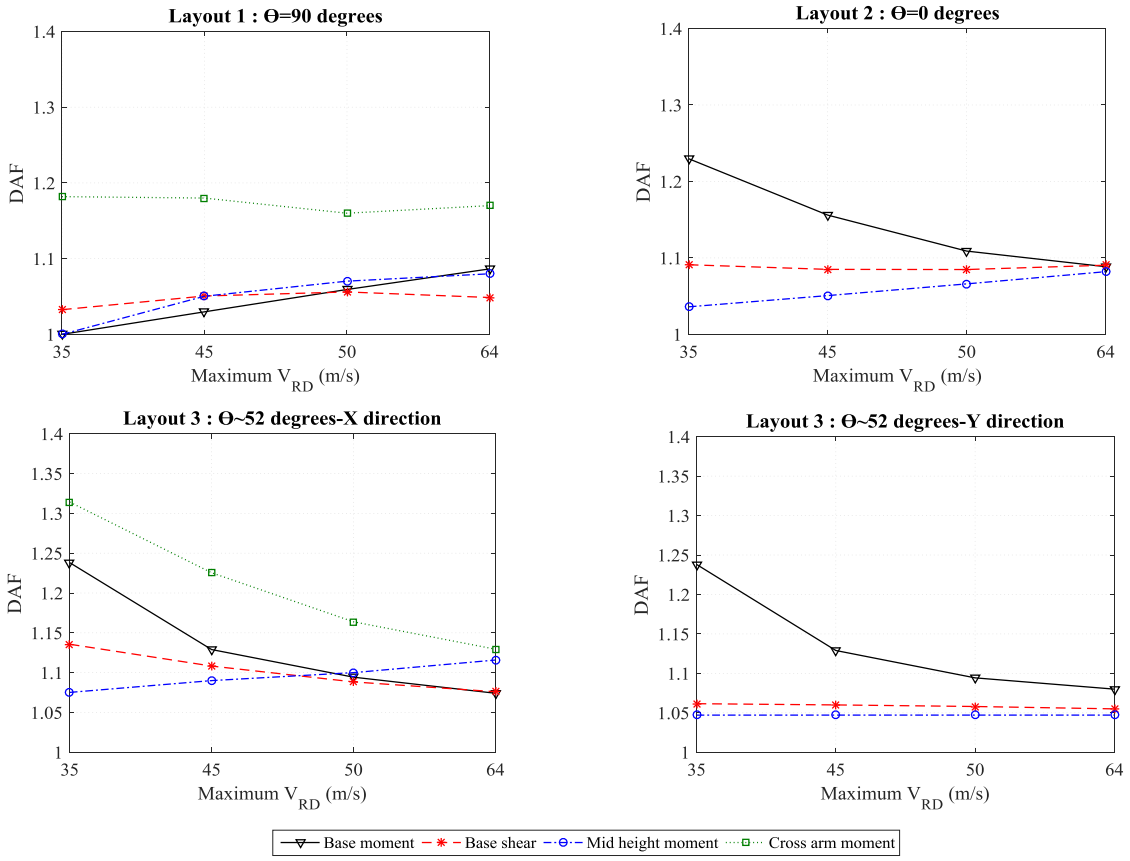

Fig. 2-31. Dynamic amplification factor DAF for the studied layouts.

In Layout 1 (maximum Q_{bX}), where there are no conductors attached to the tower, the DAF factor is found to range between 1.0 and 1.09 for the base moment, between 1.03 and 1.05 for the base shear, and between 1.0 and 1.08 the mid height moment. The DAF of the cross arm moment is found to be higher, in the order of 1.15 due to the relatively higher flexibility of the cross arm system compared to the other zones of the tower especially when the conductors are not attached to the tower; i.e., without lateral bracing. For Layout 2 (maximum Q_{bY}), the DAF factor ranges between 1.23 and 1.08 for the base moment, has a value of 1.09 for the base shear, and ranges between 1.03 and 1.08 for the mid height moment. For Layout 3- in the X direction, the DAF factor is found to range between 1.23 and 1.07 for the base moment, between 1.13 and 1.07 for the base shear,

and between 1.07 and 1.1 for the mid height moment. The DAF of the cross arm moment is found to be higher and ranging between 1.3 and 1.13. For Layout 3- in the Y direction, the DAF factor is found to range between 1.23 and 1.08 for the base moment, and has a value of 1.06 and 1.04 for the base shear the mid height moment, respectively. The results can be interpreted as follows:

- Conductors are more prone to dynamic excitation compared to the tower due to their relatively low natural frequencies. Therefore, DAF is the highest in Layout 3 where two conductor reactions (in X and Y directions) affect the response of the tower.
- When the DAF is affected by the conductor forces, the aerodynamic damping significantly affects the variation of DAF with the change in the wind speed. An expression for the aerodynamic damping, ζ, is given by **Equation (2-6)**, which was derived for the case of a uniform prismatic structure with a uniform flow and drag motion which might be different when compared to the downburst case.

$$\zeta = \left(\frac{C_D}{4\pi}\right)\left(\frac{\rho d^2}{m}\right)\left(\frac{V_{RD}}{f_1 d}\right) \tag{2-6}$$

where f_1 is the conductor's natural frequency; L is the conductor's length (m); m is the conductor's mass (kg); T is the conductor's tension (N), which is calculated using **Equation (2-4)**; C_D is the drag coefficient, which is taken to be approximately 1.0; ρ is the air density, which is taken to be equal to 1.25 kg/m^3, and V_{RD} is the maximum radial velocity at the conductor's level. The ζ expression is inversely proportional to the conductor frequency. It is expected that the value of ζ of the conductors in Layout 3 to be lower than that of conductors in Layout 2 due to the shorter span used in Layout 3. In addition, the increase in the tension force

developing in the conductors under the downburst oblique configuration results in an increase in the conductor's frequency and consequently an additional reduction in the ζ. Accordingly, the total reduction in ζ of the conductors used in layout 3 is expected to be behind the higher DAF value for the cross arm moment.

- The DAF of the mid-height moment has an increasing trend with the increase in the velocity in all the tested layouts. This means that the mid-height moment is not affected by the conductor forces particularly for this transmission line system where the majority of the conductor forces transfer directly to the ground through the guys. The increase in the DAF in this case might be due to the effect of the geometric nonlinearity which results in an increase in the tower deformations and consequently a reduction in the tower's frequency with the increase in the wind speed.
- The DAF of the base shear is affected by both the conductor forces and the tower forces. An increase in the wind speed lead to a reduction in the DAF of the conductor forces and to an increase in DAF of the tower forces. As such, those two effects tend to counter act each other.
- The DAF of the base moment is significantly affected by the conductor's aerodynamic damping where a decaying trend is noticed with the increase of the wind speeds in layout 2 and 3. By noticing that the lever arm of the conductors' forces is larger than that of the tower forces, as shown in **Fig. 2-32**, one can except that the base moment of the system will be affected by the conductor's response more than the base shear.

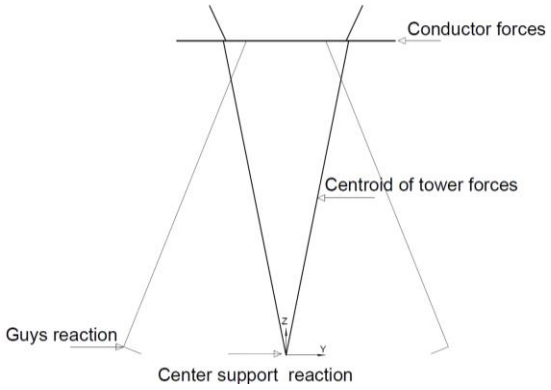

Fig. 2-32. Load path.

In general, at a typical downburst speed, i.e., V_{RD} ~ 50 to 70 m/s, the DAF for the tower and the conductors ranges between 1.1 and 1.15. Despite the difference in the span length used in Layouts 2 and 3, no significant difference in the values of the DAF factors are observed between the two layouts.

2.5. Conclusion

An aero-elastic testing of a multi-spanned transmission line subjected to downbursts is presented. The downburst wind field is generated at the WindEEE dome by pressuring air into the upper plenum first with the louver closed; then the louver is opened to create a downburst flow. The downburst wind field measured at WindEEE is characterized and validated compared to the previous numerical simulation profiles. The measurements show that the turbulence intensity of the downburst radial velocity component ranges between 0.11~0.14, values that are smaller than those for normal wind. The characterization of the downburst yields to identifying the locations of the peak radial velocities. The peak radial velocity is found approximately at a radial distance equal to 0.9 D. This is different compared to the location of the peak radial velocity previously reported by various numerical studies; R = 1.3 D (Kim and Hangan, 2007). This is

attributed to difference in the dimension of the simulation domains; i.e. H/D ratio, used in the numerical studies compared to that dimension used in the current study. A good agreement is found between the vertical profile of the downburst radial velocity obtained in the current study and those profiles developed using previous simulations.

The transmission line system considered in the current study consists of seven towers connected by conductors. The model is constructed and tested at WindEEE using a model length scale of 1:50 and a velocity scale of 1:7.07. The tower is constructed from a spine, representing the flexural and torsional stiffness, and cladding elements, representing the aerodynamics of the tower. The conductors are simulated using a steel wire, representing the line's stiffness, with discrete foam bullets being used to represent the drag. The tower is instrumented to measure the base shear, the base moment, the mid-height moment, the cross arm moment, and the accelerations. Three layouts are tested in the current study representing different configurations of the downburst acting on the line. The study first identified three critical load configurations associated with peak values for the base shear force. For each of the critical configurations, four downburst jet velocities are considered. This allows examining the effect of varying the velocity for each configuration on the response of the line. A decomposition procedure is developed in the current study to extract the resonance contribution from the total response of the tower and the conductors. First, the mean component is decomposed from the peak response. This results in a mean component varying with time and referred to here as "running-mean". The resonance response is then separated from the fluctuating response by identifying the frequencies at which abrupt changes in the slope of the power spectral density of the fluctuating response occur. Based on the results of this decomposition, the dynamic

response of the structure is characterized by calculating a dynamic amplification factor, DAF, which represents the ratio between the peak and the quasi-static responses. The study shows that the resonant response of the tower is in the order of 10~15% for all of the measurements. On the other hand, the conductor responses show a higher resonance contribution at low speeds (maximum ~30% at 35 m/s) with a decreasing trend with the increase in the wind speed (maximum ~12% at 64 m/s). The significant reduction of the conductors' DAF, which is noticed at high speeds, is believed to be attributed to the effect of aerodynamic damping. Therefore, the current aero-elastic study shows that at high downburst wind speed, the response of the tower and the conductors is mainly background. As such, for the development of design procedures by the codes of practice, a quasi-static analysis is sufficient to represent the transmission line system response to downburst loads.

2.6. Acknowledgment

The authors gratefully acknowledge Hydro One Inc., the Natural Sciences and Engineering Research Council of Canada (NSERC), and Ontario Center of Excellence OCE for the in-kind support, their collaboration, and for the financial support provided for this research. The authors also gratefully acknowledge the WindEEE Research Institute experts and technicians for their continuous assistance with the model-gauging, set-up, and testing.

2.7. References

Aboshosha, H., and El Damatty, A., (2015), "Engineering method for estimating the reactions of transmission line conductors under downburst winds", Engineering Structures 99, 272-284.

Aboshosha., H., Bitsuamlak, G., El Damatty, A., (2015), "Turbulence characterization of downbursts using LES", Journal of Wind Engineering and Industrial Aerodynamics 136, 44–61.

American Society of Civil Engineers (ASCE), (2010) "Guidelines for electrical transmission line structural loading", ASCE manuals and reports on engineering practice, No. 74, New York, NY, USA.

Australian Standard/New Zealand Standard (AS/NZS) 7000, (2010) "Overhead line design detailed procedures", Standards Australia Limited/Standards New Zealand, North Sydney, Australia.

Australian Wind Alliance, (2016): http://www.windalliance.org.au/

Chay, M., Letchford, C., (2002), "Pressure distributions on a cube in a simulated thunderstorm downburst - part a: stationary downburst observations", Journal of Wind Engineering and Industrial Aerodynamics 90, 711–732.

Choi, E., and Hidayat, F., (2002), "Dynamic response of structures to thunderstorm winds", Prog. Struct. Eng. Mech. 4, 408–416.

CIGRÉ (Conseil International des Grands Réseaux Électriques/ International Council on Large Electrical Systems), (2009). "Overhead line design guidelines for mitigation of severe wind storm damage" Scientific Committee B2 on Overhead Lines, B2. 06.09.

Darwish, M., and El Damatty, A., (2011), "Behavior of self-supported transmission line towers under stationary downburst loading", Wind and Structures 14(5), 481-4.

Darwish, M., El Damatty A., and Hangan, H., (2010), "Dynamic characteristics of transmission line conductors and behaviour under turbulent downburst loading", Wind and Structures 13(4), 327-346.

Davenport A. (1967), "Gust loading factors", ASCE J Struct Div;93(3), 11–34.

Didden, N., and Ho, C., (1985), "Unsteady separation in a boundary layer produced by an impinging jet", Journal of Fluid Mechanics 160, 235–256.

Donaldson, C., and Snedeker, R., (1971), “A study of free jet impingement, Part 1. Mean properties of free and impinging jets”, Journal of Fluid Mechanics 45, 281–319.

Failure Investigation Report, HYDRO ONE NETWORKS INC. “Failure of towers 610 and 611, circuit X503E – 500 kV guyed towers near the Township of Waubaushene”, Ontario, August 2, 2006”, Line Engineering, 2006.

Fujita, T., (1985), “The downburst: microburst and macroburst”, SMRP Research Paper 210, University of Chicago, USA.

Gattulli, V., Martinelli, L., Perotti, F. and Vestroni, F. (2007), “Dynamics of suspended cables under turbulence loading: reduced models of wind field and mechanical system”, J. Wind Eng. Ind. Aerod., 95(3), 183-207.

Hjelmfelt, M., (1988), “Structure and life cycle of microburst outflows observed in Colorado”, Journal of Applied Meteorology 27, 900–927.

Holmes, J., Hangan, H., Schroeder, J., Letchford, C., Orwig, K., (2008), “A forensic study of the Lubbock-Reese downdraft of 2002”, Wind Structures 11 (2), 137–152.

Ivan, M., (1986), “A ring-vortex downburst model for flight simulations” Journal of Aircraft 23, 232-236.

Kim, J., and Hangan, H., (2007), “Numerical simulations of impinging jets with application to downbursts”, Journal of Wind Engineering and Industrial Aerodynamics 95(4), 279-298.

Kong, L., Jeong, U., and King, J., (2009), “The Hoover Dam bypass project, section model and analysis of equivalent static loads”, The University of Western Ontario, Faculty of Engineering, Research Report, Boundary Layer Wind Tunnel Laboratory (BLWTL) SS15.

Lin, W., Savory, E., McIntyre, R., Vandelaar, C., and King, J., (2012), "The response of an overhead electrical power transmission line to two types of wind forcing" ”, Journal of Wind Engineering and Industrial Aerodynamics 100(1), 58-69.

Loredo-Souza, A., and Davenport, A., (2001), “A novel approach for wind tunnel modelling of transmission lines”, Journal of Wind Engineering and Industrial Aerodynamics, 89(11-12), 1017-1029.

McCarthy, P., and Melsness, M., (1996), “Severe weather elements associated with hydro tower failures near Grosse”.

Momomura, Y., Marukawa, H., Okamura, T., Hongo, E., and Ohkuma, T. (1997)., "Full-scale measurements of wind-induced vibration of a transmission line system in a mountainous area." J.Wind Eng.Ind.Aerodyn., 72(1-3), 241-252.

Shehata, A., and El Damatty, A., (2007), "Behaviour of guyed transmission line structures under downburst wind loading", Wind and Structures International Journal 10(3), 249-268.

Shehata, A., El Damatty, A., and Savory, E., (2005), "Finite element modeling of transmission line under downburst wind loading", Finite Elements in Analysis and Design 42(1), 71-89.

Solari, G., De Gaetano, P., Repetto, M., (2015) "Thunderstorm response spectrum: fundamentals and case study", Journal of Wind Engineering and Industrial Aerodynamics 143, 62-77.

Vermeire, B., Orf, L., Savory, E., (2011), "Improved modelling of downburst outflows for wind engineering applications using a cooling source approach", Journal of Wind Engineering and Industrial Aerodynamics 99, 801–814.

Zhang Y., (2006), "Status quo of wind hazard prevention for transmission lines and counter measures", East China Electric Power 34(3), 28-31.

CHAPTER 3

AERO-ELASTIC RESPONSE OF TRANSMISSION LINE SYSTEM SUBJECTED TO DOWNBURST WIND: VALIDATION OF NUMERICAL MODEL USING EXPERIMENTAL DATA

3.1. Introduction

Downbursts are usually associated with thunderstorms and are defined as localized cold masses of air that impinge towards the ground and then convect horizontally causing high wind speeds (Fujita, 1985). Those high wind speeds can lead to severe damage to various structures including transmission line structures which span over long distances to transport electricity from the source of production to the distributing network. The extension of transmission line systems for over many kilometers increases their vulnerability to be hit by downbursts. Many failure incidents of transmission lines/towers due to thunderstorms were reported in literature. Most recently in 2016, more than 20 transmission towers failed during a series of downburst events in South Australia (Australian Wind Alliance, 2016). In 2005, ten towers failed in JiangSu, China, during a severe thunderstorm as reported by Zhang (2006). Kanak et al. (2007) reported the failure of 18 power towers during a severe thunderstorm in Slovakia that occurred in 2003. Knowing that the failed lines were designed for a wind speed of 44 m/s, the study suggested that the failure of the power lines was due to downburst events of a velocity higher than 44 m/s. In 1996, a series of transmission tower failures in Manitoba, Canada, under severe thunderstorms was reported by McCarthy and Melsness (1996). Similar incident occurred in Ontario, Canada where two 500 kV guyed towers failed during a severe thunderstorm (Hydro One 2006). The failure was found to be localized in these two towers only and none of the towers of the

three other lines at the vicinity of the failed line were affected. Meteorological analysis indicated that a high intensity microburst (i.e. small size downburst) associated with very high wind speeds of ~ 50 m/s took place in the zone of the failed towers (Hydro One 2006). **Fig. 3-1** shows one of the failed towers. The lack of information regarding proper procedure for designing transmission line structures to resist downbursts in addition to the reoccurring failures of the transmission lines during thunderstorms motivated number of researchers to characterize the downburst wind field and to investigate the behavior of transmission line systems under downbursts.

Due to the spatial and temporal localization of downbursts, a limited number of downburst field measurements were reported in the literature such as Northern Illinois Meteorological Research (NIMROD) and the Joint Airport Weather Studies (JAWS) reported by Fujita (1990), the downburst that occurred near Lubbock, Texas in 2002 and reported by Holmes et al. (2008), and the Wind and Ports project reported by Solari et al. (2015). On the other hand, various small-scale experimental studies (such as by Donaldson and Snedeker 1971, Didden and Ho 1985, and Chay and Letchford 2002), and analytical studies (such as Oseguera and Bowles 1988, Chay et al., 2006, and Abd-Elaal et al., 2013) were conducted. Numerical simulations are another tool where various features of the downburst wind field can be modelled including the temporal and spatial variations and the roughness effect. Three numerical simulation approaches are found in the literature as follows: a) the Impinging Jet Simulations (such as by Chay et al., 2006, Kim and Hangan, 2007, Sengupta and Sarkar, 2008, Gant 2009, and Aboshosha et al., 2015); b) the Cooling Source simulations (such as by Mason et al., 2009 and 2010, and Vermeire et al. 2011); and c) the Ring Vortex Simulations (such as by Ivan, 1986 and Savory et al. 2001).

Despite the severity of downburst effects on transmission line structures, no sufficient information is available in the design guidelines to account for downbursts. Few number of studies investigated the effect of downburst winds on transmission line structures. Savory et al. (2001) conducted a failure analysis on a single transmission tower subjected to both tornado and downburst loads. The study reported that the considered tower was more vulnerable to tornado loading compared to downburst loading. However, this study did not consider the conductor forces, which are expected to be more significant in the case of downbursts because of their large size compared to tornadoes. Most of the structural studies, such as Wang et al. (2013), Yang and Zhang, (2016), and Mara et al. (2016), utilized the vertical wind profile of the peak radial velocity, V_{RD}, of the downburst while ignoring the spatial effect of downbursts. Shehata and El Damatty (2007 and 2008), Darwish and El Damatty (2011), and Aboshosha and El Damatty (2015) indicated the dependency of downburst loads on the event size (i.e., downburst diameter, D) and its relative location to the tower of interest, which can be defined by the polar coordinates R and Θ as shown in **Fig. 3-2**. This means that in order to estimate the maximum internal forces that can develop in a transmission line system, an enormous number of loading scenarios should be considered. Those loading scenarios should consider the variations in D, R, Θ, and the temporal variation of the downburst velocities. Also, the properties of the transmission line system affect the external wind forces applied on the system as well as the internal forces distribution.

Fig. 3-1. Guyed tower failure (Hydro One report, 2006)

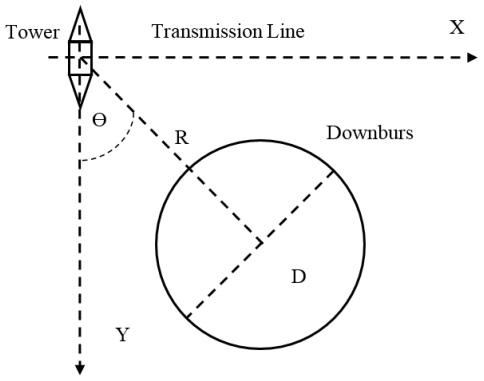

Fig. 3-2. Downburst characteristic parameters

An extensive research program started and is still going by the authors' research group focusing on studying the response of transmission line structures under downbursts and tornadoes. The research started numerically and then extended recently to include experimental studies such that the one reported in the previous chapter. This research led to the development of a comprehensive and unique computational code, called "HIW-TOWER", which was used by a number of companies in Canada in analyzing transmission line structures under downbursts and in designing them to sustain such events. The program "HIW-TOWER", incorporated the spatial and the time variation of downburst wind field based on the Computational Fluid Dynamics (CFD) simulation conducted by Kim and Hangan (2007) using both the impinging jet and the RANS approaches. This CFD data was validated by comparing the vertical profile of the peak radial velocity to previous experimental simulations (Donaldson, 1971 and Didden and Ho 1985) and to an empirical expression (Wood, 2001). This CFD data was incorporated into a finite element model (FEM) developed in-house by Shehata et al. (2005). The structural part of this numerical model was validated through comparison with bench mark numerical problems reported in the literature. The computer code was then updated by incorporating CFD data based on

Large Eddy Simulations (LES) conducted by Aboshosha et al. (2015). The advantages of the LES method is that it can model different terrain effects and can also predict turbulence. An experimental program was recently conducted and reported in the previous chapter at a unique large-scale testing facility, called the WindEEE dome, at the University of Western Ontario, and the results were used to validate the LES simulations developed by Aboshosha et al. (2015). Another update of the computer code was conducted by incorporating a semi-analytical approach developed by Aboshosha and El Damatty (2014) for the simulation of the behaviour of the conductors under downburst loading instead of modelling the conductors using finite element modeling. This led to a significant enhancement in the efficiency of the computer code in terms of a reduction in the computational time, since the prediction of the maximum effects of downbursts on transmission line structures requires conducting a large number of non-linear time incremental analyses as will be explained later. Aboshosha and El Damatty (2014) validated their semi-analytical solution through a comparison with the results obtained from modelling conductors using non-linear finite element code.

It is clear that the validation of the comprehensive computer code was conducted on individual components separately. With the availability of a large-scale testing facility, the WindEEE dome, an opportunity exists to validate the entire numerical code through a comparison with the results of the downburst tests conducted on relatively large-scale aero-elastic model at WindEEE. The validation of the numerical model is not only conducted through comparison between measured and calculated quantities, but also through an assessment for the ability of the model to predict the downburst locations leading to maximum effects on transmission line structures.

The paper starts by providing a brief description of different components of the numerical model. The experiment conducted at WindEEE is then briefly described including the wind field, the tested aero-elastic model, instrumentation, and the test plan. The test results are then presented and used to identify the critical downburst locations causing the maximum line response. The tested transmission line system is then modeled using the previously developed numerical models and comparisons are carried out between the test and the numerical results. The conclusions drawn from the study are then presented.

3.2. Brief description of the numerical tools

In this Section, a brief description of the numerical models developed by Shehata et al. (2005) and Aboshosha and El Damatty (2014) to analyze transmission lines under downburst winds is provided. Those models can be used to analyze the tower and the conductors under downbursts quasi-statically. Since the downburst field was scaled up to the gust velocity, the quasi-static analysis implicitly considers the background component of the turbulence. The models neglect the resonant response of the towers and the conductors. This was justified in several studies such as Sheheta and El Damatty (2007) and Aboshosha and El Damatty (2015) due to the relative high frequency of the tower and the existence of high aerodynamic damping of the conductors which attenuates their vibrations (Holmes 2008, Aboshosha and El Damatty 2015). The experimental study reported in the previous chapter has shown that the resonant response at high wind speeds does not exceed 20% of the total response. Given the significant uncertainty in the magnitude of the downbursts, this value can be neglected from the practical point of view.

3.2.1. Tower simulation using finite element model (FEM)

This finite element model was developed by Shehata et al. (2005) to simulate the tower members. In their model, the tower members were modelled using two noded linear three dimensional frame elements with three translation and three rotation degrees of freedom at each node. A 2-D nonlinear consistent beam element, developed by Koziey and Mirza (1994) and modified later by Gerges and El Damatty (2002) to include the geometric nonlinear effect, was used to model the conductors. In order to predict accurately the forces transmitted from the conductors to the tower, Shehata et al. (2005) recommended to consider three conductor spans on each side of the tower. In addition to the geometric nonlinearity, the model considered the effect of pretension forces, sagging, and the insulator flexibility. Shehata et al. (2005) utilized the CFD model developed by Hangan et al. (2003) to simulate the spatial and the temporal variations of the mean component of the downburst wind field. The analysis required developing a scaling-up procedure in order to transform the model-scale wind field to full-scale. The scaling procedure involved converting the radial and vertical dimensions of the wind field, the wind speed components and the time, from the model-scale to the full-scale. The conversion approach depends on the assumptions made regarding the full-scale diameter and jet velocity of the acting downburst. This means that the same CFD model was used to produce various downburst events by varying the jet velocity and the diameter of the event. This allowed Shehata and El Damatty (2007) to conduct an extensive parametric study to assess the behaviour of a guyed transmission line system subjected to a generic downburst. The analysis considered permutations between the following variations:

a. Downburst diameter varying from 500 m to 2000 m.

b. Distance ratio R/D varying from 0 to 2.2.

c. Angle of attack Θ varying from 0° to 90°.

For each load case, nonlinear analyses considering the entire time history of the wind speeds were quasi-statically conducted for the conductors and the ground wires to evaluate the conductor reactions. The conductor's reactions were then reversed and applied on the tower together with the downburst wind forces acting on the tower members and linear static analyses were then conducted.

Using the numerical approach, Shehata et al. (2005) found that the tower performance against the downburst events is affected not only by the wind intensity but also by the downburst location. Shehata and El Damatty (2007) emphasized on this finding when they identified a unique critical load case that was believed to be the reason of the failure of Manitoba Hydro towers in 1996 (McCarthy and Melsness,1996). This failure occurred in the cross arm zones. Shehata and El Damatty (2007) reported that this failure occurred under the oblique case of downburst when the touchdown point of the downburst was located at an angle of attack ranging between 15°~ 45° measured from the tower of interest. Although Shehata et al. (2005) model was able to study the behaviour of the transmission line system using the extensive parametric study, the model was computationally expensive. This was mainly due to the iterative nonlinear analysis required for the conductors. This motivated Aboshosha and El Damatty (2014) to develop a semi-analytical technique to analyze the conductrors as explained in the next section.

3.2.2. Conductors semi-analytical technique

Aboshosha and El Damatty (2014) developed a semi-analytical closed form solution to accurately and efficiently analyze multi-spanned conductors when subjected to downburst loads. The model required solving a set of equations to estimate the unknown displacements at the insulator-conductor connection points. By limiting the unknown displacements to degrees of freedom at the conductor's supports, a significant reduction in the computational time was achieved compared to nonlinear finite element analysis. The technique is able to determine the response under non-uniform loads in both the lateral and vertical directions which taking into account the insulator's flexibility, and pretension force in the conductors. Aboshosha and El Damatty (2014) derived six equations to solve the six unknowns (three displacements and three reactions) at the conductor-insulator points by considering the following: two equations resulting from the moment equilibrium of the conductors, one equation resulting from equating the conductor length with the integral of the deformed curve, and three equations resulting from the moment equilibrium of the insulator. The initial displacements were assumed first, then the reactions R_y (transverse direction) and R_z (vertical direction) were updated. This was followed by solving for the reaction R_x (longitudinal direction) and d_x (longitudinal displacement) iteratively, then updating the displacement components d_x, d_y and d_z. The whole process is repeated until convergence occurs. This technique showed superior performance (around 180 time faster) when compared to finite element analysis of transmission lines conductors. More details about the technique can be found in Aboshosha and El Damatty (2014).

3.3.Wind Tunnel Testing at WindEEE

3.3.1. Downburst wind field

The WindEEE dome is utilized to simulate a lab-scale downburst. WindEEE has a hexagonal testing chamber with a maximum width of 25 m and a height of 3.8 m as shown in **Fig. 3-3**. Along the perimeter of the testing chamber, 100 reversible fans exist to produce large scale wind profiles. To produce high intensity wind fields such as tornadoes and downbursts, the chamber is attached to an upper plenum supplied by 6 fans and a circular nozzle called the bell mouth.

To form a downburst with a chosen intensity, the air inside the upper plenum is pressurized by running the upper plenum fans together with the fans mounted on the walls of the testing chamber with a specific electricity power, then the bell mouth is opened suddenly to release the air from the upper plenum to the testing chamber. The released air impinges towards the ground of the test chamber and forms the downburst. The diameter of the bell mouth D is chosen to be 3.2 m, which leads to a height to diameter ratio of 1.2. Such a ratio is within the typical height to diameter H/D ratios of a real downburst that was reported to be between 1.0~4.0 (Hjelmfelt, 1988). **Fig. 3-4** shows the formation of the downburst at the WindEEE dome. After the downburst is formed, it interacts with the roughness elements placed on the floor of the test chamber. These roughness elements can be controlled automatically to represent various terrain exposures. In the current study, the roughness element size is selected to be 0.15 m to simulate the open terrain exposure.

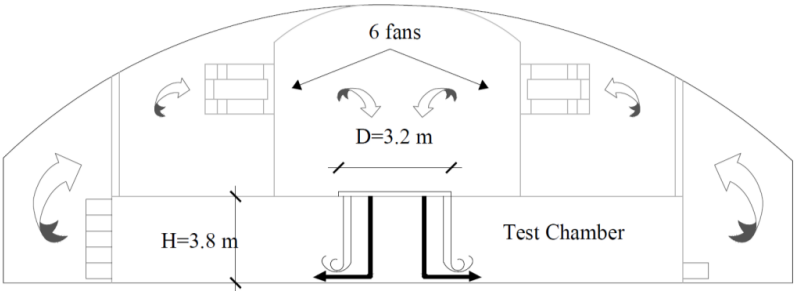

(a) Elevation WindEEE chamber

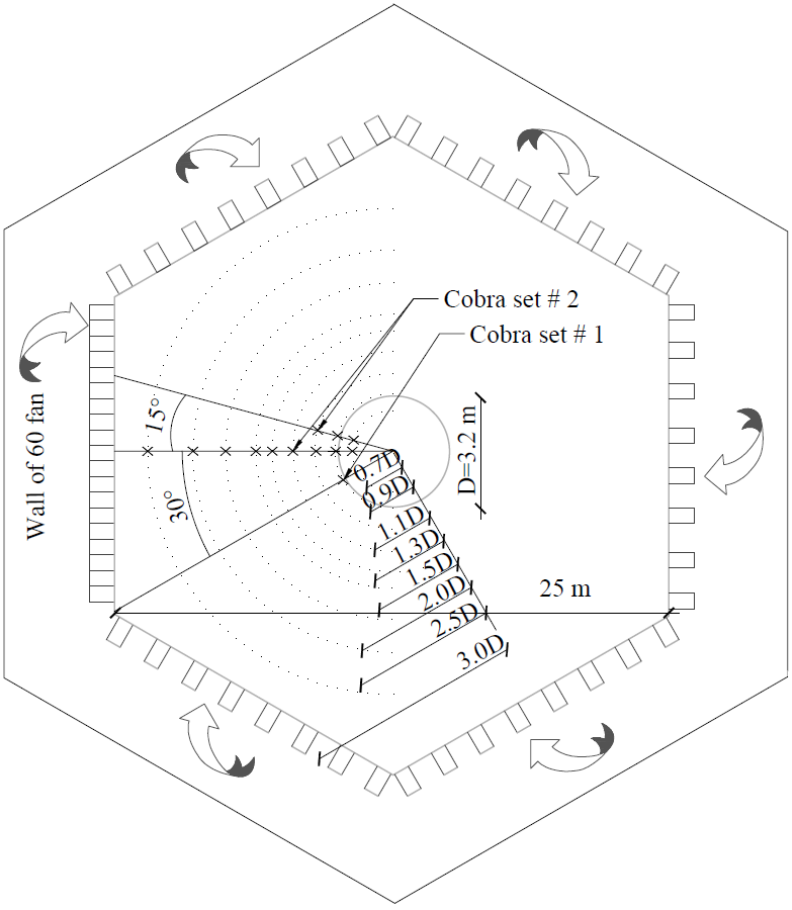

(b) Plan view of WindEEE chamber

Fig. 3-3.Testing chamber

Fig. 3-4. Downburst formation snapshot at WindEEE

The downburst wind field at the WindEEE dome is measured at various angles and radii relative from the center of the downburst to assess the homogeneity of the flow and to evaluate the variation of the wind field with the change of the distance from the center of the touchdown point of the downburst. The flow field is measured using two sets of cobra probes with a sampling frequency of 156 Hz. Each cobra probe set consists of six three-dimensional probes mounted on a column at heights of 0.1, 0.2, 0.43, 0.67, 0.9, 1.0 m. **Fig. 3-3** shows the selected locations of the cobra probe sets while **Fig. 3-5** shows a typical probe set.

During the measurements, one set is always located at a radius of 0.9D and an angle of -30, where the angle is measured from the line passing through the center of downburst perpendicular to the wall of the main fans assuming positive sign for clockwise direction, while the other set is movable. The movable probe set is placed at radii of 0.7D, 0.9D, 1.1D, 1.3D, 1.5D, 2.0D, 2.5D, and 3.0D at an angle of 0 as well as radii of 0.7, 0.9, 1.1 at an angle of +15. This is done to correlate between the time histories of the radial velocity

resulting from different events. The measured speeds recorded from the two cobra sets are correlated by unifying the time instance corresponding to the peak happening at probe set no. 1 for different downburst simulations. An example of the time history of the radial velocity, V_{RD}, is shown in **Fig. 3-6**. The figure shows V_{RD} at a point of X=0 m and Y= 2.88 (R=0.9D) measured from the downburst center at a height of Z=0.2 m. The velocity measurement at this point is recorded twice for two different downburst simulations, labeled test 1 and test 2 in **Fig. 3-6**, to ensure that the test is repetitive. The figure shows a minor difference of 3% between the peak radial velocities recorded for the two downburst simulations which means the test is reasonably repeated. The time shift between the peaks of the two tests, Test 1 and Test 2 in **Fig. 3-6**, is expected since the time instant of opening the bell mouth and the time instant of recording the velocity are manually controlled.

Downburst wind velocities are processed and decomposed into mean and fluctuating components. The mean component of the velocity is usually named as "running-mean" or the "non-stationary mean" as a result of the time dependency of the downburst velocities (Choi and Hidayat, 2002, Holmes et al. 2008, Kwon and Kareem, 2009). The running mean wind speed of the downburst is extracted using the approach described by Aboshosha et al. (2015) and explained and validated in the previous chapter. The mean radial velocities are extracted from the measured wind field for the measured radii distances. **Fig. 3-7** shows the evolution of the vertical profile of the mean radial velocities, normalized to the maximum value of V_{RD}, for the different R/D ratios for an open terrain. The figure is developed at the time instant, 4.84 sec (model-scale), corresponding to the maximum radial speed measured in the entire wind field which is fount to take place at R = 0.9D and Z = 0.03. **Fig. 3-8** shows the instantaneous vertical profiles of the mean V_{RD} normalized to the

maximum mean V_{RD} for distance ratios of R/D equal 0.7 to 3.0. More information regarding the wind field is discussed in the previous chapter.

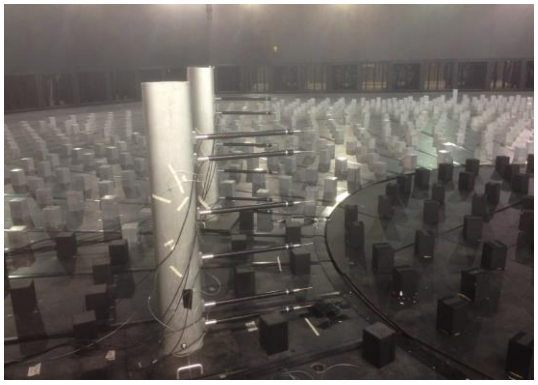

Fig. 3-5. Wind Field measurement using cobra probe devices

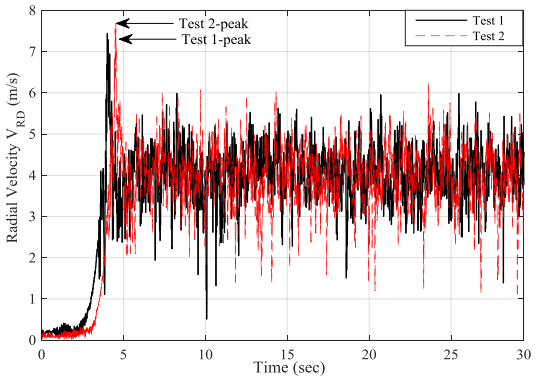

Fig. 3-6. Repeatability of the downburst wind field

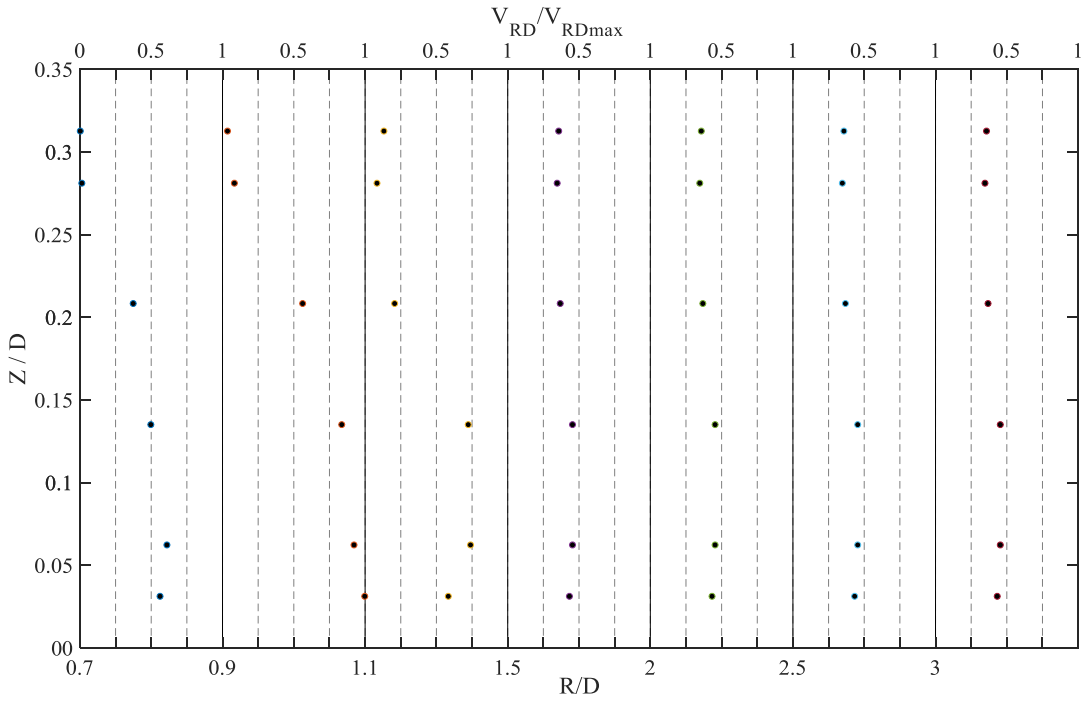

Fig. 3-7. Evolution of downburst radial profiles at time = 4.84 seconds

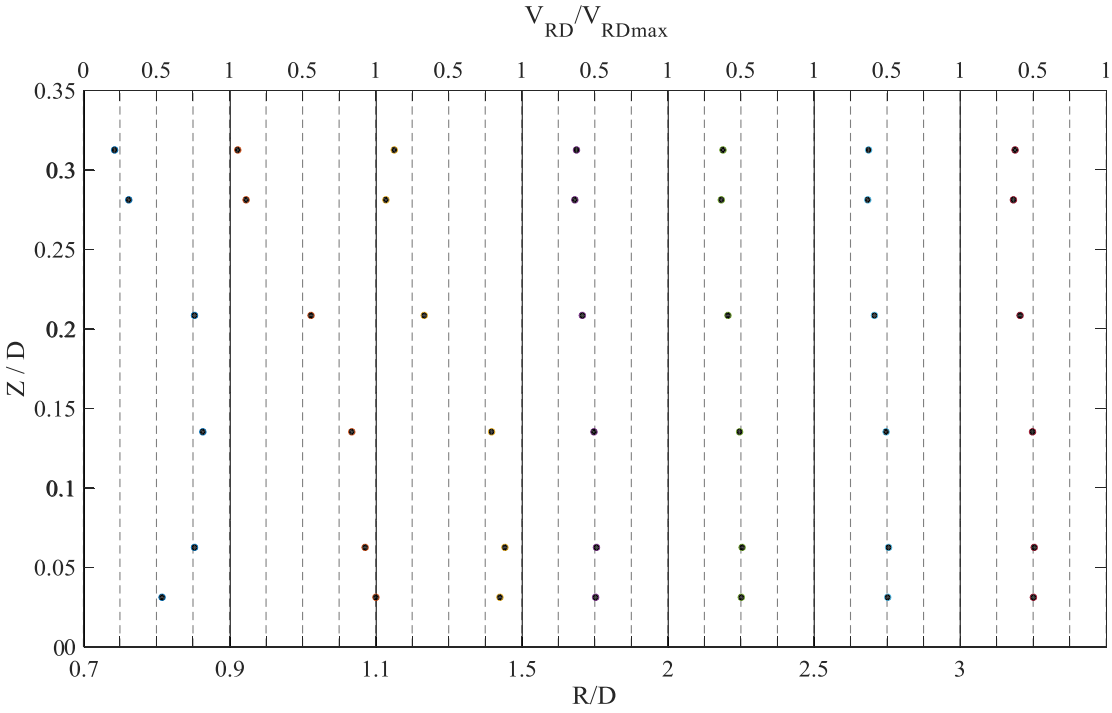

Fig. 3-8. Instantaneous of radial wind profiles

3.3.2. Aero-elastic transmission line model

A brief description of the full scale transmission line system followed by a description of the aero-elastic model and a summary of the instrumentation employed to acquire the test measurements is provided. More information can be found in the previous chapter of this study.

3.3.2.1. Full-scale transmission line system

The current study utilizes the aero-elastic transmission line designed and reported in the previous chapter which consists of seven towers as shown in the test layout provided in Fig. **3-9**. A three-dimensional perspective of the line tower is shown in **Fig. 3-10**. The global axis system used in the current study is shown in **Fig. 3-10** where the X-axis

represents the direction of the transmission line, the Y-axis is the direction perpendicular to the line direction, and the Z-axis is the vertical direction. The tower is supported by 4 guys and carries three conductor bundles at the insulators; two at the tip of each cross arm and one at the center point of the main girder. Two span cases are considered in the current test; L = 125 m or 250 m with a sag at the mid-span of 3.25 m or 6.5 m, respectively. Although this is less than the typical span length used for such towers (i.e. ~200-500 m), it is still practical and it represents the spans used in some cases. A pretension force of 11 kN is applied to all the guys. The tower is resting on the ground on a hinged support that allows the rotations at the tower center while preventing the displacements. **Fig. 3-11** shows a photo of the tested line.

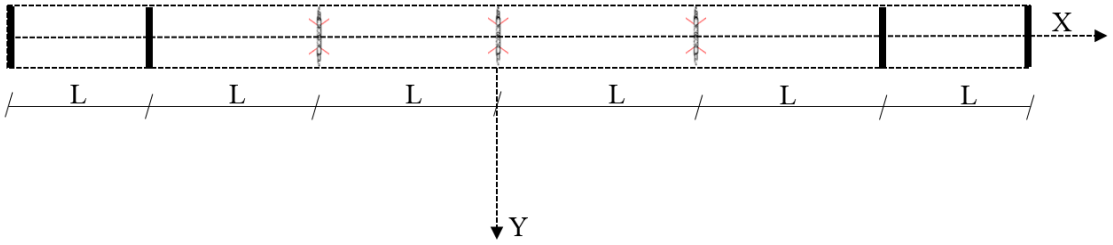

Fig. 3-9. Schematic of the test layout

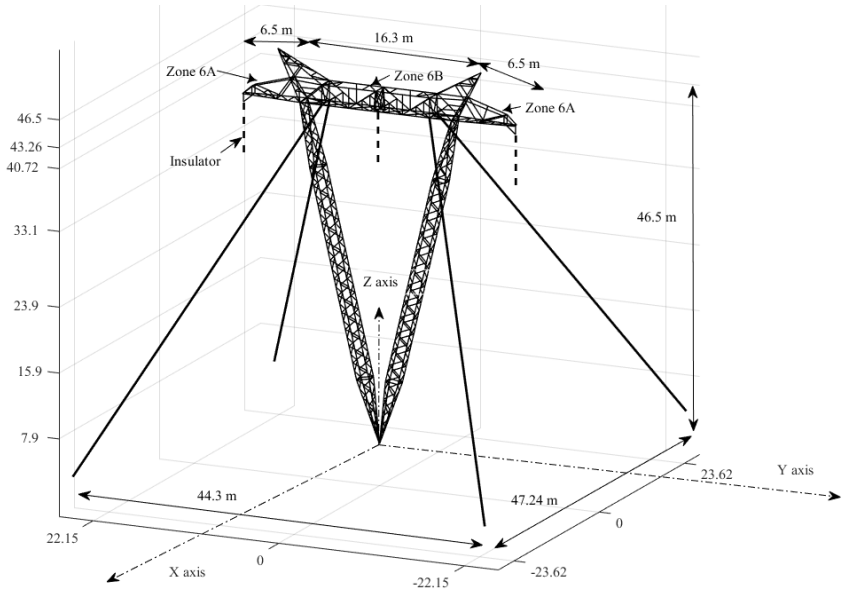

Fig. 3-10. 3-D view of the prototype tower

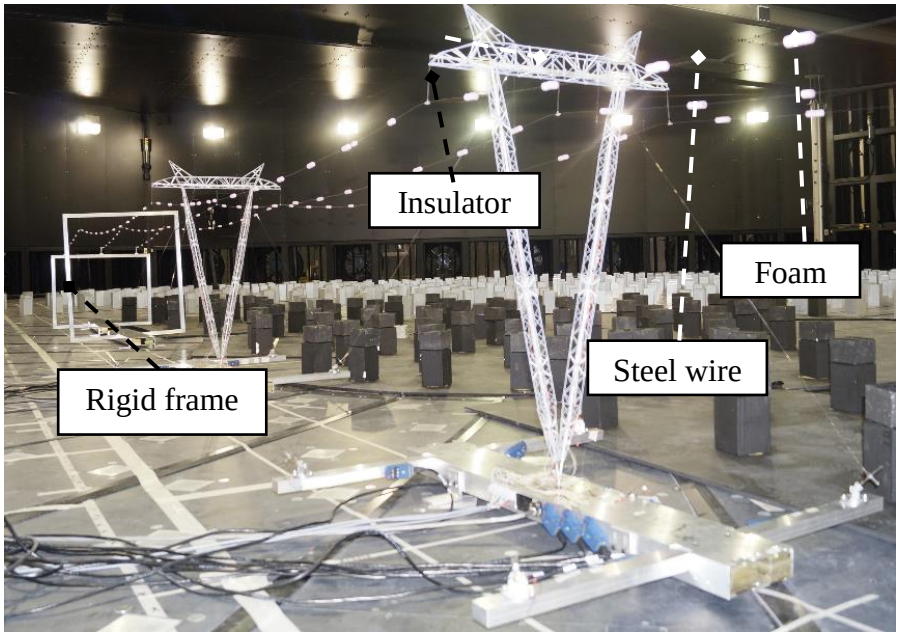

Fig. 3-11. Half-length of the assembled line

3.3.2.2. Aero-elastic modelling of the line system

The aero-elastic model is constructed at a length scale of 1:50 and a velocity scale of 1:7.07. The scaling ratios of all other forces and stiffness are given in the previous chapter.

The model of a single tower, such as towers A to C in **Fig. 3-9**, is comprised of the following components: a) an aluminum spine designed to model the lateral and torsional stiffness of the tower system, b) non-structural sections made of plastic, referred to as cladding, attached to the spine to obtain the correct distribution of masses and drag forces. Dimensions of the aluminum spine and the conductors are given in the previous chapter. The conductor bundle is simulated using a steel wire in addition to discrete aerodynamic drag elements to simulate the mass and the drag of the conductor bundle as shown in **Fig. 3-11.** The stiffness of the insulators is represented by steel rod as shown in **Fig. 3-11**. The spans of the aero-elastic line considered in the current study are 5 m and 2.5 m representing a full-scale spans of 250 m and 125 m, respectively. This means that the span to diameter ratio L/D is equal to 1.5 to 0.7, respectively.

The boundary condition of the line is satisfied using a two-degree of freedom gimbal system, 2D Universal Base Support, at the tower center together with the four guys. The intermediate support of the conductors is modeled using the insulator rod with proper flexibility. At the end of the line, the conductors are attached to rigid frames.

3.3.2.3. Instrumentations and data acquisition system

Different instruments are used to measure the line responses. Those instruments include: strain gauges to measure in-plane (Y direction) and out-of-plane (X direction) mid-height moments at the two legs (M_{i1} and M_{i2}, respectively) and out-of-plane cross arm moment

(M_{Ca}), strain gauges to measure the tension in the guys (T_{Guy}), and force balance to measure the center point forces in three principal directions. This allows to estimate the base shears (Q_X and Q_Y) and the base moments (M_{Xb} and M_{Yb}) as per the following expressions:

- Base shear = Σ Guys force in direction of interest + center support force in the direction of interest.
- Base moment= Σ Guys force in direction of interest x lever arm measured from the guy's support to the center support in the direction of interest.

3.3.3. Experimental Test plan

The test configurations and layouts are selected in view of the findings of the previous numerical studies (Shehata and El Damatty, 2007, and Darwish and El Damatty, 2011) together with the characteristics of the measured downburst field. Regarding the radial distance corresponding to the peak radial velocity, the results show that the maximum radial speed occurs at a radial distance $R \approx 0.9$ D. Therefore, in the current study, the tower of interest is placed at three different radial distances around the location of the peak radial velocity; i.e., R = 0.8, 0.9, and 1.0 D. In addition, the current study considers three orientations of the downburst with respect to the tower; $\Theta = 0°$, 90°, and a number of intermediate oblique cases. Regarding the selection of the line span, the following is considered: 1) at $\Theta = 90°$, Shehata and El Damatty (2007) showed that no conductor forces exist, therefore, only a single tower is considered; 2) at $\Theta = 0°$, Shehata and El Damatty (2007) showed that the maximum lateral loads acting on the line occur when the downburst diameter is small, i.e., at high L/D ratios. Therefore, a span of 5 m is considered for the angle of attack of $\Theta = 0°$; 3) at $0° < \Theta < 90°$, Shehata and El Damatty (2007) reported high

longitudinal force developing in the conductors when the ratio L/D is less than unity. Therefore, for the oblique configurations of the downburst loads, a span of 2.5 m is considered which leads to an L/D equal to ~0.7.

Three layouts (see **Fig. 3-12**) are considered in the current study to assess the tower responses under different configurations of the downburst. **Table 3-1** summarizes the considered layouts and the parameters used in the test. The table shows the location (X and Y distances) of the middle tower (the tower of interest) with respect to the downburst touchdown point for each layout. The towers are tested under a peak radial speed of 8 m/s model-scale, corresponding to a radial speed of 56 m/s full-scale, for an open terrain exposure. The next section describes each of the studied layouts in details.

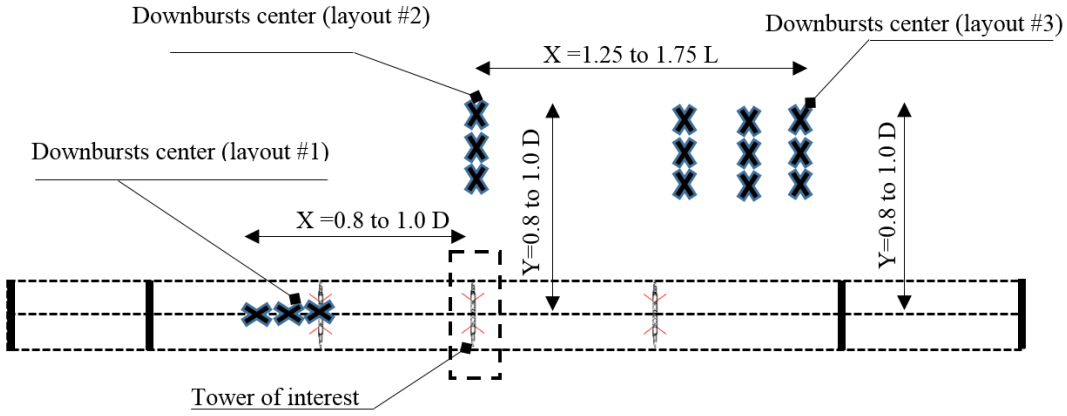

Fig. 3-12. Summary of downburst-structure orientations for the considered layouts

Table 3-1. Test layouts

Layout no.	Θ (degree)	Middle tower location			Line span (m)	No. of spans
		X (m)	Y (m)	R/D		
1	90°	2.56, 2.88, 3.2	0	0.8, 0.9, 1.0	-	-
2	0°	0	2.56, 2.88, 3.2	0.8, 0.9, 1.0	5	4
3	44° to 60°	3.125, 3.75, 4.375	2.56, 2.88, 3.2	1.26, 1.48, 1.7	2.5	6

3.3.3.1. Layout 1: Maximum longitudinal loads (Angle of attack of 90º)

In this layout, a single tower is considered in the test where no conductors are attached. The tower is placed such that the downburst winds act on the tower face perpendicular to the line direction (X-direction). A schematic of this layout is provided in **Fig. 3-13-a** showing the locations of the tested tower relative to the downburst center. The figure shows that the tower is placed at longitudinal distances X = 2.56 m, 2.88 m, and 3.2 m from the center of the downburst. This is corresponding to distance ratios R/D = 0.8, 0.9, and 1.0, respectively. **Fig. 3-13-b** shows a picture for test layout 1 inside WindEEE.

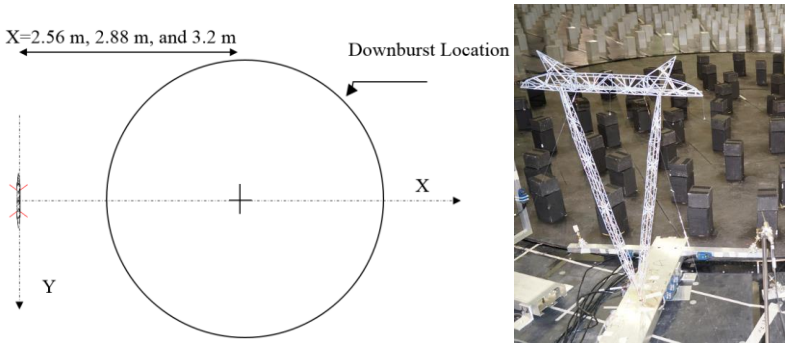

(a) Schematic plan view of layout 1 (b) Layout 1 testing at WindEEE

Fig. 3-13. Test layout 1

3.3.3.2. Layout 2: Maximum transverse loads (Angle of attack of 0 º)

In this layout, the tower is placed such that the downburst winds act on the transverse direction, Y direction, of the line. The layout considers four line spans each of 5 m. This is because the total width of WindEEE is 25 m, so two spans were removed only in this layout in order to accommodate the line with 5 m span. **Fig. 3-14**-a shows the location of the middle tower with respect to the downburst center at the testing chamber. The tower is placed at a transverse distances Y equal to 2.56 m, 2.88 m, and 3.2 m corresponding to a distance ratio R/D equal 0.8, 0.9, and 1.0, respectively. **Fig. 3-14**-b shows a picture for test layout 2 inside WindEEE.

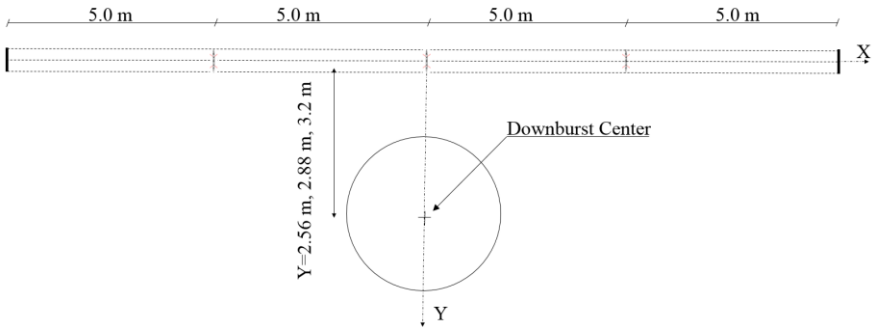

(a) Schematic plan view of layout 2

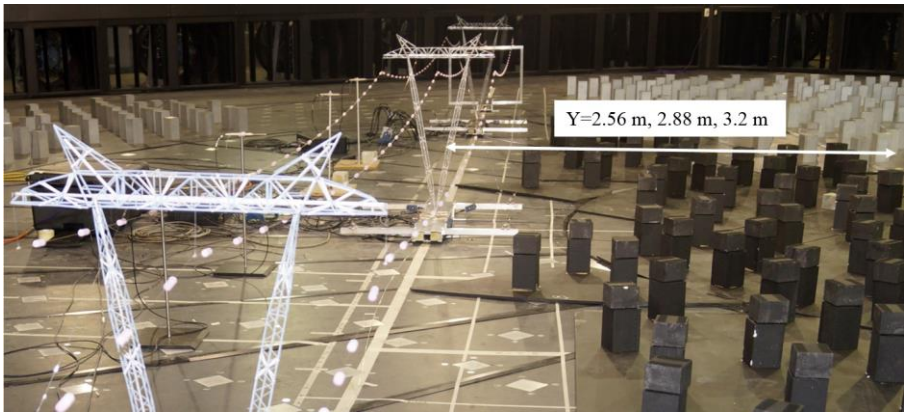

(b) Layout 2 testing at WindEEE

Fig. 3-14. Test layout 2

3.3.3.3. Layout 3: Maximum oblique loads (Yaw angles of attack):

This layout examines the tower response when the downburst acts with an oblique angle on the line. **Fig. 3-15-a** shows the considered locations of the middle tower of the line with respect to the downburst center while **Fig. 3-15-b** shows a picture for test layout 3 inside WindEEE. Nine tower locations are selected representing the permutations of distance ratios (R/D) equals 0.8, 0.9, and 1.0 in Y direction and a distance to span ratio (X/L) of 1.25, 1.5, and 1.75 in X direction.

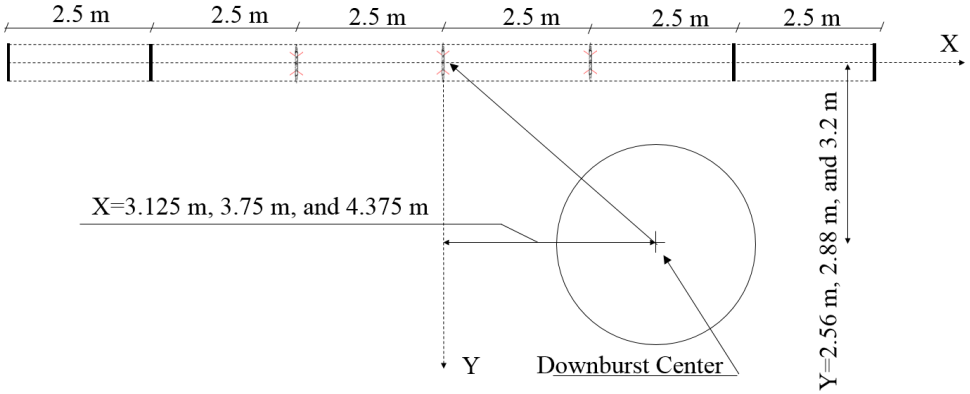

(a) Schematic plan view of layout 3

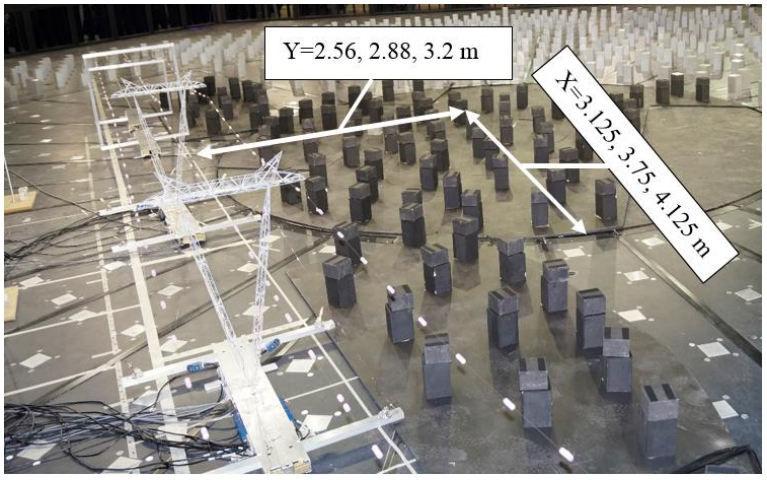

(b) Layout 3 testing at WindEEE

Fig. 3-15. Test layout 3

3.4. Variation of peak and mean responses of the aero-elastic model with the downburst location

This section discusses the tower responses for the three studied layouts in view of the measured base shears (Q_X and Q_Y), base moments (M_{Xb} and M_{Yb}), mid height moments (M_{Xi} and M_{Yi}), and cross arm moment (M_{Ca}). The section aims at examining the findings of discussed numerical studies that indicated high dependency of the tower responses on the location of the downburst event.

Fig. 3-16 shows a sample of the peak and the mean time history responses of the tower for layout 1 when the tower is located at a distance ratio R/D = 0.9 under a peak radial velocity of 8 m/s, where M_{Xb} is the base moment measured in the X direction, Q_X is the base shear measured in the X direction, T_{Guy} is the net tension force measured in the guys due to downburst loads, and M_{X1} is the mid-height moment measured in the X direction at the right leg of the tower (the leg closer to the touchdown point of the downburst).

The mean component of the structural responses is separated from the measured peak response, using the filtering function described in the previous chapter of this study, as shown in **Fig. 3-16**. The figure shows that a sudden peak of the response occurs in a very short period of the entire time history. Then, the response decreases suddenly till reaching a minimum value.

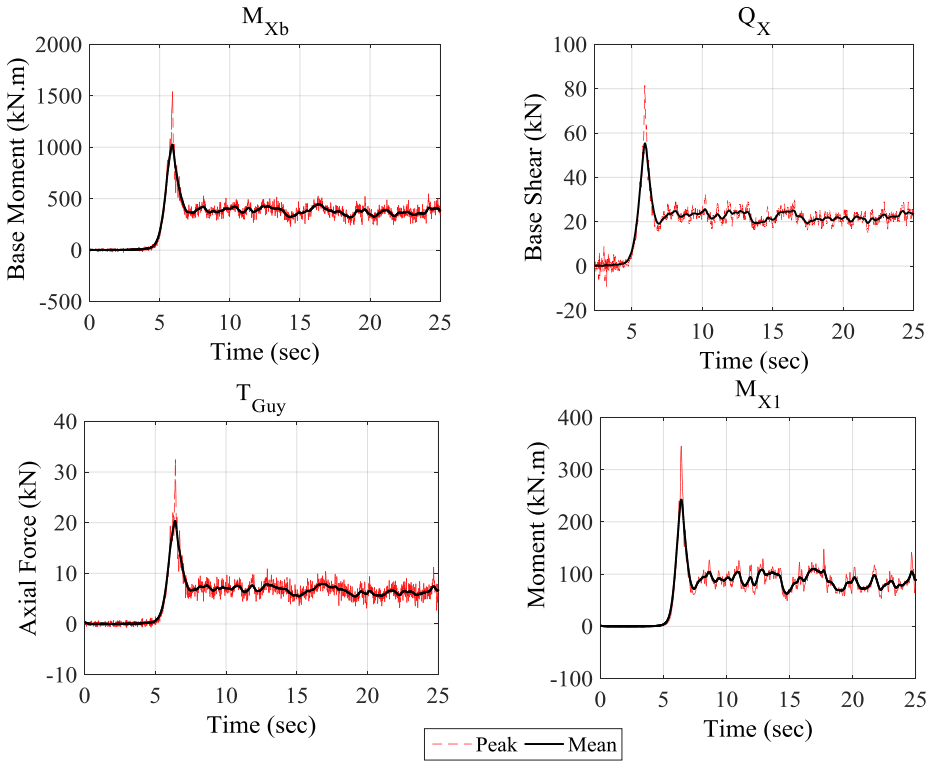

Fig. 3-16 Sample response of the middle tower subjected to downburst loads

The maximum peak and the maximum mean responses obtained from each of the three tested layouts are shown in **Fig. 3-17 to 3-20**. The figures show the variations of the base shears, Q_i, mid-height moments at the two legs, M_{i1} and M_{i2}, base moments, M_{ib}, and cross arm moment, M_{Ca}, with the distance ratio R/D, the angle of attack Θ, and the type of response; i.e., peak and mean responses.

3.4.1. Layout 1: Maximum Longitudinal Loading (Θ=90˚, Fig. 3-17)

Generally, it is found that peak responses occur at R/D ranging between 0.8 to 0.9; i.e., X = 2.56 m to 2.88 m. For example, the maximum cross arm and base moments occur at R/D = 0.8, while the maximum mid-height moment and base shear occur at R/D = 0.9. Both the base moment and the cross arm moments are more sensitive to the wind forces acting on

the cross arm level, which are maximum when downburst center is located at R/D ~ 0.8 as shown in **Fig. 3-8**. The base shear and mid-rise moment are more sensitive to the loads acting on the legs of the tower, which are maximum when R/D = 0.9. **Fig. 3-17** shows that the mid height moment M_{X1} is approximately equal to that of M_{X2} since both tower legs are exposed approximately to equal wind pressure.

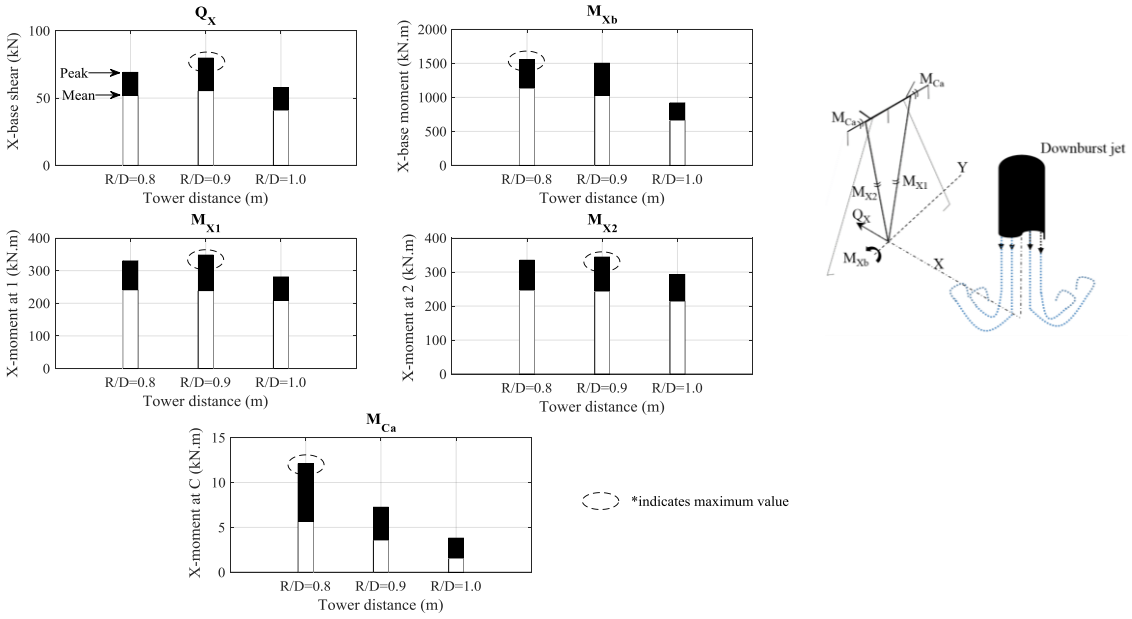

Fig. 3-17. Layout 1 maximum peak responses of the tower B

3.4.2. Layout 2: Maximum Transverse Loading (Θ=0˚, Fig. 3-18)

The test results show that the maximum base shear, base moment, and mid height moment occur when the middle tower is placed at a distance ratio R/D = 0.9. This corresponds to a distance ratio R/D = 0.8. At R/D = 0.9, the responses are slightly less than that of R/D = 0.8. The mid height moment M_{Y1} is less than M_{Y2} . The ratio M_{Y1}/M_{Y2} is found to be equal to 0.73, 0.8, and 0.67 for R/D of 0.8, 0.9, and 1.0, respectively.

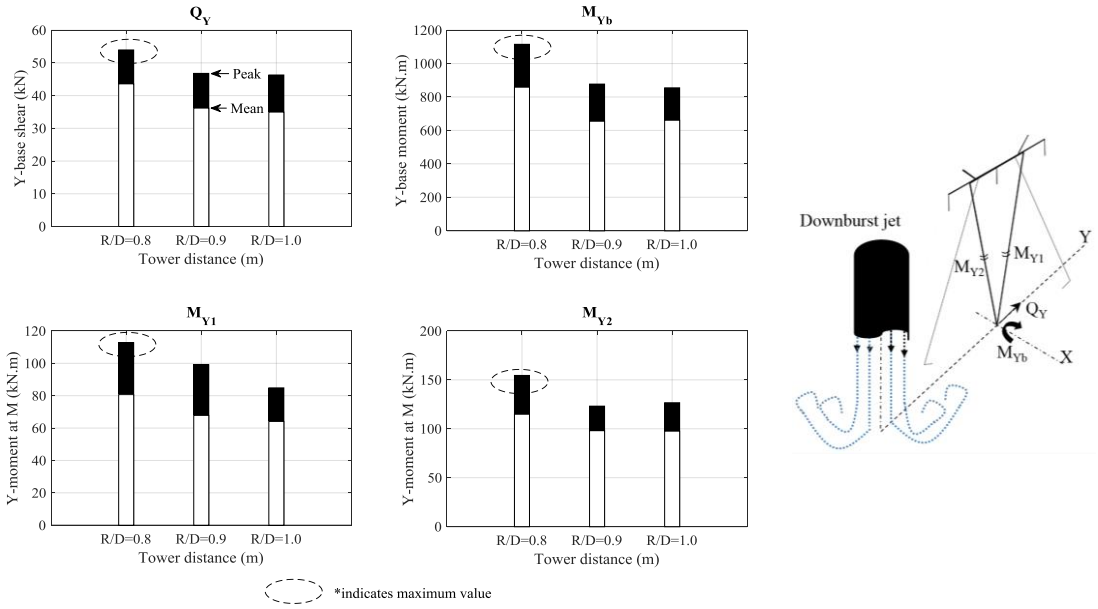

Fig. 3-18. Layout 2 maximum peak responses of the tower B

3.4.3. Layout 3: Maximum Oblique Loading (Θ=0˚, Fig. 3-19 and 3-20)

The results show that the maximum base shears, mid height moments, and out-of-plan cross arm moment occur when the middle tower is placed at a distance X = 3.125 m and Y = 2.56 m. On the other hand, the maximum base moments occur when the middle tower is placed at a distance of X = 3.75 m and Y = 2.88 m. Both cases correspond to the application of the maximum downburst speed (at R = 0.8~0.9 D) on the second line span adjacent to the tower of interset (1.25-1.5 L). This is in an agreement with the findigs of Shehata and El Damatty (2008) where the critical configuration causing the maximum longitudinal force in the conductors is fount at R = 1.6 D, Θ = 30°, and L/D = 0.5 to 0.8 which leads to a projection of the downburst center on the second span of the line measured from the tower of interst. It is also found that the base responses in the two principles directions, X and Y, are in the same order, which can be attributed to the fact that the incoming angle of attack

at the tower of interest is close to 45˚. The ratio between the conductor longitudinal to transverse reactions is found to be in the order of 58% where the longitudinal force is calculated by analyzing the cross arm moment measured in the test and the transverse force is calculated using the ASCE-74 (2010) wind force equation; i.e., *transverse force = 0.5p* $(V_{RDC})^2 d\ L$, where V_{RDC} is the radial velocity of the downburst at the conductor's level, *d* is the conductor's diameter, and *L* is the conductor's span.

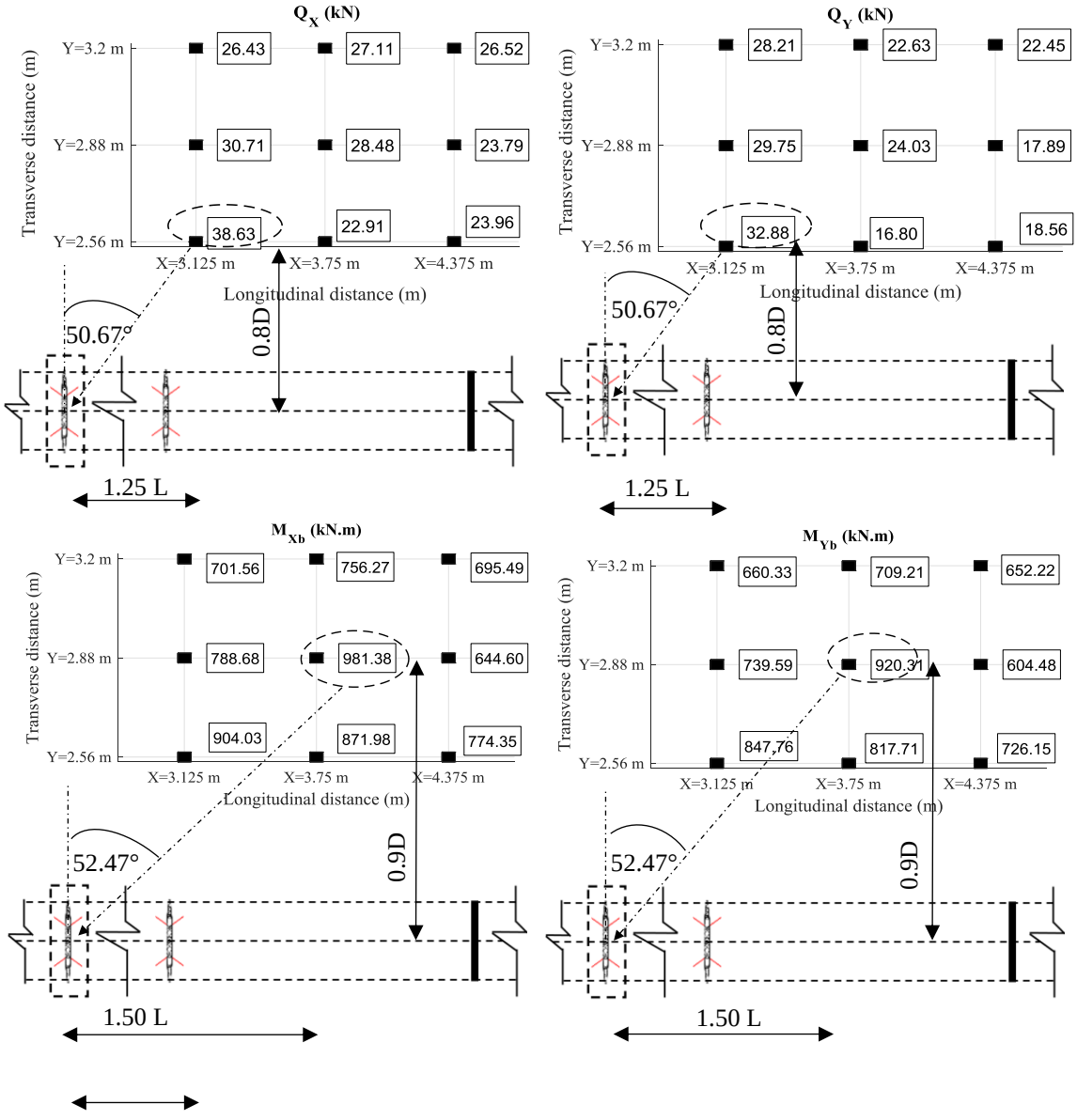

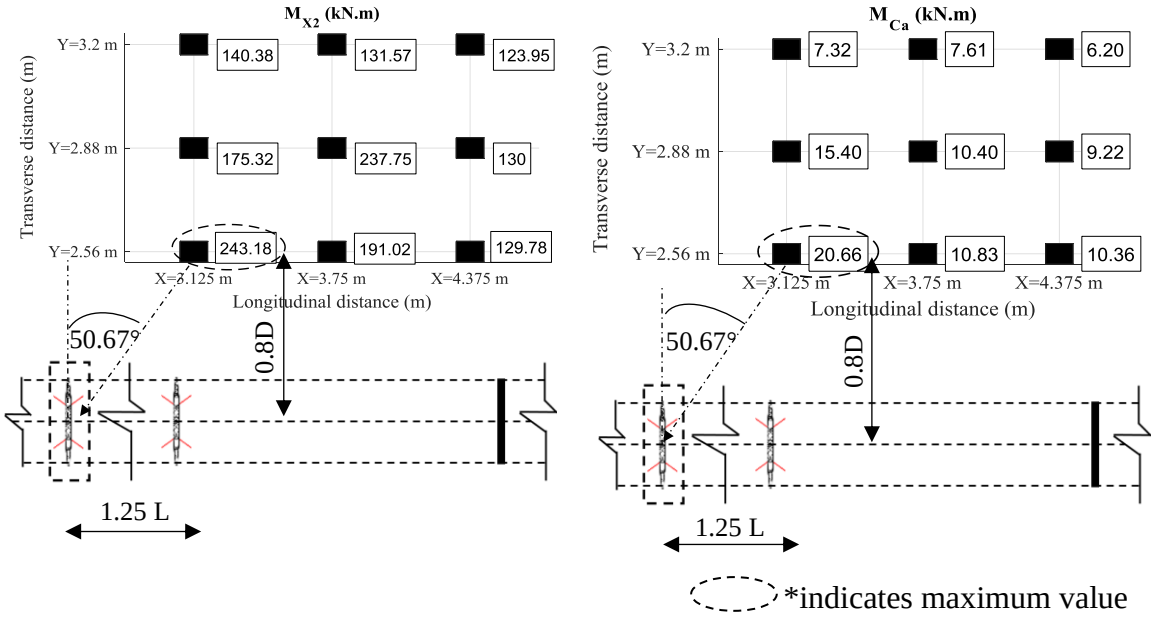

Fig. 3-19. Layout 3 maximum peak responses of tower B

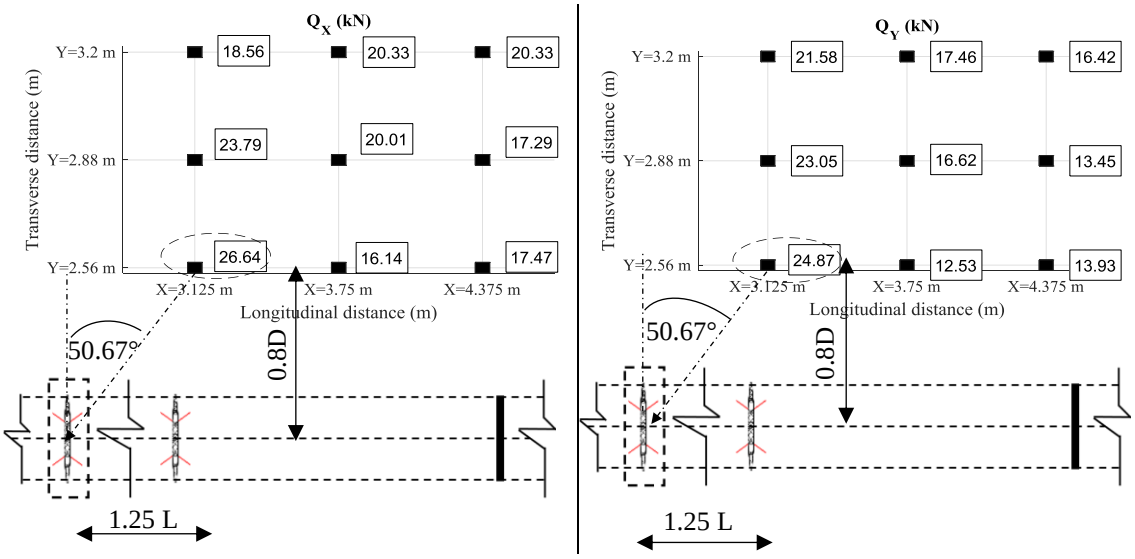

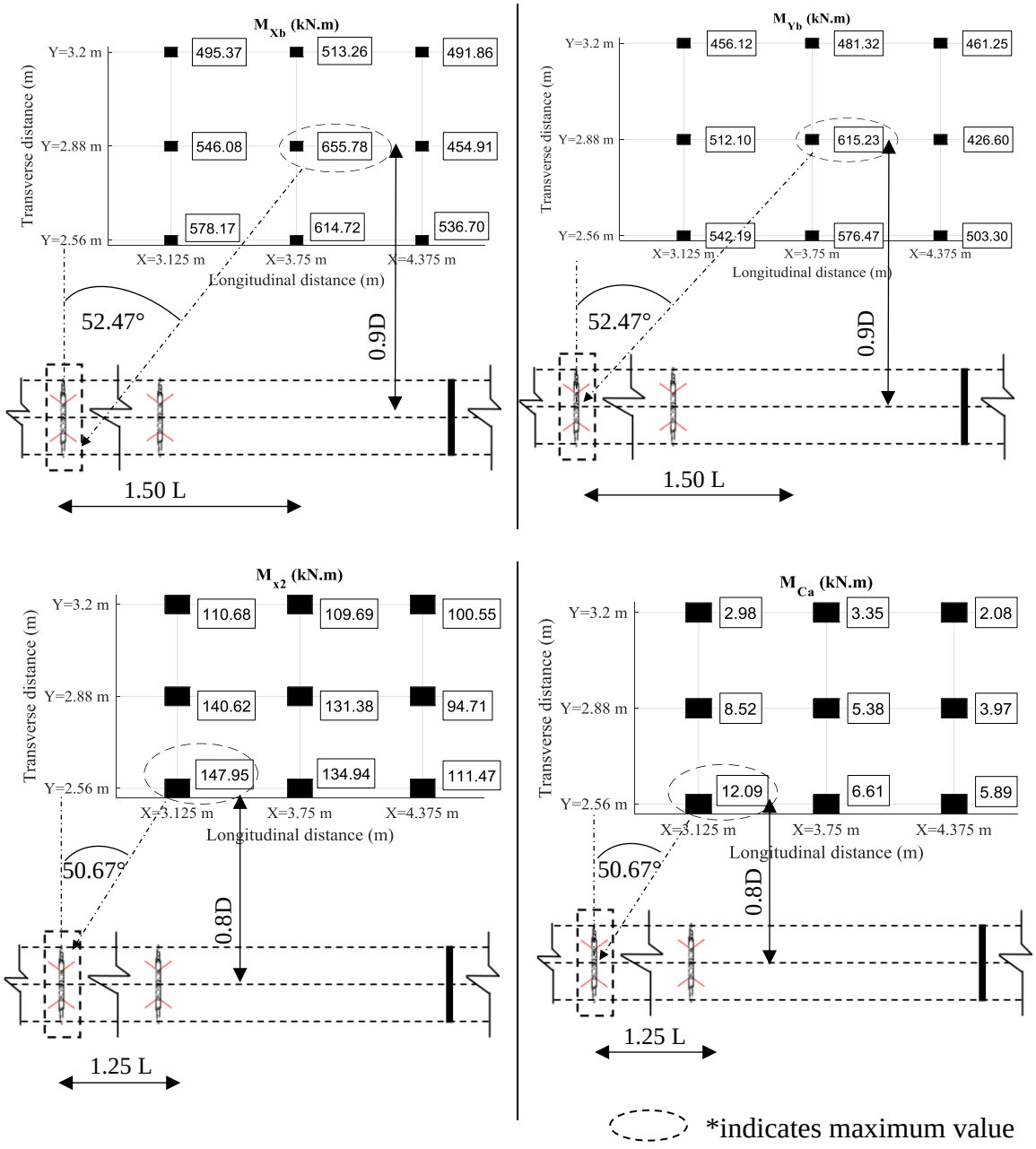

Fig. 3-20. Layout 3 maximum mean responses of tower B

The comparison between the peak response values obtained from the three tested layouts shows the followings:

- Base response in layout 1 is approximately 40% larger than that in layout 2, and also mid-height leg moment in layout 1 is almost double that in layout 2 although no conductor's loads exist in layout 1. This is attributed to the large tower projected area in the wind direction in layout 1 compared to that in layout 2.
- The cross arm moment induced from layout 3, due to the contribution of the longitudinal force developing in the conductors, is 1.7 times larger than that induced from layout 1 resulting from applying the wind loads orthogonally on the cross arm. This ratio may significantly increase with the increase of the span length, the wind intensity, or the change in the conductor's properties (Aboshosha and El Damatty, 2015-b).

Those observations agree with the previous numerical studies' findings. The test results highlight that the tower response is sensitive to the location of the touchdown point of the downburst. The results also show that a downburst location may be critical for a specific zone of the tower not all the tower zones in general. Therefore, a special attention should be taken into consideration when designing the transmission line systems to resist a generic downburst load where several loading scenarios should be considered. In the following section, the running mean wind speeds decomposed from the measured downburst wind field, reported earlier in this study, are implemented in the numerical models, described earlier in this study, to estimate the corresponding running mean responses of the tower and consequently validating the numerical models.

3.5. Results obtained from the numerical models

The built in-house numerical models are validated by comparing their aerodynamic forces, conductor reactions, and straining actions distribution to those measured during the test. The mean component of the downburst wind field is implemented in the numerical models to provide the numerical models with wind pressures similar to those applied on the tested transmission line. Four test cases are selected for the validation as summarized in **Table 3-2**: (i) one case from layout 1, (ii) one case from layout 2, and (iii, iv) two cases from layout 3. These chosen cases are found critical and responsible for the maximum responses as indicated in **Fig. 3-17 to 3-20**.

Table 3-2. Selected test cases for validating the numerical models

Case	Validation case # 1	Validation case # 2	Validation case # 3	Validation case # 4
Layout	1	2	3	3
Location	X=2.88 m Y=0 m	X=0 m Y=2.56 m	X=3.125 m Y=2.56 m	X=3.125 m Y=2.88 m
Span	Single tower	5 m	2.5 m	

Validation of the numerical models is conducted at three levels: (i) at the level of the external forces (aerodynamics) by comparing the base moments and the base shears, (ii) at the conductor level, by comparing the out-of-plane cross arm moments and (iii) at the level of distributing the straining actions, by comparing guy's tensions, center support horizontal forces, mid-height moments.

3.5.1. Validation of the external forces evaluation:

In this section, a case from Layout 1, Validation case #1, is first selected to check the accuracy of the numerical models in calculating the external forces applied on the tower members while eliminating the conductors effect. Another case is selected from Layout 2, Validation case #2, which represents the maximum transverse loads acting on both the tower and the conductors. **Fig. 3-21** shows a comparison between the base shears obtained from the experiment and the numerical models for validation cases #1 and #2, while **Fig. 3-22** shows the same comparison for the base moments. As illustrated in the figures, the maximum difference is found equal -6% in validation case #1 and 13.5% in validation case #2.

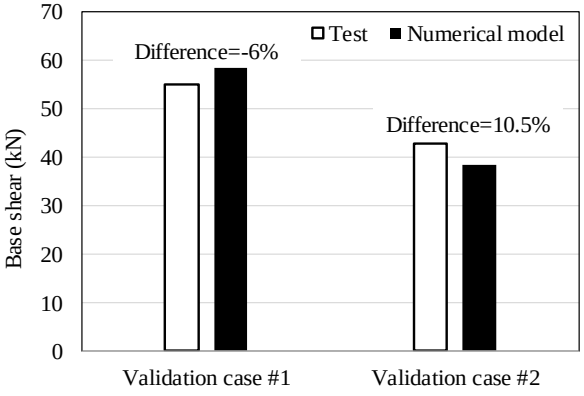

Fig. 3-21. Base shear validation

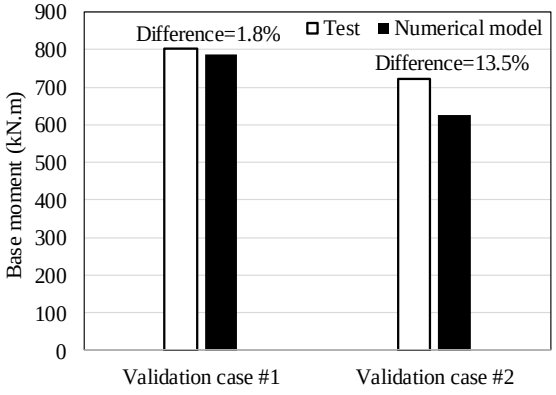

Fig. 3-22. Base moment validation

3.5.2. Validation of the conductor solution

As discussed earlier, the oblique case of the downburst loading results in a longitudinal force developing in the conductors and causing an out-of-plane bending moment on the cross arm zone of the transmission line system as illustrated in **Fig. 3-23**. Two cases are selected out of the described test cases to examine the efficiency of calculating the

longitudinal force developing in the conductors using the built in-house semi analytical technique developed by Aboshosha and El Damatty (2014). Those two cases are found to cause the largest R_X in the conductors and consequently the largest M_{Ca} in the cross arm zone. Those two cases are described in this section as the validation case #3 and 4. An excellent agreement is found in the two studied cases as shown in **Fig. 3-24** with a maximum difference of 5 %.

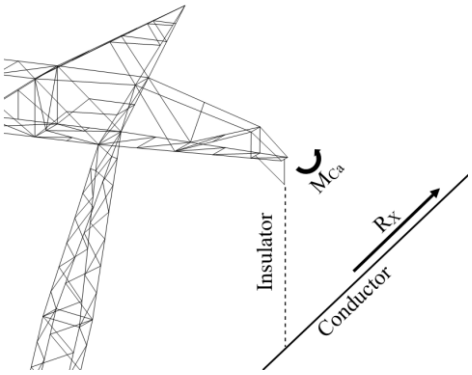

Fig. 3-23. Free body diagram of the cross arm system under the oblique case

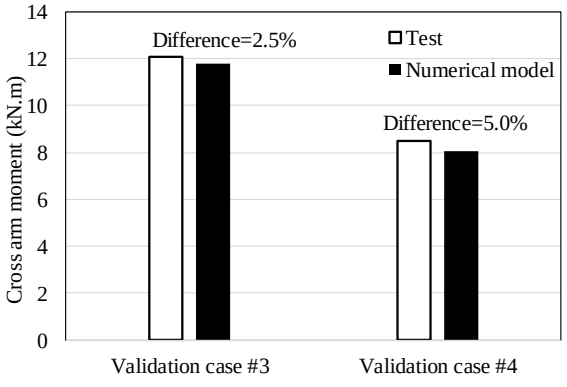

Fig. 3-24. conductor's model validation

3.5.3. Validation of straining action distributions

The third part of the validation process investigates the ability of the numerical model developed by Shehata et al. (2005) to estimate the right stiffness of the structure zones and consequently compute the distribution of the straining actions accurately. This is examined by comparing the guy's tensions, center support's reactions, and mid height moments obtained from the numerical models to those measured during the test. Validation cases #1, 2, and 3 are used to examine the numerical model solutions for different angles of attack. **Fig. 3-25** shows a comparison between the guys tensions obtained from the WindEEE

testing to those obtained using the numerical models. The analyses show that the guy tensions estimated by the two approaches are in a good agreement with a maximum difference of 12%. Similar behaviour is found for the center support reaction and the mid-height moment as shown in **Fig. 3-26 and 3-27**, respectively. As indicated from the figures, the responses obtained from the numerical models are in a good agreement with those obtained from the WindEEE test with a maximum difference in the order of 16% and 10% for the center support force and mid-height moment, respectively.

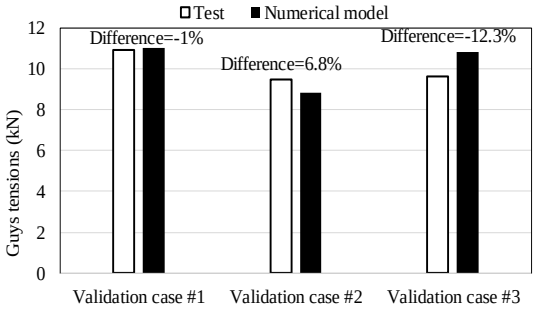

Fig. 3-25. Guys tension validations

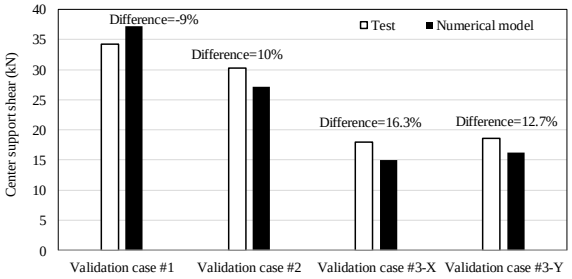

Fig. 3-26. center support force validation

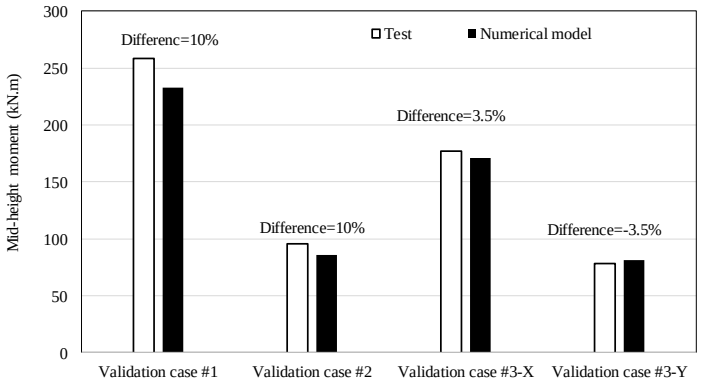

Fig 3-27. Mid-height moment validation

It is observed that higher difference exists in the validation cases where the conductors are contributing to the tower response causing extra forces. This may be attributed to the uncertain aerodynamics of the circular sections tested in wind tunnel experiments. Another

source of error is the accuracy of interpolating the wind field in the locations that were not measured in this study. Further refined research focusing on addressing the shielding and drag effects on lattice tower members subjected to downburst loading is needed.

3.6.Conclusions

An aero-elastic model of a multi-spanned transmission line system is utilized to validate two numerical models that were previously developed in-house to evaluate the response of transmission line systems under downburst loads. The aero-elastic transmission line model consists of three aero-elastic towers and other four rigid frames to simulate a total number of six spans. The downburst wind field simulated at the WindEEE Research Institute is measured in space and validated. The desired geometric scale is selected to be 1:50. A brief description the procedures and assumptions of the design of the aero-elastic model is discussed in this chapter. A detailed description of the instrumentation, boundary conditions, and the data acquisition system used in the test is provided. The profiles of the downburst radial velocities measured at different distances is provided and the location of the peak radial wind speed is determined. A review about the built in-house numerical models, that were previously developed to evaluate the response of transmission towers and their attached conductors when subjected to a generic downburst, is provided. The main findings of the numerical studies conducted using those numerical models is discussed. In order to validate these findings, three test layouts are selected to assess the response of the transmission line to different downburst configurations representing varying distances measured between the centers of the downburst and the study tower. The

study configurations also consider eleven downburst angles of attack. The following summarizes the findings of this study:

- The time history response of tower shows a typical trend where a sudden peak occurs then the response reaches a sudden minimum peak.
- The downburst wind speeds as well as the corresponding response of the tower are decomposed into running-mean and fluctuating components by adopting a cutting-off frequency greater than the shedding frequency of the main vortices of the downburst.
- The experiment results show that the main shaft of the tower experiences a critical response under an angle of attack of 90°.
- For the angle of attack of 0° where one tower leg is shielded behind the other, the shielding factor is found to be in order of 0.7~0.8. A more dedicated study is needed to accurately assess this aspect for the lattice transmission towers.
- The oblique angle of attack induces a significant longitudinal force in the conductors that causes an out-of-plan moment at the cross arm sections. This longitudinal force is found to be as high as 58% of the conductor's transverse force.
- The results show that the critical responses of the tower sections may occur under different cases of loadings. This might be of importance for the design guidelines committees responsible for determining the loading importance factors.
- The structural system of the tower of this study minimizes the vulnerability of the tower to the downburst. This is because the majority of the conductor's and the

cross arm forces transfer directly to the guys supports and consequently to the foundations.

- Four test cases are used to validate the built in-house numerical models. The mean component of the downburst wind field measured at the WindEEE dome is implemented into the in-house numerical models to provide similar wind pressure to that occurred during the test. The validation shows a very good agreement between the measured responses of the tower and the calculated responses using the numerical models.
- The discrepancies between the measured and the calculated responses increase in the oblique load cases where a significant conductor forces contributes to the tower response. This is may be attributed to the accuracy in estimating the wind forces used in the numerical models.

3.7.Acknowledgment

The authors would like to thank the generous financial support received from Hydro One and Ontario Center of Excellence to complete this project. The authors also are very grateful for experts at the Boundary Layer Wind Tunnel lab (BLWTL) and the Wind Engineering, Energy and Environment Research Institute (WindEEE RI) for their guidance throughout the stages of this project.

3.8.References

Abd-Elaal E, Mills JE, Ma X. (2013), “An analytical model for simulating steady state flows of downburst”, J Wind Eng Ind Aerodyn;115:53–64.

Aboshosha, H. and El Damatty, A.A., 2014. “Effective Numerical Technique to Analyse Transmission Line Conductors under High Intensity Winds”, Wind and Structures, Vol. 18, No. 3.

Aboshosha, H. and El Damatty, A.A., 2015 “Dynamic response of transmission line conductors under downburst and synoptic winds” Wind and Structures Vol. 21, No.2 (2015) 241-272.

Aboshosha, H., and El Damatty, A., (2015-b), “Engineering method for estimating the reactions of transmission line conductors under downburst winds”, Engineering Structures 99, 272-284.

Aboshosha., H., Bitsuamlak, G., El Damatty, A., (2015-a), “Turbulence characterization of downbursts using LES”, Journal of Wind Engineering and Industrial Aerodynamics 136, 44–61.

American Society of Civil Engineers (ASCE), (2010) “Guidelines for electrical transmission line structural loading”, ASCE manuals and reports on engineering practice, No. 74, New York, NY, USA.

Australian Wind Alliance, (2016): http://www.windalliance.org.au/

Chay, M., Albermani, F. and Wilson, R., (2006), “Numerical and analytical simulation of downburst wind loads”, Engineering Structures 28(2), 240-254.

Chay, M., Letchford, C., (2002), “Pressure distributions on a cube in a simulated thunderstorm downburst - part a: stationary downburst observations”, Journal of Wind Engineering and Industrial Aerodynamics 90, 711–732.

Choi, E. and Hidayat, F., (2002), “Dynamic response of structures to thunderstorm winds”, Prog. Struct Eng. Mech. 4, 408-416.

Darwish, M., and El Damatty, A., (2011), “Behavior of self-supported transmission line towers under stationary downburst loading”, Wind and Structures 14(5), 481-4.

Didden, N., Ho, C.M., 1985 “Unsteady separation in a boundary layer produced by an impinging jet” Journal of Fluid Mechanics 160, 235–256.

Donaldson, C., and Snedeker, R., (1971), “A study of free jet impingement, Part 1. Mean properties of free and impinging jets”, Journal of Fluid Mechanics 45, 281–319.

Failure Investigation Report, HYDRO ONE NETWORKS INC. “Failure of towers 610 and 611, circuit X503E – 500 kV guyed towers near the Township of Waubaushene”, Ontario, August 2, 2006”, Line Engineering, 2006.

Fengli, Yang., and Hongjie, Zhang., (2016), “Two case studies on structural analysis of transmission towers under downburst”, Vol. 22, No. 6, 685-701.

Fujita, T., (1985), “The downburst: microburst and macroburst”, SMRP Research Paper 210, University of Chicago, USA.

Fujita, T., (1990), “Downbursts: meteorological features and wind field characteristics”, Journal of Wind Engineering and Industrial Aerodynamics 36, 75–86.

Gant, S., (2009), “Reliability issues of LES-related approaches in an industrial context”, Flow, Turbulence and Combustion 84, 325-335.

Gerges, R., and El-Damatty, A., (2002), “Large displacement analysis of curved beams”, Proceedings of the Canadian Society of Civil Engineering Conference, Montreal, Canada, ST 100.

Hangan, H., Roberts, D., Xu, Z., and Kim, J., (2003), “Downburst simulation. Experimental and numerical challenges”, Proceedings of the 11th International Conference on Wind Engineering, Lubbock, TX, USA.

Hjelmfelt, M., (1988), “Structure and life cycle of microburst outflows observed in Colorado”, Journal of Applied Meteorology 27, 900–927.

Holmes, J. (2008), “Recent developments in the specification of wind loads on transmission lines”, Journal of Wind Engineering and Industrial Aerodynamics, 8-18.

Holmes, J., Hangan, H., Schroeder, J., Letchford, C., Orwig, K., (2008), “A forensic study of the Lubbock-Reese downdraft of 2002”, Wind Structures 11 (2), 137–152.

Ivan, M., (1986), “A ring-vortex downburst model for flight simulations” Journal of Aircraft 23, 232-236.

Kanak, J., Benko, M., Simon, A. and Sokol, A. (2007), “Case study of the 9 May 2003 windstorm in southwestern Slovakia”, Atmospheric Research, 83, 162-175.

Kim, J. and Hangan, H., (2007), “Numerical simulations of impinging jets with application to downbursts”, Journal of Wind Engineering and Industrial Aerodynamics 95(4), 279-298.

Koziey, B., and Mirza, F., (1994), "Consistent curved beam element", Computers and Structures 51(6), 643–654.

Kwon, D., and Kareem, A., (2009), "Gust-front factor: new framework for wind load effects on structures" ASCE J Struct Eng135(6), 717–32.

Mara, T., and Hong H., Lee, S., Ho, T., (2016) "Capacity of a transmission tower under downburst wind loading" Wind and Structures An International Journal 22(1):65-87.

Mason, M., Wood, G., and Fletcher, D., (2010), "Numerical investigation of the influence of topography on simulated downburst wind fields", Journal of Wind Engineering and Industrial Aerodynamics 98(1), 21-33.

Mason, M., Wood, G., Fletcher, D., (2009), "Numerical simulation of downburst winds", Journal of Wind Engineering and Industrial Aerodynamics 97(11-12), 523-539.

McCarthy, P., and Melsness, M., (1996), "Severe weather elements associated with September 5, 1996 hydro tower failures near Grosse".

Oseguera R., and Bowles R., (1988) "A simple, analytics 3-dimensional downburst model based on boundary layer stagnation flow" NASATM- 100632. Hampton (VA): NASA Langley Research Center.

Savory, E., Parke, G., Zeinoddini, M., Toy, N., and Disney, P., (2001), "Modelling of tornado and microburst-induced wind loading and failure of a lattice transmission tower", Engineering Structures 23(4), 365-375.

Sengupta, A., Sarkar, P., (2008) "Experimental measurement and numerical simulation of an impinging jet with application to thunderstorm microburst winds", Journal of Wind Engineering and Industrial Aerodynamics 96, 345–365.

Shehata, A. and El Damatty, A., (2008), "Failure analysis of a transmission tower during a microburst", Wind and Structures 11(3), 193-208.

Shehata, A. Y., and El Damatty, A. A. (2007), "Behaviour of guyed transmission line structures under downburst wind loading", Wind and Structures, an International Journal, 10(3), 249-268.

Shehata, A.Y., El Damatty, A.A. and Savory, E., (2005), "Finite element modeling of transmission line under downburst wind loading", Finite Elements in Analysis and Design., 42(1) 71-89.

Solari G, Burlando M, De Gaetano P, Repetto MP. (2015), “Characteristics of thunderstorms relevant to the wind loading of structures”, Wind and Structures, 20(6):763–91.

Vermeire, B., Orf, L., Savory, E., (2011a), “Improved modelling of downburst outflows for wind engineering applications using a cooling source approach”, Journal of Wind Engineering and Industrial Aerodynamics 99, 801–814.

Wang, X., Lou, W., Li, H., and Chen, Y., (2009), “Wind-induced dynamic response of high-rise transmission tower under downburst wind load”, Journal of Zhejiang University 43(8), 1520-1525.

Wood, G., Kwok, K., Motteram, N., and Fletcher, D., (2001), “Physical and numerical modelling of thunderstorm downbursts”, Journal of Wind Engineering and Industrial Aerodynamics 89, 535-552.

Zhang Y., (2006), “Status quo of wind hazard prevention for transmission lines and counter measures”, East China Electric Power 34(3), 28-31.

CHAPTER 4

LONGITUDINAL FORCE ON TRANSMISSION TOWERS DUE TO NON-SYMMETRIC DOWNBURST CONDUCTOR LOADS

4.1. Introduction

Downbursts are localized wind events that occur during thunderstorms. They form along with tornadoes, a category of weather events called non-synoptic High Intensity Wind (HIW). Fujita (1985) described a downburst as an intensive downdraft formed by cold air that impinges on the ground. In contrast, tornadoes are formed by an updraft of rising hot air. During the past decades, many failures of transmission line structures were reported in various locations around the globe due to downbursts. Hawes and Dempsey (1993) stated that 90% of the transmission line failures in Australia were induced by downbursts. Kanak et al. (2007) studied a downburst event that occurred in southwestern Slovakia in 2003 where at least 19 electricity transmission towers collapsed. Zhang (2006) reported the failures of 18 towers belonging to 500 kV lines and 57 towers belonging to 110 kV lines due to strong wind events such as downbursts, tornadoes and typhoons in China. McCarthy and Melsness (1996) reported the failure of 19 transmission towers located near Winnipeg, Manitoba, Canada, during a downburst event. In 2006, Hydro One Ontario, reported a failure of two guyed towers during a downburst event with an estimated wind velocity of 50 m/s. Many other towers failed in Ontario, Canada, during HIW events. Those failure incidents triggered an extensive research program at the University of Western Ontario, Canada, related to this topic. The current study focuses specifically on the behaviour of transmission line conductors during downburst events.

The location and size of downbursts affect their loading scheme on transmission line structures. Shehata et al. (2005) developed a nonlinear finite element code for transmission lines that incorporated downburst wind field simulated using Computational Fluid Dynamics model. The model considered the time history of a generic downburst event where the location and size of the event were assumed variables. Using this model, Shehata and El Damatty (2007, 2008) and Darwish and El Damatty (2011) studied the behavior of a guyed and self-supported transmission towers subjected to downburst wind induced loads, respectively. Both studies reported that the peak response of the transmission line members depends on the dimensional characteristics and intensity of the downburst event in addition to the structural system of the tower and conductor's properties. Those studies reported possible critical load cases that affected the majority of the tower members. One of those critical load cases was called the "oblique downburst" load case, which is the main focus of the current study, where the downburst acts with an oblique angle of attack on the transmission line. The oblique load case of the downburst does not appear during synoptic wind events causing a special load case acting on the tower. This occurs when the virtual (imaginary) line connecting the center of the downburst and the center of the tower is neither perpendicular nor parallel to the conductor's direction. Considering the conductor spans adjacent to the tower of interest, this downburst location will lead to uneven and non-symmetric distribution of wind loads along those spans. The segments located at one side of the tower will be closer to the downburst compared to the segments located at the opposite side of the tower. Consequently, the tension forces that develop in the segments close to the downburst will be higher than their counterpart in the segments more distant to the downburst. The difference between the conductor tension forces will then lead to a net

longitudinal force that acts on the tower cross arms. Aboshosha and El Damatty (2013) reported that the longitudinal forces, which develop in the conductors could be as high as 60% of the transverse reactions under a downburst jet velocity of 40 m/s. Current guidelines for the design of transmission line structures have very limited information about downburst loadings. AS/NZS (2010) recommends a uniform distribution of a downburst load with higher values for the span reduction factor compared to a synoptic wind. Current guidelines do not consider this oblique downburst load case, which can be very damaging to transmission line structures. This load case will introduce a net force acting on the tower along the longitudinal direction of the line, as will be explained later in this paper, and consequently, it is similar to that of the failure containment case described by the ASCE-74 (2010) design guideline where one side of the conductors are assumed broken. However, depending on the properties and the span of the conductors, and the magnitude of the downburst forces, the broken wire load case may or may not exceed the oblique downburst load case.

Many challenges arise in the evaluation of the longitudinal force associated with the oblique downburst load case. For design purposes, the maximum value of this longitudinal force needs to be estimated. This is challenging since the value of the longitudinal force depends on the location of the downburst as well as its physical size. In addition, the evaluation of this force requires conducting a nonlinear iterative analysis of the conductors taking into account the conductors' prestressing force, sagging, and material properties as well as the flexibility of the insulators, which is not an easy task for practicing engineers.

Aboshosha and El Damatty (2014) modeled six conductor spans and calculated their forces under downburst loads using closed form solution. In their study, the insulators were

simulated using link members. The conductor's pretension force was considered in the solution. In addition to the conductor's weight per unit length, the solution considered the downburst transverse loads acting on the conductor. The solution is found to be computationally inexpensive. However, the solution requires coding for a number of nonlinear and coupled equations. Later on, Aboshosha and El Damatty (2015) simplified their technique by reducing the number of the unknowns in the solution. Aboshosha and El Damatty (2015) simulated the line insulators using link element at the tower of interest, linear stiffness at the towers adjacent to the tower of interest from each side, and roller supports at the successive towers from each side. However, Aboshosha and El Damatty's simplified solution still requires sophisticated iterative solution by solving a list of equations. The current paper includes a comprehensive parametric study conducted to investigate the effect of each of the conductor's properties on the longitudinal force of the conductor developing under the critical downburst loads. Based on the results of this parametric study, a set of charts is developed to allow practitioner engineer to calculate the conductor's longitudinal force using simple set of linear interpolation equations.

The objective of the current study is to develop a procedure for estimating the maximum longitudinal force acting on transmission towers due to the oblique downburst load case. The procedure needs to be simple enough for either incorporation into the codes of practice or for direct use by practicing engineers. The procedure should account for the variations in the size and location of the downburst relative to the line span and should estimate the absolute maximum force associated with the most critical downburst configuration. Finally, it should be broad enough to account for the many parameters that define the conductor's physical

properties such as span, sag, weight per unit length, projected area, cross section, insulator length, and material properties.

To achieve that, the work presented in this paper is conducted in four consecutive phases dividing the paper into four parts. The first part focuses on the downburst wind field where an extensive parametric study is conducted to determine the critical downburst configuration, in terms of location and size, which is expected to lead to a maximum longitudinal force being transferred to the towers. The second part includes a nonlinear structural analysis to assess the variations in the longitudinal forces with various geometric and material parameters defining the conductors under the critical oblique load case identified in the first part. Based on the outcomes reached in part two, charts are then developed and a procedure established in part three to evaluate the maximum longitudinal force experienced by a general tangent transmission line system. The validation of this procedure is conducted in the fourth part of the study. Finally, the conclusions drawn from the entire study are presented.

It is important to mention that the current study is done assuming a deterministic approach. However, further studies are needed to develop downburst maps and assess the probability of occurrence of the considered critical configuration at a specific location.

4.2. Downburst Wind Field

Many parameters determine the effect of a downburst event on the structural response of a tower including the size (jet diameter, D_J) and the intensity of the downburst (jet velocity, V_J) as well as the polar coordinates of the downburst center relative to the center of the tower of interest (R and Θ), as shown in **Fig. 4-1**.

Different approaches are found in the literature regarding the numerical simulation of downbursts such as the: a) Ring Vortex Model, b) Impinging Jet Model, and c) Cooling Source Model. A review of the different simulation methods for downbursts can be found in Aboshosha et al. (2016). In the current study, the impinging jet model developed by Hangan et al. (2003) and validated by Kim and Hangan (2007) is utilized to simulate the downburst wind field. The impinging jet model is based on the analogy between an impulsive jet impinging upon a flat surface and a downburst. The Computational Fluid Dynamics (CFD) model provides a time series for the vertical component (V_{VR}) and the radial (horizontal) component (V_{RD}) of the downburst velocity field. The model incorporates only the mean component of the downburst. Although the turbulence is an intrinsic factor in evaluating the peak loads and responses of the structures, different studies such as Gattulli et al. (2007) have shown that at high velocities, the dynamic response of the conductors can be ignored due to the presence of high aerodynamic damping. As will be explained later, the background component of the turbulence is taken into account in the current study by scaling-up the wind field to the gust wind speed. This approach assumes a full-correlation of the downburst turbulence along the conductor spans which is a reasonable assumption in view of the study conducted by Holmes et al. (2008).

Hangan et al. (2003) carried out a downburst simulation on a small scale. Shehata et al. (2005) subsequently provided a procedure for scaling up this data, which is adopted in the current study. **Fig. 4-2** and **Fig. 4-3** show the variations in the radial and the vertical velocities respectively occurring along the height normalized with respect to the jet velocity. These profiles correspond to the time instant at which maximum radial and vertical velocities occur.

The maximum radial velocity corresponds to a distance ratio, R/D_J, of 1.3 as shown in **Fig. 4-2**. By examining **Fig. 4-2**, it can be shown that the absolute maximum radial velocity occurs at a height of approximately 50 m. The variations in velocity occurring between the elevations of 30 m and 70 m are within 5% of the absolute maximum. This range of 30 m to 70 m represents the range for the typical location of conductors. As such, in the current study, the wind velocity is considered to be at the height corresponding to the maximum value and by doing so, one parameter, the elevation of the conductors, is eliminated from the parametric studies. On the other hand, **Fig. 4-3** shows that the vertical velocity profile changes drastically with the variation of the R/D_J ratio. At the maximum height of typical towers (about 60 m), the vertical velocity is approximately equal to 0.2 V_J. Knowing that the wind forces are directly proportional to the square of the velocity, the vertical forces can be neglected compared to the radial forces. As such, only the radial velocity effect will be considered in this study.

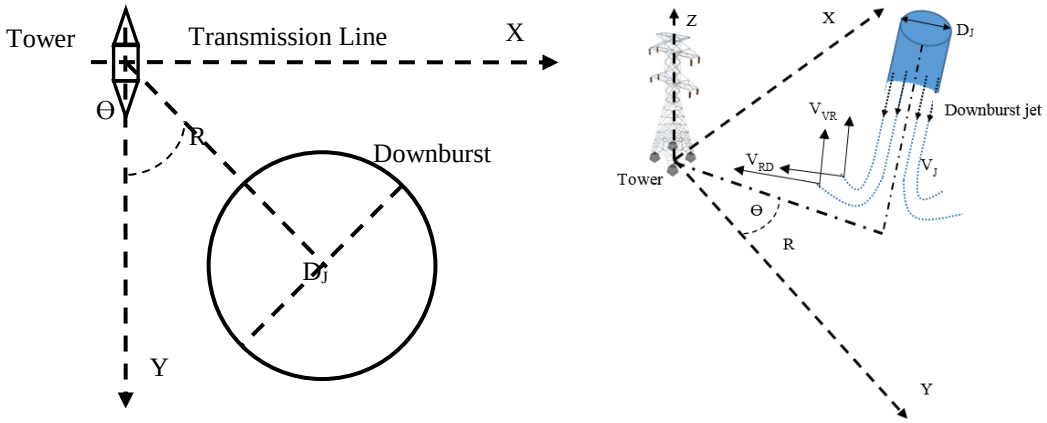

(a) (b)

Fig. 4-1. Downburst characteristic parameters.

Fig. 4-4 shows the radial velocity distribution along the full-scale time history of the downburst event (Shehata et al., 2005). The figure shows that the radial velocity increases suddenly until reaching the maximum value; it then decreases suddenly until reaching the minimum value, at which point it remains constant throughout the rest of the time history.

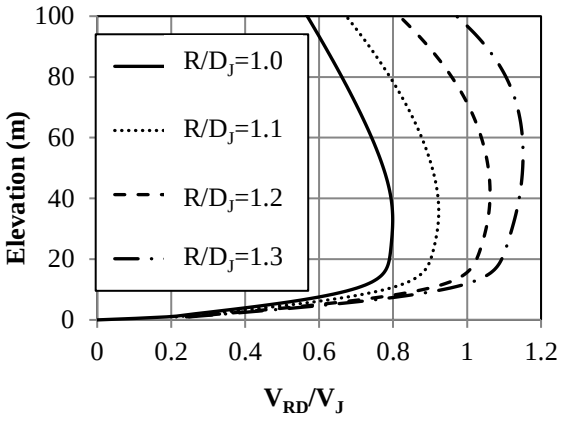

Fig. 4-2. Radial velocity profile along the height at D_J =500 m.

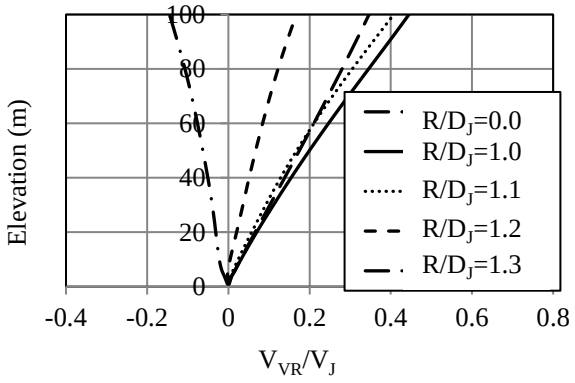

Fig. 4-3. Vertical velocity profile along the height

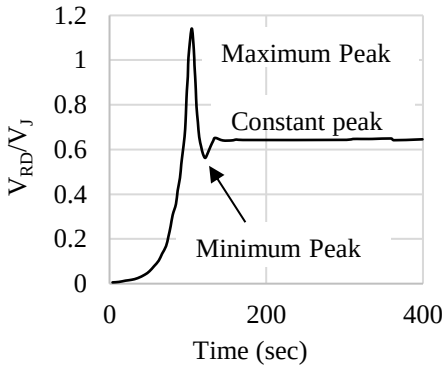

Fig. 4-4. Time history of the radial velocity at a point in space

Based on the above discussion, the downburst variables that influence the response of the conductors are D_J, V_{RD}, R, Θ, and time, t. In this section, an extensive parametric study is conducted to determine the downburst configuration that causes the maximum longitudinal force transferred from the conductors to the tower of interest.

Fig. 4-5-a shows a schematic for the distribution of the transverse velocity (transverse velocity is the component of the radial velocity acting perpendicularly on the conductors) normalized with the jet velocity (V_{TR}/V_J) along three spans from each side of the tower of interest. This distribution results from a downburst having a diameter D_J and a location relative to the tower defined by the polar coordinates (R and Θ). The consideration of the three spans from each side is based on the recommendation of Shehata et al. (2005) for an accurate prediction of the response of transmission towers to downburst loadings. For a given conductor, the wind forces depend on the square of the velocities. **Fig. 4-5**-b shows a schematic for the distribution of $(V_{TR}/V_J)^2$ along the six conductor spans. In this figure, A_1 is obtained by integrating $(V_{TR}/V_J)^2$ along the three spans (3L) located at the right hand side of the tower of interest. Similarly, A_2 is obtained by integrating $(V_{TR}/V_J)^2$ along the three spans located at the left hand side of the tower of interest. A_1 and A_2 are proportional to the total forces acting on the three right hand side spans and the three left hand side spans, respectively. By dividing A_1 and A_2 by (3L), the corresponding ratios $A_1/3L$ and $A_2/3L$ are proportional to an equivalent distributed load acting on the right hand side spans and the left hand side spans, respectively. The increase in the tension force due to the downburst loading on the right span's conductors (ΔT_R) depends on the magnitude of the acting transverse loading. As such, ΔT_R depends on the parameter $A_1/3L$. Similarly, the increase in the tension force on the left spans (ΔT_L) depends on the parameter $A_2/3L$. The difference between ΔT_R

and ΔT_L represents the conductor longitudinal force, R_X, which is transmitted to the tower due to the unbalanced load case. As such, R_X depends on the parameter $A_D = (A_1-A_2)/3L$. The purpose of the parametric study conducted in this part of the paper is to determine the downburst parameters (D_J, R, and Θ), which lead to the maximum values for the parameter A_D, and consequently to R_X, for a general conductor system. This is achieved by taking the following steps:

1. A value of the conductor span, L, is assumed.
2. For each value of L, a parametric study is conducted by varying the jet diameter, D_J, and the location of the downburst using the two parameters (R/D_J and Θ).

As mentioned earlier, the CFD data was provided by Kim and Hangan (2007) in the model scale. Shehata et al. (2005) provided a transformation equation in order to scale-up the CFD data to estimate the wind field associated with a real downburst. This time scale proposed by Shehata et al. (2005) is given by the following equation: $\Delta t_p = \Delta t_m * D_{Jp} / V_{Jp} * D_{Jm} / V_{Jm}$, where Δt_p is the time step used in the full-scale analysis; Δt_m is the time step used in the CFD model; D_{JP} and D_{Jm} are the downburst size in the full-scale and the model-scale, respectively; V_{JP} and V_{Jm} are the downburst jet velocity in the full-scale and the model-scale, respectively. For the dimensions used in the CFD, the above equation leads to a full-scale time step of $\Delta t_p = 1.23 * D_{Jp} / V_{Jp}$. The analyses show that various conductors sections along the line experience the maximum downburst transverse velocity at different times. This is a unique feature of the downburst wind field that is characterized by the coupling between time and space. As such, the analyses of the current study are conducted in a quasi-static manner where the entire time history is considered in order to capture the time instant corresponding to the peak longitudinal force R_X. For each downburst configuration defined by the specific

values of D_J, R/D_J and Θ, the time history variation of the transverse velocity profile along three spans from each side of the tower is determined. The areas A_1 and A_2 and the parameter $A_D = (A_1-A_2)/3L$ are evaluated at each time step. The maximum value of A_D, which is recorded over the entire time history of the downburst, is determined together with the instant corresponding to this value, t_{max}.

Fig. 4-6 shows the variation of the parameter A_D with the ratios R/D_J and L/D_J as well as the angle Θ. The variation of A_D is shown for R/D_J values ranging between 0.2 to 2.2, L/D_J values ranging between 0.25 to 1.0, and Θ values ranging between 15° and 60°. The ranges for the two ratios R/D_J and Θ are selected based on the study conducted by Shehata and El Damatty (2007) where they reported that the critical locations for the conductor's longitudinal forces are within those ranges. The figure shows that the downburst configuration corresponding to $L/D_J=0.5$, $R/D_J=1.6$, and Θ=30° leads to the maximum value for the parameter A_D, and, consequently, for maximum value for longitudinal force R_X.

A schematic showing the location of the downburst corresponding to this critical configuration is shown in **Fig. 4-7**. Using simple trigonometry, it can be shown that the projection of the center of the downburst on the line is located at the middle of the second span as demonstrated in **Fig. 4-7**. The jet diameter corresponding to this critical configuration (for $L/D_J=0.5$) will vary between 600 m and 1200 m for the considered spans, which is within the practical diameter for a microburst (Hjelmfelt, 1988).

The distribution of the transverse velocity along the six conductor spans (three from each side of the tower of interest) corresponding to the critical oblique downburst configuration is shown in a quantitative manner in **Fig. 4-8**. Having identified this distribution as the most

critical one producing the maximum longitudinal force acting on the tower, the rest of the study will proceed using this configuration.

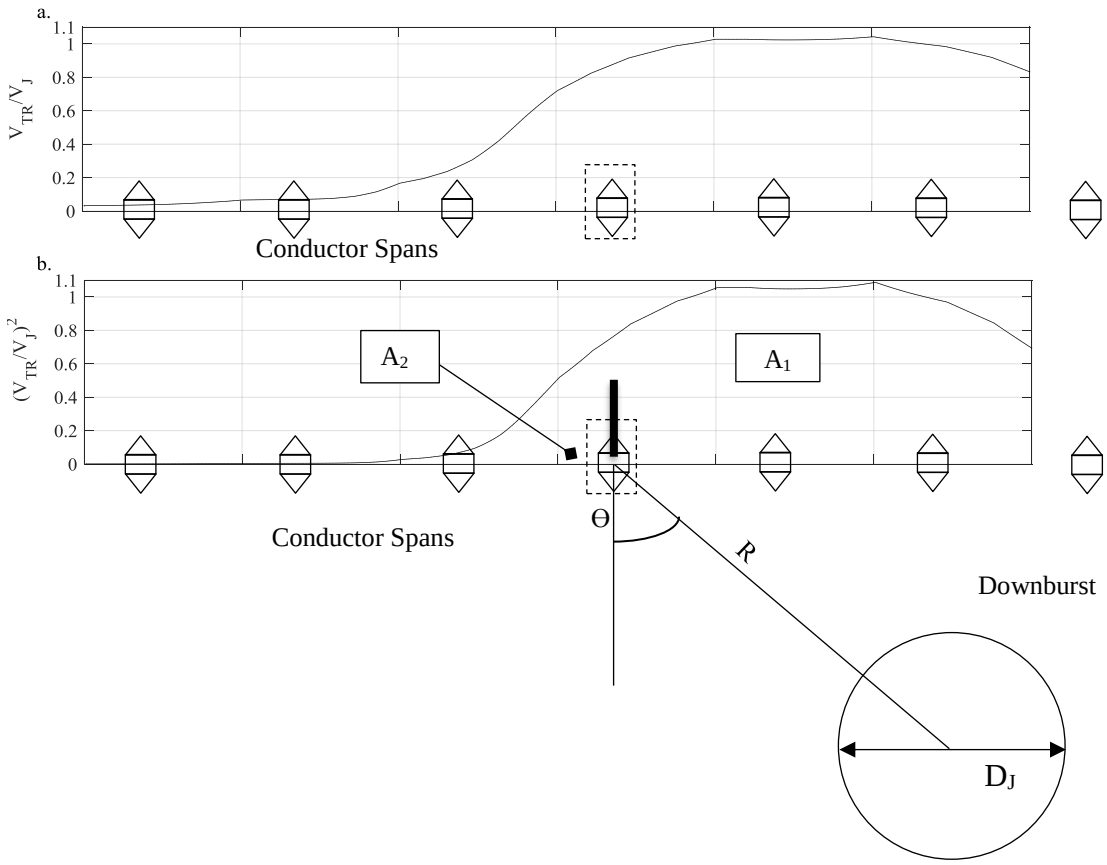

Fig. 4-5. Velocity distribution along multiple spans in the case of an oblique downburst.

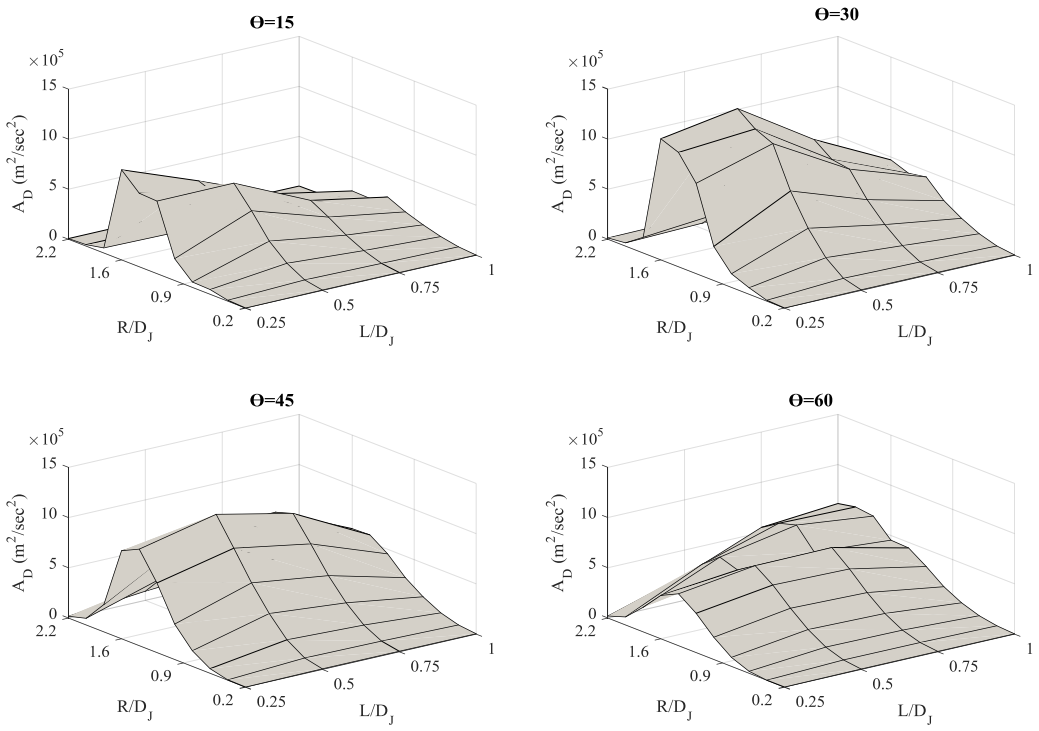

Fig. 4-6. Variations of A_D with different downburst diamaters.

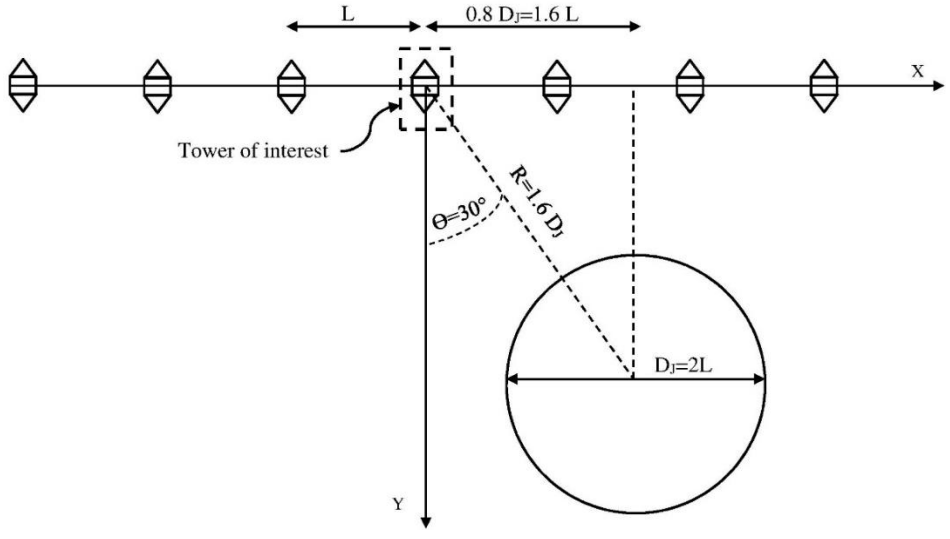

Fig. 4-7. Location of downburst corresponding to conductor's maximum longitudinal force.

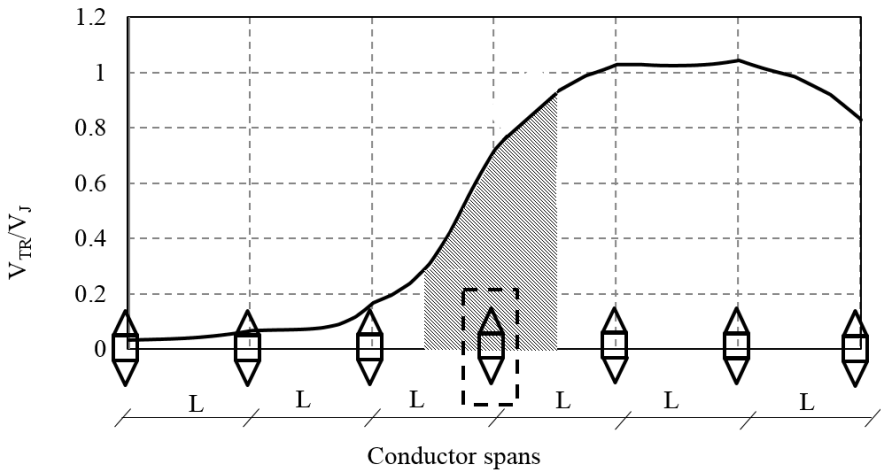

Fig. 4-8. Transverse velocity distribution for the critical oblique load case (R/D=1.6 and Θ=30° and L/D_J=0.5).

4.3. Variation of Longitudinal Force with the Conductor parameters

The objective of this paper is to present a simple procedure for the evaluation of the longitudinal force transmitted from the conductors to a tower as a result of the critical downburst configuration identified in the previous section. To do so, the variations in the longitudinal force with various geometric and material parameters of the conductors must be first assessed. This will allow the identification of the parameters that do not affect the longitudinal force as well as those that lead to both linear and nonlinear variations of such a force. The parameters that affect the response of the conductors can be grouped as follows: (a) insulator length (h), (b) wind pressure ($\alpha= 0.5*\rho*d_P*V_J^2$), (c) axial stiffness (EA), (d) weight per unit length (w), and (e) sag ratio which is the line sag divided by the span (S).

In the above parameters, d_P is the projected diameter of the conductor in the direction perpendicular to the transverse wind. The parameter α is proportional to the magnitude of the applied wind pressure of the conductor.

The structural analysis conducted in this part of the study utilizes an analytical technique developed and validated by Aboshosha and El Damatty (2014). The technique considers six conductor spans, three on each side of the tower at which the longitudinal force is to be calculated. The technique takes into account the nonlinear behaviour of the conductors associated with large deformations as well as the effect of the pretension forces. The flexibility of the insulators at the tower/conductor connections has a significant effect on a cable's longitudinal responses as indicated by Kashani and Bell (1988) and Wei et al. (1999). Using a fully-hinged boundary condition assumption at the tower-conductor's joint will cause an overestimation of the conductor's longitudinal force (Darwish et al., 2010). The flexibility of the insulators supporting the conductors is included in the Aboshosha and El Damatty (2014) analytical technique, which can predict the response under a general non-uniform and non-symmetric load distribution such as that resulting from the critical oblique downburst case identified in the previous section. The main advantage of this technique compared to the standard nonlinear finite element analysis is the computational efficiency. The former technique is approximately 185 times faster than the finite element analysis. A schematic showing the six-span conductors included in the analytical model is shown in **Fig. 4-9**. The springs shown in this figure simulate the insulators' stiffness. The non-uniform distributed load considered in the analysis is also shown in the figure. This load is obtained from the velocity distribution provided in **Fig. 4-8**, which is transformed into forces using the following equation obtained from ASCE-74 (2010):

$$F = QK_Z K_{Zt} (V_{TR})^2 G C_f A_P \tag{4-1}$$

where Q is the numerical coefficient of a value equal to 0.613; K_Z is the velocity pressure exposure coefficient taken to be 1, assuming an open terrain; K_{Zt} is the topographic factor

which is considered to be equal to 1 assuming that there are no topographic magnifier factors; V_{TR} is the transverse velocity distribution along the line given in **Fig. 4-8**; G is the gust response factor for the conductors, which is considered to be equal to 1 assuming that the downburst velocity is a gust velocity; C_f is the force coefficient taken to be 1, for circular sections; A_P is the conductor projected area per unit length (d_P*1). Thus, **Equation (4-1)** can be simplified using the following expression: $F = 0.613\,(V_{RD})^2 d_P$.

It's worth mentioning that the value of the force coefficient, C_f, recommended by the ASCE-74 (2010) code equation does not take into consideration the transient aerodynamics effect of the downburst gust. In the gust front factor framework developed by Kwon and Kareem (2009), a potential increase in the aerodynamics of the structure is suggested to take place due to the abrupt increase of the downburst velocity. Kwon and Kareem (2009) recommended to consider the amplification factor of the aerodynamics is unity until further studies are conducted.

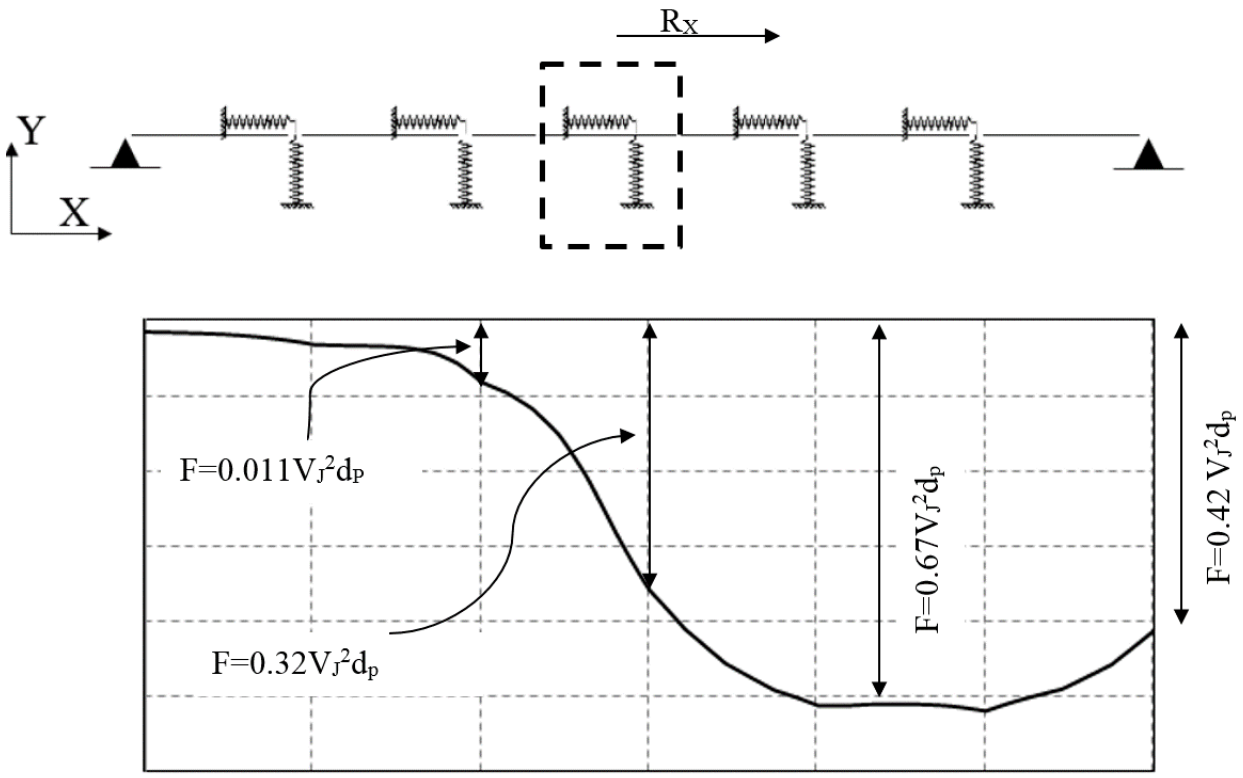

Fig. 4-9. Distribution of transverse forces on the conductor due to the critical oblique downburst case.

In the analytical solution, the response of the conductors is obtained using an iterative procedure and the longitudinal force, R_X, which is transmitted to the intermediate tower is determined. The variations of the force, R_X, with the various conductor parameters, as obtained from the analysis, are presented below. For each of the examined parameters, the practical range is determined based on recommendations received from Hydro One Ontario and from other utility companies in the USA. Two conductors, C1 and C2, are used in the parametric study. The weight per unit length, the projected diameter, and the axial stiffness of the two conductors are given in **Table 4-1**. The default value for the sag ratio for each conductor is given in this table. For each conductor, three span values are considered, which

are also given in **Table 4-1**. The numbers given in the table are the default values used in the parametric study.

Table 4-1. Conductors used to assess the effect of the conductor's parameters on R_X

Conductor index	Weight per unit length w (N/m)	Projected diameter d_P (m)	Axial stiffness EA (N)	Sag ratio S	Span L (m)	Insulator length (m)	Downburst velocity (m/s)
C1	40	0.04	1.89 E+08	4%	300, 400, and 500	3	70
C2	10	0.02	3.5E+07	2%	300, 400, and 500	2	70

For each conductor, the following parametric study is undertaken:

1. **Effect of the insulator length**: The insulator length, h, is varied from 1 m to 5 m. **Fig. 4-10** shows the variations in the force R_X with h for the two conductors and for the different span values. The figure shows that the values of R_X are inversely proportional to h. The variations of R_X with h are almost linear and a larger variation is shown for C1, especially on large spans.
2. **Effect of the wind pressure**: The wind pressure, α, is varied from 25 kg/sec^2 to 125 kg/sec^2. This corresponds to a variation in the jet velocity from 31 m/s to 70 m/s for C1 and from 44 m/s to 100 m/s for C2. **Fig. 4-11** shows the variations in the force R_X with α for the two conductors and for the different span values. As expected, R_X increases with the increase of α. For large spans, the relationship is nonlinear.
3. **Effect of the line sag**: The sag value is varied from 12 m to 18 m for both conductors. This corresponds to a sag to span ratio, S, that ranges between 2% and 4%. **Fig. 4-12** shows the variations in the force R_X with the sag values, S_L, for the two conductors and for the different span values. The results shown in **Fig. 4-12** indicate that R_X is nonlinearly proportional to the cable sag. This is obvious for the large span case of a

heavy conductor, C1. This can be justified by the fact that the increase in the conductor sag leads to a reduction in the pretension force and, consequently, to a reduction in the conductor's stiffness. As a result, the transverse deflection resulting from the downburst wind load will increase. This will lead to an increase in the conductor's longitudinal force.

4. **Effect of the conductor's weight per unit length**: The conductor weight per unit length, w, is varied from 10 N/m to 40 N/m. This range corresponds to a variation in the conductor's diameter from 0.02 m to 0.04 m for both C1 and C2. To maintain the wind pressure α at the default values, 122.5 kg/sec^2 for C1 and 62.5 kg/sec^2 for C2, the jet velocity is varied from 70 m/s to 100 m/s for C1 and from 50 m/s to 70 m/s for C2. **Fig. 4-13** shows the variations of the force R_X with w for the two conductors and for different span values. The figure shows that the force R_X decreases nonlinearly with the increase in the conductor's weight per unit length. For a fixed sag value, the initial pretension force, T, is linearly proportional to w. As such, an increase in w will result in an increase in T and consequently to an increase in the conductor's stiffness. This in turn will reduce both the transverse deflection and the longitudinal force.

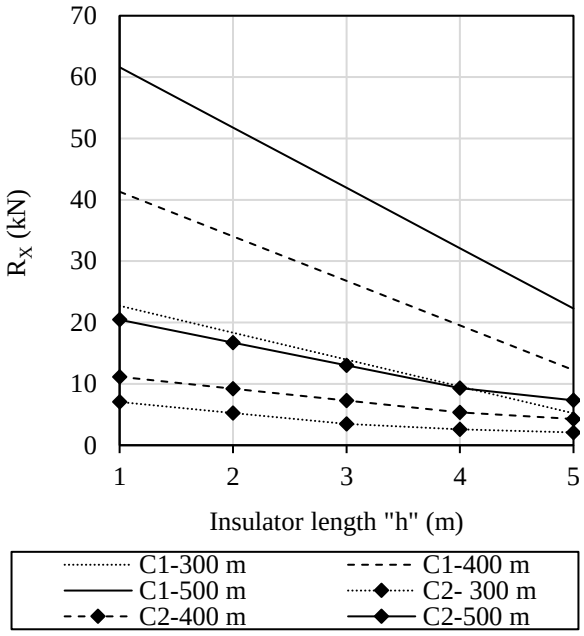

Fig. 4-10. Variations of R_X with h.

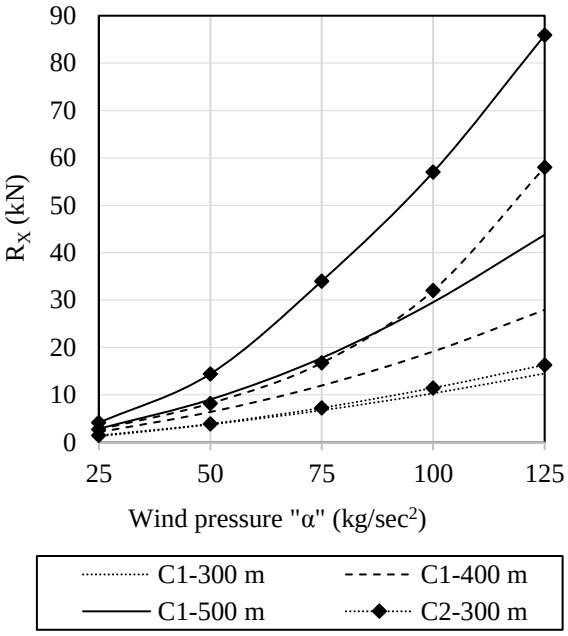

Fig. 4-11. Variations of R_X with α.

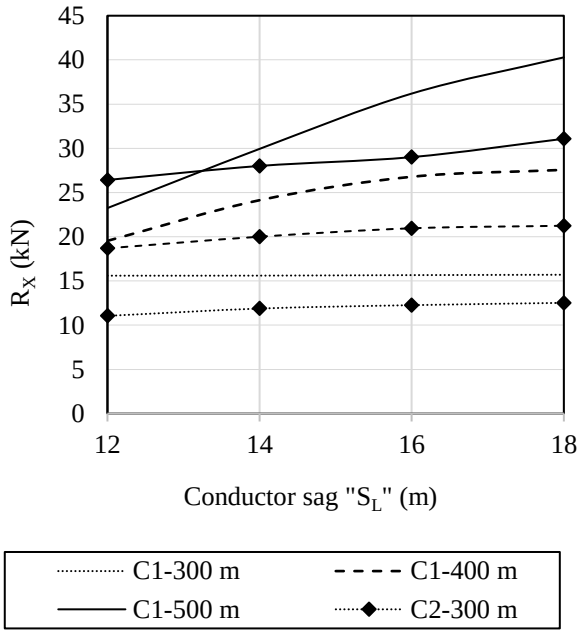

Fig. 4-12. Variations of R_X with S_L.

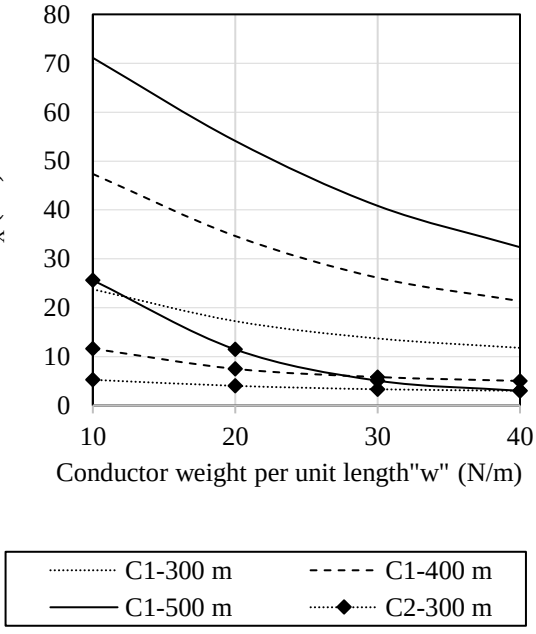

Fig. 4-13. Variations of R_X with w.

The parametric study also has shown that the axial stiffness, EA, of the conductor has a negligible effect on the longitudinal force.

4.4. Longitudinal force charts

In this section, a set of charts is developed, which is given in Appendix A, to evaluate the conductor's longitudinal force (R_X) acting on a generic tangent transmission tower under the critical oblique downburst load case obtained in section 4.2. The developed charts are based on the two main assumptions. First, the towers are aligned on a tangent line with a zero angle. Second, the conductor is attached to the tower through an insulator. As such, these charts are not applicable for the case of ground wires.

The presentation and the format of those graphs rely on the findings of the parametric study, which assist in identifying the trend of variations in R_X with each parameter. The charts are developed to cover the practical range of the variations of the parameters h, α, w, S, and L. The following findings obtained from the previously reported parametric studies are employed in the development of the charts:

1) For the considered range of h, the longitudinal force, R_X, varies linearly with h.
2) R_X varies nonlinearly with α. However, if the domain ($25 \leq \alpha \leq 125$) is divided into 4 regions, the variation of R_X with α is linear within each region.
3) The variations of R_X with L and S are nonlinear. Such variations are captured by presenting the charts in the form of the relationship between R_X and L for the different values of S.
4) In view of the above, the charts are divided into eight groups having different lower and upper limits for α and w. The ranges of those eight groups are provided in **Table 4-2**. For each group, eight graphs are developed covering all of the possible combinations of α_{min}, α_{max}, w_{min}, and w_{max} together with h_{min}= 1m and h_{max}=5m. The eight graphs illustrate the relationship between R_X and L, for the

different S ratios, for the upper and the lower limits of α, w, and h of the specific groups.

Since R_X varies linearly with α, w and h within each group, a three-dimensional linear interpolation can be carried out to obtain the value of R_X corresponding to the arbitrary values for L, S, h, w and α within the range of the group.

Table 4-2. Group range for the evaluation of R_X.

Group	α (kg/sec^2)		w (N/m)		h (m)	
	α_{min}	α_{max}	w_{min}	w_{max}	h_{min}	h_{max}
I	25	50	10	25	1	5
II	25	50	25	40	1	5
III	50	75	10	25	1	5
IV	50	75	25	40	1	5
V	75	100	10	25	1	5
VI	75	100	25	40	1	5
VII	100	125	10	25	1	5
VIII	100	125	25	40	1	5

The following steps illustrate the procedure that can be used to evaluate the maximum longitudinal force (R_X) of a conductor subjected to the critical oblique downburst load case.

1. Calculate $\alpha = 0.5*\rho*V_J^2*d_p$.
2. Based on α and the conductor's weight per unit length w, select the group that the system belongs to (I to VIII).

3. Based on the line span and the sag ratio, a user can determine eight longitudinal forces using the eight graphs of the selected group which are given in Appendix A. Those are labeled:

   R_{X1}= force corresponding to (w_{min}, h_{min}, α_{min})
   R_{X2}= force corresponding to (w_{min}, h_{min}, α_{max})
   R_{X3}= force corresponding to (w_{max}, h_{min}, α_{min})
   R_{X4}= force corresponding to (w_{max}, h_{min}, α_{max})
   R_{X5}= force corresponding to (w_{min}, h_{max}, α_{min})
   R_{X6}= force corresponding to (w_{min}, h_{max}, α_{max})
   R_{X7}= force corresponding to (w_{max}, h_{max}, α_{min})
   R_{X8}= force corresponding to (w_{max}, h_{max}, α_{max})

where h_{max}=5 m, h_{min}=1 m, w_{max} and α_{max} are the upper range of the conductor's weight per unit length and the wind pressure for selected group, while w_{min} and α_{min} are the lower ranges of the conductor's weight per unit length and the wind pressure for the selected group, respectively.

Based on the properties of the conductor under examination in terms of α, h and w, and the above-evaluated eight forces, a linear interpolation can be conducted using the set of equations shown below:

$$R_{X(1-2)} = R_{X1} + (R_{X2} - R_{X1}) * \frac{(\alpha - \alpha_{min})}{(\alpha_{max} - \alpha_{min})} \quad (4\text{-}2)$$

$$R_{X(3-4)} = R_{X3} + (R_{X4} - R_{X3}) * \frac{(\alpha - \alpha_{min})}{(\alpha_{max} - \alpha_{min})} \quad (4\text{-}3)$$

$$R_{X(h\,min)} = R_{X(3-4)} + (R_{X(1-2)} - R_{X(3-4)}) * \frac{(w_{max} - w)}{(w_{max} - w_{min})} \quad (4\text{-}4)$$

$$R_{X(5-6)} = R_{X5} + (R_{X6} - R_{X5}) * \frac{(\alpha - \alpha_{min})}{(\alpha_{max} - \alpha_{min})} \quad (4\text{-}5)$$

$$R_{X(7-8)} = R_{X7} + (R_{X8} - R_{X7}) * \frac{(\alpha - \alpha_{\min})}{(\alpha_{\max} - \alpha_{\min})} \quad (4\text{-}6)$$

$$R_{X(h\max)} = R_{X(7-8)} + (R_{X(5-6)} - R_{X(7-8)}) * \frac{(\mathrm{w}_{\max} - \mathrm{w})}{(\mathrm{w}_{\max} - \mathrm{w}_{\min})} \quad (4\text{-}7)$$

$$R_X = R_{X(h\max)} + \frac{(R_{X(h\min)} - R_{X(h\max)})}{(h_{\max} - h_{\min})} * (h_{\max} - h) \quad (4\text{-}8)$$

where α, w, and h are the actual cable parameters, α_{max} and α_{min} are the selected group's upper and lower limits of the wind pressure factor, respectively, and w_{max} and w_{min} are the selected group's upper and lower limits of the weight per unit length, respectively. **Fig. 4-14** shows a flow chart that summarizes the previous steps.

It is important to clarify that in case of multi-conductor's bundle, the estimated R_X obtained from **Equation (4-8)** must be multiplied by the number of sub conductors in the bundle assuming no shielding effect.

As shown above, the conductor's longitudinal force, R_X, depends on the value of α and consequently on the jet velocity of the downburst, V_J. **Fig. 4-2** indicates that the maximum radial velocity occurs at a 10 m height, V_{10}, which is typically measured and used to quantify the wind field, is approximately equal to the jet velocity, V_J. Maximum wind speed measured during previous strong downburst events have ranged between 50 m/s and 70 m/s (Savory et al. , 2001). As such, it is recommended to assume the value of V_J in calculating R_X using this range. Kim and Hangan (2007) showed that the wind field averaging time depends on the jet velocity and the size of the downburst event. Different studies such as Choi and Hidayat (2002), Holmes et al. (2008), Lombardo et al. (2014), and Solari et al. (2015) showed that the averaging period of downburst wind field is significantly lower than those averaging time typically used for synoptic winds. It should be noted that the wind speeds

measured during a downburst are gust and consequently they include turbulence. This means that the fluctuating component (turbulence) is taken into account in the procedure developed in this paper to estimate R_X. A full correlation of the turbulence is inherently assumed in this approach. This is a reasonable assumption since the studies conducted by Holmes et al. (2008) and Aboshosha and El Damatty (2014) reported that the turbulence associated with a downburst is more correlated than the turbulence associated with normal winds. Up to a span of 500 m, the previous studies have suggested that there is a span reduction factor resulting from the turbulence correlation, which is between 0.95 and 1.0; while for a normal wind the span reduction factor ranges between 0.75 and 1. In view of the above discussion and based on the fact that the resonant effect is attenuated by the large aerodynamic damping of conductors, the proposed approach is considered to adequately account for turbulence.

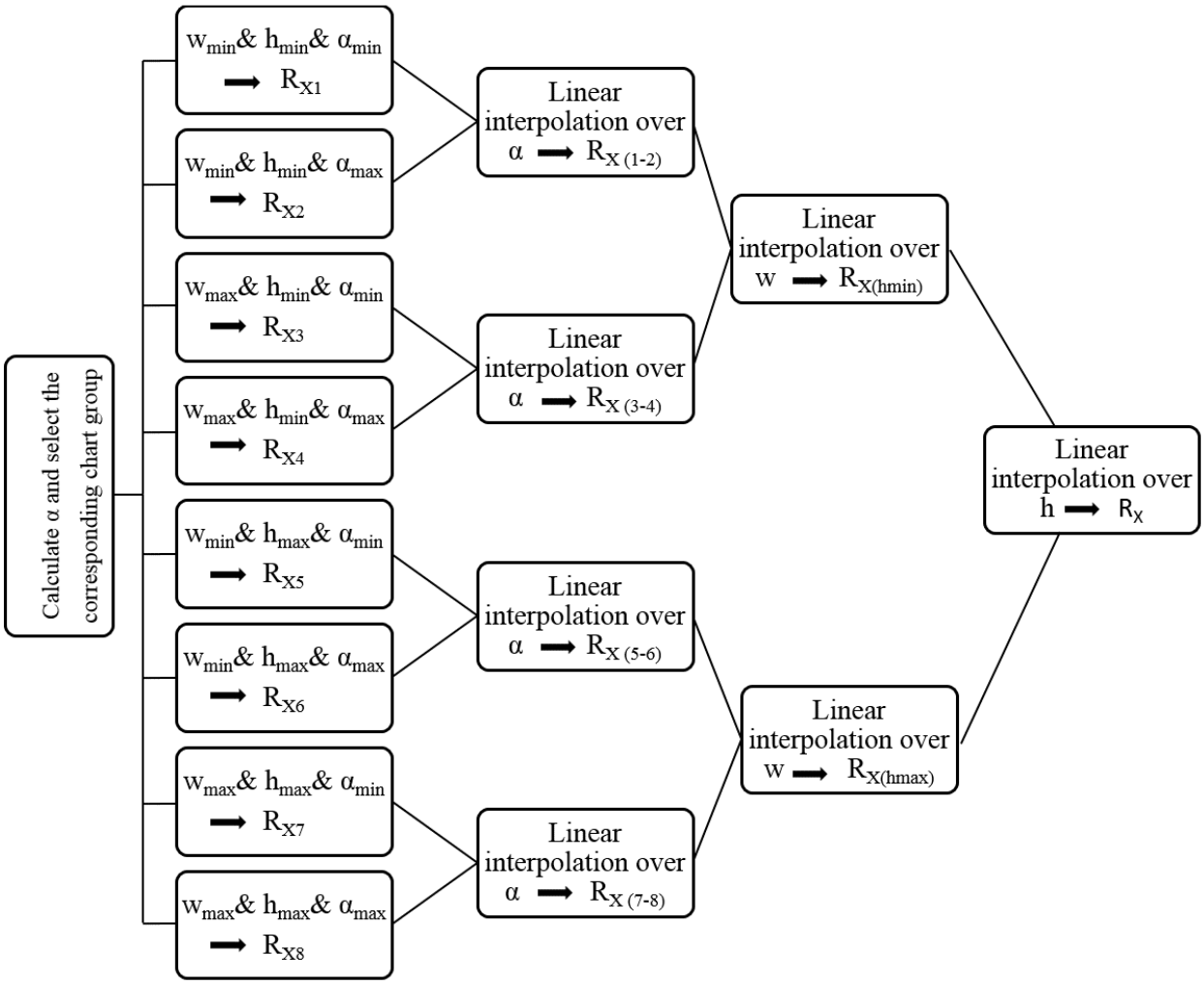

Fig. 4-14. Flow chart of the interpolation process to obtain the conductor's longitudinal force under the critical oblique downburst load case.

4.5. Transverse force

The conductor transverse force, R_Y, associated with the critical oblique downburst load case should be taken into consideration along with the calculated longitudinal force, R_X. The shaded area shown in **Fig. 4-8** represents the tributary area for the transverse velocity acting on an intermediate tower due to the critical oblique load case. By calculating this shaded area and dividing it by the span of the line, an equivalent uniform velocity, which leads to

an equal transverse force on the tower, can be estimated. This uniformly distributed velocity is found to be approximately equal to 0.65 V_J. Using this uniform velocity, the user can easily calculate the corresponding transverse force R_Y. **Fig. 4-15** illustrates the direction of the forces R_X and R_Y where they should be applied on the tower of interest."

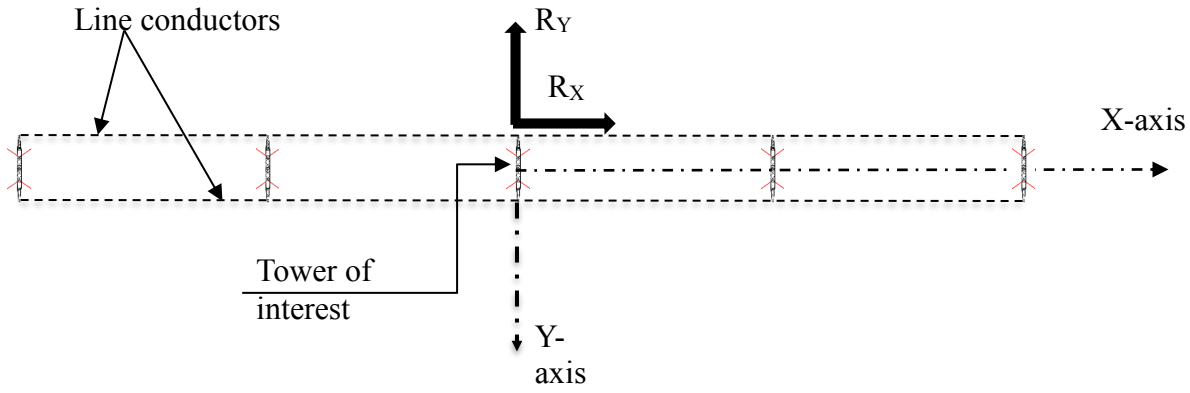

Fig. 4-15. Direction of the conductor forces R_X and R_Y.

4.6. Validation

The validation of the proposed solution is adopted by comparing the evaluated conductor forces, R_X and R_Y to those forces, R_{Xexact} and R_{Yexact}, calculated using the semi-analytical solution developed and validated by Aboshosha and El Damatty (2014) as shown in **Table 4-3**. The conductors used in the validation are selected from the data of five real transmission tower systems. The jet velocity is assumed to equal 70 m/s. **Table 4-3** shows that there is a good agreement between the results. The percentage of the error is found to be less than 6% and 3% for R_X and R_Y, respectively.

Table 4-3. Validation for the R_X and R_Y values obtained from the proposed approach

α (kg/s^2)	h (m)	w (N/m)	L (m)	S	R_X (kN)	R_{Xexact} (kN)	%Error (X)	R_Y (kN)	R_{Yexact} (kN)	%Error (Y)
156.25	2.4	18	400	3%	58.19	59.92	-2.88	26.40	25.7	2.7
187.5	3	10	300	2.50%	16.75	16.50	1.52	23.76	23.54	0.94
156.25	1.2	14	200	4%	36.88	37.25	-1.00	13.20	13.4	-1.49
132.25	4.27	34.68	460	3%	25.51	25.12	1.53	25.70	25.0	2.72
104.23	2.44	20.14	450	4.3%	44.55	42.16	5.45	19.8	19.6	1.1

4.7. Example

This section provides an example to demonstrate the solution steps required to evaluate the critical longitudinal force R_X using the developed charts.

Design Data

- Wind span =450 m
- Length of insulator assembly = 2.44 m.
- Conductor weight per unit length = 20.14 N/m
- Conductor projected diameter= 0.034 m
- Line sag= 19.5 m (~4.3% span)
- Assumed downburst jet velocity of 70 m/s

Based on the above data, the following calculations are conducted:

$$\alpha = V_J{}^2 * d_p = 70^2 * 0.034 = 166.77\ m^3/s^2$$
$$\Rightarrow 160 \langle \alpha \langle 200 \ \& \ w = 20.14\ N/m \Rightarrow 10 \langle w \langle 25 \quad \Rightarrow Group\ VII$$

Based on the charts in section 4 for Group VII, the following values are extracted:

$R_{X1} = 65\ kN$ $\quad$ $R_{X2} = 85\ kN$
$R_{X3} = 45\ kN$ $\quad$ $R_{X4} = 65\ kN$
$R_{X5} = 35\ kN$ $\quad$ $R_{X6} = 45\ kN$
$R_{X7} = 20\ kN$ $\quad$ $R_{X8} = 28\ kN$

Then the following calculations are conducted:

$$R_{X(1-2)} = R_{X1} + (R_{X2} - R_{X1}) * \frac{(\alpha - \alpha_{\min})}{(\alpha_{\max} - \alpha_{\min})}$$

$$\Rightarrow R_{X(1-2)} = 65 + (85 - 65) * \frac{(166.67 - 160)}{(200 - 160)} = 68.335\ kN$$

$$R_{X(3-4)} = R_{X3} + (R_{X4} - R_{X3}) * \frac{(\alpha - \alpha_{\min})}{(\alpha_{\max} - \alpha_{\min})}$$

$$\Rightarrow R_{X(3-4)} = 45 + (65 - 45) * \frac{(166.67 - 160)}{(200 - 160)} = 48.335\ kN$$

$$R_{X(h\min)} = R_{X(3-4)} + (R_{X(1-2)} - R_{X(3-4)}) * \frac{(\mathrm{w}_{\max} - \mathrm{w})}{(\mathrm{w}_{\max} - \mathrm{w}_{\min})}$$

$$\Rightarrow R_{X(h\min)} = 48.335 + (68.335 - 48.335) * \frac{(25 - 20.14)}{(25 - 10)} = 54.82\ kN$$

$$R_{X(5-6)} = R_{X5} + (R_{X6} - R_{X5}) * \frac{(\alpha - \alpha_{\min})}{(\alpha_{\max} - \alpha_{\min})}$$

$$\Rightarrow R_{X(5-6)} = 35 + (45 - 35) * \frac{(166.67 - 160)}{(200 - 160)} = 36.67\ kN$$

$$R_{X(7-8)} = R_{X7} + (R_{X8} - R_{X7}) * \frac{(\alpha - \alpha_{\min})}{(\alpha_{\max} - \alpha_{\min})}$$

$$\Rightarrow R_{X(7-8)} = 20 + (28 - 20) * \frac{(166.67 - 160)}{(200 - 160)} = 21.33\, kN$$

$$R_{X(h\max)} = R_{X(7-8)} + (R_{X(5-6)} - R_{X(7-8)}) * \frac{(\mathrm{w}_{\max} - \mathrm{w})}{(\mathrm{w}_{\max} - \mathrm{w}_{\min})}$$

$$\Rightarrow R_{X(h\max)} = 21.33 + (36.67 - 21.33) * \frac{(25 - 20.14)}{(25 - 10)} = 26.3\, kN$$

Then, the final longitudinal unbalanced force is evaluated:

$$R_X = R_{X(h\max)} + \frac{(R_{X(h\min)} - R_{X(h\max)})}{(h_{\max} - h_{\min})} * (h_{\max} - h)$$

$$\Rightarrow R_X = 26.3 + \frac{(54.82 - 26.3)}{(5 - 1)} * (5 - 2.44) = 44.55\, kN$$

4.8. Conclusion

A simple approach is developed in this paper that can be used to estimate the maximum longitudinal force that can act on transmission towers during downburst events. This force results from a downburst location that leads to an uneven distribution of wind velocity along the spans located adjacent to a tower. First, an assessment is done to estimate the critical downburst location that is expected to lead to the maximum values for the longitudinal forces. It is revealed that the critical downburst configuration corresponds to the situation where the ratio between the downburst distance and its diameter, R/D_J, is equal to 1.6 and the jet diameter is twice the conductor's span while the angle of attack Θ equals 30 degrees. This situation also corresponds to a downburst location having the projection of the center of the downburst on the line located at the middle of the second span adjacent to the tower of interest. At this critical location, an extensive parametric study is then conducted to assess

the variations of the longitudinal forces with various parameters that affect the conductor's response. The following findings related to the variations of the longitudinal force, R_X, with the conductor parameters are obtained:

a) R_X is inversely proportional to the insulator length h and the relationship between R_X and h is almost linear.

b) R_X increases with the increase of the wind pressure α and the relationship between R_X and α is non-linear.

c) R_X increases with the increase in the sag to span ratio, S. In most cases, the relationship between R_X and S is nonlinear.

d) R_X decreases with the increase in the conductor's weight per unit length, w. The relationship between R_X and w is non-linear.

e) R_X is not influenced by the change in the conductor's axial rigidity, EA.

It is shown that by dividing the practical range of α into four divisions and the practical range of w into two divisions, R_X varies linearly within those divisions. As such, the entire domain for the values of α and w can be divided into eight regions, where within each region, R_X varies linearly with α, w, and h. For each region, the variations of R_X with the span, L, and the sag ratio, S, are provided for the combinations of the upper and lower values of α, w, and h corresponding to each region. The force R_X for a general conductor can be then estimated from those plots by applying a three-dimensional linear interpolation between the values corresponding to the upper and lower limits of α, w, and h. A validation of the proposed approach is conducted by comparing the values estimated using the developed graphs and the interpolation procedures to those obtained directly from a semi-analytical closed form solution. Finally, an example is provided to illustrate the steps involved in the proposed

approach. Because of its simplicity and ease of application, it is expected that the developed approach will be of particular interest to practitioner engineers and developers of design guidelines. It will also assist in designing transmission towers to better resist downbursts and consequently mitigate the amount of damage resulting from the failures observed so frequently during those events.

4.9. Acknowledgement

The authors gratefully acknowledge Hydro One Ontario and the Natural Sciences and Engineering Research Council of Canada (NSERC) for their in-kind support, their collaboration in this project, and for the financial support provided for this research.

4.10. Appendix A

Group (I): 25 ≤ α ≤ 50 & 10 ≤ w ≤ 25

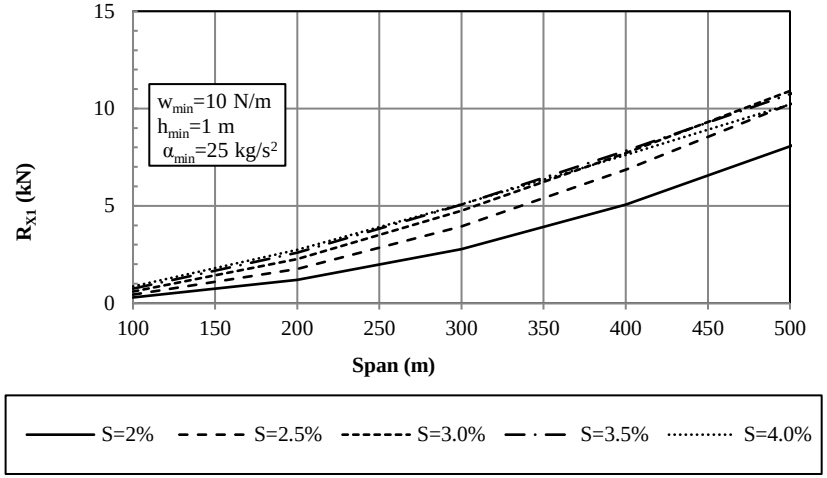

R_{X1}

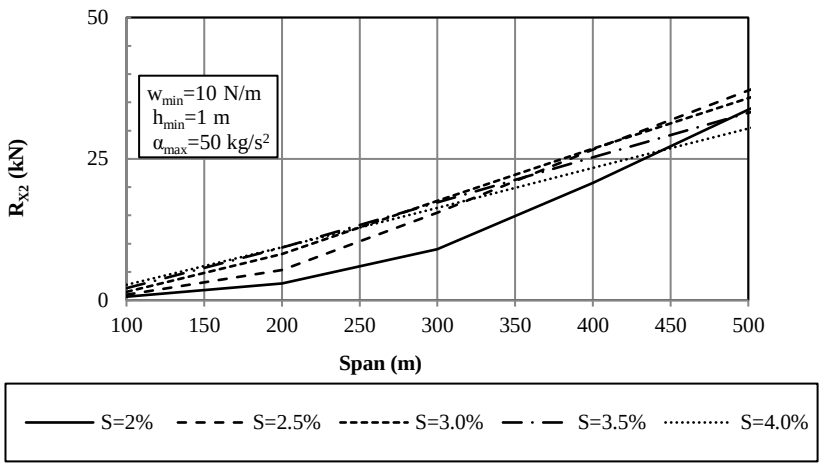

R_{X2}

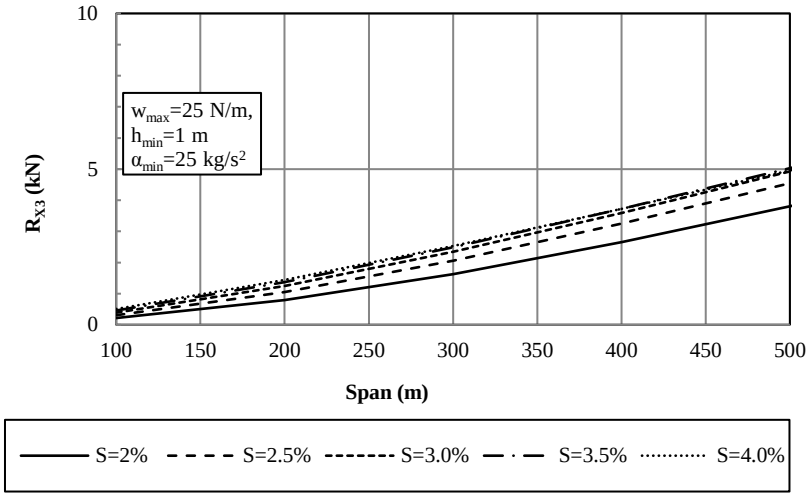

R_{X3}

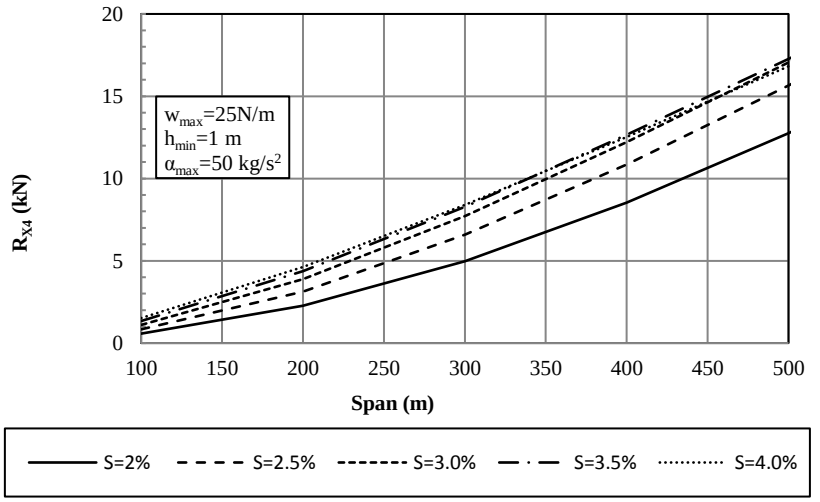

R_{X4}

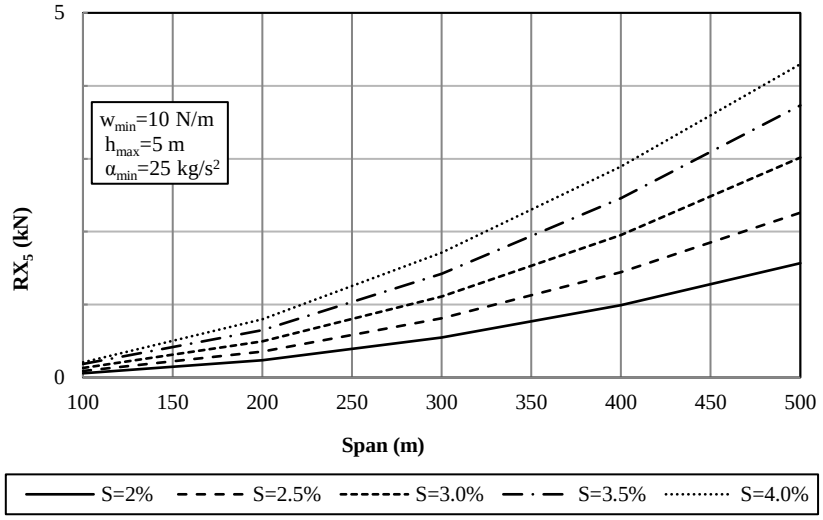

R_{X5}

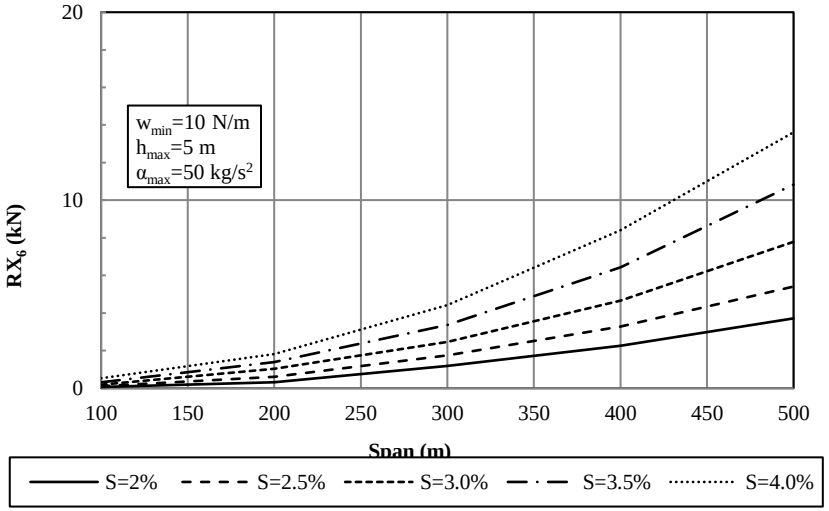

R_{X6}

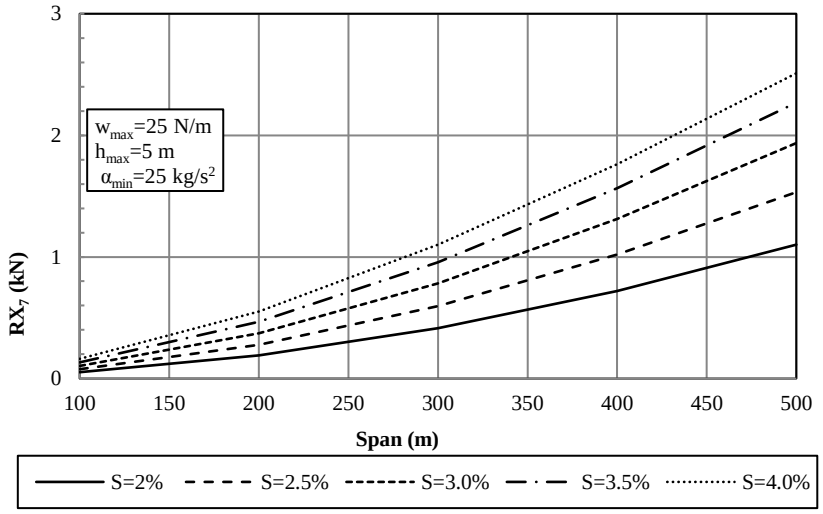

R_{X7}

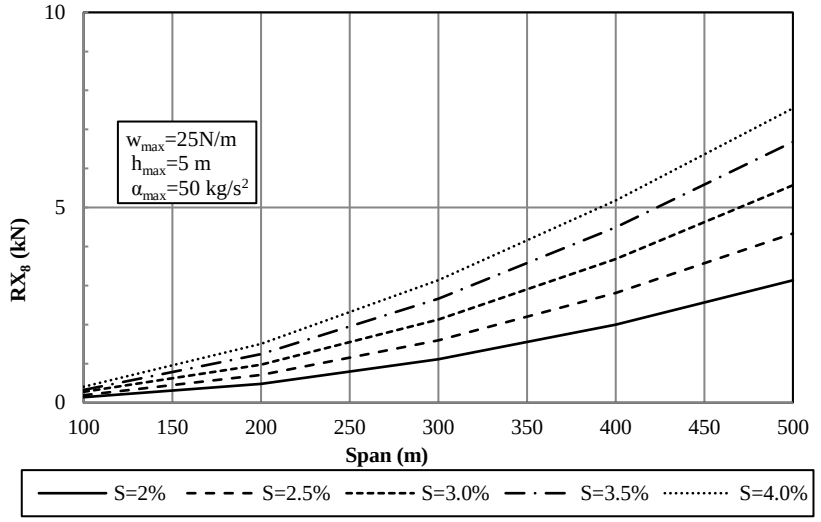

R_{X8}

Group (II): 25 ≤ α ≤ 50 & 25 ≤ w ≤ 40

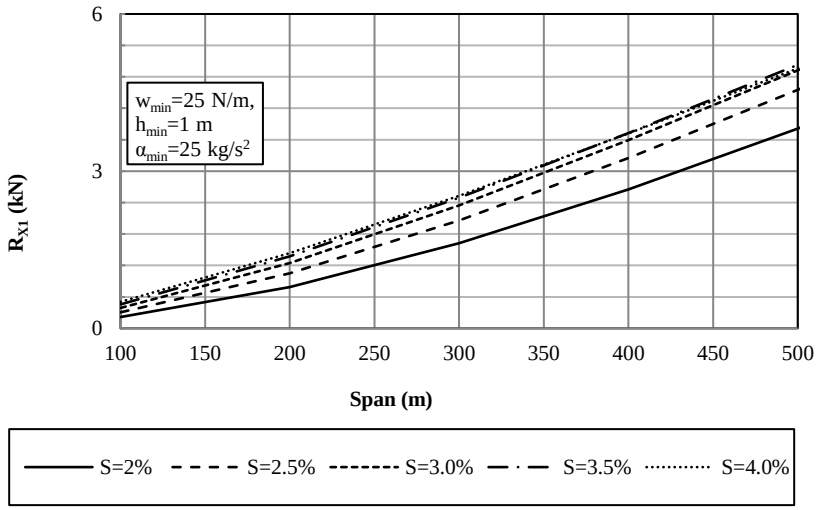

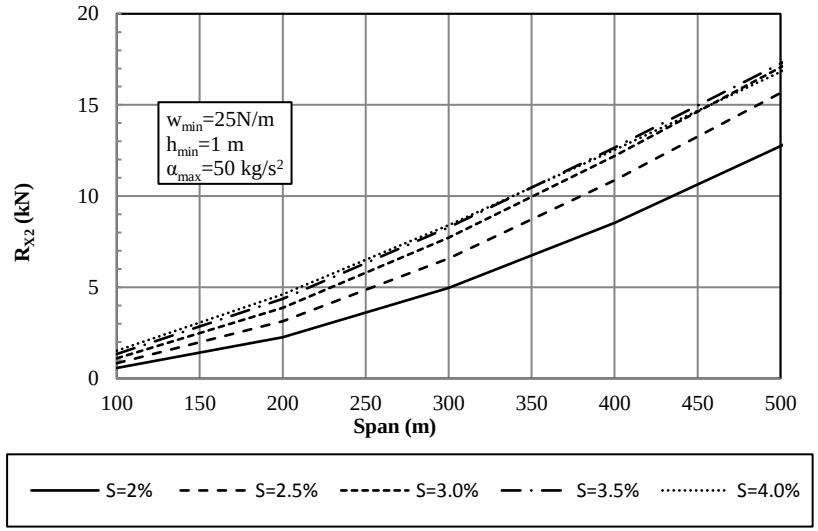

R_{X1} **R_{X2}**

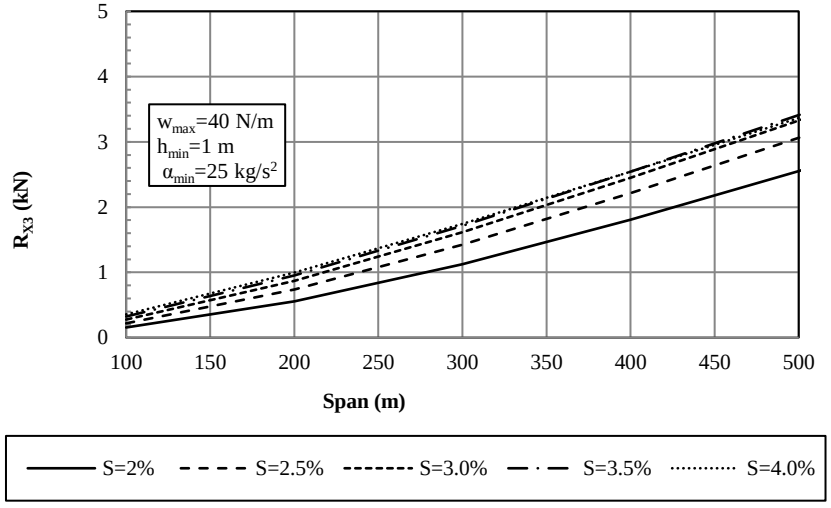

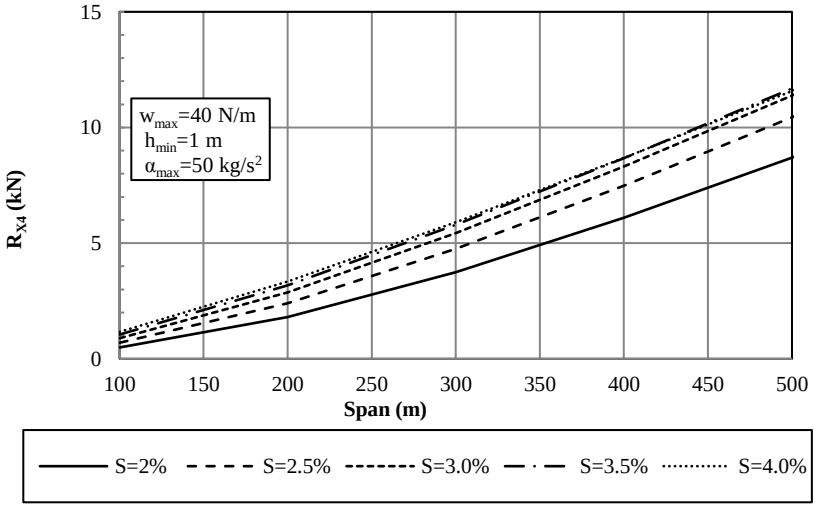

R_{X3} **R_{X4}**

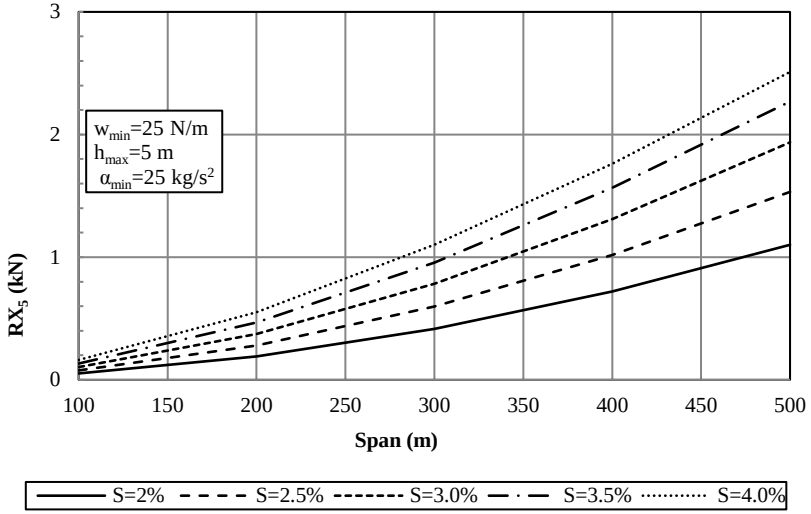

R_{X5}

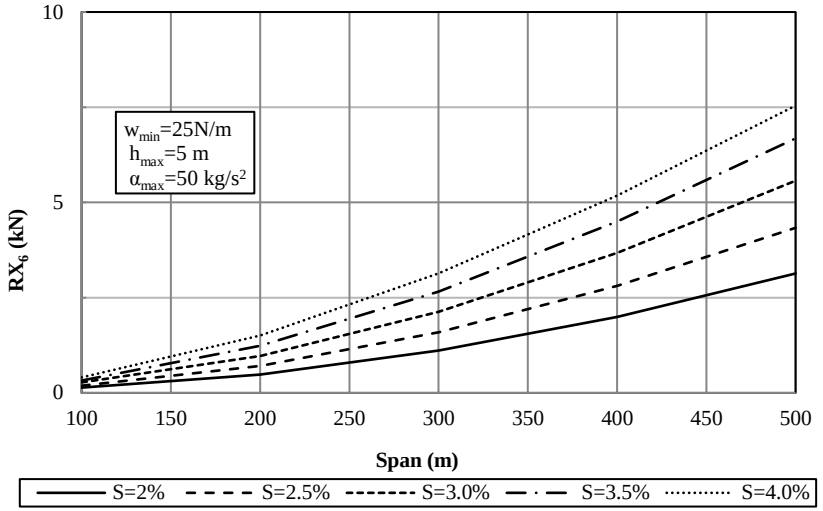

R_{X6}

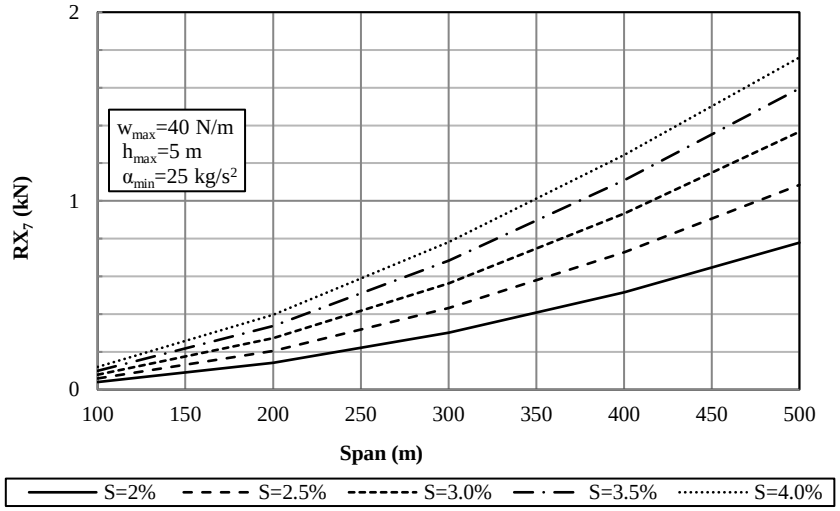

R_{X7}

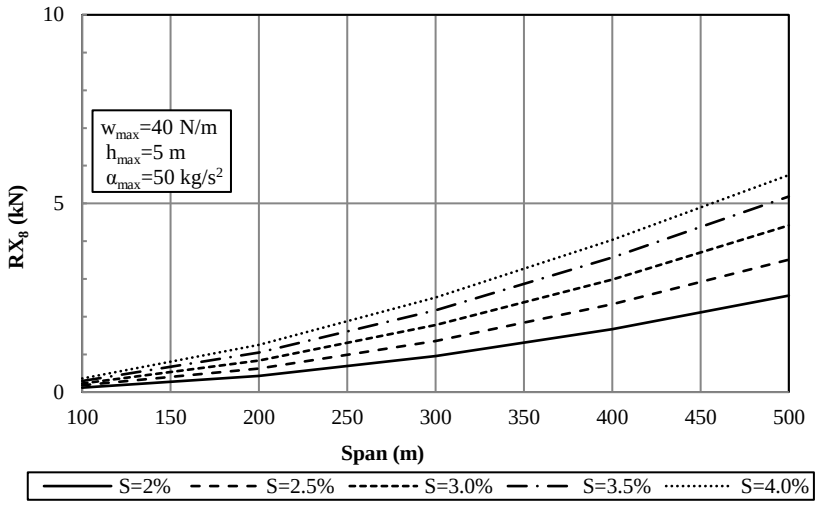

R_{X8}

Group (III): 50 ≤ α ≤ 75 & 10 ≤ w ≤ 25

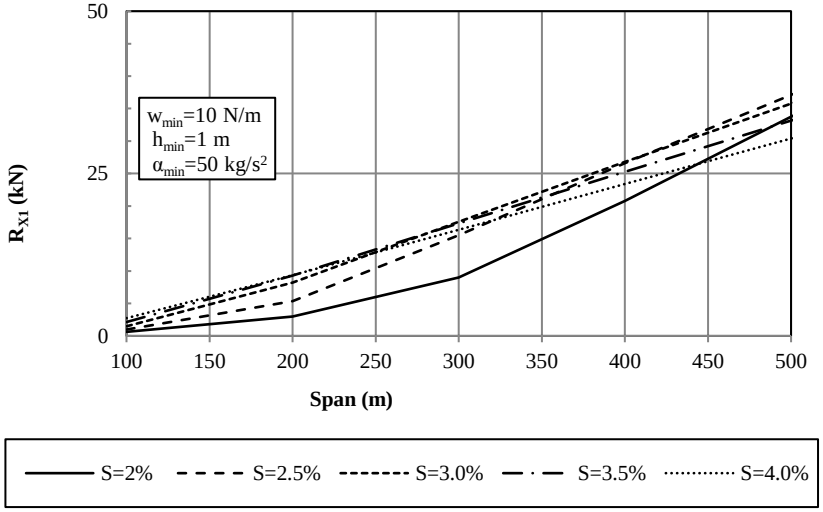

R_{X1}

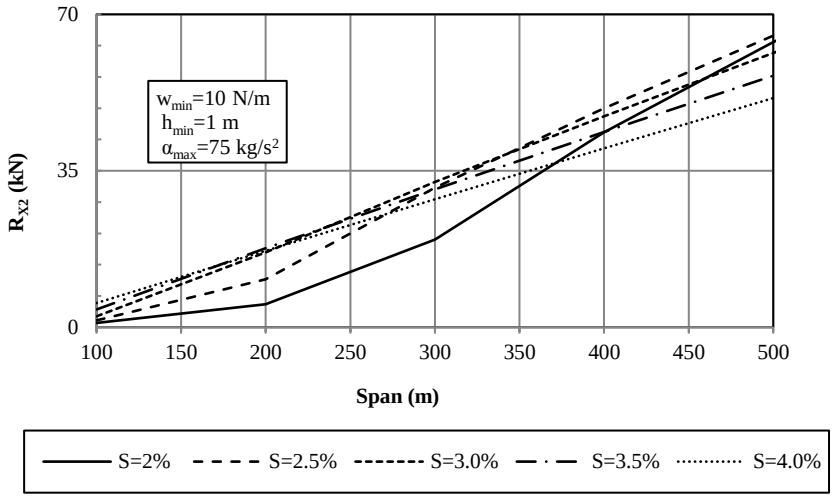

R_{X2}

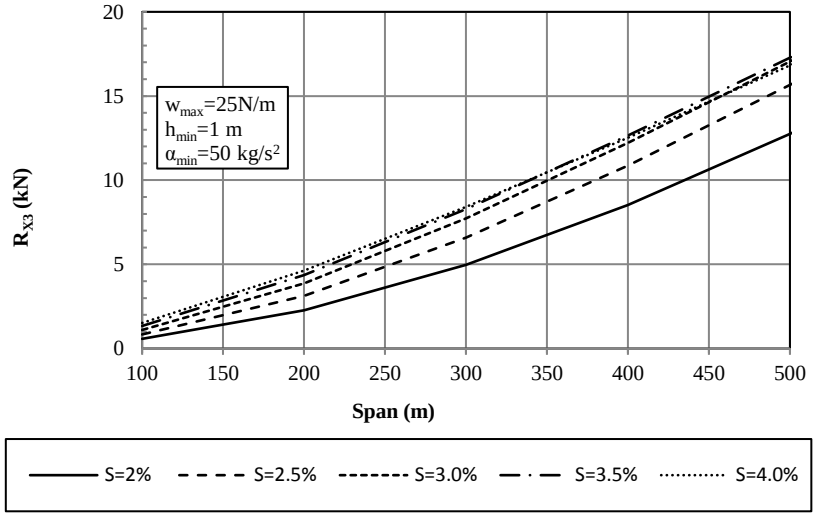

R_{X3}

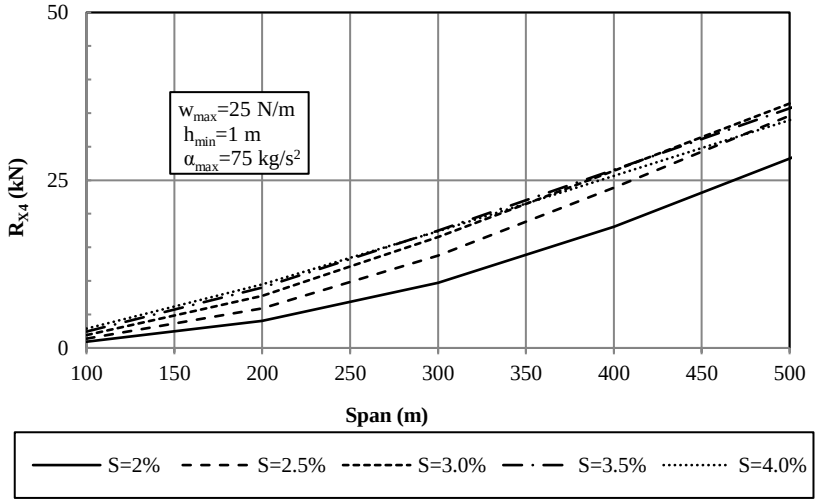

R_{X4}

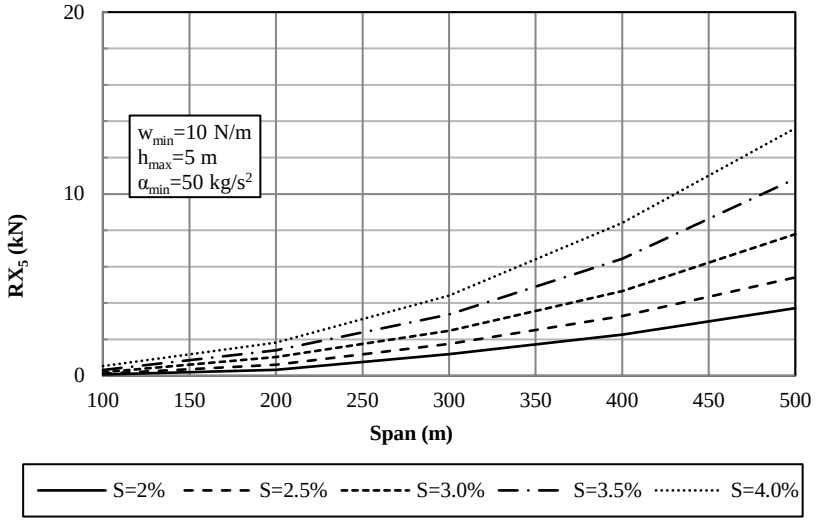

R_{X5}

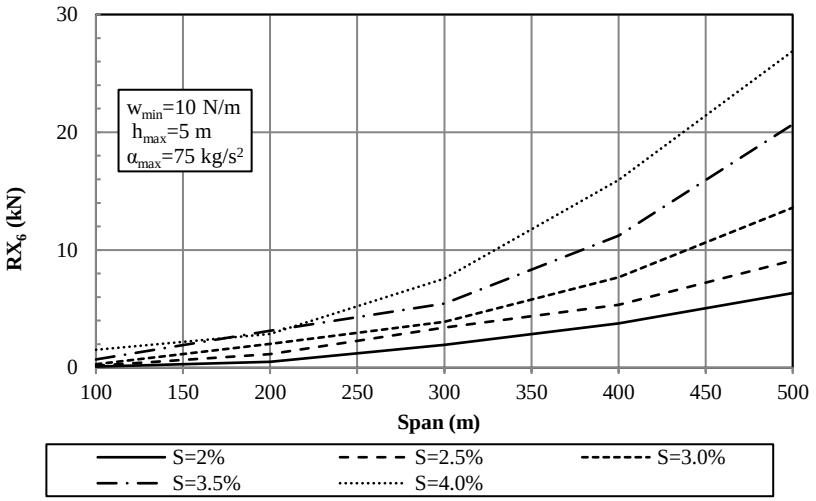

R_{X6}

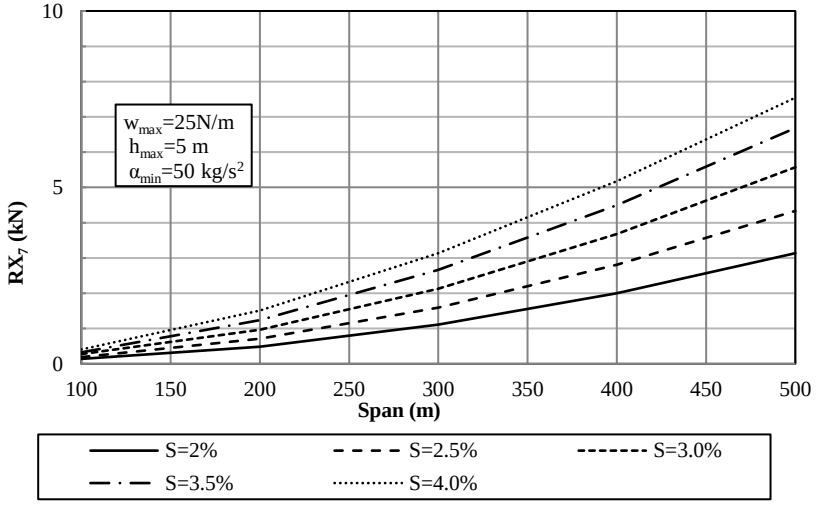

R_{X7}

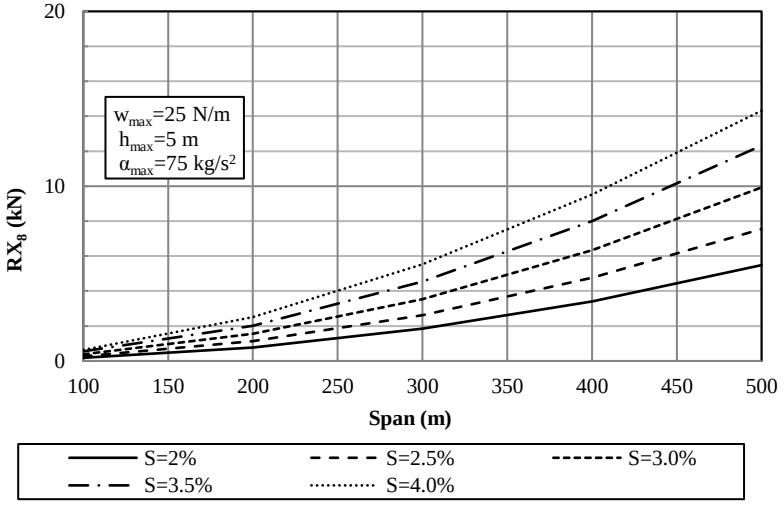

R_{X8}

Group (IV): 50 ≤ α ≤ 75 & 25 ≤ w ≤ 40

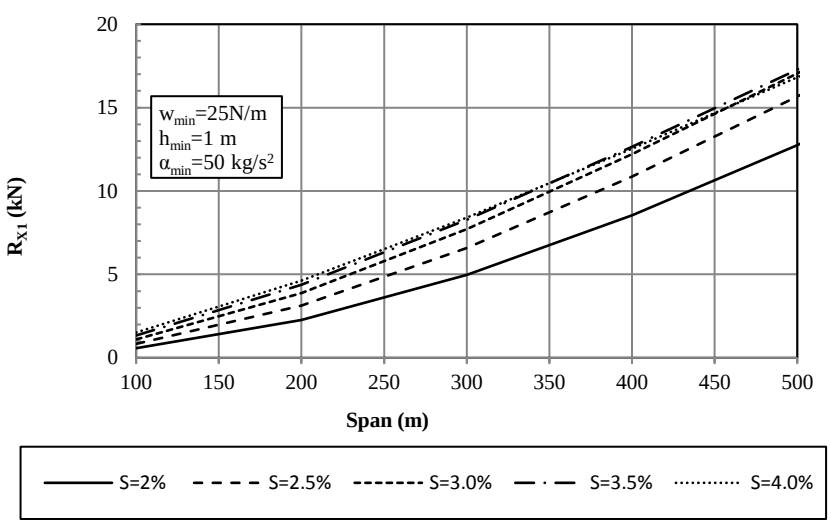

R_{X1}

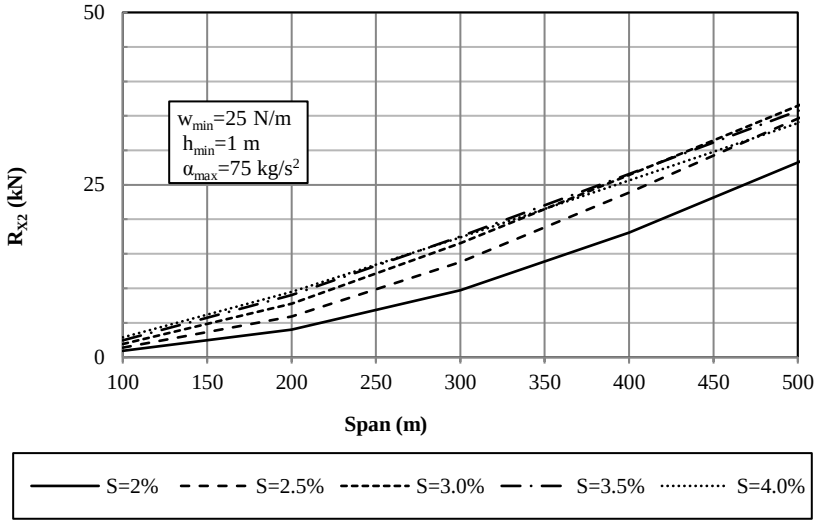

R_{X2}

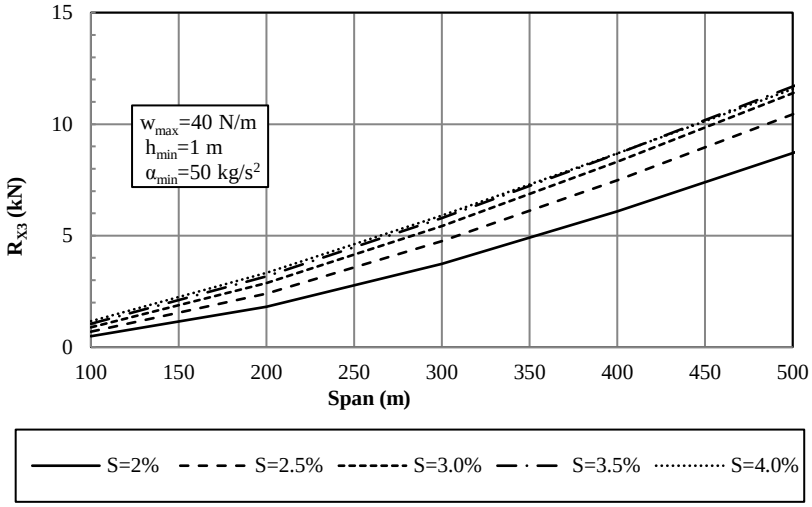

R_{X3}

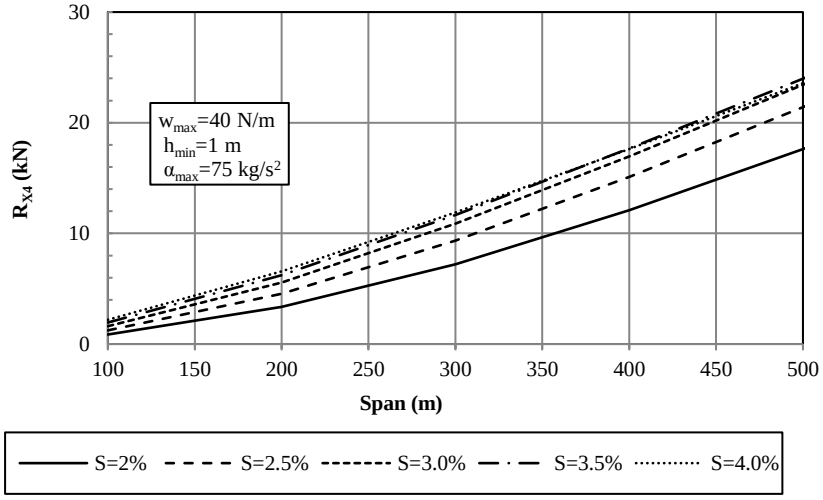

R_{X4}

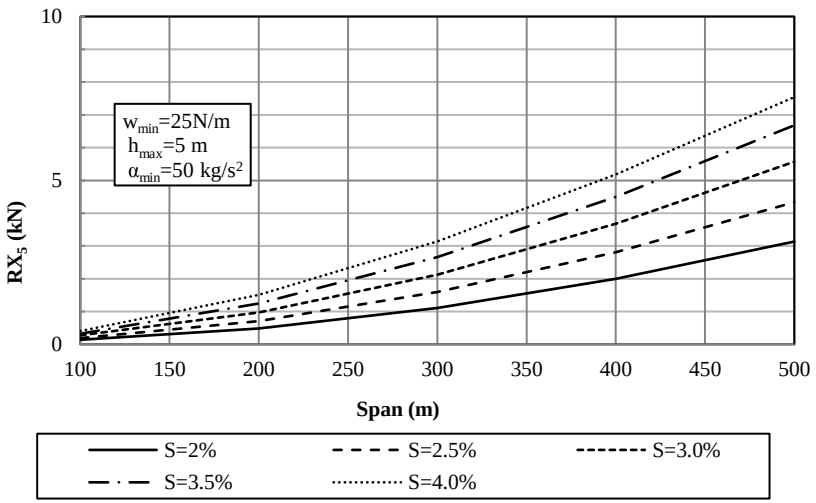

R_{X5}

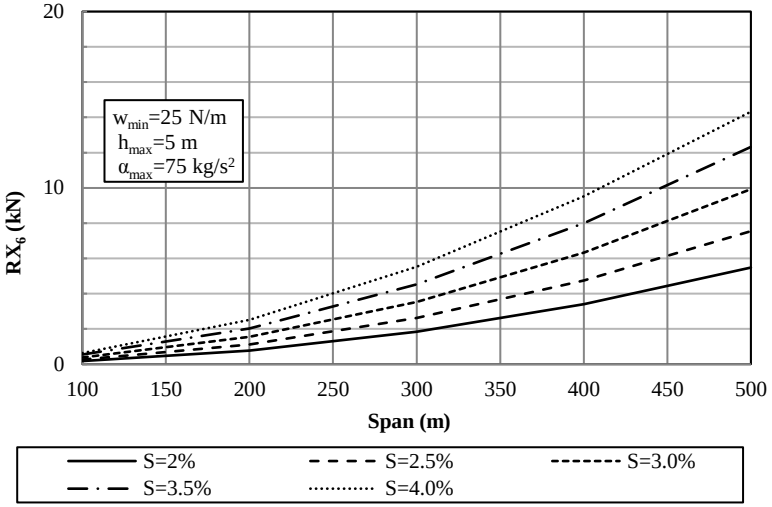

R_{X6}

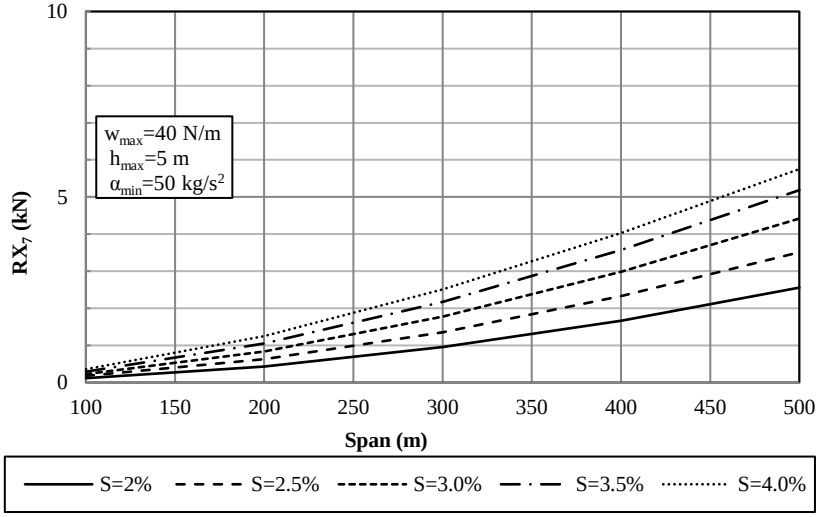

R_{X7}

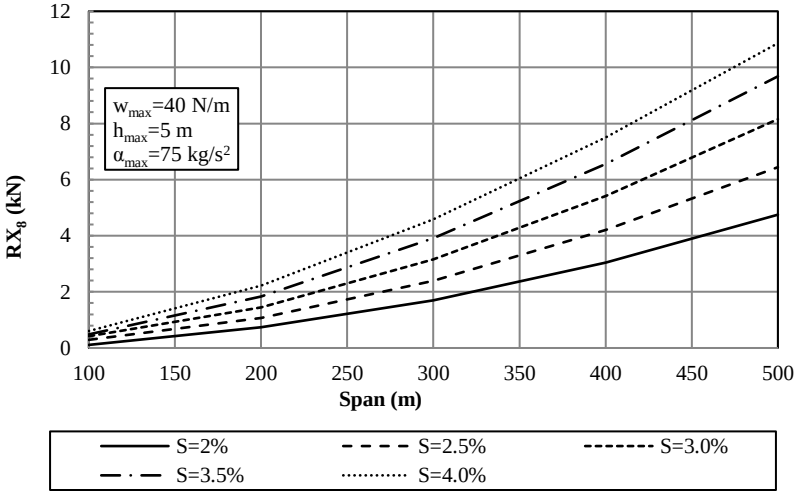

R_{X8}

Group (V): 75 ≤ α ≤ 100 & 10 ≤ w ≤ 25

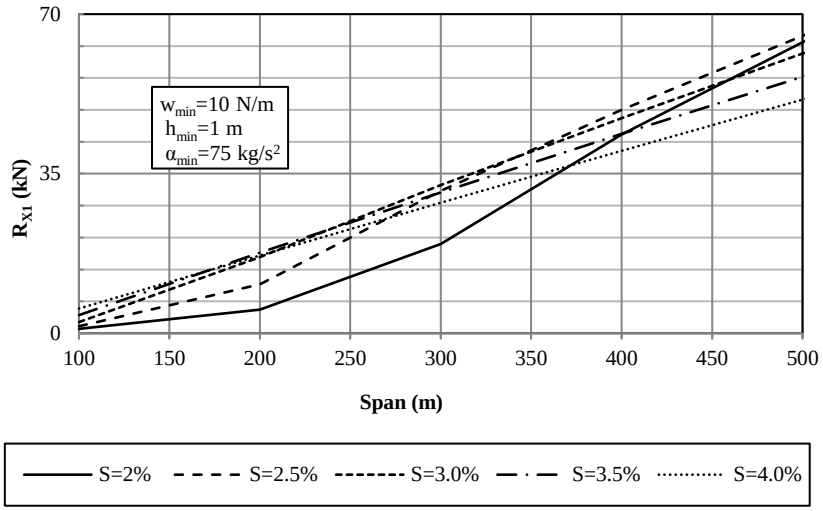

R_{X1}

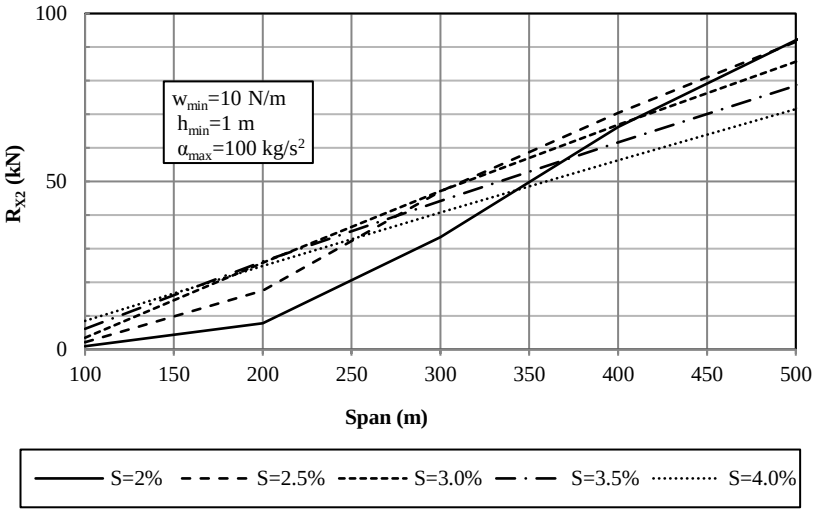

R_{X2}

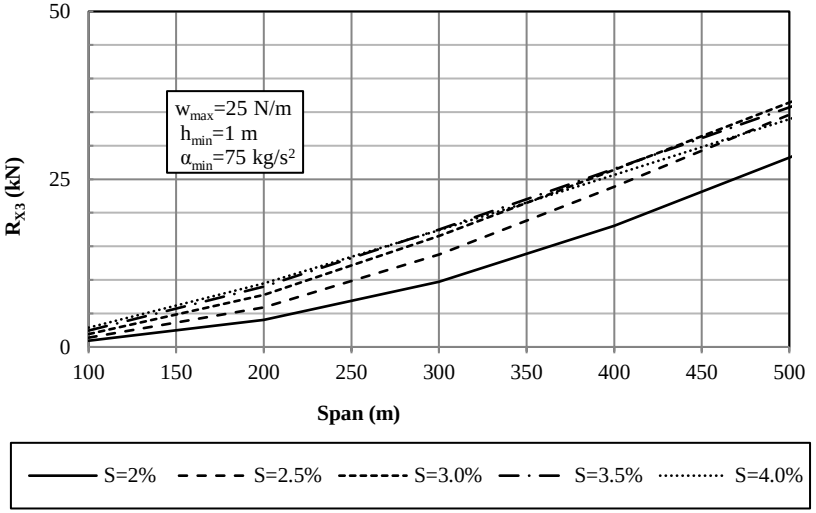

R_{X3}

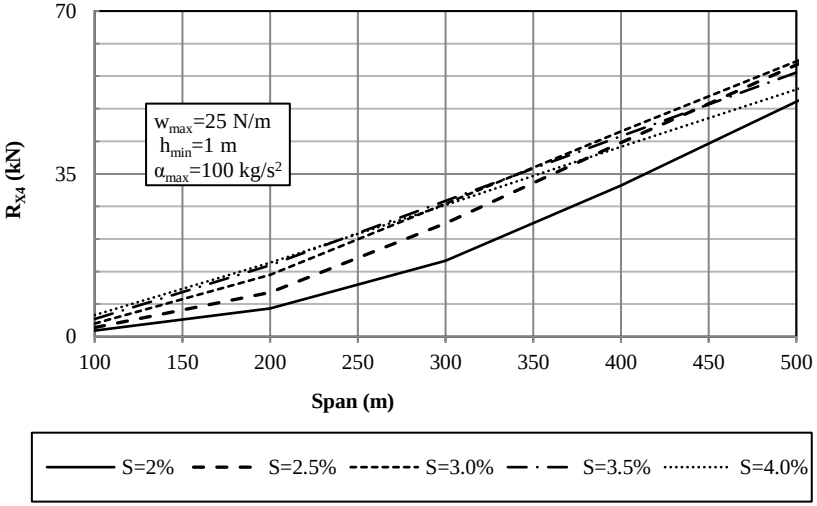

R_{X4}

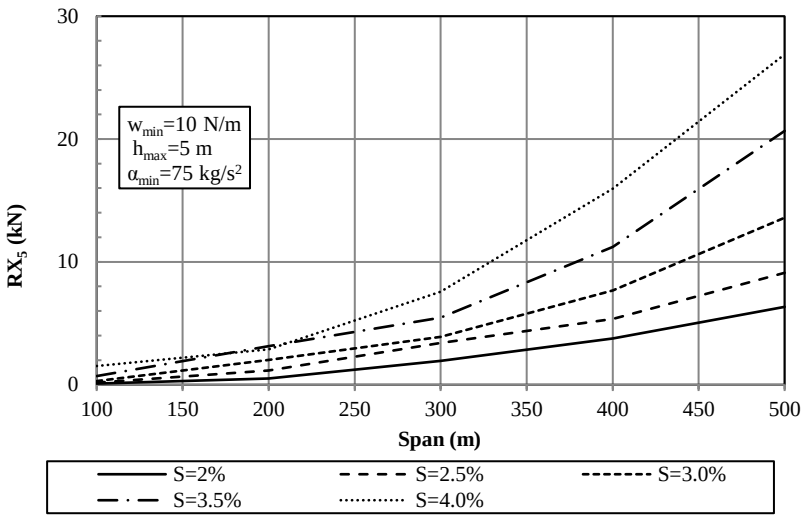

R_{X5}

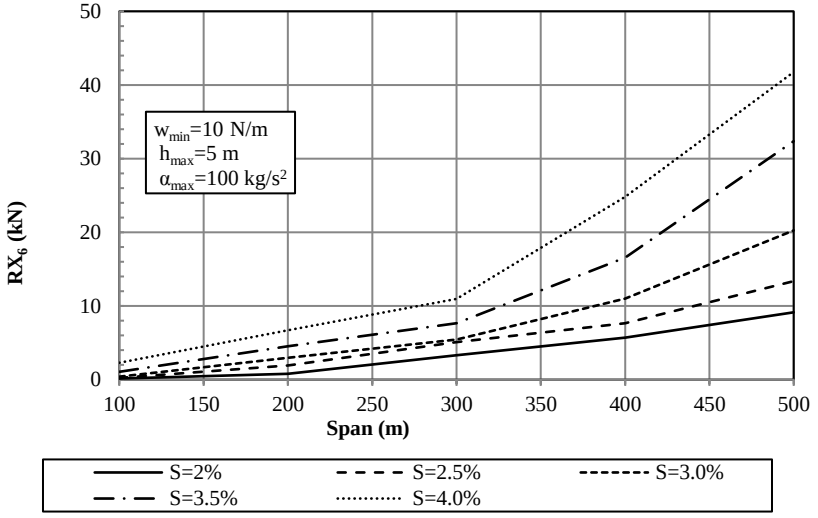

R_{X6}

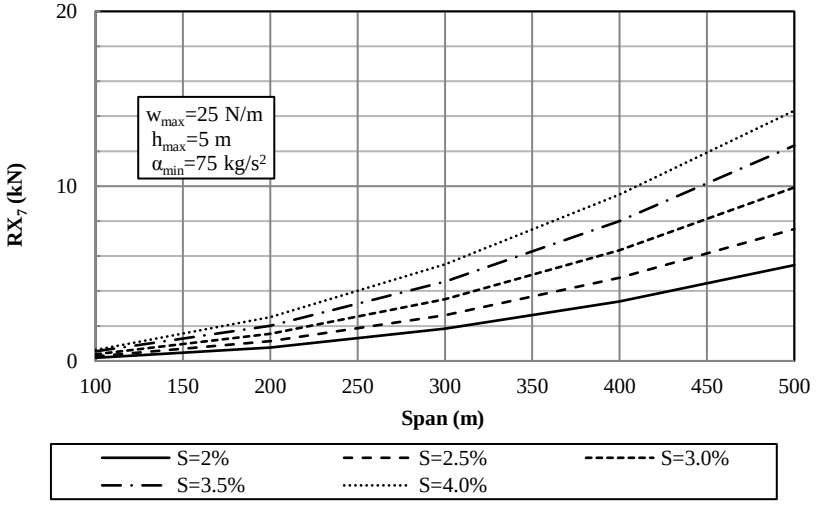

R_{X7}

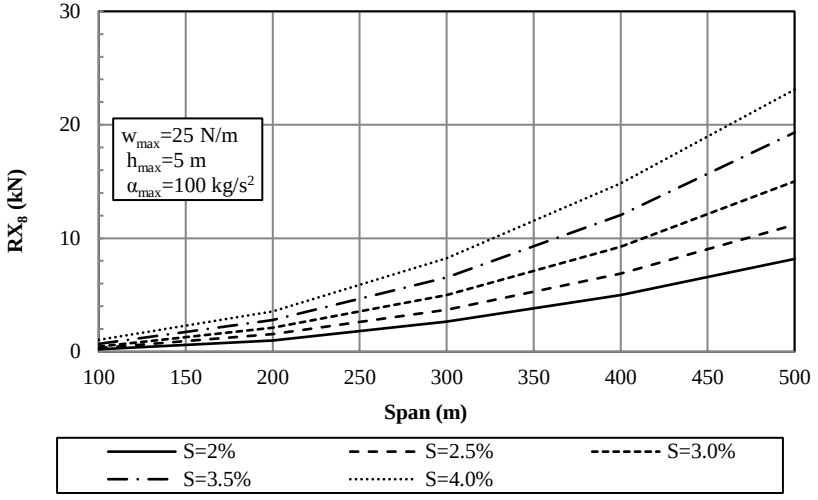

R_{X8}

Group (VI): 75 ≤ α ≤ 100 & 25 ≤ w ≤ 40

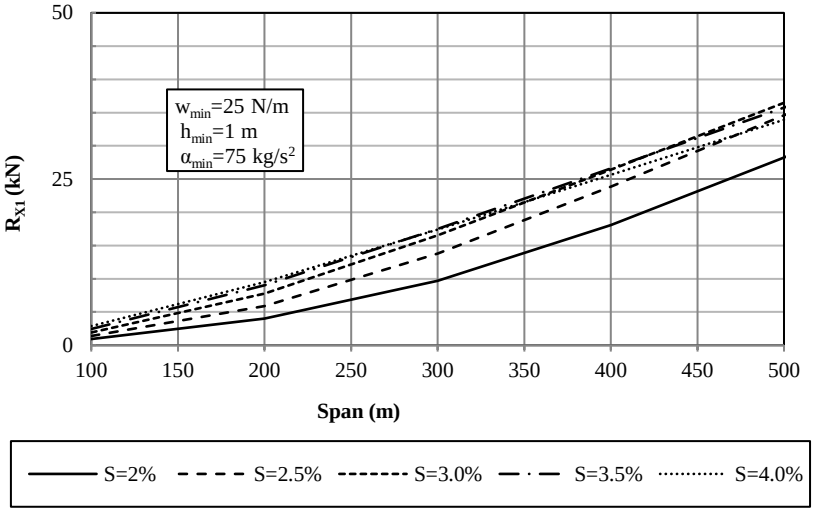

R_{X1}

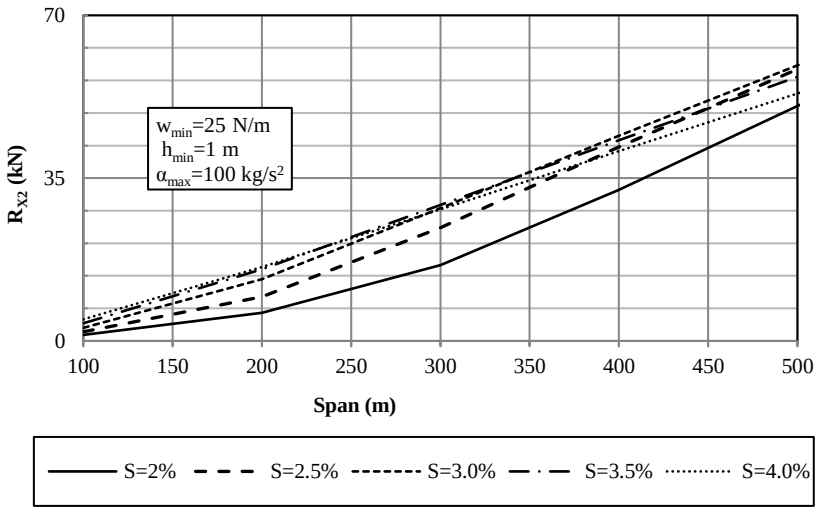

R_{X2}

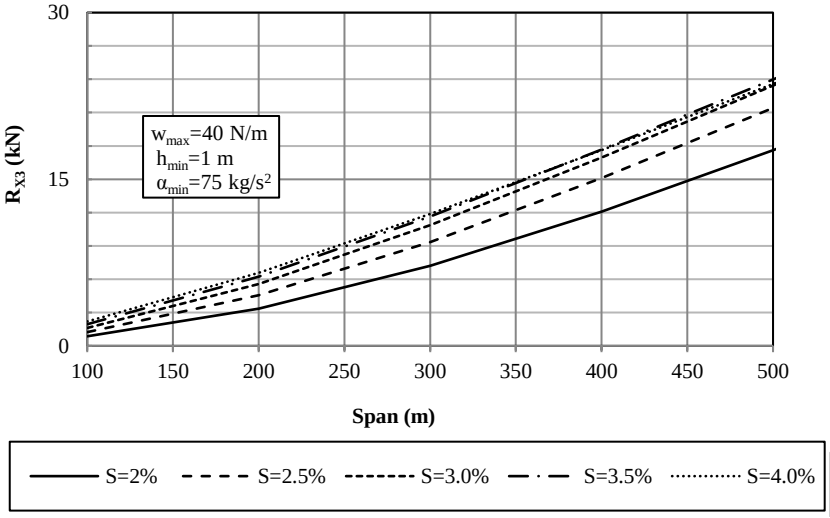

R_{X3}

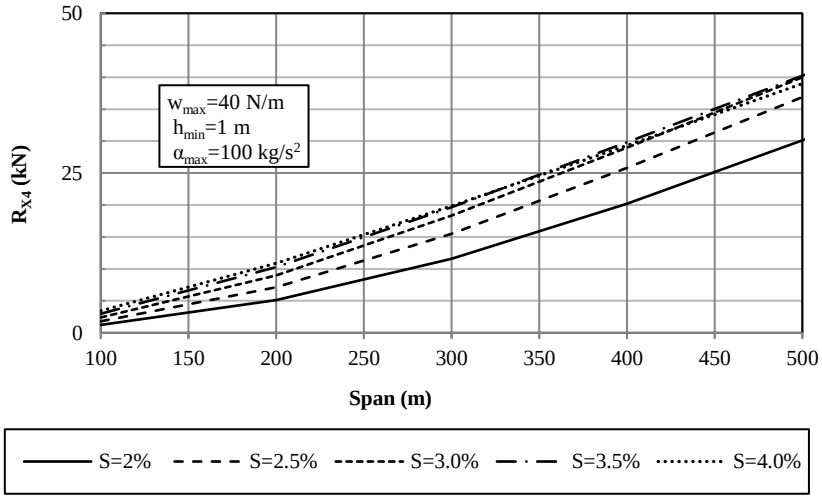

R_{X4}

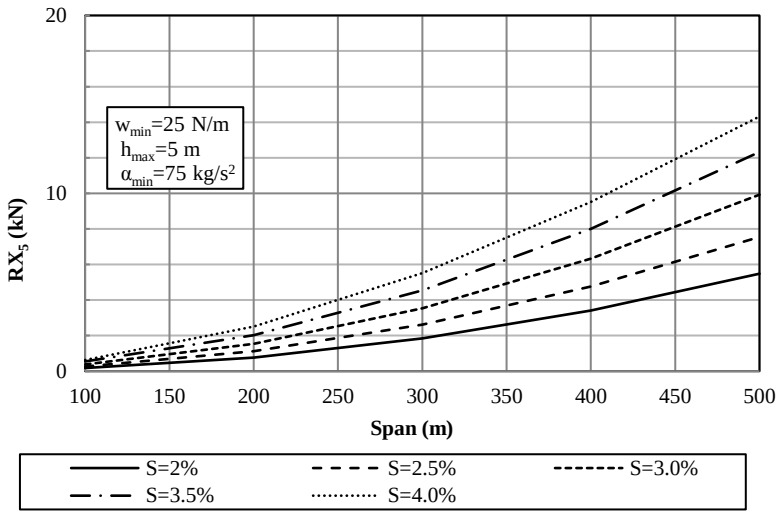

R_{X5}

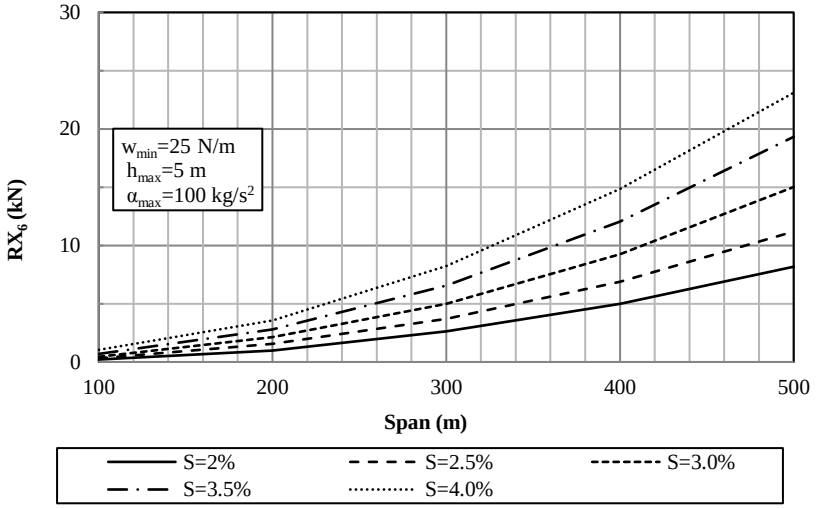

R_{X6}

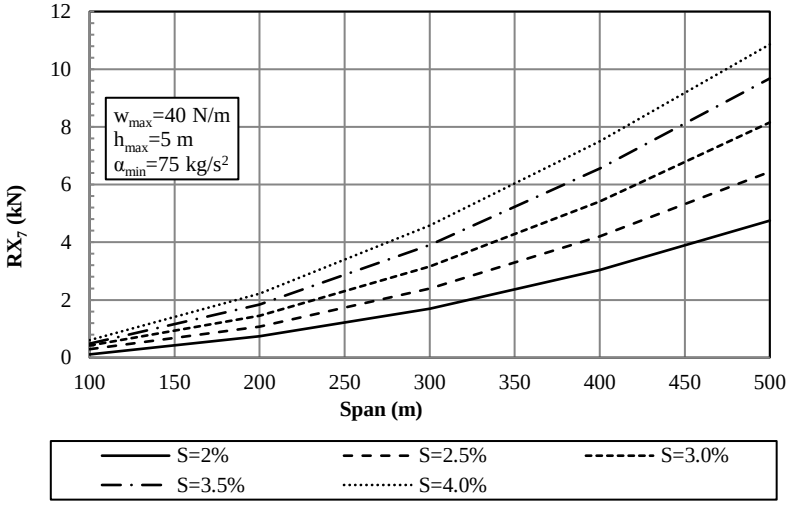

R_{X7}

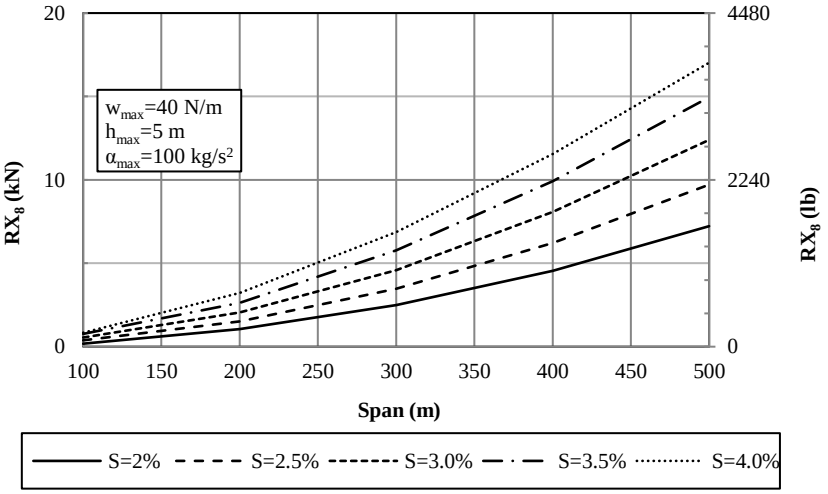

R_{X8}

Group (VII): 100 ≤ α ≤ 125 & 10 ≤ w ≤ 25

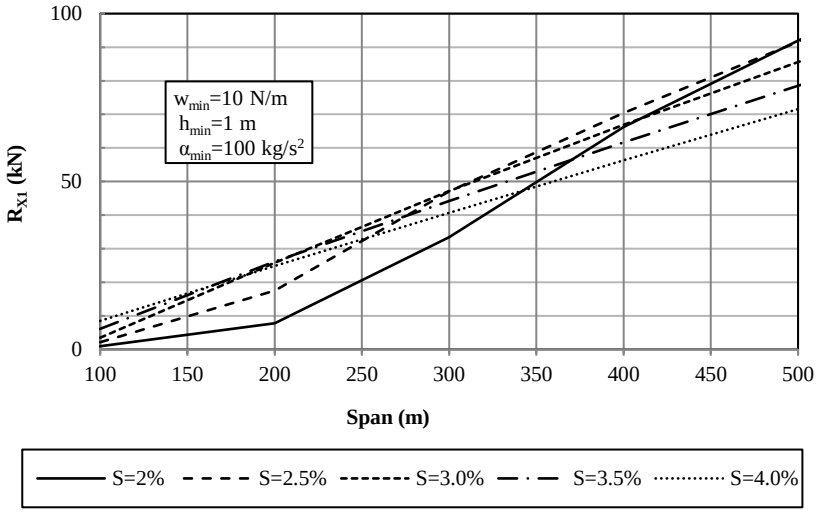

R_{X1}

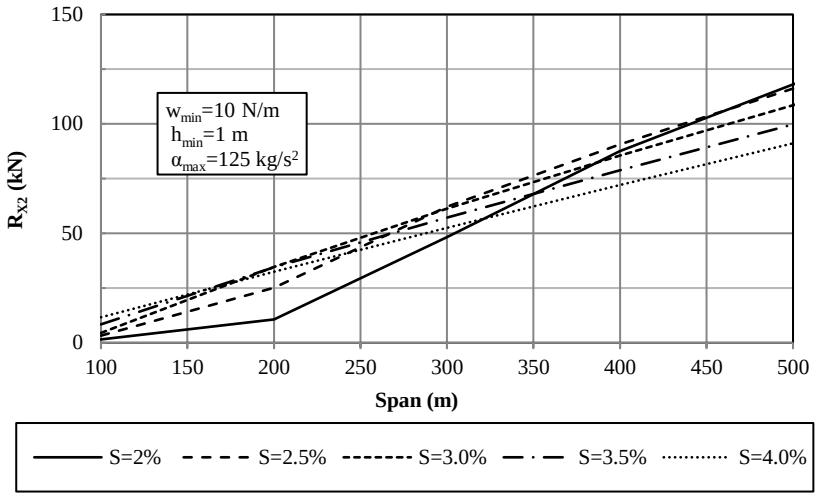

R_{X2}

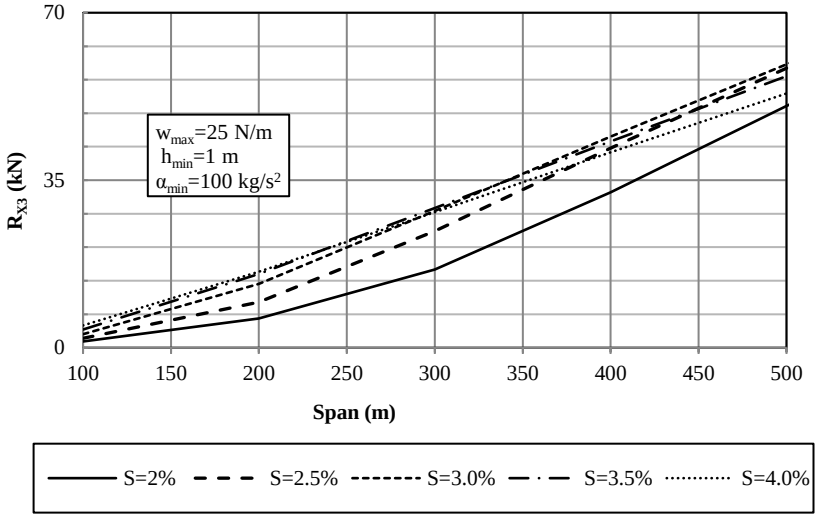

R_{X3}

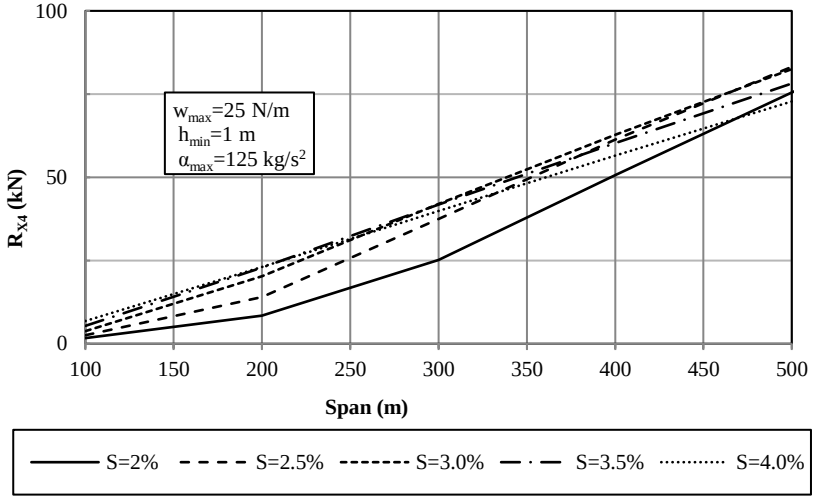

R_{X4}

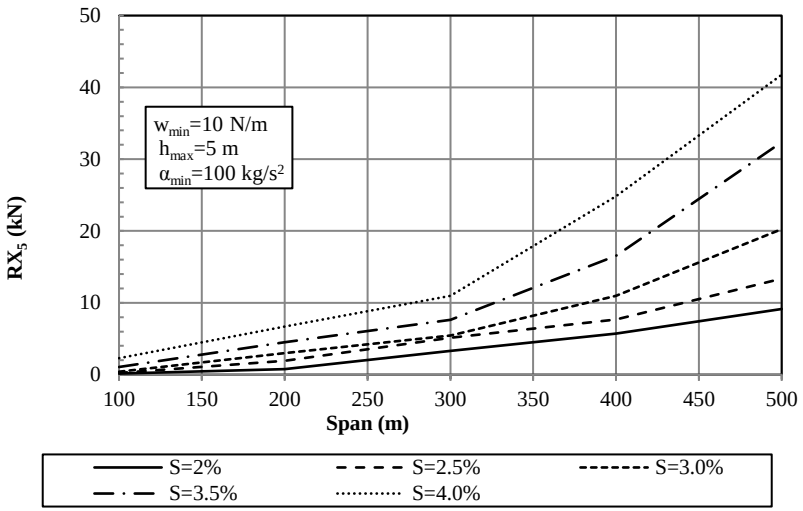

R_{X5}

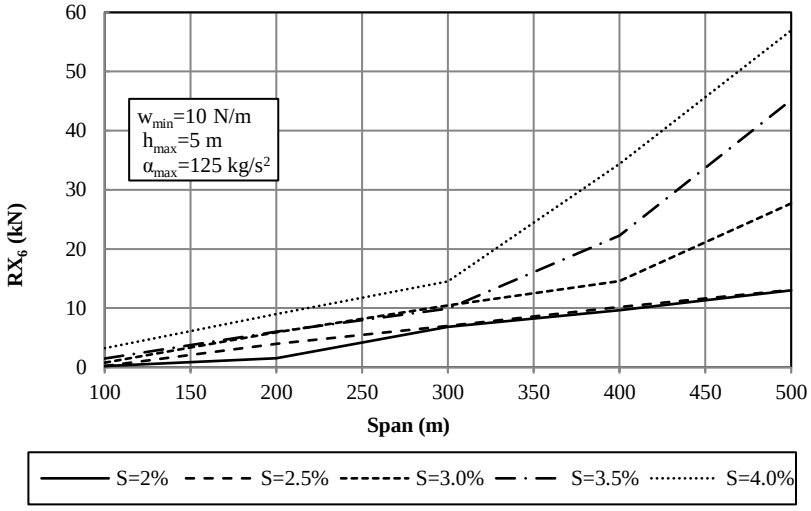

R_{X6}

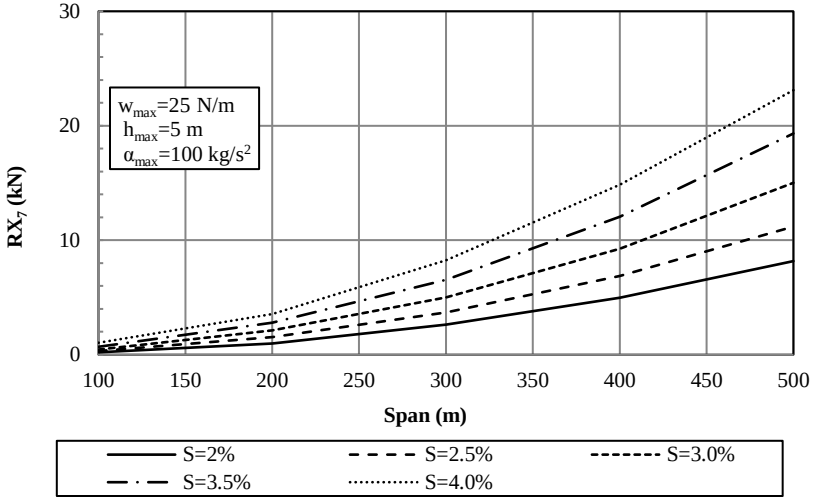

R_{X7}

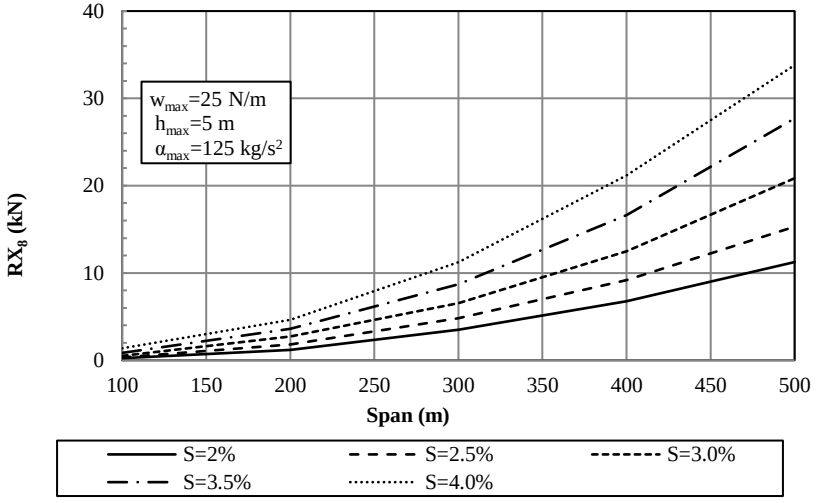

R_{X8}

Group (VIII): 100 ≤ α ≤ 125 & 25 ≤ w ≤ 40

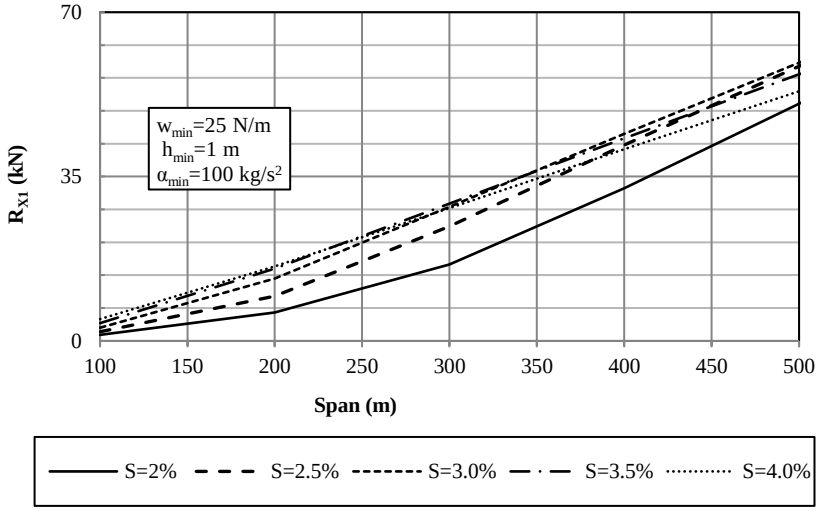

R_{X1}

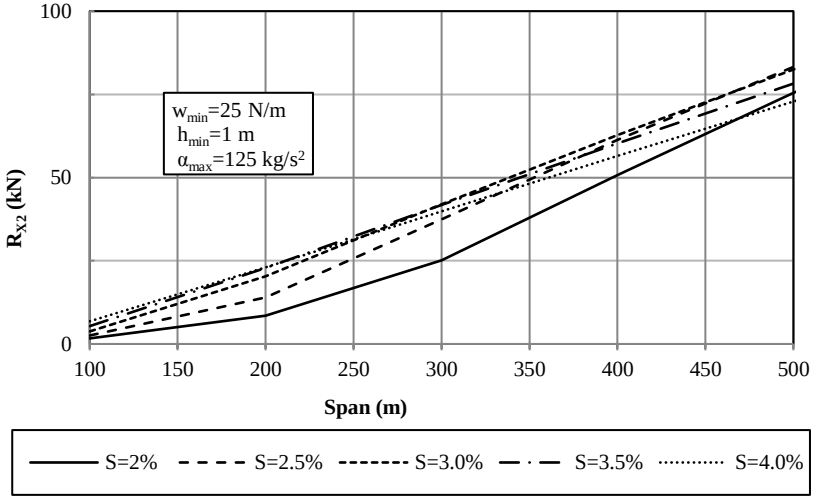

R_{X2}

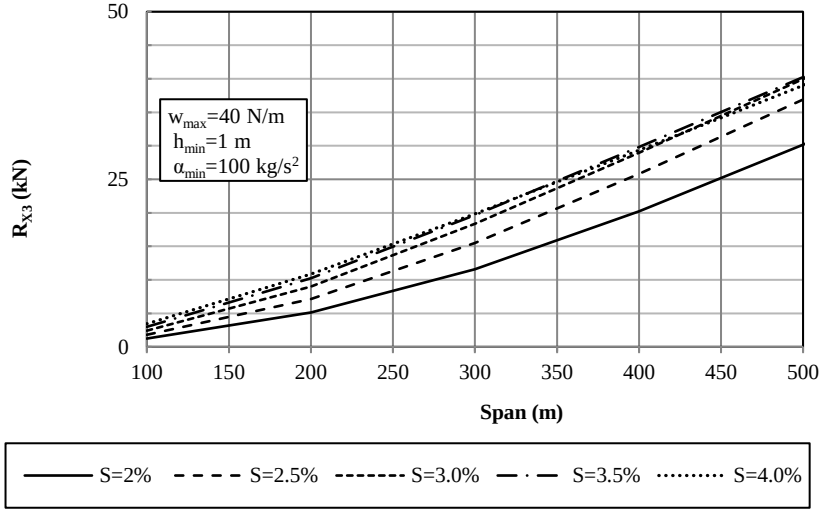

R_{X3}

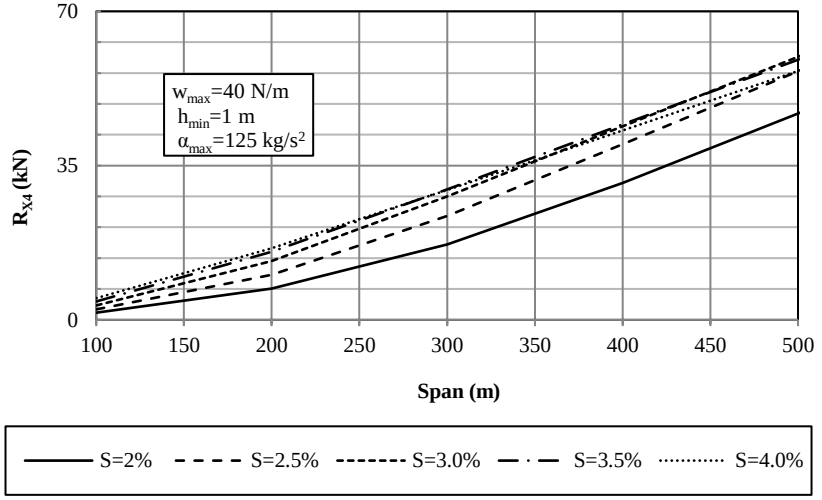

R_{X4}

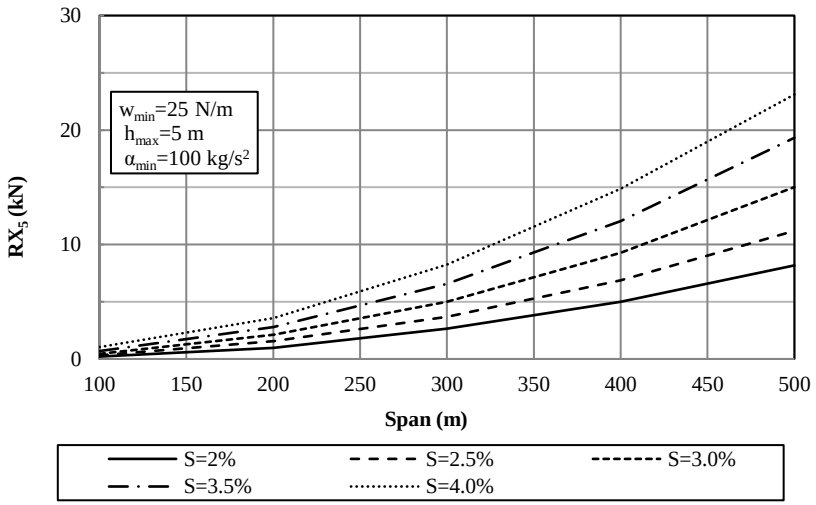

R_{X5}

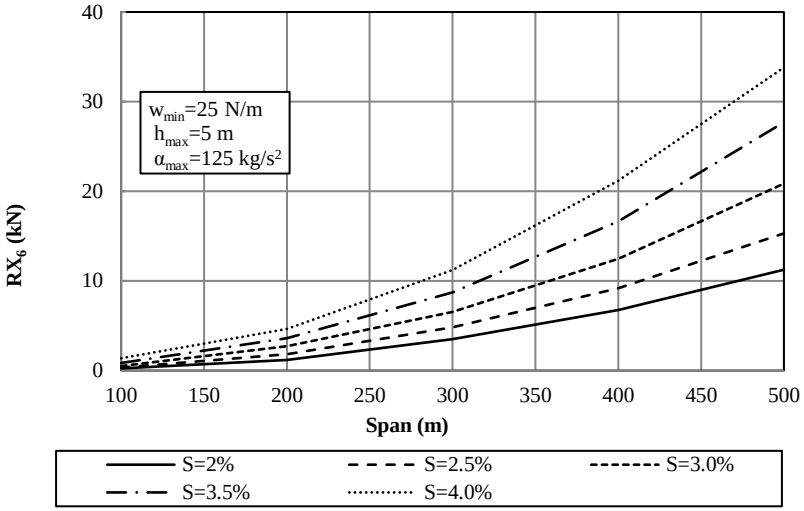

R_{X6}

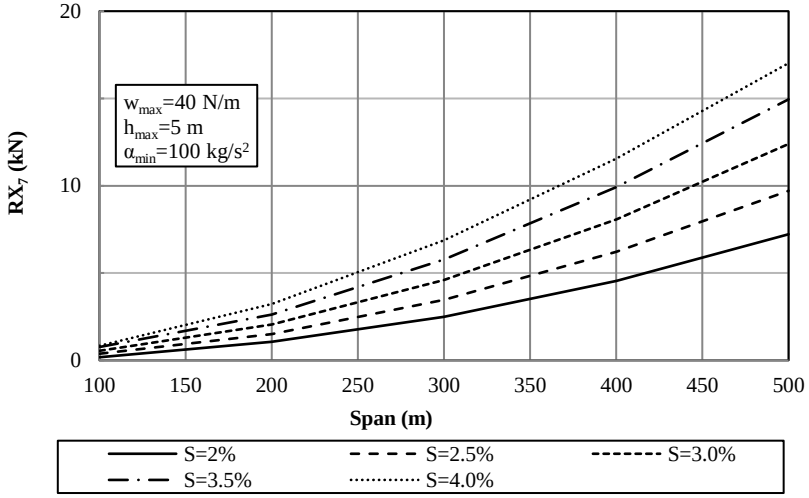

R_{X7}

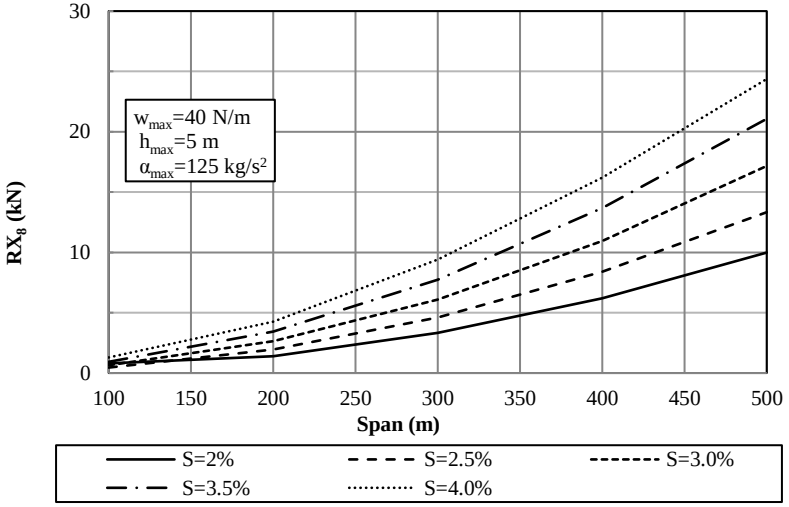

R_{X8}

4.11. References

Aboshosha H, and El Damatty, A., (2015), "Engineering method for estimating the reactions of transmission line conductors under downburst winds". Journal of Engineering Structures 142, 198–216.

Aboshosha, H., and El Damatty, A., (2013), "Downburst Induced Forces on the Conductors of Electric Transmission Lines and the Corresponding Vulnerability of Towers Failure", CSCE Conference, Montreal, QC, Canada.

Aboshosha, H., and El Damatty, A., (2014), "Span reduction factor of transmission line conductors under downburst winds". Journal of Wind Engineering 11(1), 13–22.

Aboshosha, H., Elawady, A., Elansary, A., and El Damatty, A., (2016), "Review on dynamic and quasi-static buffeting response of transmission lines under synoptic and non-synoptic winds" Engineering Structures 112, 23–46.

Aboshoshaa, H., and El Damatty, A., (2014), "Effective Technique to Analyze Transmission Line Conductors under High Intensity Winds" Wind and Structures 18(3).

Ahmadi-Kashani, K., and Bell, A., (1988), "The analysis of cables subject to uniformly distributed 27 loads", Engineering Structures 10(3), 174-184.

American Society of Civil Engineers (ASCE), (2010), "Guidelines for electrical transmission line structural loading", ASCE Manuals and Reports on Engineering Practice 74, New York, NY, USA.

Australian Standard / New Zealand Standard (AS/NZS) 7000, (2010), "Overhead line design Detailed procedures", Standards Australia Limited / Standards New Zealand, North Sydney, Australia.

Choi, E. and Hidayat, F., (2002), "Dynamic response of structures to thunderstorm winds", Progress in Structural Engineering and Materials. 4, 408-416.

Darwish, M. and El Damatty, A., (2011), "Behavior of self-supported transmission line towers under stationary downburst loading", Wind and Structures 14(5), 481-4.

Darwish, M., El Damatty, A., and Hangan, H., (2010), "Dynamic characteristics of transmission line conductors and behaviour under turbulent downburst loading", Wind and Structures, An International Journal 13(4), 327 346.

Fujita, T., (1985), "The downburst: microburst and macroburst", SMRP Research Paper 210, University of Chicago, USA.

Gattulli, V., Martinelli, L., Perotti, F. and Vestroni, F. (2007), "Dynamics of suspended cables under turbulence loading: reduced models of wind field and mechanical system", Journal of Wind Engineering and Industrial Aerodynamics 95(3), 183-207.

Hangan, H., Roberts, D., Xu, Z. and Kim, J., (2003), "Downburst simulation. Experimental and numerical challenges", Proceedings of the 11th International Conference on Wind Engineering, Lubbock, TX, USA.

Hawes, H., and Dempsey D., (1993), "Review of recent Australian transmission line failures due to high intensity winds". Proceedings of the Task Force of High Intensity Winds on Transmission Lines, Buenos Aires.

Hjelmfelt, M., (1988), "Structure and life cycle of microburst outflows observed in Colorado". J. Appl. Meteor 27, 900–927.

Holmes, J., Hangan, H., Schroeder, J., Letchford, C. and Orwig, K. (2008), "A forensic study of the Lubbock-Reese downdraft of 2002", Wind Structures 11(2), 137-152.

Kanak, J., Benko, M., Simon, A. and Sokol, A. (2007), "Case study of the 9 May 2003 windstorm in southwestern Slovakia", Atmospheric Research 83, 162-175.

Kim, J. and Hangan, H. (2007), "Numerical simulations of impinging jets with application to downbursts", Journal of Wind Engineering and Industrial Aerodynamics 95(4), 279-298.

Kwon, D., and Kareem, A., (2009), "Gust-front factor: new framework for wind load effects on structures" ASCE Journal of Structural Engineering 135(6), 717–32.

Lombardo F., Smith D., Schroeder J., and Mehta K., (2014), "Thunderstorm characteristics of importance to wind engineering", Journal of Wind Engineering and Industrial Aerodynamics 125, 121–32.

McCarthy, P., and Melsness, M., (1996), "Severe weather elements associated with September 5, 1996 hydro tower failures near Grosse".

Savory, E., Parke, G., Zeinoddini, M., Toy, N., and Disney, P., (2001), "Modelling of tornado and microburst-induced wind loading and failure of a lattice transmission tower", Engineering Structures 23(4), 365-375.

Shehata, A. and El Damatty, A., (2008), "Failure analysis of a transmission tower during a microburst", Wind and Structures 11(3), 193-208.

Shehata, A., and El Damatty, A., (2007), "Behaviour of guyed transmission line structures under downburst wind loading", Wind and Structures, An International Journal 10(3), 249-268.

Shehata, A., El Damatty, A., and Savory, E., (2005), "Finite element modeling of transmission line under downburst wind loading", Finite Elements Analysis Design 42(1), 71-89.

Solari, G., Burlando, M., De Gaetano, P., and Repetto, M., (2015), "Characteristics of thunderstorms relevant to the wind loading of structures", Wind Structures 20(6), 763–91.

Wei, P., Bingnan, S., and Jinchun T., (1999), "A catenary element for the analysis of cable 25 structures", Applied Mathematics and Mechanics 20(5), 0253-4827.

Zhang, Y., (2006), "Status quo of wind hazard prevention for transmission lines and countermeasures", East China Electric Power 34(3), 28-31.

CHAPTER 5

CRITICAL LOAD CASES FOR LATTICE TRANSMISSION LINE STRUCTURES SUBJECTED TO DOWNBURSTS: ECONOMIC IMPLICATIONS FOR DESIGN OF TRANSMISSION LINES

5.1. Introduction

A downburst is defined as a mass of cold and moist air that drops suddenly from a thunderstorm cloud base, impinges on the ground surface, and then horizontally diverges from the center of impact (Fujita, 1985). Past reports indicated that about 80% of the weather-related transmission line failures have been attributed to High Intensity Wind (HIW) events in the form of downbursts and tornadoes (Dempsey and White, 1996). In Canada, McCarthy and Melsness (1996) reported a series of transmission tower failures under HIW events that belong to the Manitoba Hydro Company. More recently, two 500 kV guyed towers failed during a severe thunderstorm in August 2006 belonging to Hydro One, Ontario, Canada (Hydro One failure report, 2006). In the USA, a recent report released by the Executive Office of the President (2013) estimated that more than 600 power outages occurred due to severe weather. The report stated that the annual average of financial losses due to the weather-related outages over this period ranged between $18 billion to $33 billion. In China, Zhang (2006) reported the failure of 18 (500 kV) and 57 (110 kV) transmission line structures that occurred in 2005 under severe wind events such as typhoons, tornadoes, and downbursts. In addition to the economic losses, the social implications for the affected society due to such outage are tremendous.

Downbursts have unique characteristics compared to synoptic winds such as hurricanes and typhoons. One of those characteristics is the localized nature of downbursts with respect to space and time. The wind field associated with downbursts is quite complicated

as it varies from one location to another depending on the distance from the downburst center. The vertical profile of the downburst wind field also varies depending on the location. This profile can differ from the typical boundary layer profile, which is currently used in the design codes. For long span structures such as transmission lines in which towers and conductors extend for many kilometers, the localized nature of the downbursts might result in a non-uniform and unsymmetrical distribution of the wind loads over the line spans. This results in load cases that do not usually exist under uniform and symmetrical large-scale wind events. Despite the large number of failures reported due to downbursts and the unique characteristics of the downburst wind field, the design codes do not provide enough information about critical downburst loads, which should be considered in the design of transmission line structures. The purpose of this research is to fill in this gap.

A number of attempts to conduct downburst field measurements are found in the literature. Wolfson et al. (1985) reported the field measurements of the FAA/Lincoln Laboratory Operational Weather Studies (FLOWS) where different intensities and durations of downbursts were recorded. Fujita (1985) characterized the downburst wind field using the field measurements of Northern Illinois Meteorological Research (NIMROD) and the Joint Airport Weather Studies (JAWS). Hjelmfelt (1988) reported a number of individual and line microbursts in Colorado. Numerical simulations of downbursts can be done using one of the following techniques: (a) Ring Vortex Model, (b) Impinging Jet (Impulsive Jet) Model, and (c) Cooling Source (Buoyancy-Driven) Model. The literature related to this subject includes a number of numerical studies conducted to characterize the downburst wind field. Zhu and Etkin (1985) used the ring vortex model to simulate the vortex ring

formed during the descent of the downburst. Vermeire et al. (2011) used the cooling source model to examine the initiation of the event inside a cloud. Kim and Hangan (2007) adopted the impinging jet approach using the Reynolds Averaged Navier-Stockes (RANS) equations to simulate the downburst wind field. This yielded a time series of the mean radial and vertical velocity components of the downbursts. Using the impinging jet model, Aboshosha et al. (2015) utilized the Large Eddy Simulations (LES) to account for the fluctuating component.

Few studies focused on assessing the behaviour of transmission tower systems under downbursts. The first study reported in the literature was conducted by Savory et al. (2001) in which they modelled a single self-supported tower with no conductors attached. In their study, the vertical profile of the downburst mean radial velocity was evaluated based on an analytical expression obtained from a wall jet simulation conducted used by Vicroy (1992). Savory et al. (2001) reported that the self-supported tower was more vulnerable to tornadoes than to downbursts. Probably this conclusion resulted from the exclusion of the conductors in the numerical modeling. Downbursts are significantly larger than tornadoes and as such they are expected to engulf a larger portions of the conductors compared to tornadoes. Shehata et al. (2005) and Darwish and El Damatty (2011) studied the behaviour of guyed and self-supported transmission line systems subjected to downburst loadings, respectively. Both studies were conducted in a quasi-static manner using the mean component of the downburst field. The two studies reported possible loading scenarios of the downburst causing peak internal forces in the towers' members. These studies showed that the spatial parameters of the downburst control the intensity of the loads imposed on the transmission line. **Fig. 5-1** illustrates the spatial parameters of the downburst that affect

the loading acting on a tower and the attached conductors. Those parameters are the downburst jet diameter (D_J), the radial distance (R), and the angle of attack (Θ). Wang et al. (2009) conducted a quasi-static analysis where they utilized an empirical lateral force model to assess the dynamic response of a high rise transmission tower, with no conductors attached, to downburst forces. Mara et al. (2016) compared the load-deformation curve of a transmission tower when subjected to both downburst and normal winds. Their study showed that normal wind capacity curves can be used as an approximate alternative for those capacity curves resulting from downbursts. Elawady and El Damatty (2016) assessed the longitudinal response of the conductors of transmission lines to the oblique downburst cases. The oblique downburst loading scenarios occur when the downburst acts with an angle of attack Θ, illustrated in **Fig. 5-1**, where $0° < Θ < 90°$. In their study, Elawady and El Damatty (2016) provided a simple approach to estimate conductor's longitudinal forces using a number of charts and linear interpolation equations. Yang and Zhang (2016) analyzed two transmission towers under both normal and downburst winds. In their study, Yang and Zhang (2016) considered the wind loads acting on the conductors as a simplified resultant vertical and lateral forces at the insulators' connections while ignoring the spatial localization of the downburst winds.

The characterization of the downburst wind field showed that the frequency of the mean component of the wind field is less than 0.05 Hz (Kim and Hangan, 2007). This frequency is much less than the frequency of the towers, which is typically higher than 1 Hz (Shehata and El Damatty, 2007). Darwish et al. (2010) found that the conductors' frequencies ranged between 0.06 to 0.1 Hz, which indicates a potential sensitivity to dynamic excitations. Darwish et al. (2010) utilized the field measurements reported by Holmes et al. (2008) and

extracted the turbulent component, which was assumed to not vary spatially. This was used to assess the dynamic response of the transmission line conductors. The study showed that the aerodynamic damping of the conductors tends to attenuate its vibration and, therefore, no dynamic response is anticipated for the conductors. This was confirmed by Aboshosha and El Damatty (2014-a) who showed that the transverse and the longitudinal forces transmitted from the conductors to the tower increased by only 5% and 6%, respectively, with the inclusion of the dynamic effect. In Chapter 2, the dynamic response of an aero-elastic model of a multi-spanned lattice transmission line subjected to downburst loads simulated at the WindEEE dome was assessed. The study showed that for the typical range of downburst velocities (50 m/s ~ 70 m/s), the dynamic response of the conductors and the tower was in the order of 15% and 10%, respectively. Taking into consideration the considerable uncertainty surrounding downburst critical loadings, due to spatial and temporal localization, one can assume that the quasi-static response of the line provides a sufficient representation of the line response.

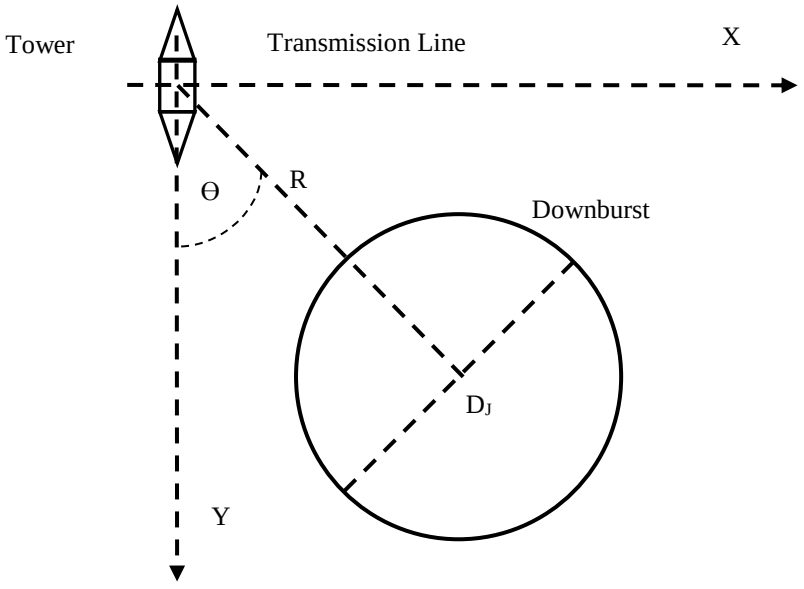

Fig. 5-1. Downburst characteristic parameters.

The objectives of the current study can be summarized as follows: (i) study the behaviour of a spectrum of transmission line systems subjected to different downburst loading configurations; (ii) identify a number of critical downburst configurations that can be generalized to apply to lattice tangent transmission lines; (iii) propose wind profiles for both the towers and the conductors associated with those critical downburst configurations, and (iv) study the economic implications of considering the proposed load cases in the design of the towers.

The current chapter starts by describing the methodology used in the study including a description of the numerical model and the applied techniques. This is followed by a description of the transmission line systems used in the conducted parametric studies. In the results section, an explanation of the behaviour of the studied transmission line systems under downburst loads is provided. Based on the behaviour observations, the study proposes a number of critical load cases simulating the critical effect of downbursts on transmission line structures for possible implementation in the codes of design. An economic study is then conducted to assess the implication of applying those load cases on the increase in the weight of the towers. Finally, the conclusions reached from the entire study are presented.

5.2. Methodology

5.2.1. Downburst Wind Field

The current study utilizes the downburst wind field developed by Hangan et al. (2003) and later validated by Kim and Hangan (2007). This Computational Fluid Dynamics (CFD) simulation provides a time series of the mean wind speed in both the radial and vertical directions for a small-scale model. The current study uses the scaling-up procedure

proposed by Shehata et al. (2005) for the CFD data in order to estimate the spatial and time variations of the wind velocities associated with full-scale downbursts. The magnitudes of the velocity components depend on the jet diameter (D_J), and the jet velocity (V_J). They also vary temporally and spatially depending on the distance (R) measured relative to the center of the downburst. Shehata et al. (2005) showed that for different D_J values, the maximum radial velocity was found to be constant at the same R/D_J ratio while the time instant of that maximum radial velocity varied with D_J. Therefore, in different structural studies, such as those conducted by Shehata et al. (2005), Shehata and El Damatty (2007, 2008), Darwish and El Damatty (2011), the distance ratio factor (R/D_J) was used to assess the structural behaviour of transmission line systems under different downburst configurations. Mara and Hong (2013) utilized the peak vertical profile of the radial component of the downburst in order to assess the capacity of a transmission tower. The study showed that the wind direction affects the force-deformation relationship. The study also showed that the capacity curves of transmission towers subjected to synoptic winds can be used for the cases of downburst winds.

The variations of the radial (V_{RD}) and vertical (V_{VR}) velocities, both normalized by the downburst jet velocity, along the height are provided in **Figs 2** and **3**, respectively. **Fig. 5-2** shows that the absolute maximum value for the radial velocity component occurs when R/D_J is 1.3. This maximum V_{RD} occurs at an elevation of approximately 50 m, which is the typical height for high voltage transmission towers. The figure also shows that the absolute maximum radial velocity is approximately equal to 1.15 V_J. This means that for a jet velocity of 50 m/sec, one would expect a maximum radial velocity to be about 57.5 m/sec. For the vertical velocity component, **Fig. 5-3** shows that the maximum value for the vertical

velocity occurs at R/D_J= 1.0. Although this distance ratio is close to those ratios corresponding to the maximum radial velocity, the elevation of the maximum vertical velocity at R/D_J=1.0 is about 150 m. At the typical height of a transmission tower, the vertical velocity component is in order of 0.2 V_J, which is less than 20% of the maximum radial velocity (1.15 V_J). Based on the fact that the wind forces are proportional to the square of the velocity, the vertical forces in the critical downburst range will be significantly less than the radial forces, and thus can be ignored.

Fig. 5-4 shows the time variations for the radial velocity components at D_J=500 m and R/D_J=1.3. The figure demonstrates the localized nature of the downburst wind field in time. Therefore, an attempt should be made to identify the time instant corresponding to the maximum radial velocity. Shehata et al. (2005) stated that the time of maximum radial and/or axial velocity depends on both the jet diameter and the jet velocity.

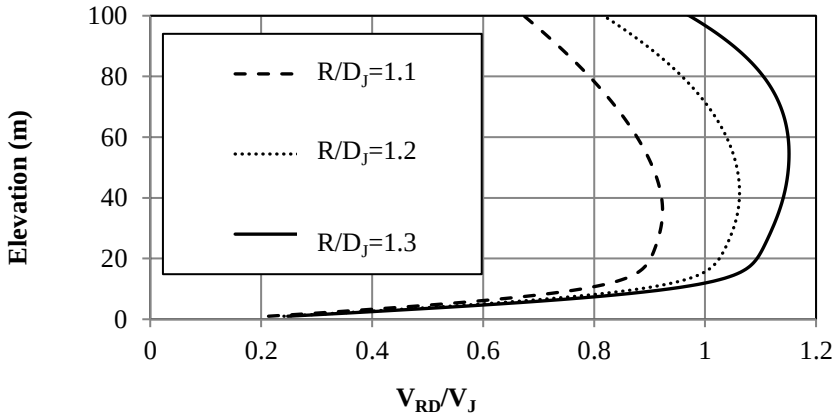

Fig. 5-2. Radial velocity profile along the height.

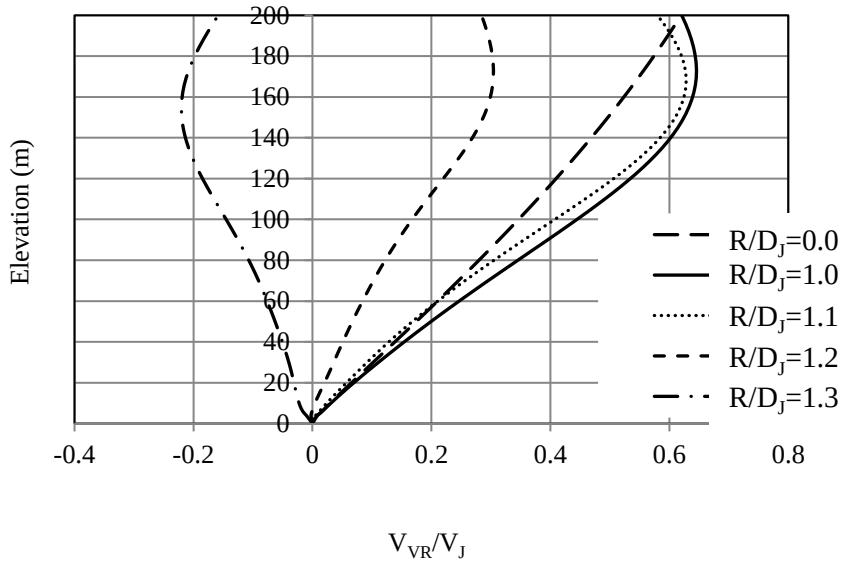

Fig. 5-3. Axial velocity profile along the height.

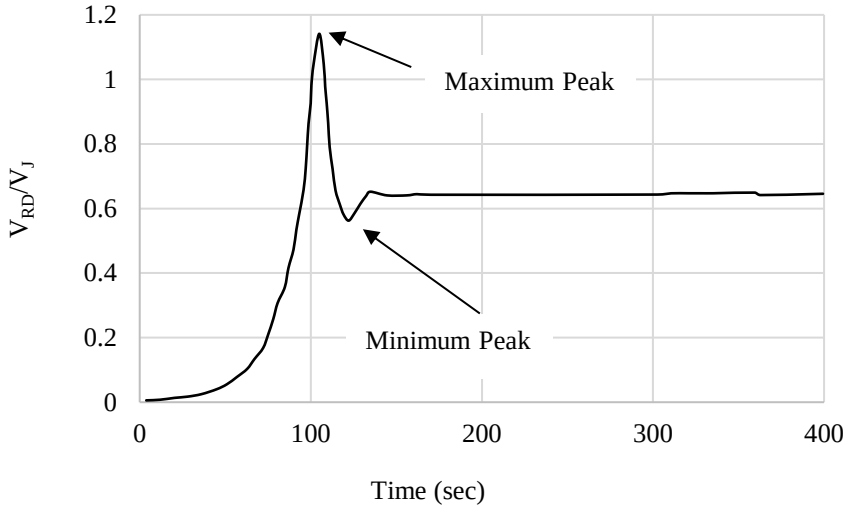

Fig. 5-4. Time history of the radial velocity at a point in space

5.2.2. Modelling Technique and Method of analysis

The current study utilizes the numerical models developed by Shehata et al. (2005) and Aboshosha and El Damatty (2014-b) and validated in chapter two to analyze the performance of the tower and the conductors, respectively. The tower members are modeled using two-noded three-dimensional frame elements with three rotational and

translation degrees of freedom at each node. The conductor's behaviour is estimated using the semi-analytical solution developed by Aboshosha and El Damatty (2014-b), which accounts for the conductor's geometric nonlinear behaviour, the pretension force, the sagging, and the insulator's flexibility. Three spans on either side of the tower of interest are modelled. Shehata et al. (2005) has shown that this number of spans is sufficient for an accurate prediction of the forces transmitted from the conductors to the tower of interest due to downburst loading. A full description of the conductor analysis technique is described by Aboshosha and El Damatty (2014-b). This technique has proven to be computationally efficient compared to typical nonlinear finite element analysis. The sequence of the analysis to predict the maximum response of a transmission line structure under downbursts is as follows:

a) A specific downburst configuration is selected based on assumed values for D_J, R/D_J, and Θ (See **Fig. 5-1** for the description of these parameters). Here V_J is assumed to be constant and equal to an arbitrary value of 70 m/s. This value represents the maximum observed downburst velocity as reported by Fujita (1985), Holmes and Oliver (1996), Orwig and Schroeder (2007), and CIGRE (2009).

b) Based on the scaling procedure described by Shehata et al. (2005), the velocity wind field is defined.

c) The external loads acting on the tower of interest and the six span conductors associated with the downburst wind field are calculated following the procedure described by Shehata et al. (2005).

d) The non-linear response of the conductors is estimated using the semi-analytical solution developed by Aboshosha and El Damatty (2014-b). This leads to the evaluation of the reactions R_X, R_Y, and R_Z at the location of the tower of interest, which are reversed to represent the forces transmitted from the conductors to the tower in the case of a specific downburst.

e) The tower is analyzed under the combined effects of the conductor forces and the joint forces acting directly on the lattice structure. This leads to the evaluation of the internal forces in all members of the tower.

f) Steps (d) to (e) are repeated through the time history of the downburst while the analysis is conducted in a quasi-static manner as discussed above.

g) The maximum internal forces obtained from the entire time history analysis are then calculated.

h) The analyses are repeated by varying the parameters D_J, R/D_J, and Θ within the following range:

- ✓ D_J=500 to 2000 m with an increment of 250 m.
- ✓ R/D_J=0 to 2.0 with an increment of 0.1.
- ✓ Θ=0° to 90º with an increment of 15º.

i) The absolute peak internal forces are obtained from the entire parametric study, which covers all of the potential downburst configurations. The downburst configurations associated with those peak forces are then recorded.

5.2.3. Structural Characteristics of Analyzed Transmission Line Systems

This studied transmission line systems consider the variations in: 1) the structural systems (guyed and self-supported), 2) the tower and cross arm configurations, 3) the conductors span and properties. The three dimensional view of the towers of the six line systems analyzed and reported in this study are shown in **Figs. 5-5** to **5-10**. The height of each tower, span of the wires as well as other conductors and ground wires' properties are summarized in **Table 5-1**.

Of the six towers, three are guyed and the other three are self-supported. The three guyed towers, G_1, G_2, and G_3 have different shapes. Tower G_1 is slender and carries two conductors, while towers G_2 and G_3 are Y and V shapes, respectively, and they both carry three conductors. The heights of the three towers vary between 43.44 m and 46.57 m and the wires' spans vary between 400 m and 480 m. The self-supported towers S_1 and S_2 are similar in shape, and they each carry six conductors. However, a large difference exists between the wire spans of the two towers (213.6 m for tower S1 and 450 m for tower S_2). Tower S_3 carries three conductors and has a different cross arm configuration compared to S_1 and S_2.

It is assumed that the six tower systems considered in the study cover a wide variety of tower support systems, tower shapes, cross arm configurations, number of conductors and conductors' spans. They provide an accurate representation for high voltage lattice towers used in the industry.

Table 5-1. Properties of selected towers

Tower	G_1	G_2	G_3	S_1	S_2	S_3
Type	Guyed	Guyed	Guyed	Self-supported	Self-supported	Self-supported
Span (m)	480	400	460	213.36	450	420
Height (m)	44.39	43.44	46.57	54.65	51.81	47.5
Width of conductor cross arm (m)	13.3	25.0	29.34	8.2& 14.3	8.2& 14.3	15.4
No. of conductors	2	3	3	6	6	3
No. of GWs	1	2	2	2	2	2
Single conductor weight (N/m)	28.97	7.98	8.67	28.97	20.14	32.7
Single conductor diameter (m)	0.0406	0.0215	0.0215	0.0345	0.034036	0.0527
No. of conductors	2 (0.48)*	4 (0.48)*	4 (0.48)*	1	1	2 (0.48)*
GW weight (N/m)	3.9	4.027	5.45	10.4	3.823	5.68
GW diameter (m)	0.009	0.0122	0.00953	0.0142	0.00978	0.0097
Insulator length (m)	4.27	4.27	4.27	2.44	2.44	4.9 & 5.9**
Conductor Sag (m)	20	16	14	3.9	19.5	15

Ground wire sag (m)	13.54	11	16	3	14	7.5
Modulus of Elasticity/ conductor (N/m^2)	6.23E +10	6.48E +10	5.18E +10	1.86E+ 11	6.48E+1 0	7.03E+10
Modulus of Elasticity/GW (N/m^2)	1.86E +11	1.05E +11	2.0E+ 11	6.23E+ 10	1.05E+1 1	1.72E+11
Guy diameter (m)***	0.016 5	0.014 3	0.019 05	N/A	N/A	N/A

*Horizontal Spacing; **V Shaped insulator; ***Galvanized steel wires.

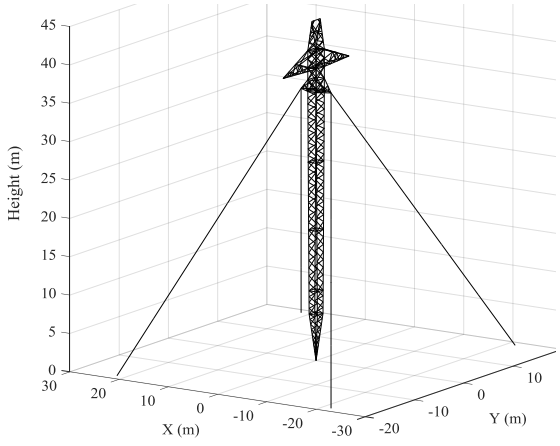

Fig. 5-5 Transmission Line System (G_1)

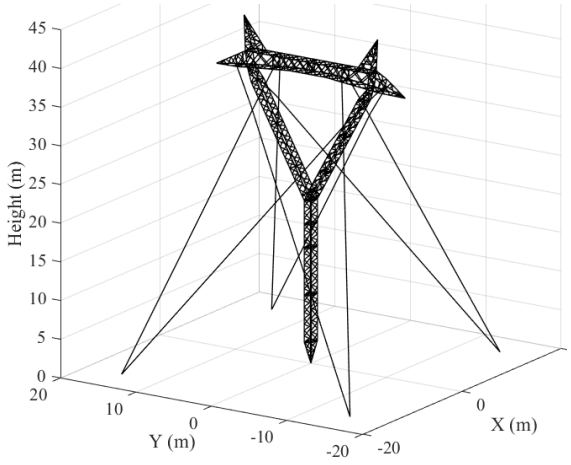

Fig. 5-6 Transmission Line System (G_2)

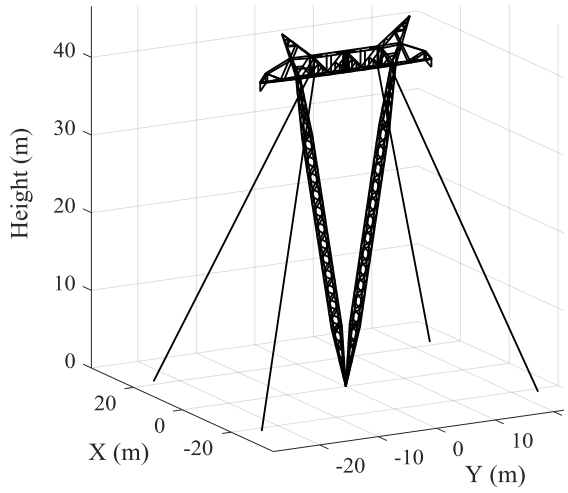

Fig. 5-7. Transmission Line System (G_3)

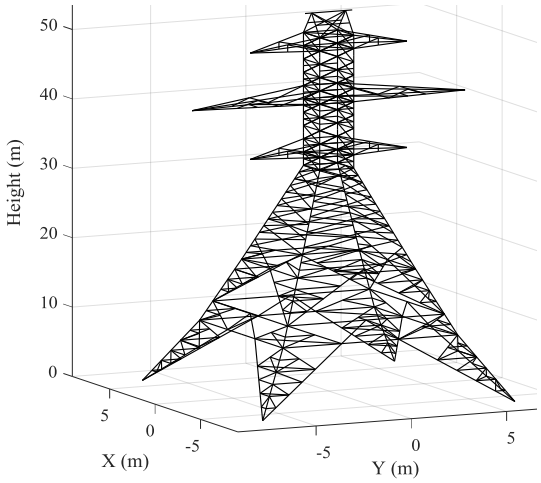

Fig. 5-8. Transmission Line System (S_1)

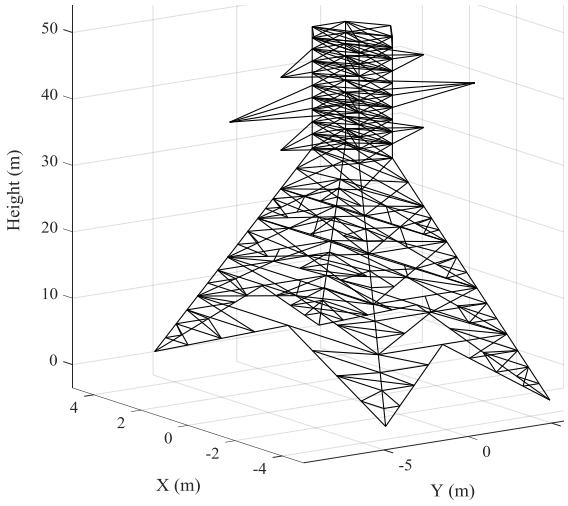

Fig. 5-9. Transmission Line System (S_2).

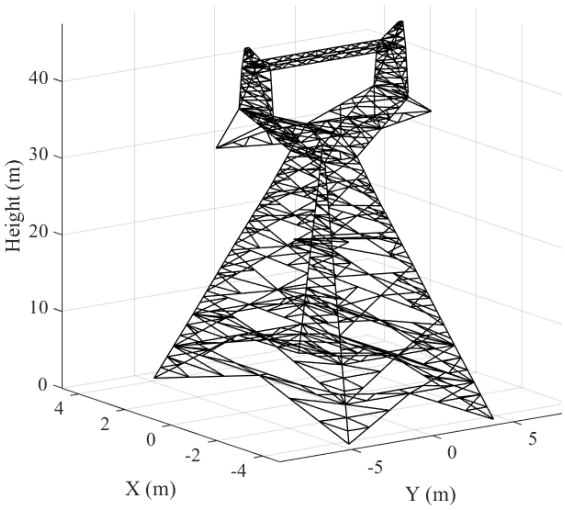

Fig. 5-10. Transmission Line System (S_3).

5.3. Results and Discussion

5.3.1. Tower response

In view of the analysis results, the behaviour of the six transmission line systems is explained with a focus on identifying the critical downburst configurations. As mentioned earlier, the downburst configurations are defined by the parameters D_J, R/D_J, V_J, and Θ, respectively, and an arbitrary value for the jet velocity of 70 m/s is selected. The choice of

the jet velocity will affect the magnitude of the internal forces but will not affect the identification of critical downburst configurations, which is the aim of this study. The results are presented by dividing the tower systems into two categories; Guyed towers and Self-supported towers. For each category, the behaviour is explained for two groups of members; members located below the cross arm, and members located within the cross arm zone.

5.3.1.1. Guyed towers

The following observations are found for the guyed towers G_1, G_2, and G_3.

Below the cross arm zone:

The peak internal forces in most of the leg members occur at a downburst configuration of $\Theta = 90°$, $R/D_J = 1.2 \sim 1.3$, and $D_J = 500$ m. The peak internal forces in few other members occur at another downburst configuration where $\Theta = 0^o$, $R/D_J = 1.2$, and $D_J = 500$ m. In order to visualize the loading associated with the configuration of $\Theta = 90°$, the reader is referred to **Fig. 5-1**. For $\Theta = 90^o$, the radial velocity profile is parallel to the conductors while for $\Theta = 0^o$, the radial velocity profile is perpendicular to the conductors. A guyed tower can be treated as an overhanging beam, where the cantilever portion is located above the guys-tower attachment point. The conductor forces act on the cantilever portion of the tower. In tower G_1, it is clear that the conductor forces tend to reduce the bending moment acting on the members below the cross arm zones, i.e., between the supports. For the case of $\Theta = 90^o$, no radial velocity profile acts on the conductors which leads to maximum forces developing in the tower zones below the cross arm. This behaviour was also described by Shehata and El Damatty (2007). On the other hand, for towers G_2 and G_3, where one cross arm is used for both the guys and the conductors, the analyses show that the conductor's forces have a

negligible effect on the tower members since a large percentage of the conductor's forces transfers directly to the ground supports through the guys. As such, the conductor's forces have a minimal effect on the internal forces developing in the tower members. However, for those two towers, the aerodynamics of the tower face, which is perpendicular to the line direction, are larger than those of the tower face which is parallel to the line direction. Therefore, most of the shaft members experience their peak internal forces at an angle of attack of 90 degrees.

The diagonal members located below the cross arm zone are found to experience peak internal forces at downburst configurations of R/D_J=1.2~1.3, D_J=500 m, and Θ=0º or 90º. As stated by Shehata and El Damatty (2007), diagonal members located in a plane perpendicular to the line, are critical under the configuration of Θ=0º; while members located in a plane parallel to the line are critical under the configuration of Θ= 90º.

<u>Cross arm zone:</u>

For tower G_1, the chord members located in the cross arm zone are found to experience peak internal forces with a downburst configuration of R/D_J= 1.4 ~ 1.7, D_J=500 m~1000 m, and Θ=15º ~ 45º. Such cases of Θ, which are not equal to either 0º or 90º, are referred to as oblique cases. By referring to **Fig. 5-1**, the oblique cases mean that the downburst is closer to one side of the line than the other side around the tower of interest. This means that the two spans adjacent to the tower will be subjected to unequal wind loads. This leads to a difference in the tension forces developing in the left and right spans resulting in a net longitudinal force acting on the tower cross arms causing an out-of-plane bending moment.

Some other members in tower G_1 and all the cross arm members in G_2 and G_3 have shown a critical response under non-oblique load configurations where $\Theta=0^o$ or 90^o, R/D_J =1.2~1.3 while D_J = 500 m ~ 750 m.

5.3.1.2. Self-supported towers

The following observations are made for the self-supported towers S_1, S_2, and S_3.

Below the cross arm zone:

For the leg members located below the cross arms, the critical downburst configurations are found to be R/D_J=1.2~1.3, $\Theta=0^o$, and D_J=500 m~750 m. A self-supported tower behaves like a cantilever. As such, the peak straining actions in the tower occur when both the tower and the conductors are fully loaded by downburst wind forces, i.e., at $\Theta=0^o$. The leg members in Tower S_2 experience the peak forces at an oblique angle of attack of $\Theta=15^o$. The properties of the conductors in tower S_2 cause a strong longitudinal force to develop in the conductors due to the oblique loading. More elaboration on this finding is provided in the next section.

Similar to the response in the case of guyed towers, the diagonal members experience their peak force at a downburst configuration corresponding to R/D_J=1.2~1.3, D_J=500 m ~ 1000 m, and $\Theta=0^o$ or 90 ^{o} depending on the plane in which each member is located. Similar to the leg members, a number of diagonals in tower S_2 experience their peak internal forces when the downburst configurations are R/D_J =1.3~ 1.5, Θ = 15^o ~ 30^o, and D_J =500 m.

Cross arm zone:

The chord members of tower S_1 and tower S_3 experience their peak internal forces under a downburst configurations of R/D_J=1.2~1.3, D_J=500 m~1000 m and $\Theta=0^o$ or 90^o. On the other hand, oblique load configurations are found to be critical for such members in tower

S_2. The analysis of tower S_2 shows that the cross arm members experience peak internal forces at downburst configurations of R/D_J= 1.5~1.6, Θ=15º ~30º, and D_J=500 m ~ 750 m. The presence of the downburst oblique cases indicates a strong impact of the conductors' longitudinal forces. The next section provides an explanation of the significance of the conductor's longitudinal forces in the six studied tower systems.

5.3.1.3. Conductor forces

An oblique downburst load configuration causes a longitudinal force to develop in the conductors and the ground wires. **Fig. 5-11** illustrates the direction of the conductor forces, which develop due to the oblique downburst scenarios. This figure shows that the transverse force, R_Y, acts in a direction that is perpendicular to the line direction; while the longitudinal force, R_X, acts in a direction parallel to the line direction. The longitudinal force R_X develops, simultaneously with R_Y, only when the downburst attacks the line at an oblique angle. In the current study, it is noticed that the oblique downburst configurations are critical for two of the towers, G_1 and S_2. In order to understand why those two towers in particular are more vulnerable to the oblique downburst configurations than the others, the magnitudes of the developed longitudinal force R_X in all the studied conductor cases are evaluated. They are then normalized by the conductors' pretension force, T, in order to get an indication of their severity. **Table 5-2** shows the downburst parameters (D_J, R/D_J, and Θ), which correspond to the maximum R_X vales developing in the conductors. The analyses show that the longitudinal force R_X increases with the increase of the conductor's diameter and the line's span. Therefore, the conductors of towers G_2 and G_3 develop a higher R_X than the conductors of G_1. For the self-supported towers, the table shows that the conductor forces of tower S_2 are significantly higher than those of tower S_1 and S_3. The

span of line S_2 is approximately double that of S_1, which results in a significant increase in R_X. Although the spans of S_2 and S_3 are approximately equal, the conductors used in line S_3 are heavier and have longer insulators compared to S_2. These differences result in a reduction in the R_X value that develops in line S_3 compared to the longitudinal force in line S_2.

Table 5-2. Downburst configurations causing maximum R_X

Tower	Downburst configuration	R_X/T^*
G_1	D_J=960 m, R/D_J=1.6, Θ=30	0.46
G_2	D_J=800 m, R/D_J=1.6, Θ=30	0.9
G_3	D_J=920 m, R/D_J=1.6, Θ=30	0.72
S_1	D_J=426m, R/D_J=1.6, Θ=30	0.09
S_2	D_J=900 m, R/D_J=1.6, Θ=30	1.25
S_3	D_J=840 m, R/D_J=1.6, Θ=30	0.47

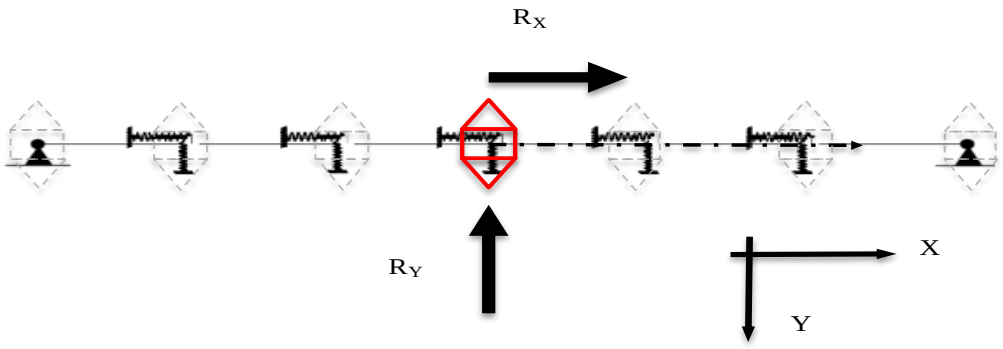

Fig. 5-11. Conductor reactions under downburst wind field.

The effect of the conductors' forces on the tower response is closely associated with the structural system of the cross arm. For the guyed towers, the ratio (R_X/T) is found to be

0.72 for G_3, 0.9 for G_2 and 0.42 for G_1. Only tower G_1 is found to experience peak internal forces due to a critical R_X developing in the conductors. This can be attributed to the difference in the structural system of the cross arms used in G_1, G_2, and G_3. Towers G_2 and G_3 have a much wider cross arm. Therefore, the cross arm forces associated with $\Theta=0^o$ are stronger in towers G_2 and G_3 compared to G_1. This effect tends to make the configuration $\Theta=0^o$ more critical compared to the oblique case for systems G_2 and G_3. It can be observed that for G_2 and G_3, the guys are attached directly to the cross arm. This tends to attenuate the twist effect resulting from the longitudinal force associated with the oblique case. However, the situation is different with tower G_1 where the guys are located at a level lower than that of the conductor cross arm. This tends to make the cross arm very sensitive to the out-of-plane effect resulting from the longitudinal force associated with the oblique case.

5.3.2. Proposed Downburst Load Cases

In view of the results of the parametric studies reported above, load cases that simulate the critical effect of downburst events on a generic tangent lattice transmission lines are identified and presented in this section.

The analyses reveal that three load cases will cover the situations leading to peak internal forces in all members of a tangent lattice tower. Those will correspond to two configurations with $\Theta = 90°$ and $\Theta = 0°$ as well as a third configuration where Θ has intermediate values between 0° and 90° (oblique case). Other parameters associated with those three configurations will be determined from the discussion carried below.

For $\Theta = 90°$, the downburst wind field is parallel to the line and therefore no conductor loads will result from this configuration. Loads will result only from the drag effect of the wind field on the tower members. As such, the downburst diameter and distance leading to

maximum wind profile on the tower are the critical parameters that should be considered with this configuration. Investigation of the wind field reveals that the maximum profile occurs for a distance ratio $R/D_J = 1.3$. It also reveals that the smaller the diameter, the larger are the values of the wind profile. As such, the critical downburst parameters associated with the configuration $\Theta = 90°$, are the minimum value of D_J which is 500 m together with $R/D_J = 1.3$.

For $\Theta = 0°$, the downburst wind field is perpendicular to the line. As such, both the tower and the conductors will be subjected to wind loads. Similar to the $\Theta = 90°$, the peak loads acting on the tower will correspond to a configuration in which $D_J = 500$ m and $R/D_J = 1.3$. The velocity profile along the conductors and consequently the conductors' loads will depend on one extra parameter, which is the ratio between the span and the jet diameter, L/D_J. To investigate the effect of this ratio, **Fig. 5-12** shows the radial velocity distribution along the two spans adjacent to a tower for different L/D_J ratios at $\Theta = 0°$ and $R/D_J = 1.3$. The larger the area enclosed by those velocity distributions, the higher are the transverse loads acting on the two conductors and consequently the force transmitted to the tower. From the figure, it can be detected that the largest enclosed area corresponds to $L/D_J = 0.25$. The area enclosed by the profile corresponding to $L/D_J = 0.5$ is slightly smaller. The reduction in the area for higher values of L/D_J is more significant. For the critical D_J value of 500 m, $L/D_J = 0.25$ will correspond to a span of 125 m. This is quite small for high voltage transmission lines where the span typically exceeds 250 m. As such, $L/D_J = 0.25$ is not deemed to be practical. It is therefore recommended to consider the distribution corresponding $L/D_J = 0.5$. This will be the right distribution for a downburst having a jet

diameter of 500 m acting on a line with a span of 250 m. For larger spans, this distribution will be conservative for the critical downburst diameter of 500 m.

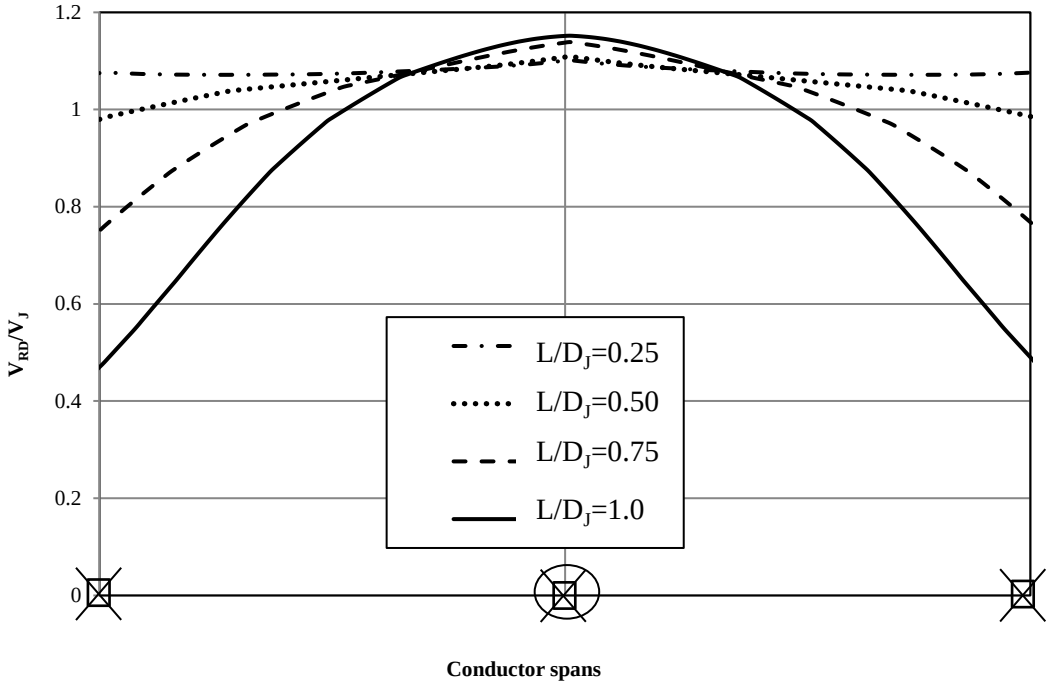

Fig. 5-12. Radial velocity distribution along line spans at R/D$_J$=1.3 and Θ=0°.

The third critical downburst configuration is called the "oblique case" and it happens for intermediate values of Θ between 0^o and 90^o. This load case will typically affect the cross arm members. At this intermediate downburst location, the magnitude and distribution of velocities and, consequently loads, along two spans adjacent to the tower will be unequal. This will lead to a difference in the conductors' tension in two adjacent spans. This difference will lead to a net longitudinal force acting on the cross arm of the towers. As such, the critical oblique downburst configuration is the one that would lead to maximum values for tis longitudinal force. In the extensive study conducted by Elawady and El

Damatty (2016), it was shown that the maximum longitudinal forces occur at a downburst configuration having $\Theta = 30°$ and $R/D_J = 1.6$, and $L/D_J = 0.5$.

Based on this discussion, the velocity profiles acting along the tower height and the line spans associated with the three critical configurations of the downbursts named herein as critical load cases, are presented below.

5.3.2.1. Load case#1: $R/D_J=1.3$, $\Theta=90º$, $D_J=500$ m

This configuration represents the maximum velocity profile acting on the tower in the direction perpendicular to the line's direction. In this load case, there are no forces acting on the conductors. The maximum velocity profile along the height of the tower is provided in **Fig. 5-13**. Equivalent uniform velocity distribution, V_{eqT} is evaluated to reproduce the overall effect of the non-uniform profile in order to facilitate its application. This is done by first squaring the velocity profile to represent forces. V_{eqT} is calculated that as the area enclosed by its squared value as well as the first moment of the squared value at the tower base are equal to or exceed the corresponding value associated with the non-uniform profile. The calculated value for V_{eqT} is found to be equal to 1.10 V_J.

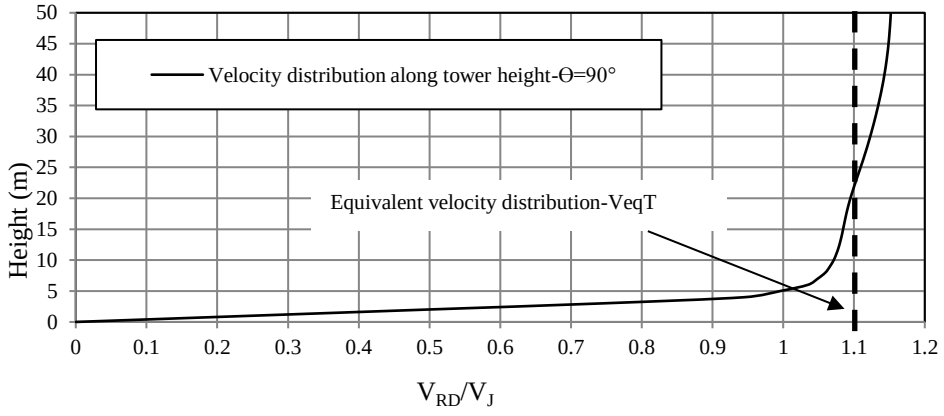

Fig. 5-13. Radial velocity distribution along tower height- Θ=90°.

5.3.2.2. Load case#2: $R/D_J=1.3$, $\Theta=0^o$, $L/D_J=0.5$

This configuration represents the maximum velocity profile acting on the tower and the conductors in the direction parallel to the line direction. The critical velocity profiles along the height of the tower as well as along the spans adjacent to the tower of interest are given in **Fig. 5-14** and **5-15**, respectively. Equivalent uniform velocity distributions, V_{eqT} and V_{eqC}, are evaluated to reproduce the overall effect of the non-uniform profiles in order to facilitate their application using the same approach described in load case 1. The calculated values for V_{eqT} and V_{eqC} are found to be equal to 1.10 V_J and 1.06V_J, respectively.

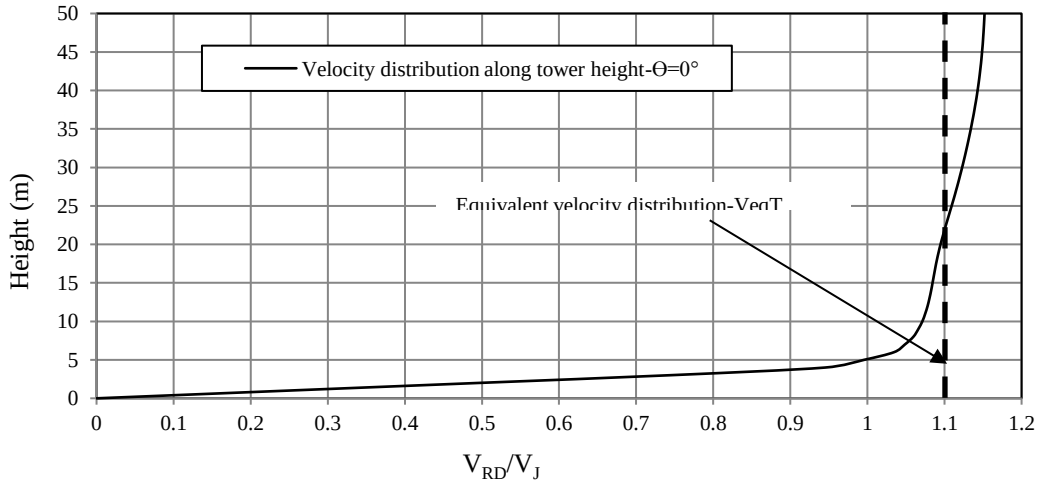

Fig. 5-14. Radial velocity distribution along tower height Θ=0°.

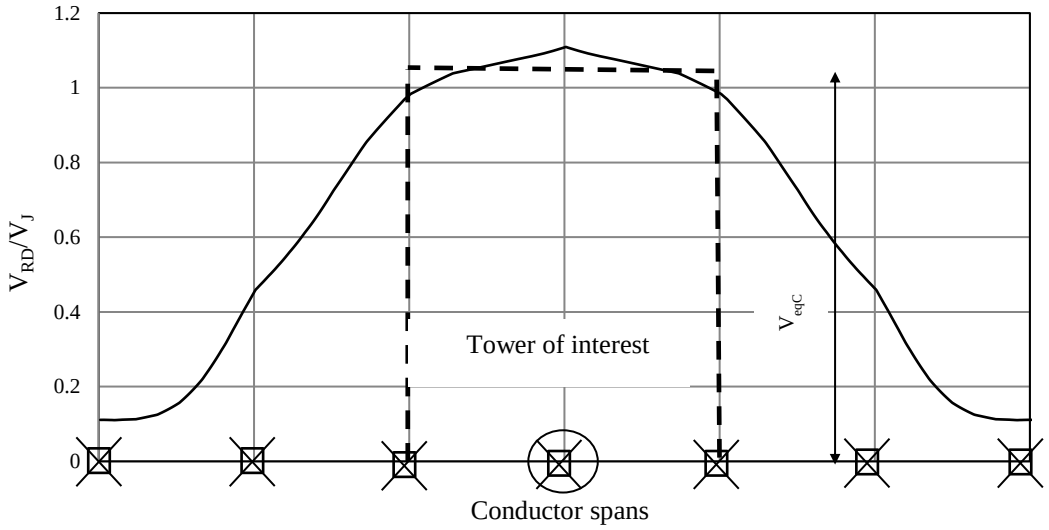

Fig. 5-15. Radial velocity distribution over six conductor spans Θ=0°

The 3-second gust velocity is usually used as a reference for the downburst events. Therefore, the studies conducted by Holmes et al. (2008) and Aboshosha et al. (2015) reported a span reduction factor that can be applied to account for the non-correlation in turbulence along the spans of the line. The relation between the length of the span and the span reduction factor of the downburst is provided in **Fig. 5-16**.

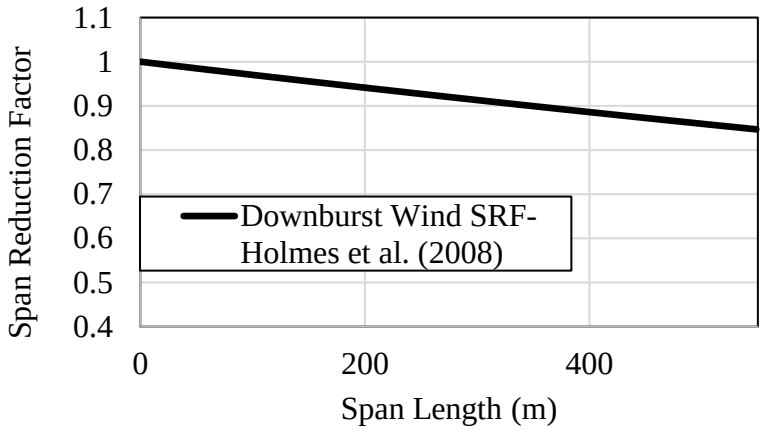

Fig. 5-16. Downburst span reduction factor

5.3.2.3. Load case#3: $R/D_J=1.6$, $\theta=30^o$, $L/D_J=0.5$

This configuration represents the maximum oblique velocity profile acting on the tower and the conductors. **Fig. 5-17** shows the radial velocity distribution along the tower height for both the transverse and the longitudinal directions associated with this load case. **Fig. 5-18** shows the radial velocity distribution of the critical oblique downburst configuration along the line spans associated with this load case. Similar to the previous load cases, equivalent uniform velocities of V_{eqTT}, and V_{eqTL}, and V_{eqC} are evaluated to replace the nonlinear velocity profiles in the tower's transverse direction, the tower's longitudinal direction, and the conductor's transverse direction, respectively. The calculated values for V_{eqTT}, and V_{eqTL}, and V_{eqC} are found to be equal to 0.8 V_J and 0.47 V_J, and 0.65 V_J, respectively. It is important to mention that the value of V_{eqC} can be only used to calculate the transverse reaction R_Y under this load configuration. The longitudinal reaction R_X depends on the conductor's properties and requires conducting a nonlinear analysis for the conductors under non-uniform loading. A set of graphs and an interpolation procedure that takes into account the variation in loading and conductors' properties was developed by Elawady and El Damatty (2016) to facilitate the evaluation of those forces manually.

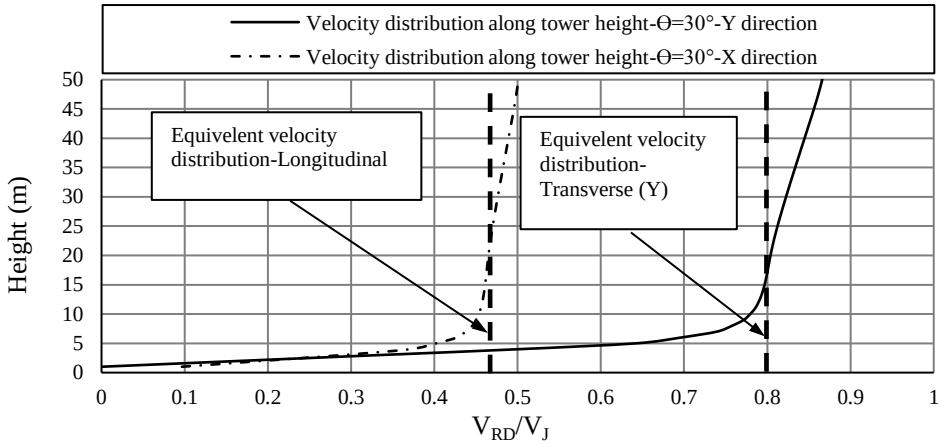

Fig. 5-17. Radial velocity distribution along tower height at $R/D_J=1.5$ and $L/D_J=0.5$, and $\Theta=30°$.

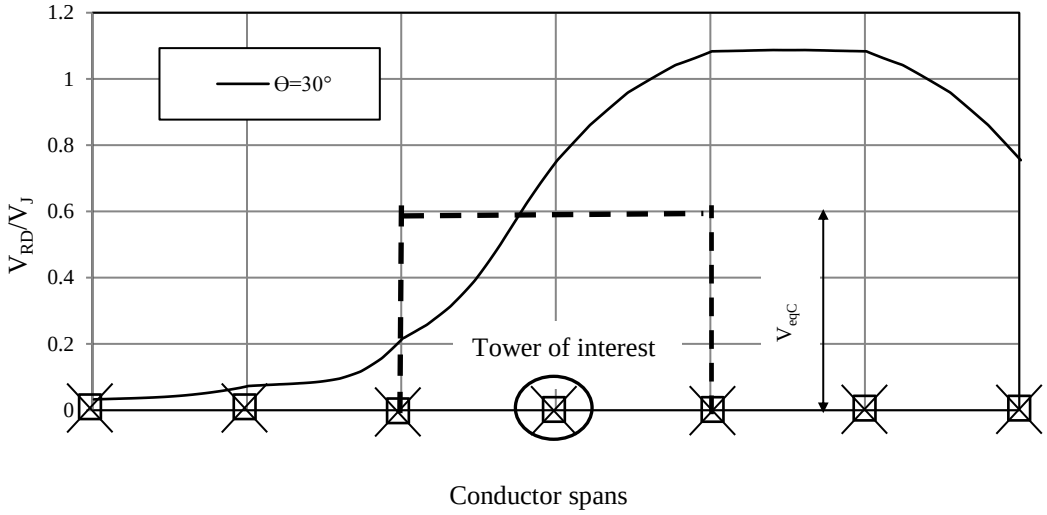

Fig. 5-18. Radial velocity distribution over six conductor spans at $R/D_J=1.5$ and $L/D_J=0.5$, and $\Theta=30°$

5.3.3. Load Cases Validation

Three hypotheses have been made in order to propose the three critical load cases discussed in the previous section. First, three critical load cases are selected out of the entire parametric study, which consisted of approximately 900 load cases, to represent the critical

loading scenarios anticipated for the tangent transmission towers subjected to the downbursts. Second, the proposed load cases are then simplified from nonlinear to linear wind velocity profiles to facilitate their applications by practitioners. Third, the dynamic response of the tower and the conductors is assumed to be only background while neglecting the resonant response, which varies between 10~15%. These three hypotheses need to be validated. In this section, the forces developing in each member of the studied towers due to the extensive parametric study (FP) are compared to those forces developing in the members due to the proposed critical load profiles (FC). The comparison graphs are shown in **Fig. 5-19**. The vertical axes of these figures represent the ratio between the envelopes of the forces experienced by each member under the considered downburst configurations (FP), approximately 900 load cases, to the envelopes of the forces in those members under the three proposed simplified load cases (FC). The analysis shows that the internal forces developing in most of the tower members under the proposed simplified load profiles are either greater than or equal to those resulting from the parametric study.

Several research studies are currently ongoing to address the probabilistic environment of thunderstorms. Other uncertainties arise from the fact that the peak forces developing in the members (FP) are based on the assumption of having an extreme loading scenario that takes place at a specific downburst diameter, at a specific location of the downburst relative to the tower and at a specific time. However, the probability that such a combination will simultaneously occur for a specific tower is low. Transmission line towers often possess sufficient redundancy and ductility (Mara and Hong, 2013), which allows them to function under extremely stressful circumstances. Therefore, the authors believe that such a difference between FP and FC is acceptable.

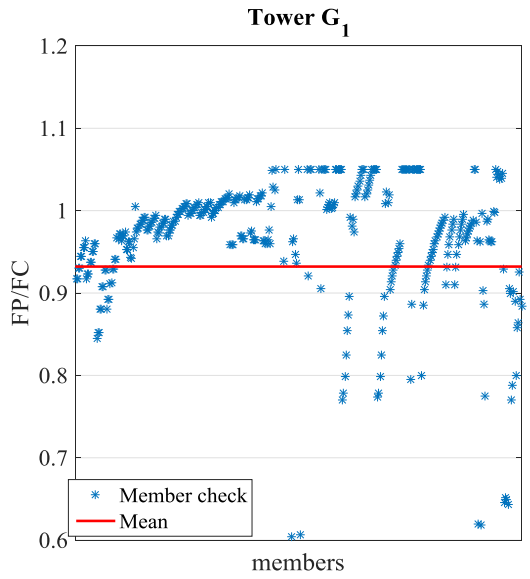
Tower G1
1.2
1.1
1
0.9
0.8
0.7
0.6
FP/FC
Member check
Mean
members

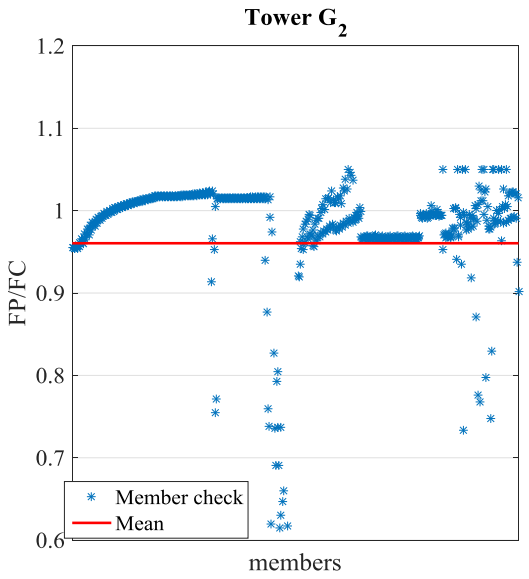
Tower G2
1.2
1.1
1
0.9
0.8
0.7
0.6
FP/FC
Member check
Mean
members

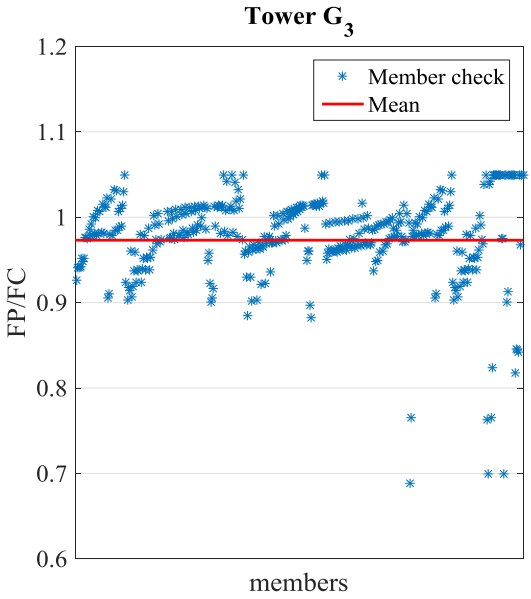
Tower G3
1.2
1.1
1
0.9
0.8
0.7
0.6
FP/FC
Member check
Mean
members

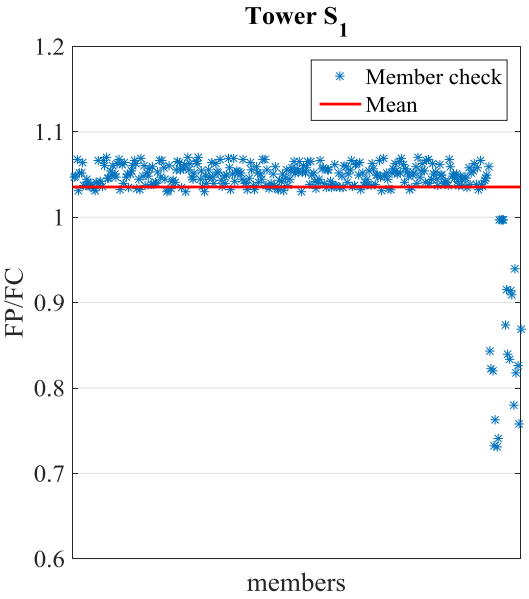
Tower S1
1.2
1.1
1
0.9
0.8
0.7
0.6
FP/FC
Member check
Mean
members

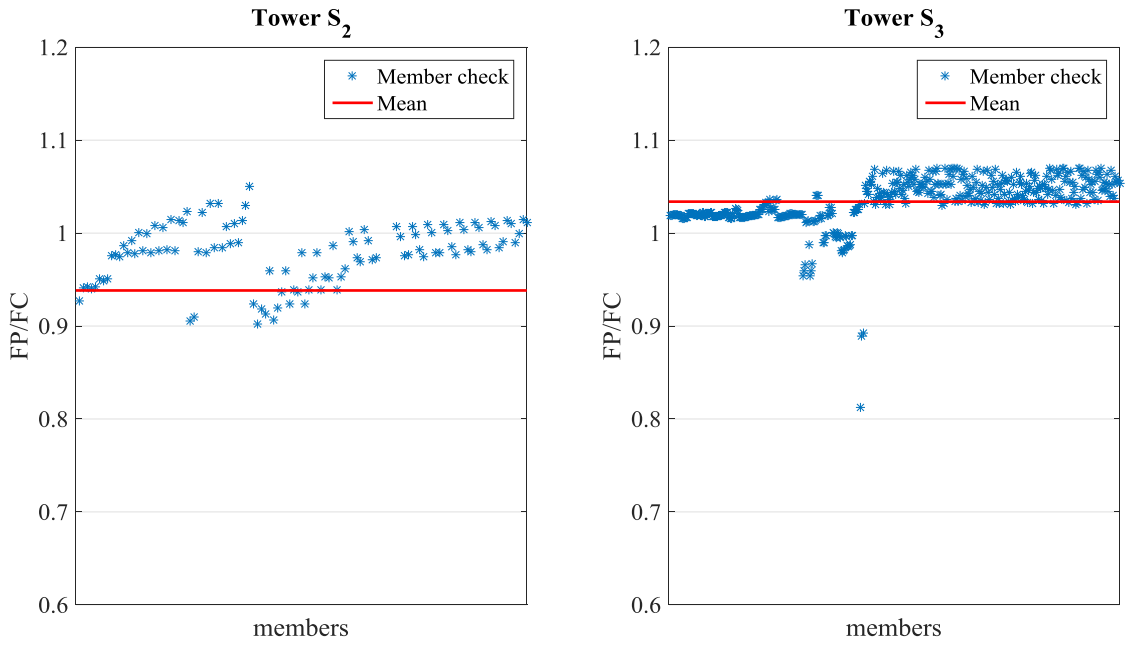

Fig. 5-19. Load cases validation.

5.3.4. Economic Implications

In this section, the economic implications of considering the identified downburst load cases in the design of the towers is assessed. The change in the total weight of the towers resulting from considering those load cases is the parameter used to assess the economic implications. The three downburst load cases are used to evaluate the peak internal forces developing in the tower members for the six considered systems. Those internal forces are then compared to the members' capacity. Since the downburst internal forces can switch from tension to compression depending on the location of the downburst, the member's capacity are assumed to be governed by their compression strengths since they are usually less than the corresponding tensile strengths. The ratio between the internal force and the strength is evaluated for all members. When this ratio is found to exceed unity, the cross section of the member is upgraded such that this ratio is slightly below unity. The weight

of the upgraded towers is evaluated and compared to the initial weight in order to assess the economic implication of designing the towers to resist downburst loadings. A downburst jet speed of 50 m/sec is assumed in this study. The compression capacity of the tower members is calculated based on the recommendations given in ASCE 10 (1997) for angle cross sections.

For a number of selected members, **Table 5-3** identifies the critical downburst load cases and the corresponding peak internal forces found in each member (F_{DB}). The table also shows the ratio between F_{DB} and the corresponding member capacity, $F_{Capacity}$. The table shows that the ratio $F_{DB}/F_{Capacity}$ randomly varies depending on the studied system and the member locations. **Table 5-4** shows the failed members, in red and solid lines, in each of the studied towers due to the effect of the downburst loads. **Table 5-5** summarizes the results of the economic study where the increase of weight relative to the initial weight of each tower is provided. The upgrade required for each of the studied towers to resist the downburst load cases is provided below:

For the guyed towers:

Different zones require an upgrade for the three studied guyed towers. For G_1 which was originally designed to resist a 32 m/s wind speed, the analysis shows that the members located in the main body of the tower below and above the cross arm zones do not need any upgrade. Out of 48 members in the cross arm zone, 22 members are found to need an upgrade. The total weight of the tower is increased by 3% in order to resist the downburst loads. For tower G_2 which was originally designed to resist a 36 m/s wind speed, below the cross arm zone, 290 members are shown to experience internal forces exceeding their strength capacities, while with the exception of a few

diagonal members, the rest of the cross arm members do not need any upgrade. The resulting increase in the total weight of the upgraded tower is 23% compared to the original design. For G_3 which was originally designed to resist a 36 m/s wind speed, 156 members located in the tower's main legs and the girder are shown to exceed their strength capacities. The upgrade of those members results in a 14% increase in the total weight of the tower. The significant increase in the weight required for G_2 and G_3 compared to G_1 is a result of their relative high flexibility. In addition, the aerodynamics of G_2 and G_3 is much higher than that of G_1 under the critical load case of $\Theta = 90°$ which is observed for the studied guyed towers. This triggered higher downburst loads acting on the tower.

For the self-supported towers

Tower S_1 is found to sustain the three downburst load cases without any need for upgrade. For tower S_2, 190 members in various locations in the tower are shown to exceed their strength capacities. The upgrade of the member's cross sections results in 16.3**%** increase in the total weight of the tower. For tower S_3, only 10 members, all located in the cross arm zone, are shown to need an upgrade resulting in a 1% increase in the total weight of the tower. Although the transmission tower system used in S_2 is similar to that one of S_1, a significant upgrade is estimated for tower S_2 to sustain the downburst loads. This is due to the high longitudinal force developing in the conductors of S_2 compared to S_1 and S_3. In addition, the original design wind speed of S_2 (34 m/s) was significantly lower than that of S_1 (45 m/s) and S_3 (40 m/s).

Table 5-3. Results of the economic study

Member	Type	Downburst linear profiles		$F_{DB}/F_{Capacity}$
		Critical Load Case	F_{DB} (kN)	%
Guyed tower G_1				
30P	Chord	2	-30	16
351P	Chord	1	-98	35
430P	Guys Cross arm diagonal	2	-53	200
437P	Guys Cross arm diagonal	3	-42	227
Self-supported tower G_2				
40P	Chord	2	-144	103
132P	Chord	2	-753	442
308P	Chord	1	-237	139
955P	Cross arm chord	1	-25	10
Self-supported tower G_3				
539P	Chord	2	-220	110
726P	Chord	2	-132	76
352P	Chord	2	-180	43
95P	Cross arm chord	3	-144	115
Self-supported tower S_1				
217P	Chord	1	-462	71

434P	Chord	1	-320	62
528P	Chord	1	-272	45
799P	Cross arm chord	3	-13	9
Self-supported tower S_2				
2P	Chord	1	-686	295
41P	Chord	3	-632	272
52P	Chord	1	-403	60
331P	Cross arm chord	3	-72	138
Self-supported tower S_3				
85P	Chord	1	-584	40
566P	Chord	1	-481	31
725P	Chord	1	-467	30
928P	Cross arm chord	3	-35	149

*Chord: vertical member below the cross arm

Table 5-4. Failed members under downburst load case of a jet speed equal to 50 m/s.

G_1 (Design speed 32 m/s)	G_2 (Design speed 36 m/s)	G_3 (Design speed 36 m/s)
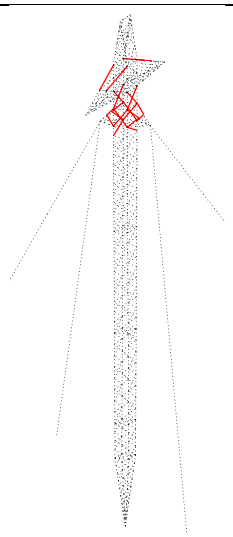	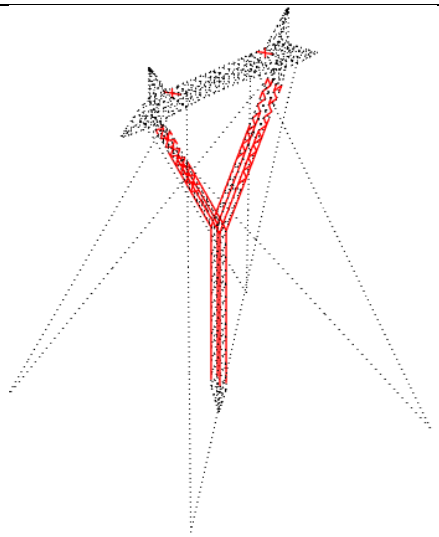	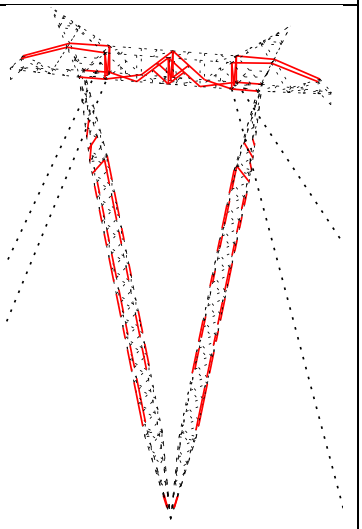
S_1 (Design speed 45 m/s)	S_2 (Design speed 34 m/s)	S_3 (Design speed 40 m/s)
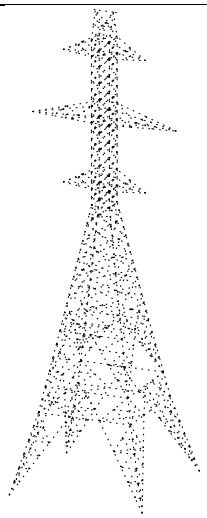	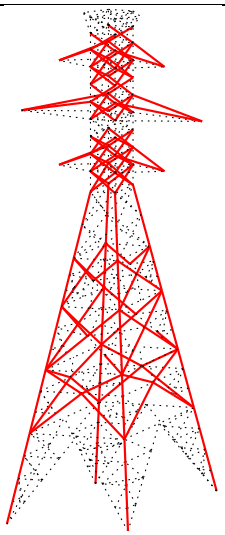	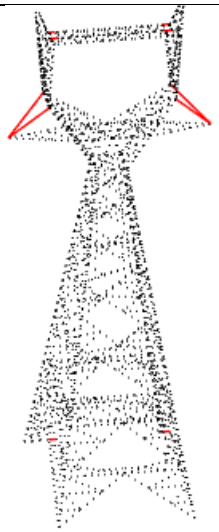

Table 5-5. Summary of the economic implications of the downburst.

Tower	No. of failed members	Location of failed members	Weight increase
G_1	22	Cross arms	3%
G_2	290	Main shaft chords	23%
G_3	156	Main tower shaft+cross arm	14%
S_1	0	N/A	0%
S_2	190	All tower zones	16.30%
S_3	10	Cross arm	1%

5.4. Conclusion

An extensive parametric study is conducted to identify the critical downburst load cases acting on lattice transmission line systems. Six different transmission lines are analyzed with respect to several downburst loads representing different tower systems, spans, heights, and conductor properties. The study investigates the effect of different parameters describing the downburst configuration on the internal force of the tower members. For each transmission line system, the parametric study considers varying the downburst jet diameter (D_J), the distance ratio (R/D_J), and the angle of attack (Θ). The behaviour of the studied towers under the considered downburst load configurations is explained and the following observations are made:

- The load configuration of $\Theta = 90^o$, $R/D_J = 1.3$ results in maximum longitudinal loads on the transmission towers. This load configuration, which does not induce loads on the conductors, is found to be critical for guyed towers. This is because the guyed towers act as a hanging beam where the conductor forces reduce

the maximum bending moment acting on members located between the cross arm and the ground support.

- The load configuration of $\Theta = 0^o$, $R/D_J = 1.3$ causes the maximum transverse loads on the line. This load configuration is found to be critical for the self-supported towers where the tower behaves in a manner that is similar to a free cantilever.

- For both tower systems, either $\Theta = 0^o$ or 90^o is found to be critical for diagonal members depending on the plane in which the diagonal members are located. For members located in a plane parallel to the line direction, an angle of attack of $\Theta = 90^o$ is found to be critical; while for members located in a plane that is perpendicular to the line direction, an angle of attack of $\Theta = 0^o$ is found to be critical.

- In some cases, an oblique load case (at $0° < \Theta < 90°$) is found to be critical for members located in the cross arm zones. This result is due to the large longitudinal forces transmitted to the towers in the oblique load cases. Those forces result from the difference in the tension forces that develop in the conductor spans adjacent to the towers because of the uneven distribution of the external loads between those spans.

- The results of the parametric study are used to propose three critical load cases, corresponding to $\Theta = 0°$, $\Theta = 90°$, and an intermediate value for Θ, respectively. An analysis is made to select the critical downburst parameters for each case, in terms of jet diameter, distance to jet ratio and span to jet diameter ratio. The recommended velocity profiles along the height of the tower and along

the spans of the conductors are provided for the three critical load cases. Those profiles are found to have a nonlinear distribution and thus are simplified to equivalent uniform profiles to facilitate their application by practitioners. A validation of the simplified load cases is conducted by evaluating the internal member forces resulting from applying the simplified velocity profiles and comparing them to the corresponding values obtained from the extensive parametric studies. The analyses show that considering the simplified velocity profiles can provide very close internal forces in the tower members compared to these forces obtained from the extensive parametric study.

The economic implications of upgrading the resistance of the towers of six studied transmission line systems to sustain the proposed downburst load cases are then assessed. A downburst jet velocity of 50 m/sec is assumed. The ratio of increase in the weight of the upgraded towers relative to the initial towers is used to assess the implication of designing the towers to resist the downburst loads. For the three guyed tower systems, the increase in weight is found to be 3%, 23%, and 14%, respectively. Meanwhile, for the towers of the three self-supported systems, this increase is found to be 0%, 16.3%, and 1%, respectively. The significant increase in the tower weight required for S_2, 16.3%, is a result of the high longitudinal force developing in the conductors compared to that found in S_1 and S_3. Meanwhile, the significant increase in the weight of G_2, 23%, might be attributed to the low original wind speed used in the design of this tower.

5.5. Acknowledgements

The authors gratefully acknowledge Hydro One Ontario and the Natural Sciences and Engineering Research Council of Canada (NSERC) for their in-kind support, their collaboration in this project, and for the financial support provided for this research. The authors are grateful for the valuable feedback received from the members of the ASCE-74 code committee responsible for updating the transmission lines manual.

5.6. References

Aboshosha, H., and El Damatty A., (2014-a), "Span reduction factor of transmission line conductors under downburst winds", Journal of Wind and Engineering, Vol. 11, No. 1, Jan. 2014, pp. 13-22.

Aboshosha H., El Damatty A., (2014-b), "Effective Technique for the Reactions of Transmission Line Conductors under High Intensity Winds" Wind and Structures, an International Journal. 18(3) 235-252.

Aboshosha, H., Bitsuamlak, G., El Damatty A., (2015), “Turbulence characterization of downbursts using LES”, Journal of Wind Engineering and Industrial Aerodynamics. 136, 44–61.

American Society of Civil Engineers (ASCE) (1997), “Design Of Latticed Steel Transmission Structures”, ASCE Manuals and Reports on Engineering Practice, No. 10, New York, NY, USA.

Conseil International des Grands Réseaux Électriques/ International Council on Large Electrical Systems (CIGRÉ), (2009), "Overhead line design guidelines for mitigation of severe wind storm damage", Scientific Committee B2 on Overhead Lines, B2. 06.09.

Darwish M., El Damatty A., and Hangan, H., (2010), "Dynamic characteristics of transmission line conductors and behaviour under turbulent downburst loading", Wind and Structures 13(4), 327-346.

Darwish, M.M. and El Damatty, A.A., (2011), "Behavior of self-supported transmission line towers under stationary downburst loading", Wind and Structures 14(5), 481-4.

Dempsey, D., White, H., (1996) “Winds wreak havoc on lines”, Transm Distrib World 48(6), 32-37.

“Economic Benefits of Increasing Electric Grid Resilience to Weather Outages” The White House, Executive Office of the President, USA, August 2013.

Elawady, A. and El Damatty, A., (2016), “Longitudinal Force on Transmission Towers Due to Non-Symmetric Downburst Conductor Loads” Engineering and Structures 127:206-226

“Failure of towers 610 and 611, circuit X503E – 500 kV guyed towers near the Township of Waubaushene, Ontario, August 2, 2006”, Failure Investigation Report, HYDRO ONE NETWORKS INC. - Line Engineering, 2006.

Fengli, Yang., and Hongjie, Zhang., (2016), “Two case studies on structural analysis of transmission towers under downburst”, Vol. 22, No. 6, 685-701.

Fujita, T.T., (1985). "The downburst: microburst and macroburst", SMRP Research Paper 210. University of Chicago.

H. Hangan, D. Roberts, Z. Xu, J. Kim, Downburst simulation, Experimental and numerical challenges, in: Proceedings of the 11th International Conference on Wind Engineering, Lubbock, Texas, Electronic Version, 2003.

Hjelmfelt, M., (1988), “Structure and life cycle of microburst outflows observed in Colorado”, Journal of Applied Meteorology 27, 900–927.

Holmes J.D., Oliver SE. (1996) "A model of downburst winds near the ground for transmission line loading", CSIRO Div. of Building, Construction and Engineering, Australia. Report DBCE Doc 96/3 (M), January 1996.

Holmes, J.D., Hangan, H.M., Schroeder, J.L., Letchford, C.W. and Orwig, K.D. (2008), "A forensic study of the Lubbock-Reese downdraft of 2002", Wind and Structures 11(2), 137-152.

Kim, J. and Hangan, H., (2007), "Numerical simulations of impinging jets with application to downbursts", Journal of Wind Engineering and Industrial Aerodynamics 95(4), 279-298.

Mara, T., and Hong H., Lee, S., Ho, T., (2016) “Capacity of a transmission tower under downburst wind loading” Wind and Structures An International Journal 22(1):65-87.

McCarthy, P., and Melsness, M., (1996), “Severe weather elements associated with September 5, 1996 hydro tower failures near Grosse”

Orwig, K. D. and J. L. Schroeder, (2007), "Near-surface wind characteristics of severe thunderstorm outflows", Journal of Wind Engineering and Industrial Aerodynamics., 95, 565-584.

Savory, E., Parke, G.A.R., Zeinoddini, M., Toy, N., and Disney, P. (2001), "Modelling of tornado and microburst-induced wind loading and failure of a lattice transmission tower", Engineering Structures 23(4), 365-375.

Shehata, A.Y. and El Damatty, A.A., (2007) "Behaviour of guyed transmission line structures under downburst wind loading", Journal of Wind and Structures, 10(3) 249-268.

Shehata, A.Y., El Damatty, A.A. and Savory, E., (2005), "Finite element modeling of transmission line under downburst wind loading", Finite Elements in Analysis and Design., 42(1) 71-89.

Vermeire, B., Orf, L., Savory, E., (2011a), “Improved modelling of downburst outflows for wind engineering applications using a cooling source approach”, Journal of Wind Engineering and Industrial Aerodynamics 99, 801–814.

Vicroy, D., (1992), “Assessment of microburst models for downdraft estimation”, Journal of Aircraft 29, 1043-1048.

Wang, X., Lou, W., Li, H., and Chen, Y., (2009), “Wind-induced dynamic response of high-rise transmission tower under downburst wind load”, Journal of Zhejiang University 43(8), 1520-1525.

Wolfson, M., DiStefano, J., Fujita, T., (1985), “Low-altitude wind shear characteristics in the Memphis, TN area”, Proceedings of the 14th conference on severe local storms, American Meteorological Society, Indianapolis, IN, USA., 322–7.

Zhang Y. (2006), “Status quo of wind hazard prevention for transmission lines and countermeasures”, East China Electric Power, 34(3), 28-31

Zhu S, Etkin B. (2006), “ Model of the wind field in a downburst”, J Aircraft 1985; 22:595–601.

CHAPTER 6

SUMMARY AND CONCLUSIONS

6.1. Summary

The research conducted in this Thesis consist of two distinctive parts that are believed to provide significant advancement in the subject of transmission line structures under downburst loading. The first part reports the first experimental program conducted on a multi-span aero-elastic transmission line model subjected to a reduced-scale simulated downburst. The test is conducted at the WindEEE dome facility, which is the only three-dimensional wind facility in the world that can simulate reduced-scale downbursts. Characterization of the downburst wind field produced at WindEEE is reported. The aero-elastic test has two main objectives. The first objective of the test is to assess the dynamic response of the tower and the conductors under various downburst loading scenarios. The second objective of the test is to validate a non-linear numerical model previously developed in-house for the simulation and prediction of the response of transmission line structures under downbursts. The wind field measured at WindEEE is implemented into the numerical code that is used to simulate the tested aero-elastic model. Comparisons are made between the numerical predictions and the test measurements. The validation is made at three different levels; validation of the conductor's simulation, validation of force calculations and validation of the finite element model for the tower.

In the second part of the studies, a comprehensive procedure for the evaluation of a set of critical load cases that can be used to design transmission line structures under downbursts has been developed. This part of the study is conducted using the numerical model that is

validated experimentally in the first part of the Thesis and is presented in two separate chapters. Chapter four focuses on a particular load case that appears only in the case of localized High Intensity Wind that leads to non-uniform and unequal distribution of the loads along the spans located at opposite sides of a tower. This leads to a net force acting on the tower cross arm along the longitudinal direction of the line. The evaluation of this force requires conducting sophisticated nonlinear analysis for the conductors under a set of non-uniform loads. A set of graphs and linear interpolation procedure are developed in this chapter providing a practical and simplified approach for the practitioners to estimate this longitudinal force.

By conducting an extensive parametric study in Chapter five, three load cases are provided to simulate the critical effect of downbursts on a generic transmission line system. Those load cases are provided in a form of simplified velocity profiles that can be easily applied by the practitioner. Those profiles, together with the simplified procedure for the evaluation of the longitudinal forces, provide a complete set for downburst load estimation that can be incorporated in the codes and simulations of transmission line loading.

6.2. Conclusions

The main conclusions pertaining to the aero-elastic model study reported in chapter two and three are:

- The radial distance corresponding to the location of the maximum downburst radial velocity depends mainly on the ratio between the height of the wind field domain to diameter of the downburst (H/D) used in the simulation of the wind field.
- The maximum vertical profile of the radial velocity is independent from the H/D ratio.

- The turbulence intensity of the downburst wind field is in order of 10~14%.
- At typical wind speed of downbursts, the Dynamic Amplification Factor (DAF) of the tower is in the order of 10 ~ 15%.
- The WindEEE test results show that the longitudinal force developing in the conductors under the oblique case of loading can be as high as 60% of the corresponding transverse force of the conductor.
- For a studied guyed tower, the variation of the downburst configurations affects the response of the conductors and the tower.
- The numerical models are validated using the experiment conducted in this study.

The main conclusions pertaining to the critical load case studies reported in chapter four and five are:

- The maximum longitudinal force developing in the conductors under the downburst oblique case (R_X) occurs when the projection of the downburst center on the line is on the second span measured from the tower of interest. At that point, the transverse velocity of the downburst is the maximum along the spans.
- R_X is inversely proportional to the insulator length in an approximate linear manner.
- The increase in the wind pressure results in a nonlinear increase in R_X.
- R_X is proportional to the Sag to Span ratio. The relation between the R_X and the Sag to Span ratio is found to be non-linear in most of the cases.
- R_X is non-linearly decreasing with the increase in the conductor's weight per unit length.
- The conductor's axial rigidity is found to have a negligible effect on the R_X.

- The maximum transverse loads affect the line and the tower when the downburst loads act with an angle of attack of 0° and distance ratio R/D_J equal 1.3. This load configuration is found to be critical for self-supported tower systems.
- Maximum longitudinal forces occur when the downburst acts at an angle of attack of 90° and a distance ratio R/D_J equal 1.3. This load configuration is found to be critical for the guyed tower systems.
- For both the self-supported and the guyed towers, the cross arm zones are found to be critical under oblique angles of attack where high longitudinal force (R_X) develops in the conductors.
- Three downburst critical load cases are proposed based on the observations of the parametric study conducted on six different transmission line systems. The proposed profiles are nonlinear. As such, a simplified linear profiles are suggested and validated.
- The economical implications of considering the proposed downburst profiles are evaluated. The study revealed that an upgrade for the weight of the tower ranging between 3% to 23% is required for the guyed towers and 0% to 16% is required for the self-supported towers.

6.3. Recommendation for future work

The current study discussed the static and dynamic responses of tangent transmission lines due to the downburst loads assuming an open terrain. For future research, the following investigations are suggested:

- Estimate the Dynamic Amplification Factor assuming different terrain exposures. This can be done experimentally or numerically by employing the turbulent component of the downburst winds.
- Expand the study conducted in chapter 4 to account for the effect of the non-correlated turbulence.
- Expand the study conducted in chapter 4 to account for the angle line cases. An increase in the R_X is expected when the transmission line has an in-plane angle.
- Implement the downburst critical load cases to perform nonlinear analyses on different transmission lines to assess their inelastic capacity.
- Expand the numerical studies conducted to assess the critical response of an individual tower subjected to downburst loads to include progressive failure studies of the entire line.
- Study the effect of the topography variations on the proposed downburst load profiles.
- Develop a framework aiming to consider the probability of occurrence of downburst events and the propagation of the uncertainties involved in the proposed design guidelines.
- Propose a safety factor for the proposed design load cases.

CURRICULUM VITAE

Name: Amal Elawady

EDUCATION

Master of Science in Structural Engineering 2008-2012
***Department of Civil & Environmental Engineering**, Ain Shams University, Cairo*

Bachelor of Engineering Science 2003-2008
***Department of Civil & Environmental Engineering**, Ain Shams University, Cairo*

RELATED WORK EXPERIENCE

Instructor Fall 2016
Department of Civil & Environmental Engineering, UWO, London, Ontario, Canada

Teaching Assistant 2012-2016
Department of Civil & Environmental Engineering, UWO, London, Ontario, Canada

Teaching Assistant 2008- 2012
Department of Civil & Environmental Engineering, Ain Shams University, Cairo, Egypt

AWARDS

O.H. Ammann Research Fellowship	08/2016
Dr. Robert Addie Graduate Scholarship in Wind Engineering	08/2016
Best Student Paper Award, CSCE Annual Conference	06/2016
Alan G. Davenport Award of Excellence	08/ 2015
Graduate Scholarship in Structural Engineering	07/ 2015
Ontario Centers of Excellence (OCE) Internship	05/2015
Julie Lassonde Award	01/ 2015
PCI Big Beam Contest Winner	07/ 2014
Western Graduate Research Scholarship	2012 -2016
Certificates of Honor for Excellent Students	2003-2008

PUBLICATIONS

Referred Journal Papers (published)

Elawady, A., and El Damatty, A., (2016), "Longitudinal Force on Transmission Towers due to Non-Symmetric Downburst Conductor Load", Journal of Engineering Structures, *Vol. 127, 206-226*.

Aboshosha, H., **Elawady, A**., EL Ansary, A., El Damatty, A., (2016) *"Review on Dynamic and Quasi-Static Response of Transmission Lines under Synoptic and Non-Synoptic Winds"* Journal of Engineering Structures,112, 23-46.

Elawady, A., Okail, H., Abdelrahman, A., Sayed-Ahmed, E., (2014) *"Seismic Behaviour of High-Rise Buildings with Transfer Floors"* Electronic J. of Structural Engineering, Vol. 14, 57-70.

Elawady, A., Okail, H., Abdelrahman, A., Sayed-Ahmed, E., (2012) "*Structural Performance of High Rise Building with Transfer Floors"* J. of Al-Azhar University Engineering Sector, Vol. 7, 23-38.

Conference Proceedings

El Damatty, A., and **Elawady, A.,** (**2016**), *"Development of Code Provisions for Transmission Lines under Downbursts Using Numerical Modeling and WindEEE Testing "* The 2016 World Congress on Advances in Civil, Environmental, and Materials Research (ACEM16), Jeju Island, South Korea.

El Damatty, A., **Elawady, A.,** M. Hamada, (2016), *"Transmission Line Failures during Tornadoes and Downbursts- Can they be avoided"***,** SEMC 2016 - Sixth International Conference on Structural Engineering, Mechanics and Computation, Cape Town, South Africa, September 7-9.

Elawady, A., Aboshosha, H., El Damatty, A., Bitsumlak, G., (2016) "*Large Scale Wind Tunnel Testing of a Multiple Span Aeroelastic Transmission Line Subjected to Downburst Wind"*, CSCE, London, Ontario, June 1-4, 2016**.**

Elawady, A., El Damatty, A., EL Ansary, A., (2016) "*Critical Load Cases Simulating Downbursts- Economical Implication on Design of Transmission Lines*", Cigre-IEC Colloquium conference, Montreal, Canada, 9-11 May, 2016**.**

El Damatty, A., and **Elawady, A.,** (**2015**), *"Critical Load Cases for Lattice Transmission Line Structures under Downbursts"* The 14th International Conference on Wind Engineering, ICW14, June 21-25, Brazil.

El Damatty, A., **Elawady**, **A.,** Hamada, A., Lin, E., (2014) *"State-of-the-Art Knowledge about Behaviour of Transmission Line Structures under Downbursts and Tornadoes"* proceedings of The 2014 World Congress on Advances in Civil, Environmental, and Materials Research (ACEM14), Korea.

El Damatty, A., **Elawady, A.,** Hamada, A., (2014) *"Resilience of transmission lines to Localized High Intensity Wind Events"* EMI 2014 Engineering Mechanics Institute Conference August 5-8, 2014, Canada.

Aboshosha, H., **Elawady, A.,** Peddie, K., Rofail, A., Bitsuamlak, G., (2014), *"Parametric study on the natural ventilation of a building with large atrium using hybrid CFD-wind tunnel approach"* The 6th International Symposium on Computational Wind Engineering - CWE2014, June 8 - 12, Germany.

A. El Damatty, A. Hamada, **A. Elawady** (2013), *"Development of Critical Load Cases Simulating the Effect of Downbursts and Tornados on Transmission Line Structures"*, proceedings of the Eighth Asia-Pacific Conference on Wind Engineering, Chennai, India.